The Okavango delta through the deformation of its surface : multi-proxy approach from hydrology to tectonics

Anne-Morwenn Pastier

ANNÉE 2018

UNIVERSITÉ DE RENNES 1

UNIVERSITE BRETAGNE LOIRE

THÈSE / UNIVERSITÉ DE RENNES 1
sous le sceau de l'Université Bretagne Loire

pour le grade de

DOCTEURE DE L'UNIVERSITÉ DE RENNES 1

Mention : Sciences de la Terre et des Planètes

Ecole doctorale Écologie, Géosciences, Agronomie, Alimentation

Anne-Morwenn Pastier

Préparée à l'unité de recherche UMR 6118
Géosciences Rennes – UFR Sciences et Propriété de la Matière

The Okavango Delta through the deformation of its surface : multi-proxy approach from hydrology to tectonics

Thèse soutenue à Rennes le 2 février 2018:
devant le jury composé de :

David NASH
Professor, University of Brighton / *rapporteur*

Cécile DOUBRE
Physicienne adjointe CNAP, EOST, Strasbourg / *rapporteure*

Damien DELVAUX
Senior geologist, Royal Museum for Central Africa, Tervuren, Belgique / *président du jury*

Guillaume RAMILLIEN
Chargé de recherche, CNRS, Géosciences Environnement Toulouse / *examinateur*

Olivier DAUTEUIL
Directeur de recherche, Géosciences Rennes / *directeur de thèse*

Mike MURRAY-HUDSON
Senior researcher, Okavango Research Institute, Maun, Botswana / co-*directeur de thèse*

Frédérique MOREAU
Maître de Conférence, Géosciences Rennes */ co-directrice de thèse*

Andrea WALPERSDORF
Physicienne CNAP, ISTerre, Grenoble / *membre*

Résumé :

Le Delta de l'Okavango est un système endorhéique formant un cône alluvial dans la dépression du Kalahari. L'écosystème y est rythmé par une crue annuelle en provenance de l'Angola et entravée par l'escarpement des failles normales du graben de l'Okavango. Ce régime annuel est très variable, car la répartition de la crue annuelle diffère tous les ans. À plus grande échelle temporelle, du millénaire au Ma, l'endorhéisme du Delta peut varier entre des marais (actuel), un mega-lac ou perdre son caractère endorhéique (rivière).

Les processus pouvant contrôler ces variations de régime sont 1) l'hydrologie du système, 2) l'activité des failles du graben, 3) l'apport sédimentaire et 4) l'écosystème. Cette étude apporte des contraintes quantifiées éclairant deux de ces processus à travers l'observation de la déformation de la surface terrestre par l'enregistrement de stations GPS permanentes. Le signal observé est annuellement impacté par la charge hydraulique résultant de la saison des pluies, et inter-annuellement par les variations de cette charge, ainsi que l'activité tectonique du graben.

Les satellites GRACE fournissent un enregistrement quasi-continu de la variation du stock d'eau continentale, rendant possible la modélisation de la déformation élastique de la surface terrestre sous l'effet de cette charge. Le signal de déformation ainsi modélisé est comparable au signal saisonnier enregistré, validant les données satellitaires GRACE et révélant un important aquifère dans le bassin de l'Okavango. GRACE fournit ainsi un nouveau proxy permettant de suivre l'évolution de l'aquifère, et de valider le modèle hydrologique calibré précédemment pour le bassin. Les variations inter-annuelles d'eau souterraine dans le bassin validées par GRACE confirment le rôle de tampon des variations climatiques joué par l'aquifère sur la modulation des variations climatiques. La phase des variations du stock d'eau met de plus en évidence un effet de seuil dans la recharge de ce stock, en fonction de l'intensité des premières pluies. La faible résolution spatiale des variations du stock d'eau continental fournie par GRACE peut finalement être mieux contrainte par un examen plus détaillé des signaux GPS dans le bassin.

Les vitesses de déformation horizontales de part et d'autre du graben révèlent une déformation tectonique faible sur l'ensemble du graben, de 1 mm/an exclusivement décrochante dextre. Une si faible déformation exclut une influence significative de l'activité tectonique et sismique du graben sur la variabilité de la distribution de la crue. Cette déformation observée remet en question le modèle géodynamique admis dans la région, soit une phase précoce de rifting liée à la propagation d'une branche SW du Rift Est-Africain. Un recensement des nombreuses études géophysiques réalisées dans la région dans la dernière décennie et un réexamen de la sismicité de l'Afrique australe n'amène aucune preuve significative de rifting dans le graben de l'Okavango. Un autre modèle géodynamique pour l'Afrique australe est proposé, basé sur l'accommodation lointaine de la déformation associée à l'ouverture à taux différentiels du Rift Est-Africain et le déplacement du craton du Kalahari par rapport au reste de la plaque nubienne.

Abstract :

The Okavango Delta is an endorheic system forming an alluvial fan in the Kalahari depression. The local ecosystem is paced by the annual flood coming from the Angolan highlands, blocked downstream by the normal faults scarps of the Okavango graben. This annual regime is highly variable, with the spatial distribution of the flood differing every year. At the geological time scale, from millenary to mega-annual, the Delta's endorheism can also vary between wetlands (current regime), mega-lake or loose its endorhism to turn into a river.

Processes driving these regime variations are 1) the hydrological system, 2) the faulting of the graben, 3) the sedimentary input and 4) the ecosystem. This study brings quantitative constraints regarding two of these processes through the deformation of the Earth's ground surface monitored by permanent GPS stations. The observed signal is impacted seasonally by the hydrological loading resulting from the rainy season, and inter-annually by the variations of the terrestrial water storage, as well as the tectonic activity of the graben.

GRACE satellites provide a quasi-continuous record of the variations of the Earth's continental water storage, allowing the modelling of the elastic deformation imposed on the Earth's crust by loading. The resulting modelled deformation signal is well correlated to the observed seasonal signal, hence validating the GRACE data products and revealing a large aquifer in the Okavango basin. GRACE thus provides a new proxy to monitor the evolution of water storage, and to validate more robustly the hydrological model calibrated for the basin. The variations in terrestrial water storage (TWS) in the basin validated by GRACE confirm the buffer effect of the aquifer in the modulation of climatic variations. The phase of the TWS variations moreover highlights a threshold in the recharge of TWS during the rainy season, depending on the intensity of the first rains. Finally, the poor spatial resolution of TWS variations provided by GRACE can be further constrained by a detail examination of the GPS signals in the basin.

Horizontal displacements rates across the graben reveal a low tectonic deformation rate, of 1 mm/yr, exclusively along a dextral strike-slip component. Such a low deformation rate excludes a significant influence of the graben faulting on the variability of the flood distribution. The observed deformation calls into question the current geodynamic model for the area, i.e. incipient rifitng due to the propagation of a southwestern branch of the East African Rift System. A review of the numerous geophysical studies in the study area over the last decade, as well as a re-examination of the seismic data in southern Africa does not provide significant evidence for rifting in the Okavango graben. An alternative geodynamic model is proposed, based on the far-field accommodation of the deformation resulting from the differential extension rates in the Rift Valley, and the displacement of the Kalahari craton relative to the Nubian plate.

Contents

List of Figures

List of acronyms:

CAB: Congo Air Boundary
CHIRPS: Climate Hazards Group InfraRed Precipitation with Station data
CNES: Centre national des Études Spatiales
CSR: Center for Space Research
DRC: Democratic Republic of Congo
DS: Distributary system
DWA: Department of Water Affairs
EARS: East African Rift System
ERT: Electrical Resistivity Tomography
ET: Evapotransipration
EWH: Equivalent Water Height
GNSS: Global Navigation Satellite System
GPS: Global Positioning System
GRACE: Gravity Recovery And Climate Experiment
GRGS: Groupe de Recherche de Géodésie Spatiale
IGS: International GNSS Service
ISC: International Seismological Centre
ITCZ: Inter-Tropical Convergence Zone
ITRF: International Terrestrial Reference Frame
JAXA: National Aeronautics and Japan Aerospace Exploration Agency
MODIS: Moderate-Resolution Imaging Spectroradiometer
MT: MagnetoTelluric
NASA: National Aeronautics and Space Administration
NOAA-CPC: National Oceanic and Atmospheric Administration - Climate Prediction Center
ODS: Okavango Dyke Swarm
OG: Okavango Graben
ORI: Okavango Research Institute
PREM: Preliminary Reference Earth Model
RFE: RainFall Estimator
SASSCAL: Southern African Science Center for Climate Change and Adaptive Land Management
SH: Spherical Harmonics
SRTM : Shuttle Radar Topography Mission
SSZ: Sekaka Shear Zone
SWEA: SouthWestern Extension Area
TRMM: Tropical Rainfall Measurement Mission
TWS: Terrestrial Water Storage
WMO-GTS: World Meteorological Organization - Global Telecommunication System

Résumé en Français :

Le Delta de l'Okavango, au nord du Botswana, est le terminus du système endorhéique de l'Okavango, dont le bassin versant est également réparti sur l'Angola et la Namibie. Le Delta forme un cône alluvial lié à la rupture de pente topographique au sein du graben sismiquement actif de l'Okavango (OG). Les chenaux divergents de l'Okavango sont entourés de plaines d'inondation, ponctuées d'îles de tailles variable. Ce cône alluvial fortement végétalisé forme un vaste marais dans le milieu semi-aride du désert du Kalahari, et subit donc une très forte pression environnementale. Le niveau d'eau, et par conséquent l'étendue des plaines inondées, varie au cours de l'année sous l'effet du régime climatique très contrasté. La saison des pluies, d'octobre à avril, constitue le seul apport de précipitations. De plus, il pleut deux fois plus dans le bassin versant angolais (∼800 mm/an) que dans le Delta (∼400 mm/an). Sous l'effet du très faible relief, le ruissellement s'accumule dans le bassin versant au cours de la saison des pluies, puis s'écoule lentement vers le Delta sous la forme d'une crue. Un décalage conséquent de trois mois sépare ainsi le pic de précipitations (vers janvier) du pic de débit de l'Okavango à l'apex du Delta (vers avril). Trois mois supplémentaires sont nécessaires pour inonder le Delta jusqu'à sa partie distale.

Cette crue annuelle est extrêmement variable. En termes d'étendue, elle varie de 6 000 km^2 à 12 000 km^2. La relation entre la quantité de précipitations, dans le bassin versant et/ou dans le Delta, et l'étendue de la crue n'est pas linéaire. Alors que les précipitations locales affichent un cycle d'environ 18 ans, le débit de l'Okavango à l'apex du cône semble indiquer un cycle d'environ 70-80 ans. Sa distribution spatiale est également variable. Des parties entières du Delta peuvent rester asséchées pendant des décennies, avant d'être à nouveau inondées. Parmi les marqueurs les plus évidents de cette variabilité se trouvent les éxutoires du Delta, qui sont irrégulièrement inondés.

Plusieurs processus sont possiblement responsables de cette variabilité. Concernant l'étendue de la crue, l'hydrogéologie, soit la variation des réserves d'eau souterraine, ainsi que leurs relations avec les réservoirs hydrologiques de surface pourrait conditionner le ruissellement généré au cours des pluies, ainsi que la progression de la crue. La région est malheureusement sous-instrumentée et l'absence de piézomètre dans le bassin versant ne permet pas de valider ou infirmer cette hypothèse. Concernant la variabilité spatiale de la crue annuelle, les interactions entre sédimentation, hydrologie et végétation, processus parmi les plus documentés dans le Delta, sont responsables des fréquentes avulsions de chenaux, caractéristiques des cônes alluviaux. Il a également été proposé que la tectonique active locale puisse bouleverser le gradient topographique lors des séismes, au point de modifier la distribution de l'eau dans les différents chenaux. Depuis les années 1970, cette tectonique locale est couramment associée à une propagation d'une branche sud-ouest du Rift Est-Africain. Ici encore, le manque de données, lié non seulement au manque d'instrumentation, mais également à la couverture omniprésente des sables du Kalahari, n'a pas permis la vérification de cette théories. Pour aller plus loin dans la compréhension des processus contrôlant la propagation de la crue dans le Delta de l'Okavango, il est donc nécessaire d'apporter de nouvelles quantifications.

Le réseau géodésique déployé en 2010 par l'AfricaArray/UNAVCO fournit de nouvelles données permettant ces nouvelles quantifications grâce aux séries temporelles des stations GPS. Elles montrent en effet un signal annuel de forte amplitude (jusqu'à 5 cm) corrélé à

la saisonnalité, ainsi qu'une tendance pluri-annuelle pouvant résulter à la fois de processus tectoniques et de l'évolution pluri-annuelle de la charge de (sub)surface, soit la quantité d'eau souterraine. Le couple de satellites GRACE, mesurant les variations du champ de gravité terrestre, indique une variation de masse annuelle et pluri-annuelle dans les bassins de l'Okavango et du Zambèze. En modélisant les phénomènes de charge liés à ces variations de masse, il est alors possible de décorréler les contributions tectonique et hydrologiques dans le signal de déformation observé par GPS.

En effet, la flexure de la surface terrestre liée aux phénomènes de charge est modélisable à partir des solutions GRACE à l'aide d'une fonction de Green, et des paramètres rhéologiques des enveloppes terrestres. Pour ce faire, quatre solutions GRACE sont utilisées dans cette étude : deux solutions provenant du Center for Space Research (CSR), et deux solutions provenant du Groupe de Recherche de Géodésie Spatiale et du Centre National des Études Spatiales (GRGS-CNES). Les signaux observés par GPS et modélisés à partir des solutions GRACE montrent de forts coefficients de corrélation (jusqu'à 0.94) pour toutes les stations situées dans les bassins de l'Okavango et du Zambèze. De plus, cette déformation est temporellement corrélée au régime climatique : la flexure de la croûte s'initie vers le mois de novembre, en début de saison des pluies, tandis que la relaxation de la croûte démarre vers le mois d'avril, dès que les précipitations diminuent drastiquement. Les plus faibles coefficients de corrélation des autres stations de l'Afrique australe sont liés à une absence de charge saisonnière, aussi bien révélée par les solutions GRACE que par les observations GPS. L'interprétation des solutions GRACE en termes de variation de charge hydrologique dans les bassins de l'Okavango et du Zambèze se trouvent ainsi validées et peuvent désormais être considérées comme un proxy pour la surveillance des eaux continentales.

Dans les bassins de l'Okavango et du Zambèze, les amplitudes annuelles du signal de déformation modélisé à partir des données GRACE sont cependant plus modérées que les amplitudes annuelles observées par GPS. Les hypothèse pour expliquer cette moindre amplitude peuvent concerner : 1) le traitement des données GPS potentiellement accentuant la défomation annuelle, 2) les solutions GRACE potentiellement lissant la déformation modélisée, ou encore 3) les paramètres rhéologiques utilisés pour cette modélisation.

La faible résolution spatiale des solutions GRACE ($\sim$300 km) peut être mieux contrainte par l'analyse des trois composantes du signal de déformation observé par GPS. En utilisant conjointement 1) l'amplitude et la phase des déplacements verticaux, et 2) horizontaux, ainsi que le ratio entre les déplacements verticaux et horizontaux, cette étude a permis de déterminer plus précisément la localisation de la charge saisonnière principale. Celle-ci se trouve particulièrement concentrée autour de la région de Mongu (Zambie). Ce résultat est confirmé par la présence de nombreux marqueurs géomorphologiques indiquant une intense circulation d'eau souterraine (pools et dambos).

Les modèles hydrologiques sont des outils nécessaires à une gestion durable des ressources en eau, notamment comme outil de prédiction des conséquences des futurs aménagements anthropiques ou du réchauffement climatique. Dans le bassin de l'Okavango, ces modèles ne sont contraints que par les chroniques du plus petit résevoir du système, le débit des rivières. Le nouveau proxy que sont les solutions GRACE pour l'évolution du stock d'eau continentale permettent de valider le modèle de Pitman (précipitatons-ruissellement) couplé à un modèle

de réservoirs. Le coefficient de corrélation entre les simulations du modèle et les solutions GRACE atteint 0.94 pour la solution du CSR. L'amplitude et la phase annuelle de la prédiction du modèle de Pitman se trouve ainsi validée par les solutions GRACE. Ainsi, la recharge annuelle de l'aquifère du bassin versant de l'Okavango est initiée après deux à trois mois de précipitations, selon leur intensité. Elle se poursuit jusqu'au mois d'avril, où les précipitations plus rares et moins intenses ne permettent plus cette recharge. L'évapotranspiration (ET) prend alors le dessus et la décharge de l'aquifère s'amorce.

La phase du signal fourni par les satellites GRACE, ainsi qu'une particularité des signaux GPS, permettent d'amener de plus fortes contraintes sur l'évolution annuelle de l'ET. L'Okavango étant un système endorhéique, toute eau apportée par les pluies est soit infiltrée, soit évaporée. Les bilans hydriques réalisés à l'aide de données satellitaires ne reproduisent pas le signal fourni par les solutions. L'ET estimée à partir des mesures des instruments de MODIS est largement sous-estimée, le bilan hydrique résultant étant largement excédentaire. L'ET estimée par le modèle GLEAM à partir d'un jeu de données satellitaires plus vaste permet de reproduire l'amplitude et l'évolution pluri-annuelle du stock d'eau continentale. En revanche, il ne permet pas de reproduire la phase du signal des solutions GRACE, et montre un décalage systématique d'un à deux mois. Seule l'ET estimée au sein du modèle de Pitman par la méthode de covariance des turbulences permet de reproduire à la fois l'amplitude et la phase des variations du stock d'eau continentale.

Une des particularités des signaux GPS observés dans le bassin de l'Okavango permet d'amener des contraintes supplémentaires sur les estimations de l'ET. Ils montrent un palier au cours de la phase de relaxation durant les mois de juillet et août. La résolution temporelle à 10 jours de la solution GRACE du GRGS permet de constater un palier similaire dans la décharge annuelle du stock d'eau continentale. Ce palier, apparaissant au cours de la saison sèche, ne peut être dû qu'à une diminution, voire un arrêt, de l'ET au cours de l'hiver austral. Cet arrêt est possiblement lié au minimum annuel de température à cette saison, ne permettant plus l'ET de l'humidité du sol.

Enfin, la tendance pluri-annuelle du signal de GRACE est elle aussi reproduite, avec une recharge d'année en année de l'aquifère entre 2002 et 2011-2012, et une décharge depuis. Cette corrélation permet d'affirmer non seulement la validité des prédictions du modèle, mais également la perception par les satellites GRACE du cycle naturel de l'aquifère. Un léger défaut d'amplitude est visible dans cette tendance pluri-annuelle, dont une part réside possiblement dans la calibration du modèle. Mais la présence d'une masse d'eau principale localisée dans le Zambèze supérieur par cette étude permet d'affirmer que les solutions GRACE pour le bassin de l'Okavango sont très probablement légèrement surestimées par ce voisinage.

La déformation liée à la tectonique de l'OG est quant à elle visible dans la tendance pluri-annuelle des déplacements horizontaux, peu impactés par l'évolution pluri-annuelle de la saturation de l'aquifère. Le modèle géodynamique de ce graben prédisait une forte déformation extensive. Or, l'étude géodésique des trois stations entourant l'OG révèle un faible taux de déformation (~ 1 mm/an), exclusivement décrochante dextre. Cette contradiction est donc la base d'un réexamen des critères définissant une zone de rifting à partir des récentes prospections géophysiques.

L'un des principaux arguments pour la théorie de l'extension du Rift Est-Africain est la distribution de la sismicité en Afrique australe. Les observations sismiques révélaient jusqu'en

2004 un alignement de foyers sismiques depuis le lac Malawi jusqu'au Delta de l'Okavango. Or, un nouveau déploiement de stations sismiques à travers le sous-continent révèle une distribution spatiale différente, notamment sur 3 points : 1) une distribution des épicentres bien plus diffuse, et non plus sur des alignements NE-SW, 2) une extension de cette zone de sismicité jusqu'à la côte atlantique et non plus arrêtée dans l'OG, et 3) une sismicité plus importante dans la région du Kalahari central que dans l'OG. La magnitude de complétude de cette dernière zone était restée, jusqu'à la dernière phase d'instrumentation, trop élevée pour y détecter la sismicité. Ce résultat a été confirmée par l'occurrence, en avril 2017, d'un séisme de magnitude 6.3 dans le central Kalahari.

L'épaisseur de la lithosphère dans la région révèle un amincissement local, passant de $\sim$250 km sous le craton du Congo et $\sim$220 km sous le craton du Kalahari à $\sim$160 km sous l'OG. Rien n'indique que cet amincissement soit récent et actif. Il peut en revanche s'expliquer par l'histoire tectonique de la région, issue de l'orogène pan-africain dont le pic de métamorphisme est daté à $\sim$500 Ma. Les deux cratons environnants (3.2 et 2.7 Ga) présentent ainsi naturellement une lithosphère plus épaisse, plus froide et donc plus rigide. L'histoire géologique de la région permet également d'expliquer la localisation et l'orientation des failles, remobilisant des structures tectoniques de l'orogène pan-africain. Aucune donnée significative ne vient attester d'un amincissement de la croûte terrestre. Enfin, les plus récentes études ne montrent pas d'anomalie de Bouguer ni de flux de chaleur significatifs sous l'OG.

Aucun critère de rifting continental n'est donc mis en évidence par les dernières études géophysiques. En revanche, les déplacements observés, l'héritage tectono-métamorphique de la région ainsi que les déplacements des (sous-)plaques adjacentes permettent de proposer un nouveau modèle géodynamique, basé sur l'accommodation de la déformation lointaine liée à 1) l'extension, à taux variables, du Rift Est-Africain et 2) la rotation horaire du craton du Kalahari par rapport au reste de la plaque nubienne. La lithosphère plus jeune et donc moins rigide des ceintures pan-africaines, par rapport aux cratons environnants, en fait un lieu de déformation privilégiée.

Cette étude a donc permis d'amener les quantifications nécessaires à une meilleure compréhension des processus contrôlant la distribution de la crue annuelle dans le Delta de l'Okavango. L'état de saturation antérieur de l'aquifère dans le bassin de l'Okavango est un facteur déterminant pour la génération de ruissellement et donc pour le débit de l'Okavango. Dans le Delta, cet état de saturation est également critique. L'élévation de la table d'eau ne varie généralement que d'un an à deux mètres. Mais la grande porosité des sables du Kalahari formant le substrat de l'aquifère rend l'état de saturation antécédente à chaque critique, puisqu'un mètre de battement de nappe représente la moitié du débit annuel de l'Okavango à l'apex du Delta. L'antécédence de la saturation de l'aquifère, et son évolution pluri-annuelle permettrait donc d'expliquer la différence de cyclicité observée entre les précipitations et l'étendue de la crue annuelle.

La déformation tectonique observée semble quant à elle trop faible pour être susceptible de provoquer un basculement du gradient topographique du cône alluvial. L'OG a subi une période de forte sismicité durant la période d'enregistrement des stations GPS, n'entraînant aucune perturbation dans la vitesse de déplacement inter-annuelle. La tectonique locale ne semble donc avoir aucune influence sur la dynamique du cône alluvial, bien plus influencée par les avulsions de chenaux.

Chapitre 1

Introduction

Endorheic systems are continental closed drainage systems showing no outlet connected to the ocean. They are distributed all over the world, mainly in intraplate contexts (Figure 1.1A). Instead of joining the sea, water gathers to form lakes, as large as the Caspian sea, or wetlands, as in the Tarim basin, China, which can be permanent, like in the Okavango Delta, or transient, alternating with seasonal aridity, as in the Etosha Pan. Some of these systems are even desertic, like the Gobi desert. On the geological time scale, they form sedimentary basins.

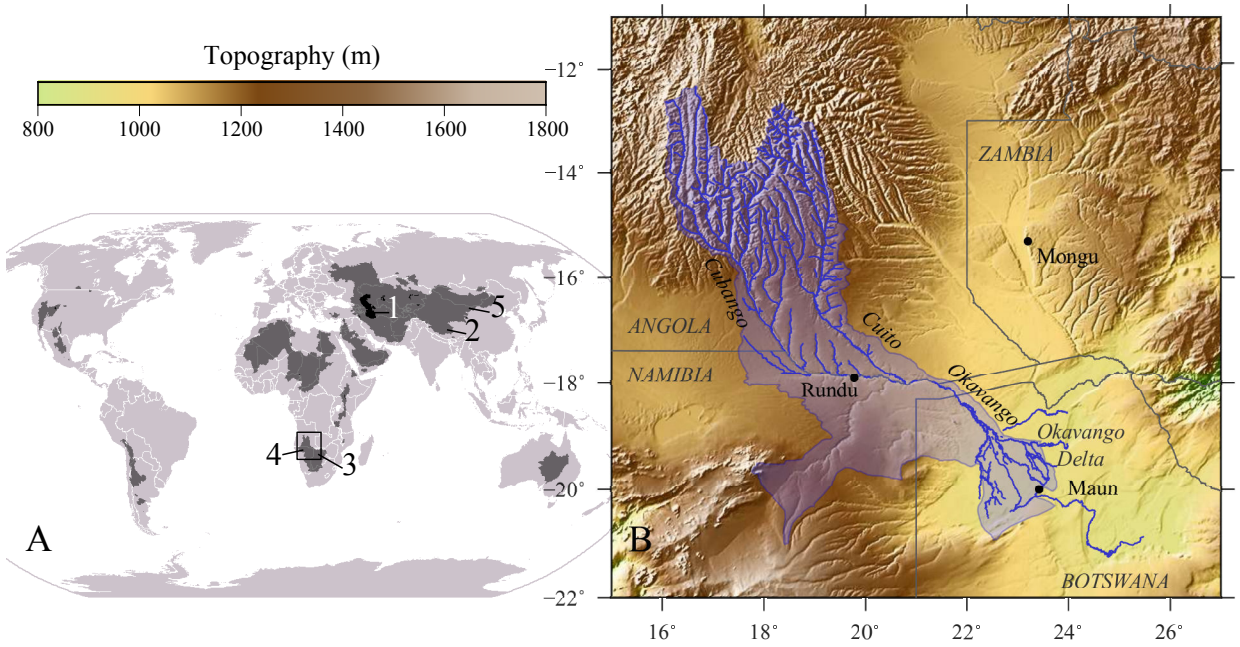

FIGURE 1.1 – A : World map of endorheic systems (dark grey) and major endorheic lakes in black (source : Citynoise, from the USGS Hydro1K data set) 1 : Caspian Sea, 2 : Tarim basin, 3 : Okavango Delta, 4 : Etosha Pan, 5 : Gobi desert. B : Location and physiography of the Okavango hydrological basin. Topography is provided by SRTM3. Black dots show the location of the permanent GPS stations used in this study.

Such systems are controlled by water balance and basin physiography (e.g., Hartley et al.,

2010). The former is exclusively depending on regional climate at the basin scale. But the latter results from different processes : crustal deformation creates relief while sedimentation and erosion smoothen the large scale topography, but can also create small scale relief. Finally, the ecosystem can influence water flow and depositional processes. Moreover, these four processes, hydrology, tectonics, sedimentation, ecosystem, exert more or less strong feedbacks on each other. Balance between these processes controls the regime of endorheic systems (lakes, marshes or desert), which can evolve through time with variations of the initial conditions of the system (basin deformation rate, climate, sedimentary input, etc.).

Among these systems, the Okavango Delta, northern Botswana, is the largest and most pristine wetland in southern Africa and is as such inscribed on the UNESCO World Heritage List (Figure 1.1B). Surrounded by the semi-arid Kalahari desert, its marshes host a hot spot of biodiversity and remain well preserved from intensive anthropogenic disturbance. The water level in the Delta's channels is paced by an annual flood pulse coming from the Angolan catchement area. The Okavango Delta is topographically controlled by an active hemi-graben, the Okavango Graben (OG). First, the break in slope induced by the graben initiates the alluvial fan and turns the Okavango river into several distributary channels. Then, fault scarps constrain the flow of water at the distal part of the Delta.

The Delta is a very variable system, at different time scales. Annually, the distribution of the inundated areas varies under the influence of the very contrasted climate, as the flood wave coming from the Angolan upper catchment inundates the Delta's floodplains. Blocked by the fault scarps and submitted to the intensive evapotranspiration (ET), water level in the channels then decreases until next flood. Inter-annually, the spatial distribution of the inundated areas also varies, with some channels receiving more water than others. Major changes in the flood distribution occurred in the past two centuries, with entire systems being dried up, and others flooded back (Wilson, 1973; Shaw, 1984; McCarthy, 2013). Such variations in the spatial distribution of the flood happen at the scale of distributary systems within a decade to centuries (e.g., Ellery et al., 1993). This annual to centennial time scale of flood distribution variations is also called the management time scale here. Obviously, the flood extent and distribution depend on water inputs, and larger inflows usually provide larger floods. But the response of both the whole catchment area and the Delta to water inputs variations is not linear, and more intense rainfall/inflow does not necessarily result in larger floods (Wolski and Murray-Hudson, 2008).

At a longer time scale, of thousands of years, variations of the endorheic regime of the Okavango also occur. Geological evidence shows that variations in tectonic activity, sedimentary input, regional climate have already turned the wetlands of the Delta into a permanent lake (Burrough et al., 2007), a flowing river (Ringrose et al., 2008) or possibly an exclusively seasonal wetland. This millenial to mega-annual time scale of endorheic regime variations is called the geological time scale here.

Identifying the drivers responsible for the variability of the Delta is crucial as the Okavango basin is submitted to a high environmental pressure, while being one of the areas with permanent water in Botswana, Namibia and south Angola. In the meantime, data products from the GRACE satellites revealed the Okavango-Zambezi basin as one of the most important area of variation of continental water and decadal accumulation on Earth (Ramillien

et al., 2008, 2014; Hassan and Jin, 2016). The three countries underlying the catchment area are developing countries, counting on water resources to develop their economic activity (agriculture, industry, tourism). Given the pristine nature of the basin, we are presented with a unique opportunity to implement social-ecological development based on sustainability principles. Being located at the end of the system and mainly depending on the inflow from the upper catchment, the future of the Okavango Delta depends on a careful management of water resources in all three countries. A better understanding of the drivers controlling the spatial extent and distribution of the flood is required to evaluate future water flows and assess impact of land use change due to both economic development (Andersson et al., 2006) and upcoming climate change (Hughes et al., 2011; Wolski et al., 2012).

Among other alluvial fan, the Okavango Delta has the peculiarity to be highly vegetated. It is also of noticeable gentle slope. The flood distribution in the Delta is therefore controlled by four processes strongly interacting with each other : 1) hydrology, as relationships between the atmosphere, the surface and groundwater control the water balance, 2) the fault activity in the graben, controlling the local topography under the influence of regional geodynamics, 3) the sedimentation/erosion processes shaping both small and large scale topography and 4) the functioning of the Delta ecosystem. Each of these processes plays a role in the distribution of the flood, sometimes in several ways, and at different time and space scales. But their respective influences have not yet been all determined, at both management and geological time scale. While previous studies have provided quantitative insight into some aspects of individual drivers, each process is at best poorly quantified and their integrated effects are not well understood. At the system scale, several important questions arise.

What is the role of each process in the non-linear response of the system to climatic variations ? How important is the aquifer in the hydrological system ? How is it responding to climatic variations ? What is the tectonic deformation rate ? Can it influence the distribution of the flood ? How is the current balance between the processes ?

The aim of this study is to bring new quantifications through the interpretation of the deformation of the ground surface observed by the permanent GPS stations. In the poorly monitored basin, permanent GPS stations (AfricaArray/UNAVCO) are recording the displacements of the ground surface since 2010. It is indeed expected that the current deformation of the Earth's surface is impacted in the study area by two of the controlling processes. First, the contrasted climate provides a seasonal hydrological loading, inducing a periodic flexure of the crust. This periodic loading is revealed by the very large amplitude of the gravity field variations observed with the GRACE satellites (Ramillien et al., 2014), which suggest a pluricentimetric annual flexure of the crust. The hydrological contribution to the deformation signal can be used to validate the GRACE data products. This data set can in turn permit the modelling of the deformation of the crust exclusively due to seasonal loading. Subtracting the modelled signal to the observed one in the study area then provides insight into tectonic processes, as in Fu and Freymueller (2012). The significant seismicity and the EARS extension hypothesis imply a crustal deformation significant enough to be monitored, as tectonics presumably stretch the crust in the OG and induces the subsidence in the Delta. Quantifying and qualifying tectonic deformation will bring new insights on the possible in-

fluence of neo-tectonics on the spatial variability of the flood, at the management time scale. Finally, the interpretation of the quantifications provided by the deformation of the surface in terms of controls on the variability of the Okavango Delta at the management and geological time scales requires a contextualisation regarding the numerous feedbacks between the driving processes. It will also bring new insights on the regional geodynamics, in an area where data concerning the current stress regime are scarce. These new insights, as well as the reexamination of the geological evidences available in the graben bring elements of response on the age of tectonic structure, and its implication on the variations of the endorheic regime on the geological time scale.

This study thus begins with a description of the study area and a review of the four controlling processes, hydrology, tectonics, sedimentation and the biotic component of the ecosystem, in order to circumscribe their potential influence on the deformation of the surface, on the variability of the flood distribution at the inter-annual to centennial time scale, and finally their influence on the endorheic regime at the geological time scale. Some of the interactions between the processes are detailed in order to highlight the deep complexity of the feedbacks.

The first issue to reach the scientific goal of the study is **how to discriminate tectonic and hydrological signals in the observed deformation ?** Indeed, only TWS variations can induce an annual periodic flexure of the crust due to variations in continental mass distribution (Tapley et al., 2004). But both inter-annual variations of TWS and tectonics impact the inter-annual trend of the observed deformation, especially on the vertical component. Comparison between the observed and the modelled deformation based on GRACE TWS (e.g., Farrell, 1972; Chanard et al., 2014) allows the validation of the great amplitude of TWS variations revealed by GRACE.

This new proxy on water storage is then used to validate the hydrological model in the catchment area, which finally allows an overview of the hydrological cycle and the relationships between the different hydrological reservoirs of the system. The GPS signals are then examined in more details to provide constraints on the GRACE signals and the hydrological cycle. The horizontal seasonal deformation is used to indicate the region of maximum TWS variation in the broad gravity anomaly provided by GRACE over the Okavango-Zambezi basin. Peculiarities in the GPS time series in the area allow better constrants on the drivers of TWS variations. Finally, the conclusions drawn about the aquifer in the basin are compared with piezometric data available in the Okavango Delta.

The current deformation across the whole graben can be quantified from the horizontal displacement rates provided for the GPS stations straddling the OG. The tectonic displacement rate and orientation are complemented by a review of several recent geophysical studies bringing new elements regarding the structure of the local crust and lithosphere, along with a reexamination of the seismicity in southern Africa. Regarding these new quantified data, the origin of the tectonic activity, so far attributed to the extension of the East African Rift System (Scholz et al., 1976), is called into question, and an alternative proposition for the regional geodynamic model is formulated.

Finally, the quantified inputs brought by this study are interpreted regarding the controls on the variability of the Okavango Delta at the management and geological time scale.

Chapitre 2

Context of the study area

The Okavango Delta consists of regions which are permanently (proximal to the inflow) to seasonally (distal part) inundated and located between the Gumare fault and the Thamalakane and Nhabe rivers, flowing along the Thamalakane fault (Figures 2.1, 2.2 and 2.3). The tectonic structure responsible for the local topographic depression, the Okavango graben, extends from the Sekaka Shear Zone (SSZ) in the southwest to the Chobe fault in the northeast, and from the Gumare fault in the northwest to the Nare fault in the southeast. At a larger scale, the Okavango basin is the hydrological basin, as defined on figure 1.1.

The Okavango graben is, along with the Makgadikgadi pans, the lowest part of the Kalahari basin. The area shows very low relief, thus small variations in the topography can induce major geomorphological and hydrological shifts. The alluvial fan is initiated by just such a very gentle break in slope, as well as constrained in its distal part by subtle topographic scarps locally barely reaching a few meters high. Thus very slight changes in the drivers of the topography (such as fault activity and sedimentation) can potentially induce major changes in the spatial distribution of the annual flood at the inter-annual to centennial time scale, or on the endorheism of the system at the geological time scale.

The Okavango Delta is a complex system comprised of a collection of numerous complex sub-systems, namely the channels, floodplains and islands. Each of these features represents a different balance between the processes controlling the Delta, which main characteristics are detailed in the following sections. The distribution and functioning of these features may vary across and along the fan. Each driving process, hydrology, sedimentation, tectonics and the ecosystem, exerts a particular influence on the flood extent and distribution. The sections following the presentation of the Delta detail these processes, their influence on the flood, as well as the forcings driving them.

FIGURE 2.1 – Satellite view of the study area. Dark grey lines mark the topographic fault scarps and black straight lines the location of the topographic profiles in figure 2.5 (Source : Landsat/Copernicus 2016-2017 from Google Earth).

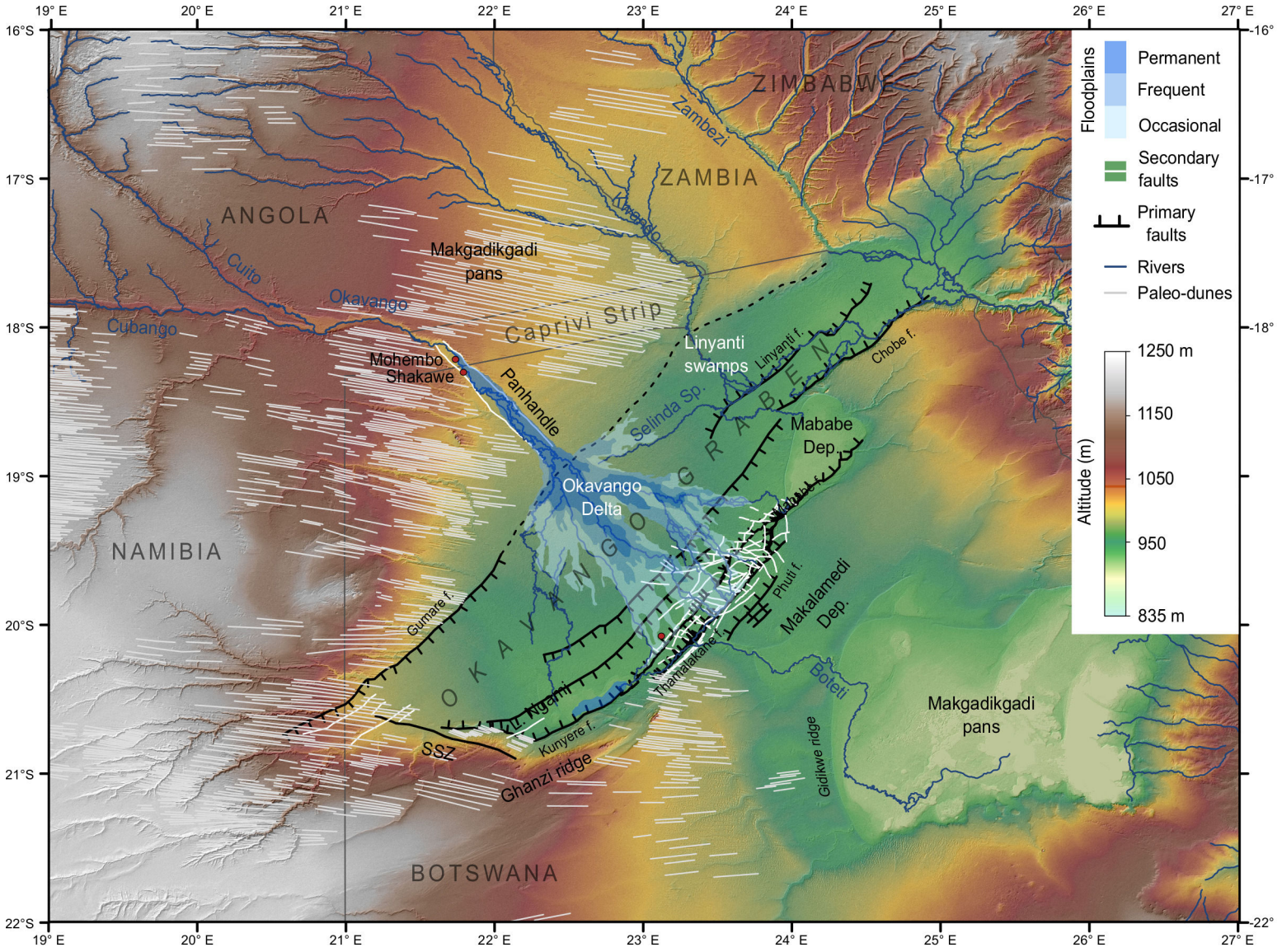

FIGURE 2.2 – Topography of the study area with location of the main faults (modified from Kinabo et al. 2007 and Campbell et al. 2006), rivers and channels, floodplains and dune fields.

FIGURE 2.3 – Satellite view of the Okavango Delta. Note the Selinda Spillway currently relating the Okavango to the Kwando, thus the Zambezi, since the major flood of 2011. Yellow lines delineate the upper, middle and lower Delta as defined by Stanistreet and McCarthy (1993) and detailed in the following section.

2.1 Description of the study area

2.1.1 Overall topography

African topography is remarkable because of its dichotomy (Figure 2.4), with the southern and eastern part of the continent (around 1000 m high) being elevated well above the northwestern sub-continent (about 300 m high), and above most continental interiors globally. This topographic anomaly, called the African Superswell (Nyblade and Robinson, 1994), reaches about 500 m and is not only visible on the continental plateaux, but also extends southwestwards in the ocean. The African superswell is related to the upwelling of hot mantle material from the mantle-core boundary, called the African superplume (Nyblade and Robinson, 1994; Simmons et al., 2007). In the East African Plateau, the influence of the plume is directly related to continental rifting. But the much broader and homogeneous southern African plateau is not directly related to any shallow mantellic anomaly. The deep hot mantle constituting the African plume is considered responsible for the topographic anomaly, which could be due to thermal dilatation of the mantle (e.g., Nyblade and Sleep, 2003) and/or dynamic topography consequent to the gravity anomaly (e.g., Lithgow-Bertelloni and Silver, 1998).

The southern African Plateau shows a central gentle depression, the Kalahari Depression, leading to intra-continental sedimentation and forming the Kalahari basin (Thomas and Shaw, 1990; Haddon et al., 1999). The Okavango Delta lies in the center of the Kalahari Depression, in an area presenting very low relief, with elevation varying from about 970 m on the northern block, to 919 m in the lowest Mababe Depression, within a distance of 160 km. Hence very slight changes in the topography can induce major change in the hydrogeomorphology of the channels.

Local topography is shown in figure 2.2 and in detailed profile in figure 2.5. The latter reveals the three major blocks of the OG, all dipping southeastward, like the Panhandle (Gumbricht and McCarthy, 2001). Beside the Panhandle (grey profile on figure 2.5, see location on figure 2.1), the northern block shows the steepest slope of 0.05%, which is reduced to 0.023% within the Panhandle. The difference in elevation between the two profiles decreases downstream. This difference is mainly due to the sudden incision of the Okavango River just downstream of the lowest knick-point in the river, the Popa Falls, which initiate the Panhandle. At the downstream end of the Panhandle, the Gumare fault does not exhibit any scarp, neither within the Panhandle, nor on the northern block.

The slope increases subtly in the central block southeast of the Gumare fault to reach 0.025%. The break in slope is associated with the meandering river of the Panhandle diverging into several sinuous anastomosing channels. The topographic gradient is remarkably uniform across the fan surface, which exhibits a sub-perfect conical shape (Gumbricht and McCarthy, 2001). This conical shape does not show any regional tilting deviating from the southeastern regional trend.

The southern block is not as regular as the northern and central ones. The regional southeastern tilting is not obvious as it is disturbed by faults and ridges. The most regular area nevertheless shows the lowest SE slope of only 0.18%. The area is mainly impacted by a SE depression : the Makalabedi Depression.

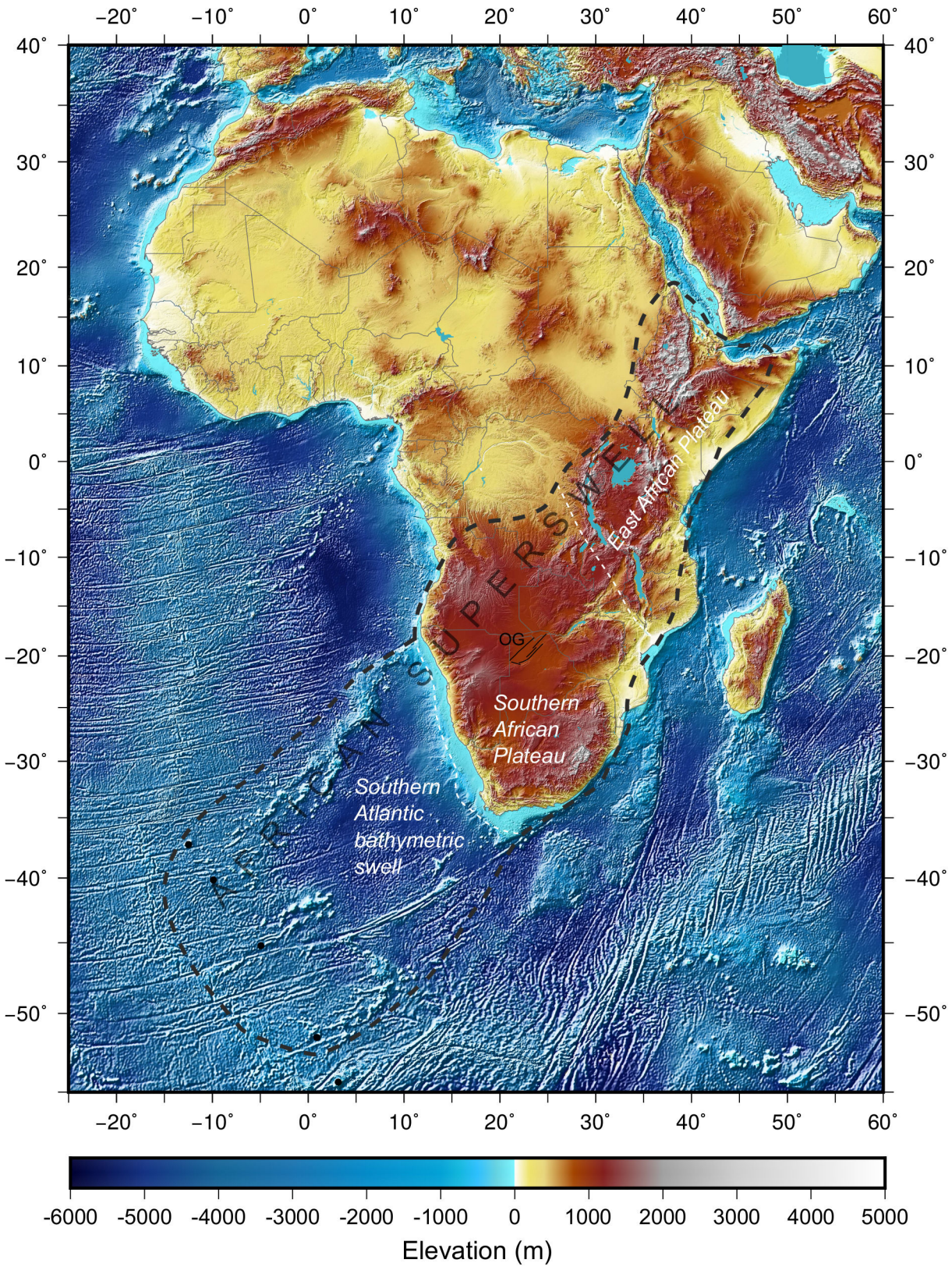
−20° −10° 0° 10° 20° 30° 40° 50° 60°
40° 30° 20° 10° 0° −10° −20° −30° −40° −50°
AFRICAN SUPERSWELL
East African Plateau
OG
Southern African Plateau
Southern Atlantic bathymetric swell
-6000 -5000 -4000 -3000 -2000 -1000 0 1000 2000 3000 4000 5000
Elevation (m)

FIGURE 2.4 – Topographic map of Africa and location of the African Superswell as defined by Nyblade and Robinson (1994), comprised of the East African Plateau, the Southern African Plateau and the Southern Atlantic Bathymetric Swell. The concave Southern African Plateau hosts the Kalahari Depression. OG : Okavango graben.

2.1.2 The Panhandle

Downstream of the border of Botswana, the river immediately turns into a highly sinuous channel actively meandering in the surrounding floodplain, as it enters the 20 km wide flat-bottomed valley called the Panhandle (Figure 2.3 and 2.5 A, B, and C). This 100 km long pre-Delta area crosses the Kalahari desert on the OG northern block. It is bordered by topographic scarps, locally reaching 15 m high. Two plausible and probably complementary processes could be responsible for these scarps. Tectonics could control the orientation of the depression through either a narrow graben (Stanistreet and McCarthy, 1993; Haddon, 2005) or a single fault (Gumbricht and McCarthy, 2001). This is highlighted by the difference of elevation between the higher eastern side of the Panhandle relative to the lower western side (Figure 2.5, Gumbricht and McCarthy, 2001). The difference in topographic gradient between the inner panhandle and the rest of the northern block shows increasing topographic scarps from the apex to the Delta, revealing the second process, the progressive incision of the Okavango river in the northern block. Moreover, some of the edges of the Panhandle are scalloped by erosion from the river, which probably widens the elongated depression.

The main channel anastomoses and forms numerous loops all along the Panhandle (Figure 2.5 B). Floodplain and meandering-related features mark the whole landscape within the topographic scarps. Scroll bars and oxbows are common evidence of the active evolution of the river. While the distance between the topographic scarps increases downstream, the width of the main channel narrows from 90 m in Mohembo to 50 m at the exit of the Panhandle, with a constant average depth (McCarthy, 2013). The loss of water due to infiltration or evapotranspiration is too low to explain this halving of width. Instead, it highlights the increasing accommodation of water flow in the floodplains with widening of the Panhandle. Finally, the Gumare fault not only induces a break in slope, but also releases the river from the confinement of the Panhandle.

2.1.3 The Okavango Delta

The Okavango Delta is an inland delta, which is better described as an alluvial fan (Stanistreet and McCarthy, 1993; Hartley et al., 2010). The geological term delta is not exactly appropriate as the river does not discharge into a standing water body, but the place was named by the first cartographers of the area, possibly Stigand (1923), and the name remained in the common usage. The Delta is the largest subaerial fan on Earth with a mean radius of 150 km. While diverging channels would finally anastomose under the control of the topographic scarps in the Panhandle, they can definitively diverge in the Delta, to form isolated distributary systems.

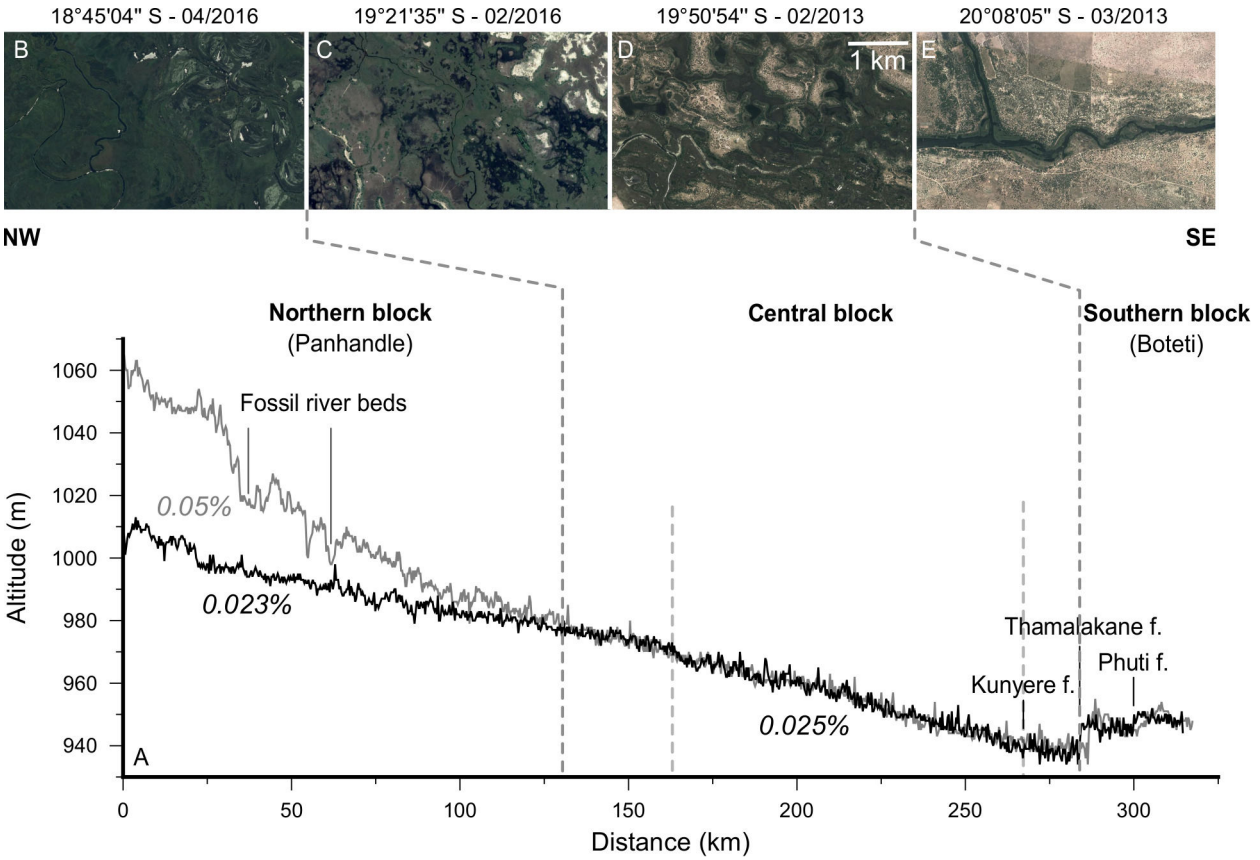

FIGURE 2.5 – A : Topographic profiles across the entire Delta from Mohembo to Maun (black line), and parallel profile SW, crossing the southern block (grey line) (data from SRTM). Different portions of the Delta are defined by topographic gradient (italicized) and morphological differences. Location of the profiles is shown in figure 2.1 Upper pictures show characteristic landscapes in the different parts of the Delta. B : The main channel, floodplain and scroll bars in the Panhandle, C : Middle Delta, D : Lower Delta, E : southern block, with bifurcation of the Thamalakane river into the Nare and Boteti rivers (images from Google Earth).

Unlike most alluvial fans, the Delta is highly vegetated. The landscapes in the Okavango Delta consist of a braided system of channels surrounded by floodplains, more or less permanently covered with vegetation, and punctuated by islands (Figure 2.6). The distribution of the inundated areas varies within each year under the influence of the annual flood, from 3 500-6 000 km^2 in January/February to 6 000-12 000km^2 August/September (Wolski and Murray-Hudson, 2008).

The Delta can be morphologically and hydrologically subdivided into three parts (Figure 2.5, Stanistreet and McCarthy, 1993). The upper Delta is comprised of permanent marshes, flooded all through the year. The middle Delta hosts more islands and some of its floodplains are seasonal, inundated each year with the flood pulse and progressively drying out during the rest of the year. The lower fan exhibits sand tongues, seasonal channels and occasional, only flooded during years of high flood, to seasonal floodplains (Figure 2.2). This morphological

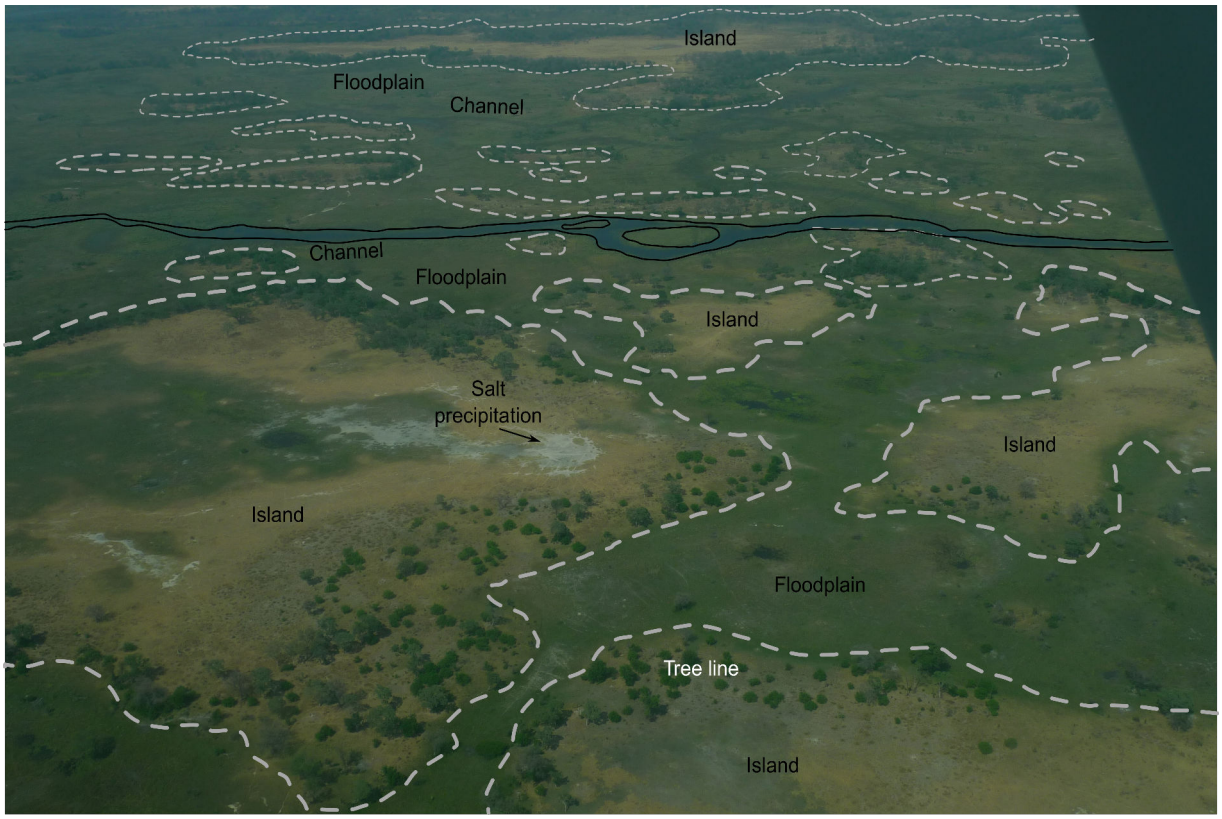

FIGURE 2.6 – Aerial photograph in the Okavango Delta, SE of Chief's Island, October 2014, at the end of the dry season and beginning of flood recession. Most of the floodplains are dry, but are still covered with grass and papyrus. Islands are delineated with dashed gray line. White areas in their centre reveal salt precipitation. Tree line is sometimes incomplete. The island in the foreground on the left is possibly declining as grass grows in the center, revealing seasonal flooding (Personal photo credit).

---

gradient, from permanent wetlands to seasonal floodplains and rivers (see landscapes in figure 2.5 C to E), reveals the loss of water along the almost perfectly linear slope of the Delta due to intense evapotranspiration (Wilson and Dincer, 1976).

The permanent swamps of the upper Delta form a relatively unbounded system of floodplains (Wolski and Murray-Hudson, 2008), in which channels are (semi-)confined by permeable levees made of peat and sand (Ellery et al., 1993; Tooth and McCarthy, 2004). The topographic slope is very gentle and even presents local flats. Several meandering channels diverge from the Okavango River and form the different distributary systems (DS) carrying water across the Delta. The upper Delta is thus a strategic area for water distribution in the whole fan as it is the location of the attribution of water among the distributary systems (Wolski et al., 2006). The flourishing vegetation forms peat aggrading in the floodplains, which accumulates water, and progressively releases it after the flood, with the decline of water level.

In the middle Delta, the slope very slightly increases. Channels are less active and sinuous. The spread of water produces seasonal floodplains and allows the occurrence of occasional

floodplains on the edges of the fan. The increasing density of islands forms chains of islands which cause the differentiation into more isolated distributary systems (Wolski and Murray-Hudson, 2008). In the central area, Chief's island virtually cuts the Delta in two parts. This island is the largest land mass in the Delta. Its surface is marked with paleo-channels and paleo-floodplains, revealing previous inundations, but these features seem less well preserved than those in recently dry areas, such as the Thaoge system. The middle Delta being less permanently inundated, peat accumulated in the floodplains is more subject to fires and is consequently less preserved.

The lower fan exclusively hosts seasonal to occasional floodplains, surrounding extensive drylands, between the south of Chief's Island and the Thamalakane river. Some perennial rivers currently flow all through the year (Thamalakane, Boro), but most of the rivers indicated on figure 2.3 are seasonal and only flow with the arrival of the flood (Shashe, Nxotega, Boteti rivers). In this part of the Delta, channels are not confined by vegetation and water spreads laterally more easily. The lower fan presents not only more islands, but mainly more sand tongues, forming major interfluve areas. It is the domain of the outlets, small, sometimes seasonal rivers and intermittent water bodies. As the end of the system, the lower fan is a primary area for the manifestation of the inter-annual variability of the inundation.

Distributary systems

Distributary systems are networks of anastomosing channels, connected to lagoons and floodplains. In the upper Delta, DS are more or less connected by water flow through the floodplains, and their boundaries are hard to delineate. Distributary systems evolve through time due to variations in water inputs, local topography and vegetation growth. Some of these channels are directly connected to the main channel (Thaoge, Nqoga, see figure 2.3), but some channels arise from the floodplains saturated with water and show no direct hydraulic connection to the Okavango River (Jao/Boro, Xudum, Selinda spillway). Most distributary systems acquire their flow from systems of collector lagoons which serve to concentrate broad floodplain flows into flows which have high enough velocity to build channels (Porter and Muzila, 1989).

The first distributary to diverge southwards from the main channel, at the southern extent of the Panhandle, is the Thaoge system, directly related to the Okavango river. In the 1850's, the Thaoge was an important channel, which used to directly feed Lake Ngami (Stigand, 1923; Shaw, 1984) from the main channel. In the late 1880's, the channel was repeatedly blocked by Papyrus growth. Attempts of dredging have been made several times without any success (Wilson, 1973). The downstream channels and floodplains are now dry but remnants of former islands and channels still impact the morphology of the landscape and the distribution of the vegetation.

The Nqoga system is actually the residual water (base flow) directly flowing from the main channel after spillage in the floodplains. It flows eastwards and divides north of Chief's Island into two DS, the Mboroga system, flowing south and feeding the Santantandibe and Gomoti rivers, and the Maunachira system then turning into the Khwai system. This distributary has been failing since the early 1920's (McCarthy and Ellery, 1995a)

The Boro system arises from the floodplains and the flats of the upper Delta, as no channel connects it directly to the the Okavango river. The perennial anastomosing, variable width

channel crosses the Delta to reach the distal Thamalakane river. The Boro currently carries the main inflow of the Thamalakane river.

The Xudum also arises from the floodplains, but no distinct channel is clearly perennial and primary for water flow. It is mainly comprised of extensive floodplains with short portions of channels fading into floodplains or feeding closed lagoons.

Finally, the Selinda spillway is an intermittent system. Currently flooded, it can stay dry for decades. This channel, when flooded, hydrologically connects the system to the Kwando, further flowing into the Zambezi. No actual flow occurs between the two systems, as the connection lies in a topographic low between the Linyanti swamps and the Okavango Delta. This hydrological link allows biotic connectivity responsible for the low endemicity observed in the Delta (Ramberg et al., 2006).

Outlets

The swamps of the Okavango Delta drain into several outlets, finally gathering to reach one of the three termini of the system : Lake Ngami in the south, currently fed by the Kunyere river, the Mababe Depression in the north east, currently fed by the Mababe river, albeit with low volumes, and the Makgadikgadi pans in the southeast (Figures 2.1 and 2.2).

At the SE end of the Delta, the Thamalakane fault drives the flow of the eponym river, gathering the outflow of the Mboroga and Boro systems. Although close to the relatively deep Mababe Depression and initiated on the eastern side of the conical fan, the Thamalakane river flows southwestwards. It is noticeable that the river does not cross the fault scarp at its lowest point, but further SW. It is also noticeable that the river divides into the Nhabe river, flowing towards Lake Ngami, and the Boteti river.

The amount of water going out of the Delta through the Boteti is estimated as approximately 2% of the inflow (Wilson and Dincer, 1976). It carries water to the **Makgadikgadi pans** when inflows are large enough. These temporary lakes represent the sump of the Kalahari desert, regional terminus of groundwater flow, where the intense evaporation accumulates salt. Their depression is fault-controlled (Haddon, 2005) and is the lowest area of the Kalahari depression.

The southwestern terminus of the system, **Lake Ngami**, has been more frequently dry than wet over the last 150 years (Shaw, 1984, 1985a). Its current flooding began in 2004, when the Kunyere river further received water from the Delta. But it was properly flooded, as a lake, only thanks to the 2011 major flood. The lake reached a maximum extent in 2012 and has been regressing since then. Its bed is the second lowest area of the OG, with a minimum altitude of 919 m (Shaw et al., 2003). The lake is currently primarily fed by the Kunyere river, joined by the Nhabe river. These two outlets are not directly related to the Okavango River but to channels arising from the floodplains. The current sedimentary input in the Lake is thus drastically lower than the bed load transported by the Thaoge system to the lake directly from the river before the XIXth century blockage. Paleo-shorelines are visible in the topography on the western side of the Lake and testify to former higher water levels in the Lake (Shaw et al., 2003; Burrough et al., 2007).

In the north east, the opposite terminus is the heart-shaped **Mababe Depression**, the bed of which reaches the lowest altitude in the OG (917 m according to the SRTM3). The Depression has not been properly flooded for the last two centuries (Shaw, 1984) but still

receives enough water to assure limited expanses of occasional to seasonal swamps, through the Mababe river in the east, and the Savuti channel in the north.

All three termini show major paleo-shorelines, indicating past wetter periods in the last millenia, when the graben hosted a megalake possibly joining the Mababe Depression, Lake Ngami, and the Makgadikgadi pans (Shaw, 1985a,b; Gumbricht and McCarthy, 2001; Burrough et al., 2007; Burrough and Thomas, 2008; Burrough et al., 2009). The datings gathered so far show that Lake Ngami has been much more regularly flooded than the two other termini at both management and geological time scale.

2.1.4 Morphological features in the Delta

Channels

Channels in the Delta have been extensively studied (e.g., McCarthy et al., 1991; Ellery et al., 1993; McCarthy and Ellery, 1995a; Tooth and McCarthy, 2004), and a detailed review is not the aim of this study. But their evolution through the floods is critical for the variation of the distribution of the flood. In order to comprehend the factors controlling this distribution, an overview of the channels particular characteristics is necessary. Channels carry the main part of fluviatile sediments and they concentrate rapid flow. In the upper and middle Delta, channels are flanked by permeable levees. They result in markedly elevated channel systems towards the distal ends of distributary channels. They also result in elevated surface water in the channels relative to the surrounding floodplains (McCarthy et al., 1991).

The evolution of channels depends on the ratio between the velocity of its flow and the vegetation growing from the banks (Ellery et al., 1995). They form relatively stable features on the long wavelength (tens of km), but portions of channels can suddenly shift. Channel avulsion (McCarthy et al., 1992; Ellery et al., 1993) is the main cause of such shifts, and may occur in a few years or over more than a century, as the current failure of the Nqoga channel (McCarthy and Ellery, 1995a). Avulsion can produce important variations of water attribution if occurring in a strategic area, such as the upper Delta. Channel avulsion can be conceptually summarized as in figure 2.7.

Stage I shows a mature depositional channel flowing on a topographic high formed by peat aggrading levees. Lateral water flow in the floodplain initiates preferred pathways, possibly helped by hippopotamus (McCarthy et al., 1998) or elephant paths. The juvenile neighbour channel erodes its bed in the Kalahari sands, remobilising sediments further downstream. Stage II shows the initiation of vegetation blockage further slowing down the water flow and encouraging sedimentation on the bed of the channel, while water flow velocity is increasing in the erosional neighbour. In stage III, the second channel captures water flow from the old failing channel in its final stage of deposition. With direct water flow comes the sedimentary load and the second channel now aggrades and forms its permeable levees. The incipient third channel drains water flow from the surrounding floodplains. Stage IV illustrates the null balance of organic aggradation in the Delta in the long term, due to the almost systematic occurrence of peat fires. The topography formed by the former peat levees is removed and only remains the sediments accumulated in the bed of the channel, leading to topographic inversion recording fossil channel beds in the landscape. Seismic events, inducing topographc

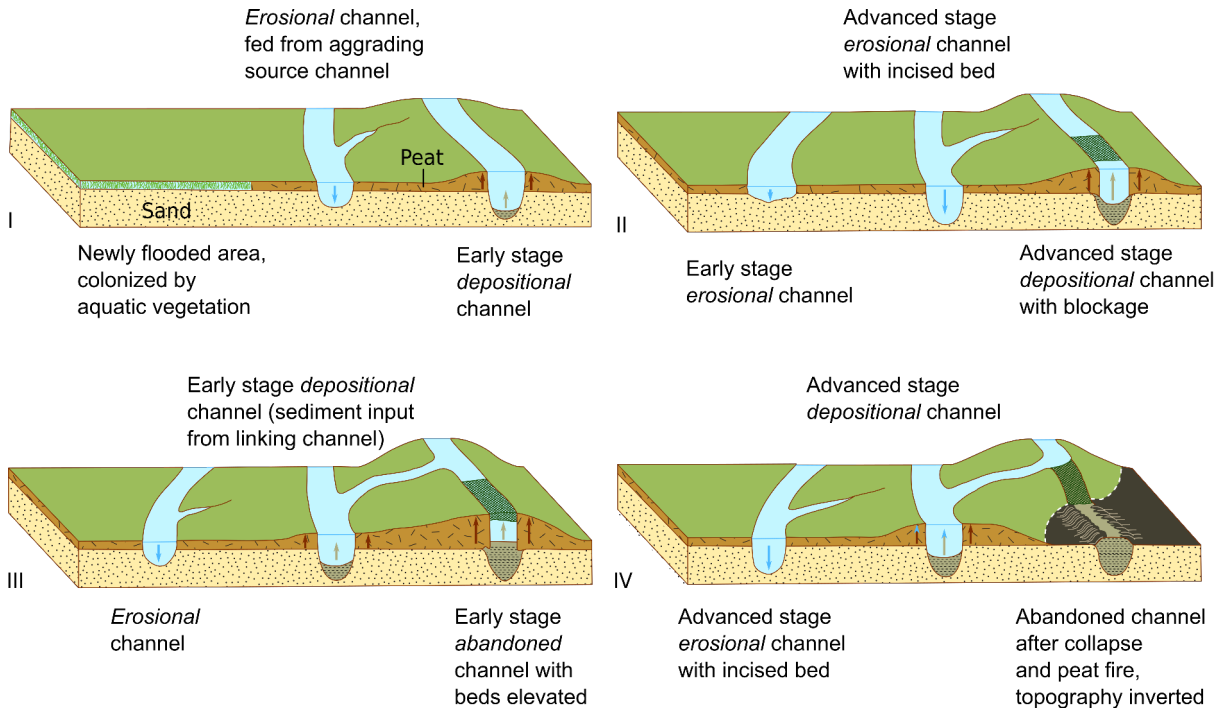

FIGURE 2.7 – Conceptual model of channel dynamics (redrawn from Ellery et al. (1993)) reflecting strong interactions between water flow, sedimentation/erosion and vegetation. See description in text.

---

offsets in the order of centimetres have been proposed to encourage some channel avulsions (Pike, 1970; McCarthy et al., 1993).

Floodplains

Surrounding channels or covering the whole surface, floodplains are extensive flat areas permanently or seasonally flooded. They are covered with mainly emergent aquatic vegetation such as sedges and grasses, but where deep water persists, floating-leaved and submerged vegetation also occurs. Floodplains in the Delta can be permanent, as in the Upper Delta, seasonal, i.e. dry during winter and spring, but filled every year during the flood, when the increasing water level in the channels outreaches the banks. Floodplains can finally be occasional, and be filled only some years, during major floods (see distribution on figure 2.2). While flow velocity is the highest in the channels, the floodplains are actually the loci of the greatest flow volume (McCarthy, 2013). Water flows through the vegetated water column, between and around the stems of the emergent plants, slower than in channels but over the entire area. As roots trap sediments along the edges of channels, almost no clastic sediment is transported through the floodplains. Floodplains play a great role in the ecosystem as they are critical dry season resources for terrestrial herbivores (Fynn et al., 2015).

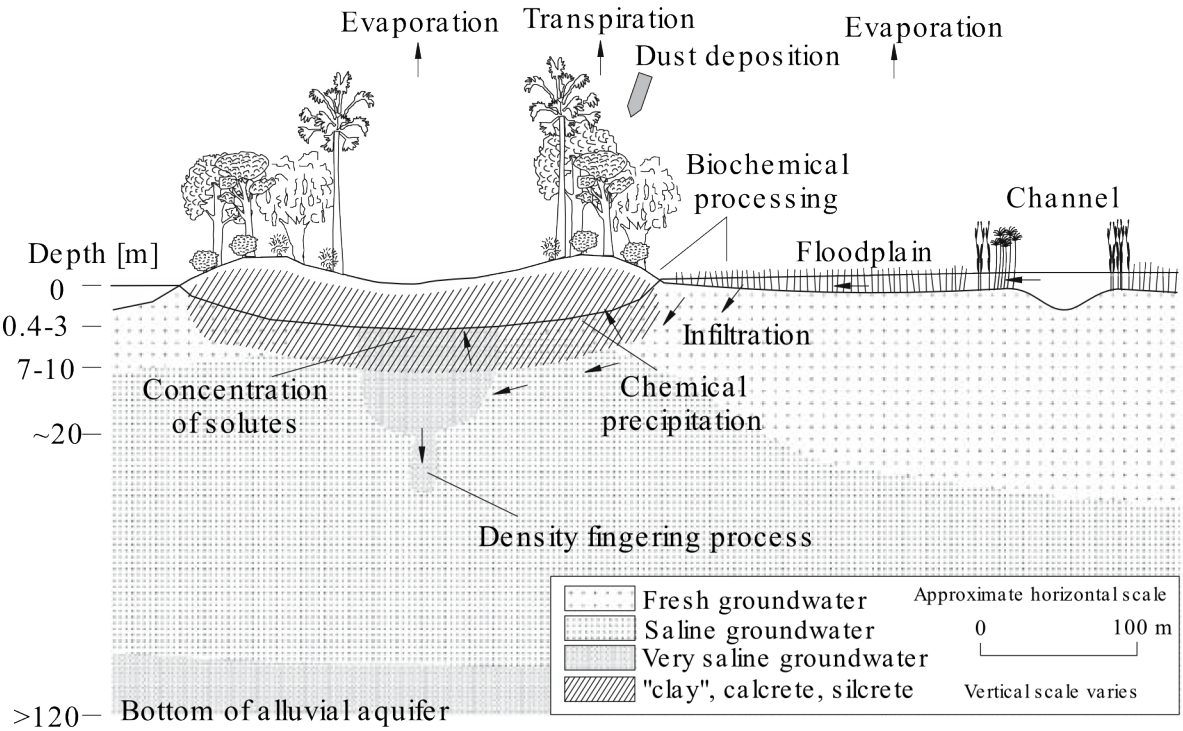

FIGURE 2.8 – Groundwater circulation beneath islands, driven from the floodplain by evapotranspiration. Chemical precipitation beneath the fringes of islands coupled with evaporation in the center concentrates the remnant water in solutes and induces a vertical density-driven current charging the deep saline aquifer (Ramberg and Wolski, 2008).

Islands

Islands are numerous in the Delta and play a crucial role in the freshness of water (McCarthy and Ellery, 1994). They are distributed along an increasing gradient from the Panhandle, hosting very few islands, to the lower Delta, inversely correlated to the amount of water (Gumbricht and McCarthy, 2003). They show a great variety in both size, from a few m^2 to several km^2, and shape, rounded, elongated, crescented, etc. Islands are entirely or partially outlined by a tree line forming a local topographic high (Figure 2.6 and 2.8). Towards the center of the island, elevation decreases and vegetation turns from trees to shrubs and grasses. The center of islands consists of barren soil whitened by efflorescence of carbonates of calcium, magnesium and sodium (McCarthy and Metcalfe, 1990; Ramberg and Wolski, 2008).

Islands most probably represent the strongest feedbacks between water flow, sedimentation and the ecosystem in the Delta (McCarthy et al., 1993; Wolski et al., 2005; Ramberg and Wolski, 2008; McCarthy et al., 2012). The large trees bordering the islands, coupled with clayey centre soils, induce a high evapotranspiration which deflates the water table and creates a centripetal groundwater flow (McCarthy et al., 1991; Bauer et al., 2004). This hydrological cycling is responsible for the increasing concentration of solutes, leading to the chemical precipitation of magnesian calcite and silica beneath the edges of islands (McCar-

thy et al., 1993) and progressive concentration of conservative solutes like sodium in island centre groundwater. Vegetation is thought to play an important role in the transport of the carbone necessary to the formation of carbonates at depth (McCarthy and Ellery, 1994). The remaining groundwater migrating towards the center of the islands is saturated in salt, which prevents growth of large trees and progressively leads to disappearance of vegetation. Capillary-driven evaporation in the centre of islands finally amplifies the increase of salt concentration in the remaining water and maintains a density-driven episodic flow of the salty shallow groundwater to the deep salty aquifer (Bauer et al., 2006; Bauer-Gottwein et al., 2007). The islands thus function as saline pumps recharging the deep aquifer and by doing so act as sinks for inorganic solutes coming from the catchment area (Gieske, 1996), as well as nutrients (Wolski et al., 2005), and are thus responsible, through these numerous feedbacks, for the freshness of the water in the Delta (Ramberg and Wolski, 2008).

Islands are initiated during periods of minor floods by the growth of vegetation on topographic highs, either formed by termite mounds (Dangerfield et al., 1998; McCarthy et al., 2012) or sedimentological features resulting from previous floods, such as scroll-bars or inverted channels (McCarthy and Ellery, 1998). In drier periods when the annual flood is sufficiently low, vegetation colonizes the relief and shrubs and trees can develop. The subsurface growth of grains of calcite, under the influence of tree transpiration, causes the upward expansion of the substrate and is partly responsible for lateral growth of islands (Gumbricht and McCarthy, 2003). Calcite and amorphous silica precipitation is estimated to account for 30 to 40% of the volume of islands (McCarthy et al., 2012). Another significant process for island growth is the trapping of airborne dust by the trees (Krah et al., 2004; Humphries et al., 2014). Strong winds pick up silt and clay from the floodplain and deposit them in the tree line as the velocity of the wind declines. After initiation, termites further contribute to island growth by collecting silts and clays for the construction of their mounds (McCarthy et al., 1998). Finally, islands can disappear due to erosion or drying up of their DS.

Islands are most probably long-term aggradation features. Based on modelling, Bauer-Gottwein et al. (2007) estimate the time for the onset of density-driven flow to between 100 and 1000 yr. Based on assessment of the amount of carbonates beneath two small islands ($\sim$200 m and $\sim$1 km long) and calcite accumulation rate, McCarthy et al. (2012) estimated the ages of the islands between 15 000 and 150 000 yr, depending on evapotranspiration rate. Finally, Ramberg and Wolski (2008) estimated the age of well-developed islands based on calcite mass balance between 100 000 and 400 000 yr. While these estimations are crude, they still provide an order of magnitude of the age of islands, from thousands to possibly hundreds of thousands of years.

2.2 Hydrological system

Climatic variations are a main forcing on the Okavango Delta, but the basin, as well as the wetlands, do not respond instantaneously to variation in water inputs. The hydrological system, i.e. the relationships between the different reservoirs (infiltration, evapotranspiration, runoff), exerts a moderating influence on the rainfall variability (e.g., Hughes et al., 2006; Wolski and Murray-Hudson, 2008).

2.2.1 Regional climate

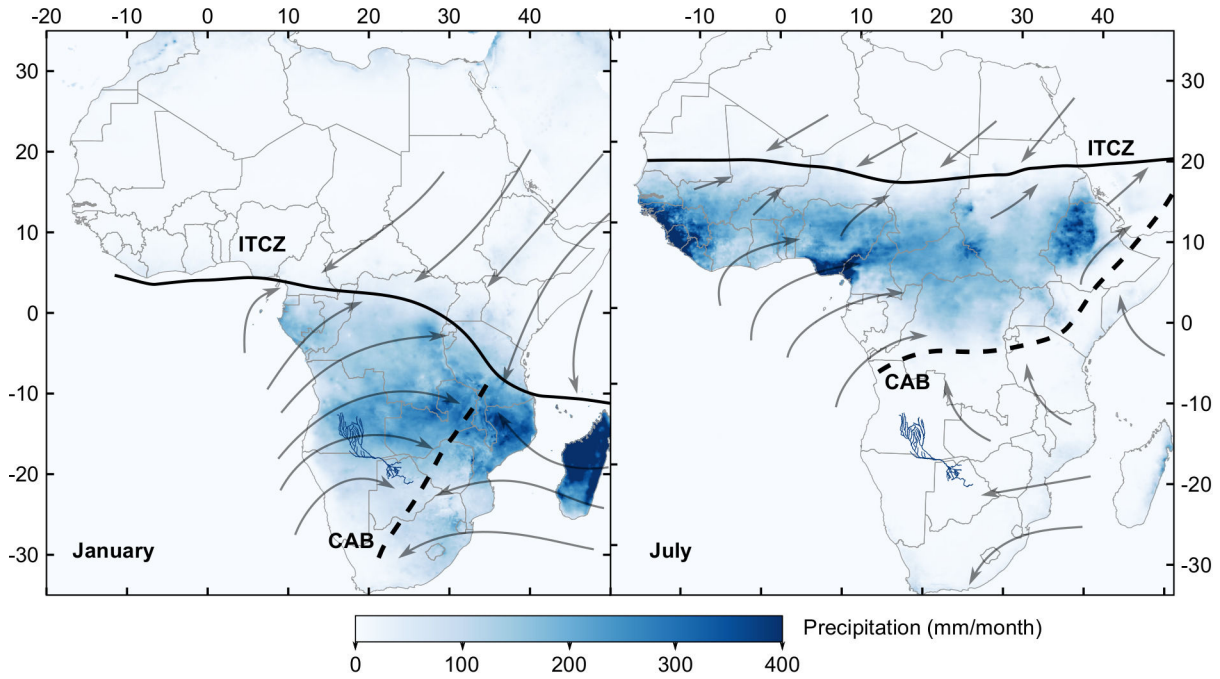

FIGURE 2.9 – Migration of the Inter-Tropical Convergence Zone (ITCZ) and Congo Air Boundary (CAB) between the austral summer (January, rainy season in study area) and the austral winter (July, dry season). Precipitation data show the mean monthly rainfall over 2001-2010 from CHIRPS. Location of ITCZ and CAB is interpreted on the distibution of precipitation and based on Nicholson (2000), as well as the general patterns of winds (grey arrows).

Precipitation in Africa is controlled by two main atmospheric boundaries : the Inter-Tropical Convergence Zone (ITCZ) and the Congo Air boundary (CAB), visible in figure 2.9. The ITCZ is formed by the convergence of the northern and southern hemisphere anticyclonic circulations driving hot air masses filled with water vapor, and thus carrying massive rainfall. The CAB is the limit between the easterlies coming from the Indian Ocean, and the westerlies, originating from the circum-polar circulation (e.g., Nicholson, 2000; Schefusz et al., 2011). The ITCZ migrates from one hemisphere to another along with the Earth's tilt during its revolution.

The Okavango basin is located in the Southern African Summer Rainfall Zone (Tyson et al., 2002). During the southern winter, an atmospheric continental high-pressure cell brings stable cold dry conditions over the southern part of the continent, preventing the arrival of hot and humid air masses (Figure 2.9). In the austral summer, the ITCZ migrates southwards and brings tropical low pressures of wet air into the dry basin. The CAB migrates southeastwards and limits the propagation of the westerlies. These migrations are different over the years, in both spatial and temporal distribution, providing variations of water inputs in the basin. Inter-annual variations are related to variations in the Sea Surface Temperature of the Indian Ocean, i.e. El Niño (e.g., Nicholson and Kim, 1997; Dieppois et al., 2015).

This climatic regime results in a strongly seasonal climate. The austral summer is characterised by a rainy season from October to April, while the austral winter is defined by a dry season, without any significant rainfall in the study area. Consequently, the hydrological year is defined in the basin by the intergovernmental Permanent Okavango River Basin Water Commission (OKACOM) from 1^{st} October to the following 30^{th} September (OKACOM, 2010). The yearly migration of the ITCZ also results in a strong regional gradient in rainfall distribution, with the Angolan headwaters receiving 800-1200 mm/yr, while the distal Delta receives on average 450 mm/yr.

Within the Okavango Delta, the spatial distribution of precipitation can also be very heterogeneous as rainfall mainly occurs during convective episodic storms that can be contained within a few km^2. This heterogeneity is problematic for the assessment of rainfall from spatially discrete rain-gauged stations. As centimeters of rain can fall within a few hours, satellite based data can also be biased by their temporal resolution. Moreover, rainfall estimates based on cloud-top temperatures are notoriously inaccurate, and tend to overestimate quantities. These issues are discussed in chapter 4.

While rainfall is nevertheless somewhat constrained, the process responsible for water loss in the basin, actual evapotranspiration, is poorly constrained. In the Delta, attempts of estimation were done in the field and vary from 2.3 to 5 mm/day (Pike, 1970 in Wilson and Dincer, 1976) to 0.06 to 4.3 mm/day, based on the diurnal groundwater level fluctuations due to tree activity in island (Bauer et al., 2004) and from 0.01 to 11.15 mm/day in the dry woodlands southeast of the Thamalakane fault during the ephemeral Fluxnet tower site (Oak Ridge National Laboratory Distributed Active Archive Center, 2015). Estimations of ET are also provided by at least two remote sensing data sets : Global Land Evaporation Amsterdam Model (GLEAM, Martens et al., 2017) and MODerate resolution Imaging Spectroradiometer (MODIS, MOD16, Mu et al., 2011).

The wide range of variation is not only due to the strong seasonality or to difficulty of the estimation and the contrasted climate. The Okavango Delta also exhibits a great variety of different landscapes differently impacting ET, from open water to the intensively transpiring floodplains, islands fringes or passive barren soil. This variety of landscapes is mainly responsible for the wide range of proposed values. ET obviously also varies very regularly with seasons, with higher rates when water is more easily available, ambient temperatures higher, and day length longer increasing photosynthesis, a major driver of ET. But estimations differ on the phase of ET variations, with the peak occurring either at the beginning or the end of the rainy season, and a minimum situated between june (Pike, 1970) and October (MODIS). As 96% of the incoming water is thought to finally leave the Delta by evapotranspiration (Wilson and Dincer, 1976), a more reliable and accurate estimation is necessary to assess a proper water balance.

2.2.2 Basin physiography and water cycle

The Okavango River arises from the Angolan highlands through two tributaries, the eastern Cuito and the western Cubango, joining at the Namibian border, between Rundu and Andara (Figure 2.10). The catchment area, as presently defined, extends over $\sim$225,000 km^2.

The definition of its boundaries varies amongst studies, as different parts are either seasonal, occasional, episodic or even fossil. The boundaries used in this study are based on the topographic catchment area, thus including fossil rivers upstream of Mohembo, but are limited downstream by the junction of the Delta, the Mababe Depression and Lake Ngami, thus excluding the Makgadikgadi pans.

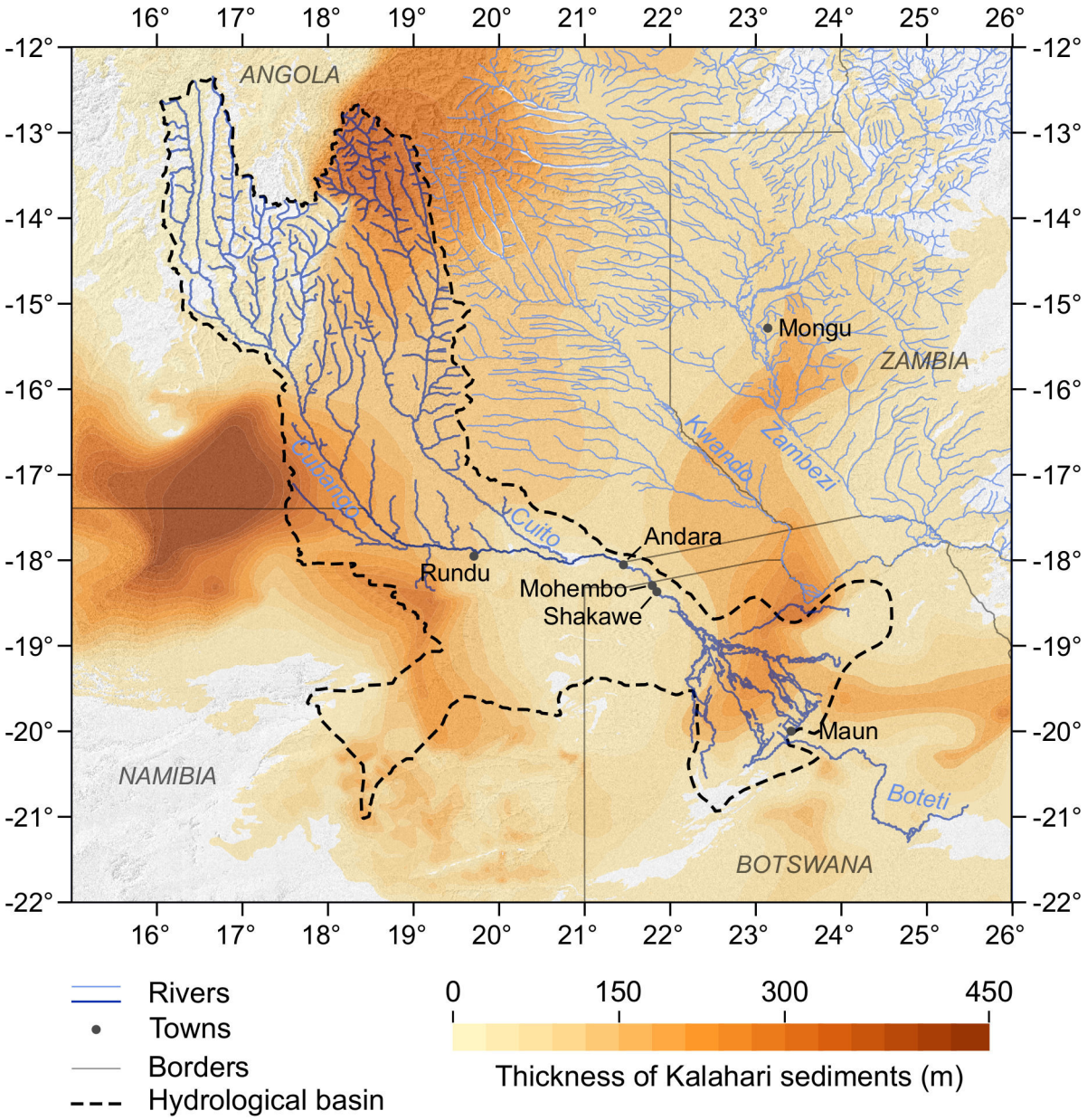

FIGURE 2.10 – Map of the hydrological basin showing thickness of Kalahari beds modified from Haddon et al. (1999) and CGMW-BRGM (2016), boundaries of the catchment area used in this study and main tributaries for the Okavango (dark blue) and the Kwando and Zambezi (light blue).

During the rainy season, runoff mainly generates streamflow in the headwater tributaries

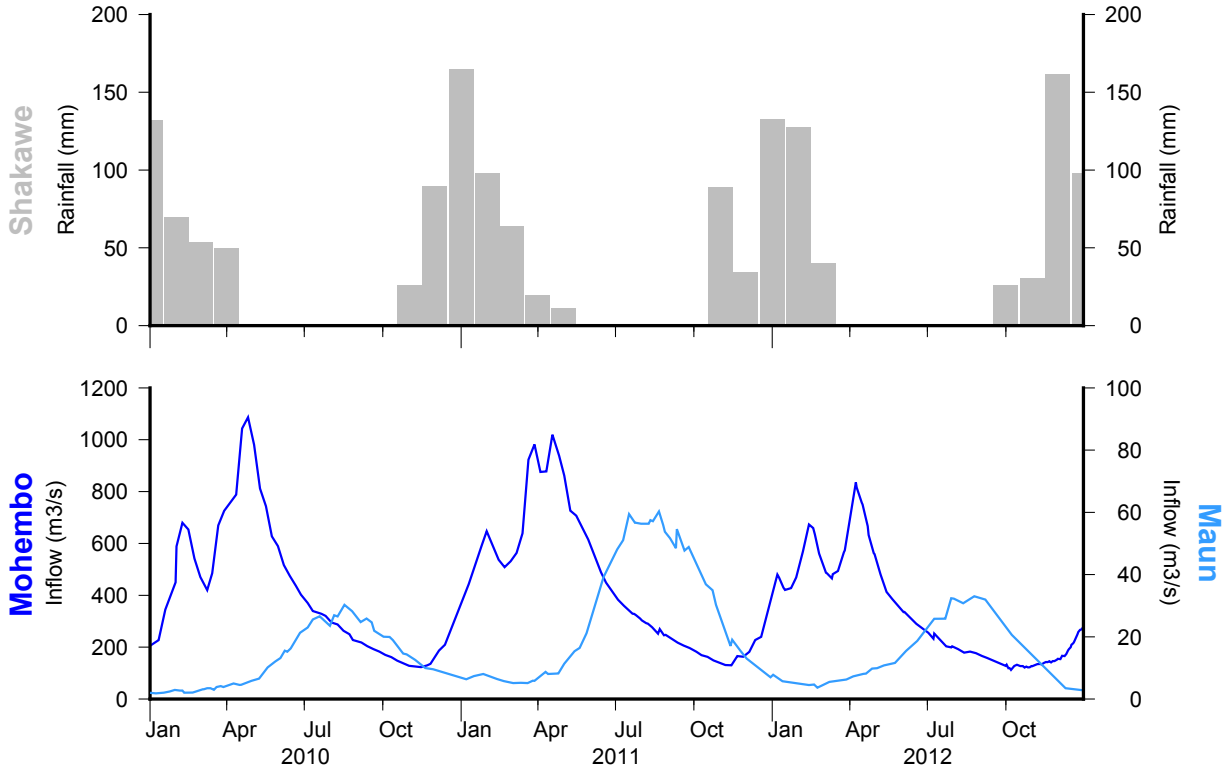

FIGURE 2.11 – Bottom plot shows the discharge at the apex of the Panhandle (Mohembo, data from Department of Water Affairs) and at the distal part of the fan (Thamalakane river, at Maun, data from Mike and Frances Murray-Hudson) and top histogram shows precipitation in Shakawe (see locations on figure 2.10, data from SASSCAL WeatherNet). The temporal offset between the peak of local rainfall and water level is due to the propagation of the flood from the Angolan headwaters to the Okavango Delta. Note the change of scales for discharge in the two stations. All data can be found at `www.okavangodata.ub.bw/ori`.

---

where rainfall is more abundant (Figure 2.9 and Wilk et al. 2006). The slope of the river bed provides a progressively lower topographic gradient downstream, which leads to the accumulation of runoff in the catchment area (Wilson and Dincer, 1976; Hughes et al., 2006). The resulting water body then forms a flood pulse, flowing slowly along the ∼600 km separating the Angolan headwaters from the Okavango Delta. The travel time results in a relatively sudden increase of the discharge observed at Mohembo approximately three months after the peak of rainfall (Figure 2.11). This flood wave then takes three more months to propagate through the distributary systems of the Delta to reach its distal part, at a distance of 250 km and a velocity of ∼5 cm/s (Wilson and Dincer, 1976). During the propagation of the annual flood pulse accross the Delta, water from the channels spills the banks, flowing into the surrounding floodplains. Spread in the floodplains and finally blocked by fault scarps, the surface water is then intensely evapotranspired and the water level progressively declines until falling below the root zone in the soil profile.

The flood pulse coming from the Angolan highlands usually is the only contribution to the rise of water level in the Delta, seldom influenced by local rainfall. The water level in the

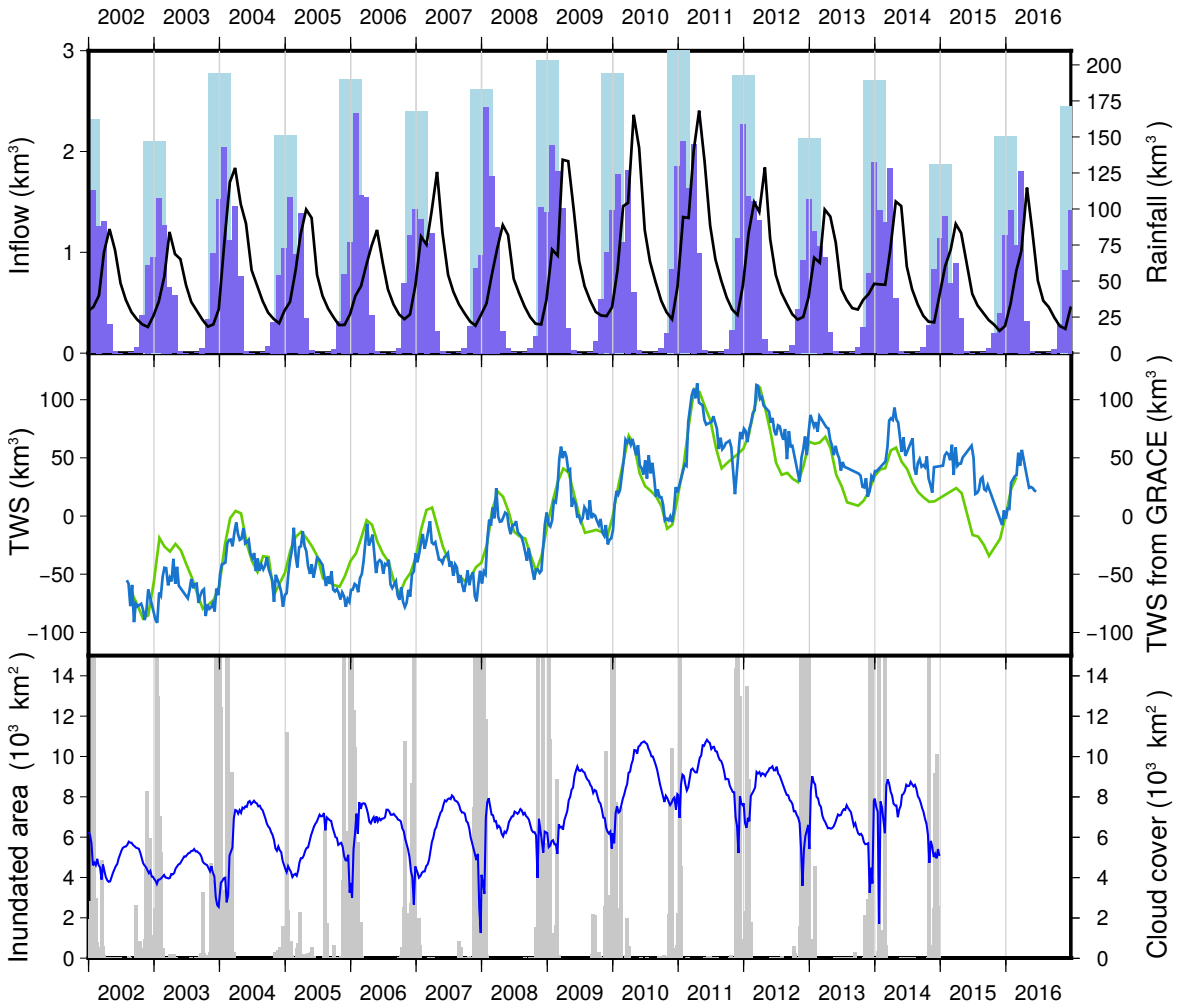

FIGURE 2.12 – Variation of hydrological fluxes in the Okavango basin and Delta. From top to bottom : monthly (dark blue) and annual (light blue) rainfall integrated over the catchment area and the Okavango Delta (CHIRPS), monthly discharge measured at Mohembo (black line, DWA), ΔStorage interpreted from GRACE data (green lne for CSR solution, blue line for GRGS solution) integrated over the catchment area and the Delta, extent of inundated areas (dark blue line Wolski et al., 2017) with grey bars showing cloud cover on the image.

Delta (Figure 2.11) and the extent of inundated areas (Figure 2.12) start decreasing as soon as the flood pulse has flowed downstream. This decrease slows down or is even stopped during the rainy season, but is rarely reversed before the end of heavy rainfall. Rainfall on the Delta itself, while it constitutes more than a third of total water inputs in terms of volume (Wilson and Dincer, 1976 and Table 2.1), influences water level only in years of exceptionally high total precipitation, and large antecedent flood extent. It can prolong outflows under both these circumstances, too. In most years however, local rainfall effects are rapidly ameliorated by the high ET that occurs during the hot summer months (Wilson and Dincer, 1976). Hence, the water level in the Delta is under strong influence of climatic factors in Angola (Wilson and Dincer, 1976; Mazvimavi and Wolski, 2006; McCarthy, 2013).

The extent and evolution of the aquifer remained unknown in the catchment area until very recently, as no piezometric monitoring has ever been implemented in Angola. The presence of an important aquifer was already suspected due to the nature and thickness of the superficial sediments (Wilson and Dincer, 1976; Gieske, 1997; Hughes et al., 2006). In the last 15 years, the GRACE satellites recorded the variations of the Earth's gravity field and proposed the Okavango-Zambezi basin as one of the major areas of annual variation of Terrestrial Water Storage (TWS) on Earth (Ramillien et al., 2008; Hassan and Jin, 2016). Moreover, the Okavango-Zambezi basin is one of the rare areas to show an increase in TWS since 2002. Groundwater may hence stand for the most important, while least observed, reservoir in the whole hydrological system (see details in chapter 4).

In the Delta, piezometers have been installed as early as 1975 (Gieske, 1997). Boreholes from the Department of Water Affairs (DWA) allowed a first order mapping of the aquifer (McCarthy et al., 1998). It has been revealed to correspond to the precise extent of the wetlands, with a water table varying from the surface to a maximum of about 10 m deep, while its depth drastically falls to over 40 m deep within a few kilometers from the alluvial fan. No lateral flow away from the fan margins in the groundwater has been determined at the regional scale, and vertical movements prevail in the relationship between surface, groundwater and the atmosphere. More detailed studies have been realised around the city of Maun to provide fresh water to the increasing population (e.g., Campbell et al., 2006), but mainly to determine the volume of the potential fresh aquifer. The lack of information on this reservoir at the scale of the Delta is an obstacle to properly assess water balance for the hydrological system.

Groundwater in the Delta is distributed between the unsaturated zone, the shallow aquifer and the deep aquifer. All three are hosted in the hundreds of meters of unconsolidated sands of the Kalahari beds, in which former channel systems have formed lenses of clay locally forming aquicludes. The shallow aquifer is filled with fresh water and is recharged almost entirely by runoff infiltration during flood propagation (Gieske, 1997; Wolski et al., 2006). Its depletion is due to the intense evapotranspiration, occurring not only from open water, but mostly through transpiration from the vegetation. The deep aquifer contains saline water, as illustrated in figure 2.8, and is fed by the saline pumps constituted by islands.

Inputs	Inflow	8.780	58%
	Rainfall	6.260	42%
Outputs	Evapotranspiration	14.910	98%
	Outflow	0.26	2%

TABLE 2.1 – Mean annual water balance (Mm^3/yr) in the Okavango Delta according to Wolski et al. (2006), over January 1969–December 2002.

Water balance in the Okavango basin is an intransigent problem. Precipitation has not been monitored in the Angolan catchment since the Angolan war (1970's) and extrapolated or satellite based data sets exhibit significant differences. Problems regarding the choice of data sets are discussed in chapter 4. Moreover, ET is not well constrained by data while it represents the quasi-totality of water outputs. If the Delta's inundated areas are less remote

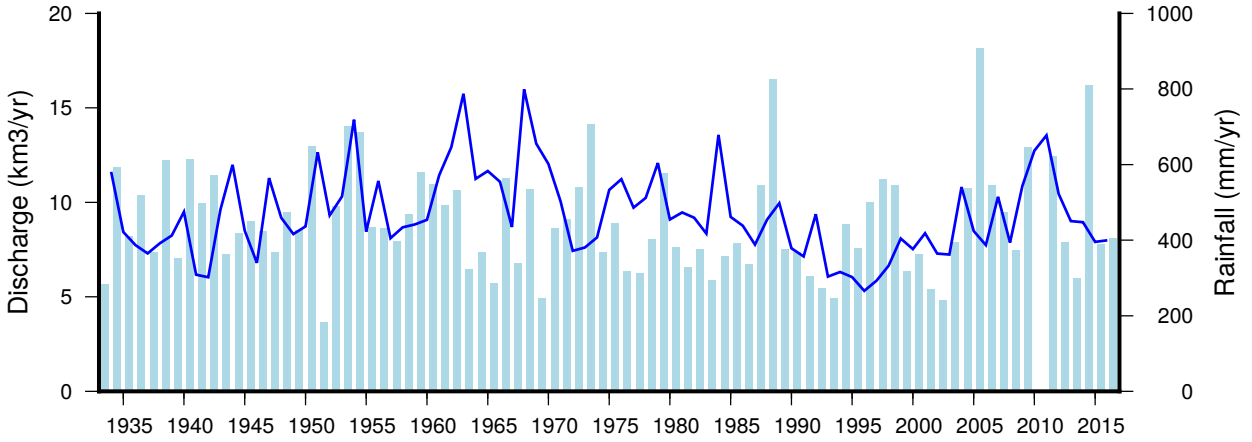

FIGURE 2.13 – Annual discharge of the Okavango river measured at Mohembo (blue line, DWA) and annual rainfall in Maun (Maun airport station from 1933 to 2009, FMMH station since 2010). All data are available on ORI's website : `www.okavangodata.ub.bw/ori`

---

and inaccessible than the catchment area, they are distributed so heterogeneously that flux measurements, and consequently water balance, are still difficult. Indeed, hydrological relationships differ between the islands, the floodplains and the channels and the small spatial extent of each feature does not allow automatic mapping from remote sensing. The foundational work of Wilson and Dincer (1976) led to the first overview of the hydrological system in the Delta and to the first attempt of water balance assessment. Hydrological models have subsequently progessively been developed to face this challenge (Dincer et al., 1987; Gieske, 1997; Hughes et al., 2006; Wolski et al., 2006; Milzow et al., 2011). These models are all calibrated based on discharge. A major step forward was realised by Gieske (1997), allowing constant hydrological parameters over the decades, by taking groundwater into account. The present understanding of water balance for the Okavango Delta, according to Wolski et al. (2006), is summarized in Table 2.1. The Okavango basin is assumed to be a closed system, with no groundwater being lost to the neighbouring basins (McCarthy et al., 1998), apart from $\sim$2% of the incoming water, flowing in the Boteti river.

The response of the hydrological system to variations of water fluxes is not linear, from the catchment area (Mazvimavi and Wolski, 2006) to the distributary systems of the Delta (Wolski and Murray-Hudson, 2008). The catchment area does not respond linearly to climatic variations (Mazvimavi and Wolski, 2006). Years of above-average rainfall do not necessarily provide major inflows (e.g. 2005-2006 in figure 2.12) and years of minor rainfall can still provide important inflow (2015-2016). Moreover, while regional rainfall shows a variability with a main period of $\sim$18 yr (Tyson et al., 2002; Dieppois et al., 2016), the variation of inflow at Mohembo exclusively exhibits a possible 70-80 yr periodicity (Figure 2.13). Unfortunately, the 84 yr long chronicle for the Okavango discharge at Mohembo is insufficient to allow the confirmation or rejection of this latter hypothesis. The variability of discharge seems to be primarily due to regional climate variations as the Zambezi shows similar discharge variations (Mazvimavi and Wolski, 2006; Wolski et al., 2012), implying a constant regime for the hydrological system over the decadal time scale.

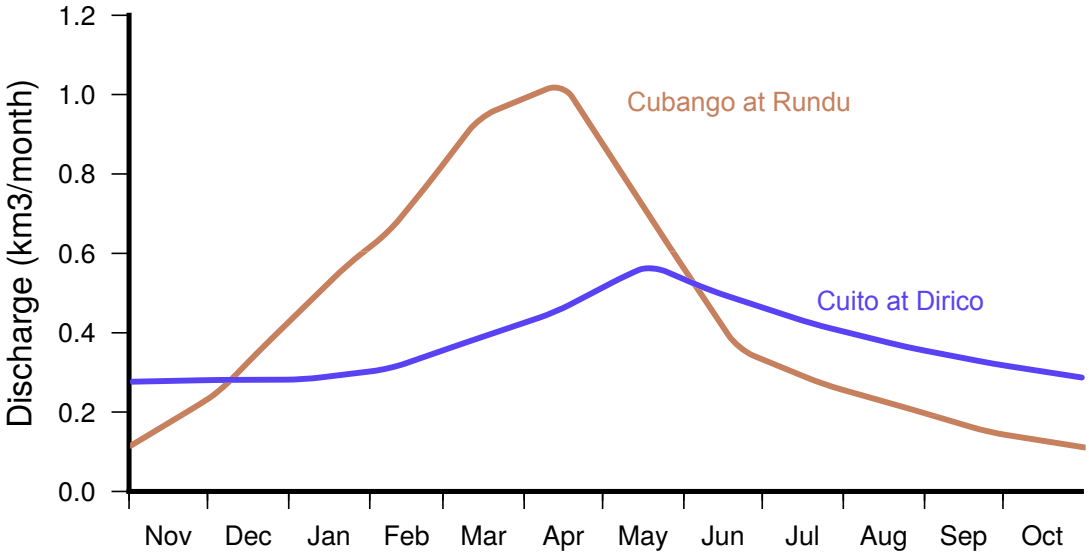

FIGURE 2.14 – Comparison between the annual evolution of water level in the Cuito and Cubango. The higher amplitude of variation in the Cubango is due to the absence of the Kalahari beds in the sub-basin. In counterpoint, the Cuito assures the base flow of the Okavango all through the year due to the hundreds of meters of Kalahari sands providing a suitable substrate for a significant aquifer (Modified from Mendelsohn et al. 2010).

A possible influence on this non-linearity is the poorly quantified shallow aquifer. Annually, the runoff generated in the Cuito and Cubango headwaters differs despite overall similar rainfall characteristics (Figure 2.14 and Hughes et al., 2006). Runoff is generated more instantaneously in the Cubango headwaters, leading in a greater amplitude of variations of the river water level. The Cubango thus has more influence on the timing and amplitude of the flood pulse. The discharge of the Cuito is more constant and this tributary thus assures the baseflow of the river through the year (McCarthy et al., 2000; Mendelsohn et al., 2010). This difference is due to the different substrates and topographies available for the aquifer (Hughes et al., 2006; Milzow et al., 2011). Indeed, while the basin almost entirely lies on the unconsolidated sands of the Kalahari, the thickness of the sand beds is not homogeneous (Figure 2.10). The headwaters of the Cuito lie on up to ∼300 m in thickness of Kalahari sands (Haddon et al., 1999), allowing infiltration of rainfall, water storage and groundwater discharge during the dry season. On the other hand, the headwaters of the Cubango partly directly lie on the metamorphic bedrock or on a few tens of meters of unconsolidated sands, preventing infiltration and generating preferentially rapid thus seasonal runoff.

Similar to the catchment area, the response of the Delta to variations in water input is not linear and higher inflow does not necessarily provide larger floods (Wolski and Murray-Hudson, 2008). The increase of inflow between 2006 and 2007 by a factor of 1.5 did not produce the same variation in the flood extent, and the duration of inundation of the floodplains was in fact shorter (Figure 2.12). Some explanation for this non-linearity can once again be found in the properties of the aquifer, especially in its responses to antecedent hydrological conditions at the arrival of the flood (Wolski and Murray-Hudson, 2008). During its propagation, the flood wave recharges the aquifer in the Delta. The flood propagation

thus depends on the pre-existing degree of saturation of the aquifer. The more saturated the aquifer already is, the less water infiltrates and the further and faster the flood wave will flow.

This non-linear response can be quantified by the ratio between inundated areas and inflow, defined as the flood regime (Wolski and Murray-Hudson, 2008). Flood regimes differ between distributary systems, but also through time within a single system, in both a transient or permanent manner (Wolski et al., 2012). Major floods or long periods of dryness can trigger changes in the flood regime, for instance through modifying the local vegetation. The non-linear response of the Delta to climatic variations thus partly relies on the integration of the non-linear response of the DS to variations of water inputs.

While groundwater is thought to exert a strong influence on the extent of the annual flood (Gieske, 1997; McCarthy et al., 1998; Wolski et al., 2006), the forcings controlling its evolution are not clearly defined yet. Infiltration of surface water during the propagation of the flood is the main recharge of the shallow aquifer, and it is thought that local rainfall does not exert a significant influence on the elevation of the water table. ET is responsible for the decline of water level observed after the flood wave, and probably influences the ability of individual rainfall events to recharge the surface aquifer (Wilson and Dincer, 1976).

2.2.3 Conclusion

The water level in the Delta is strongly influenced by climatic factors : inflow, rainfall and evapotranspiration. This influence is moderated by the relationships between the different hydrological reservoirs in the system, namely the hydrology of the Okavango basin, which is at least partly responsible for the non-linearity of the variations in the inflow at the entrance of the fan and in the spatial distribution of the flood in the Delta. The aquifer has been revealed to be a major reservoir in the system, possibly playing a crucial in the non-linearity of the system. Unfortunately, the absence of monitoring of groundwater in the catchment area did not allow so far the validation of this hypothesis. Hydrological models developed to overcome the lack of monitoring are generally only calibrated on the outflow of the catchment area, and are thus poorly constrained. Improved constraints for such a validation may henceforth be provided by the variations of the Earth's gravity field recorded by GRACE satellites to answer this fundamental question (see Sections 3 and 4). As the deformation of the surface can be affected by seasonal hydrological loading, **can it be used along with GRACE solutions as a monitoring proxy in terms of TWS in the catchment area, and thus help to assess the volume and amplitude and phase of the variations of the aquifer ?**

2.3 Geological settings

Being located in an active graben, the Okavango Delta is under the influence of tectonic processes. At the management time scale, earthquakes are thought to be possibly partly responsible in the variation of the flood distribution between the distributary systems, either by inducing local topographic offsets large enough to trigger channel avulsion, or by modifying the topographic slope at the scale of the Delta (Pike, 1970; McCarthy et al., 1993). This

hypothesis is only supported by a sensitivity test of a numerical hydrological model for the Delta (Bauer et al., 2006), in which the overall distribution of water during the flood would be disturbed by a tilting of the inner graben of only 0.00014°. Such a tilt represents a topographic offset of several cm in the northwestern part of the Delta.

Tectonics influences the basin geometry at the geological time scale by creating and maintaining the depression necessary for the system to be despite the sedimentary filling. It rejuvenates accommodation space for future sediments. The structure of the OG is strongly controlled by the long and complex tectonic history of the area. The tectonic deformation is thought to be related to a southwestern extension of the East African Rift System (EARS) since the 1970's (Scholz et al., 1976). The extensive Kalahari sands cover almost the entire area, hence providing very few outcrops of the bedrock. In the past decade, geophysical studies have brought new insights on the tectonic structure, which are reviewed in Pastier et al. (2017) in chapter 5.

2.3.1 Regional geology

Cratons

The OG is located between two old and rigid blocks : the Congo Craton in the northeast and the Kalahari Craton in the south (Figure 2 in Pastier et al., 2017 in Section 5.1). These Archean shields are formed by the assemblage of smaller cratons by Archean to Proterozoic belts. In the Congo Craton, the oldest datings in the southernmost Kasai block yield an age of 3.5 Gy (Cahen et al., 1984). The Kalahari Craton is formed by the Kaapvaal Craton, in which the oldest dated granite-gneiss yields an age of 2.928 Gy (Kamo et al., 1995) and the Zimbabwe Craton, with the earliest greenstone belts dated at 3.5 Gy (Carney et al., 1994), joined by the Archean Limpopo belt. The peak of metamorphism related to this collision is probably about 2.7 Gy (Barton and van Reenen, 1992). The precise extent of the cratons is still under debate, and it has been recently established that they extend further at depth than previously thought (Begg et al., 2009; Khoza et al., 2013).

Mobile belts

The Kalahari and Congo cratons are joined by a series of Paleo- to Neo-Proterozoic belts (Figure 2.15), the last one resulting from the Pan-African orogeny. The formation of the Damara/Ghanzi-Chobe belt is a multi-stage event which began with an episode of rifting possibly around 1106 My (Modie, 2000), named the Ghanzi-Sinclair rifting. This rifting led to the deposition of the sedimentary rocks forming the Ghanzi-Chobe belt and occurred on the same NE trend as the current faults of the OG (Borg, 1988; Haddon, 2005). A first collision between the Congo and Kalahari (KH) cratons is thought to have led to a first episode of deformation of the sediments of the Ghanzi-Chobe belt around 1 Gy. The rifting associated with the Damaran orogeny was initiated between 800 and 730 My and allowed the deposition of the sediments of the future Damara belt. An episode of deformation in the rocks of the Ghanzi group, dated around 650 My, possibly marks the initiation of the subduction bringing the Congo and Kalahari cratons back together for the Damaran collision occurring around 550 My (Miller 1983 in Haddon 2005). The peak of metamorphism for this orogeny is

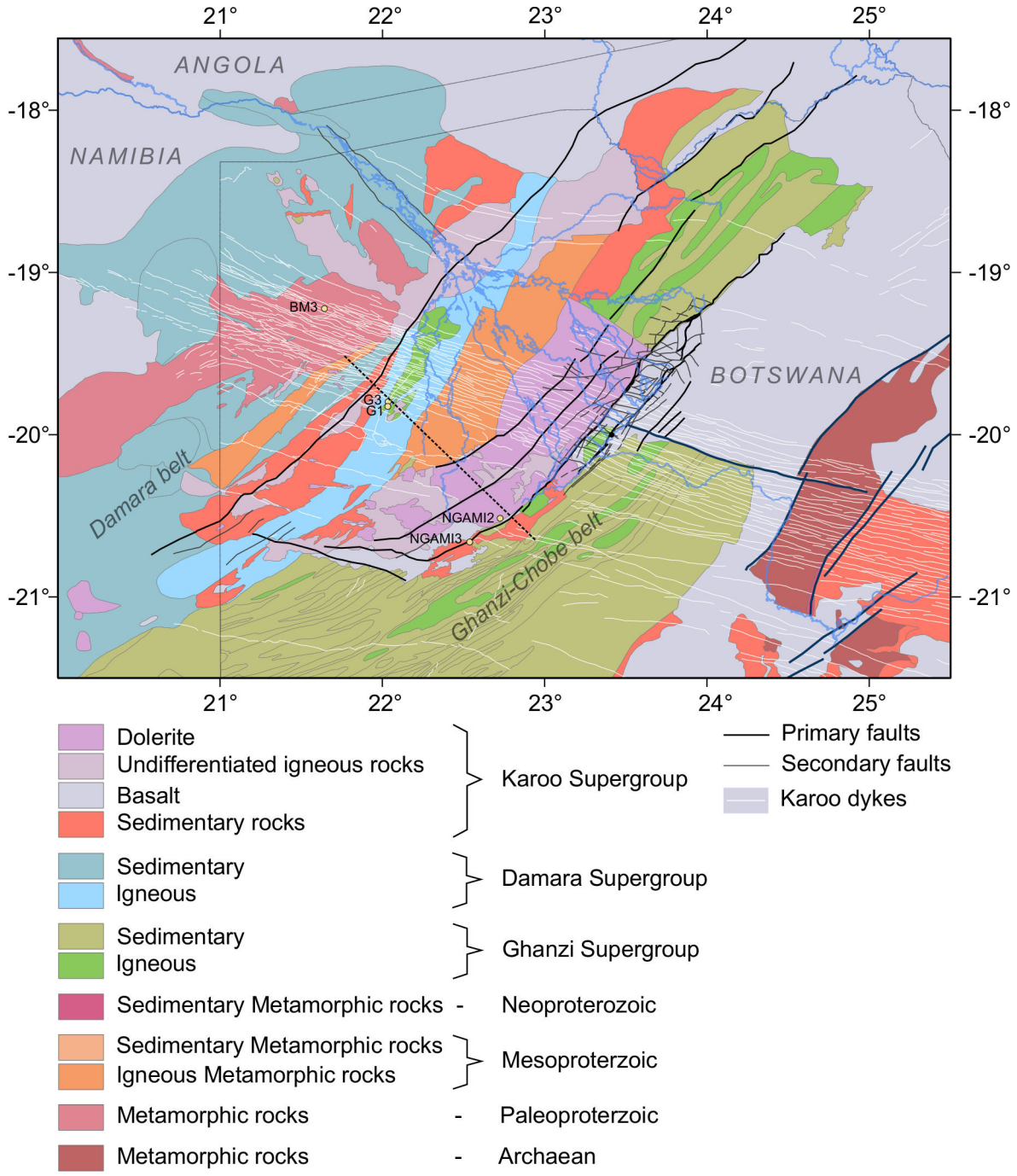

FIGURE 2.15 – Simplified sub-Kalahari geological map of the area (modified from Haddon 2005). The two mobile belts, the Damara belt and the Ghanzi-Chobe belt join beneath the graben but are covered by sedimentary and igneous rocks of the Karoo Supergroup. The orientation of the faults of the OG follow the same trend than the structural features of the Ghanzi-Chobe folded belt. Dashed line show location of the profile for figure 2.18 and yellow dots show location of the cores from Linol (2013). Note the perfect alignment of the OG faults and folds in the Ghanzi-Chobe belt, detailed in Botswana. Some parts of the OG faults also delineate the basalt floods of the Karoo.

dated at 520-528 My (Haddon, 2005). Cooling and subsequent continental collapse occurred in the Early Ordivician (Gray et al., 2006), leading to the dismantling of the belt through erosion, doming, folding, until the Permian (Miller and Burger, 1983).

In the study area, the bedrock has only been sampled in the northern block of the OG and the northern central block, where it consists of quartzite, dolomite or gneiss from the Damara belt. The boundary between the northern Damara belt and the southern Ghanzi-Chobe belt lies in the central block of the Okavango Graben (Key and Ayres, 2000; Kinabo et al., 2008). The single northwestern Gumare fault is located on the youngest highly metamorphised Damara belt. The numerous southeastern faults, however, are located in the Ghanzi-Chobe folded belt. Kinabo et al. (2007) showed that the pattern of the faults of the OG perfectly superimposes with the previous folds of the Ghanzi-Chobe, with their respective orientation simultaneously varying from 30-50°N in the north to 60-70°N. The faults are hence strongly controlled by the Proterozoic structures inherited from the Pan-African orogeny and are possibly ancient faults of the Ghanz-Chobe belt now reactivated.

Karoo

The rocks of the Karoo Supergroup lie uncomformably over the Precambrian bedrock. The Karoo period (late Carboniferous to Jurassic) is associated with intense rifting throughout Africa related to the break-up of the Gondwana super-continent (e.g, Bumby and Guiraud, 2005). Thick sedimentary deposits are preserved in grabens in southern Africa, mainly in the central to southern part of Botswana, along a NE trend, such as the OG (Key and Ayres, 2000; Modisi, 2000). The intense Karoo sedimentation can be divided into four groups : the Dwyka, Ecca, Lebung and Beaufort groups. It was capped by the volcanic episode of the ∼184-178 My Karoo Large Igneous Province (Duncan et al., 1997; Gall et al., 2002). This intense volcanic activity produced the rocks of the Stormberg group : large covers of basalt floods, locally reaching a thickness of 1000 m (Key and Ayres, 2000), intrusions of dolerite sills and the ESE Okavango Dyke Swarm (ODS), crossing the OG in its southwestern part (Figure 2.15). The 70 km wide cluster of dolerite dykes cuts all the local structures inherited from the Precambrian tectonics with a 110°N orientation (Modisi, 2000; Jourdan et al., 2004).

Sequences of Karoo sediments are found in the Okavango graben (Linol, 2013). Lower Karoo sequences are only found in the northern block, and consist of rhythmites and black shales. Their thickness can reach up to 100 m. Upper Karoo sequences (Lebung group) are found in the northern block as well as in the central part of the OG, sometimes in thick layers consisting in red fluvial sandstones. A borehole south east of the Gumare fault exhibits 170 m thick of red beds without reaching the bedrock.

Igneous rocks of the Stormberg group are thought to broadly lie in the southwestern part of the inner graben as basalt floods or dolerite sills (Key and Ayres, 2000), delimited by the SSZ and the Kunyere and Thamalakane faults. The other magmatic striking feature in the area is the Okavango Dyke Swarm. This set of dolerite dykes, oriented N110° extends from the Limpopo belt in Zimbabwe to the north of Namibia, through the OG. It has been dated around 178 My (Gall et al., 2002).

Karoo sequences are capped by a paleosoil marking an erosional surface. This surface erodes the Nxai-Nxai kimberlite, which intrudes the Karoo sediments and is dated at 83 My (Batumike et al., 2007 in Linol et al., 2015). The distribution of the basalts has been

impacted by the paleotopography. But the important contrasts observed in the available logs are strongly related to the current faults. Consequently, the preservation of hundreds of meters of Karoo sediments south of the Gumare fault and dolerites north of the Kunyere fault most probably indicate an active phase of the graben during and/or after the Karoo sedimentation and volcanism to preserve the deposit from Late Cretaceous erosion.

The Kalahari supergroup

The extensive Kalahari basin covers an area from southern Democratic Republic of Congo (DRC) to northern South Africa, and from the Etosha pan to the Zambezi catchment area and western Zimbabwe. Figure 2.16 shows the boundaries and isopachs of Kalahari sediments in the basin according to Haddon et al. (1999). Linol (2013) extended the limits of the basin to another depocenter in DRC, not drawn on the map. The stratigraphy and chronology of the Kalahari are poorly constrained, not only due to a lack of data, but also because of its great spatial variability (Thomas and Shaw, 1991; Haddon, 2005).

Although extensive, the Kalahari basin is shallow with a maximum thickness of 450 m. The very spatially variable stratigraphy of the group is generally formed of basal conglomerates, sandstones, limestones, clay and is regularly capped by the most recent unconsolidated sands (Thomas and Shaw, 1991; Haddon, 2005). Three main depocenters form the basin in southern Africa. The Etosha depocenter shows the highest thickness of sediments, in which sands can reach up to 200 m thick. The Angolan depocenter is exclusively documented by the geological of Angola, thus poorly constrained and detailed. Finally, the last depocenter extends along a N-S axis and can be divided into a Zambian depocenter, south of Mongu's GPS station, and the Okavango-Chobe depocenter, further detailed in the following section. The Zambian depocented comprises a unit of unconsolidated sands, the Mong sand member, reaching 120 m thick 220 km ESE of Mongu.

In the area of the OG, Kalahari sediments uncomformably cover either the Upper Karoo red beds, basalts or the metamorphic bedrock. The erosion surface marking the interface between the KH and Upper Karoo sediments, is also visible in the bedrock in sequences deprived of Karoo deposits. The intersection of this surface with the Nxai-Nxai kimberlite, defines 83 My as the oldest boundary for the age of initiation of KH sedimentation. The same configuration is found in the Orapa kimberlite, dated between 87.4± 5.7 and 92.4± 6.1 My (Haggerty et al., 1983; McCarthy, 2013). To date no duration of the erosion phase has been determined in the area, but close examination of the sediments directly overlying the crater of these kimberlites indicate an initiation of sedimentation relatively soon after the kimberlites eruptions.

The Kalahari sediments are divided in two distinct facies. 10 to 30 m of sandy carbonates and calcretes are found in all cores in Linol (2013) except one located between the Chobe and Linyanti faults. They reveal a palustrine environment, thus wetter than today, and are terminated by a cap calcrete, a consequence of final emersion and revealing a hiatus in the sequence. The Kalahari beds finally cover the carbonates with a few tens to 300 m of fine well-sorted sand (Figure 2.10). The origin of these sands is still controversial between aeolian and fluviatile transport (Thomas and Shaw, 1990) and in-situ weathering of the underlying Precambrian basement (McFarlane et al., 2010). These sands most probably have been remobilised several times as occuring in the paleo-dune field (McFarlane et al., 2005)

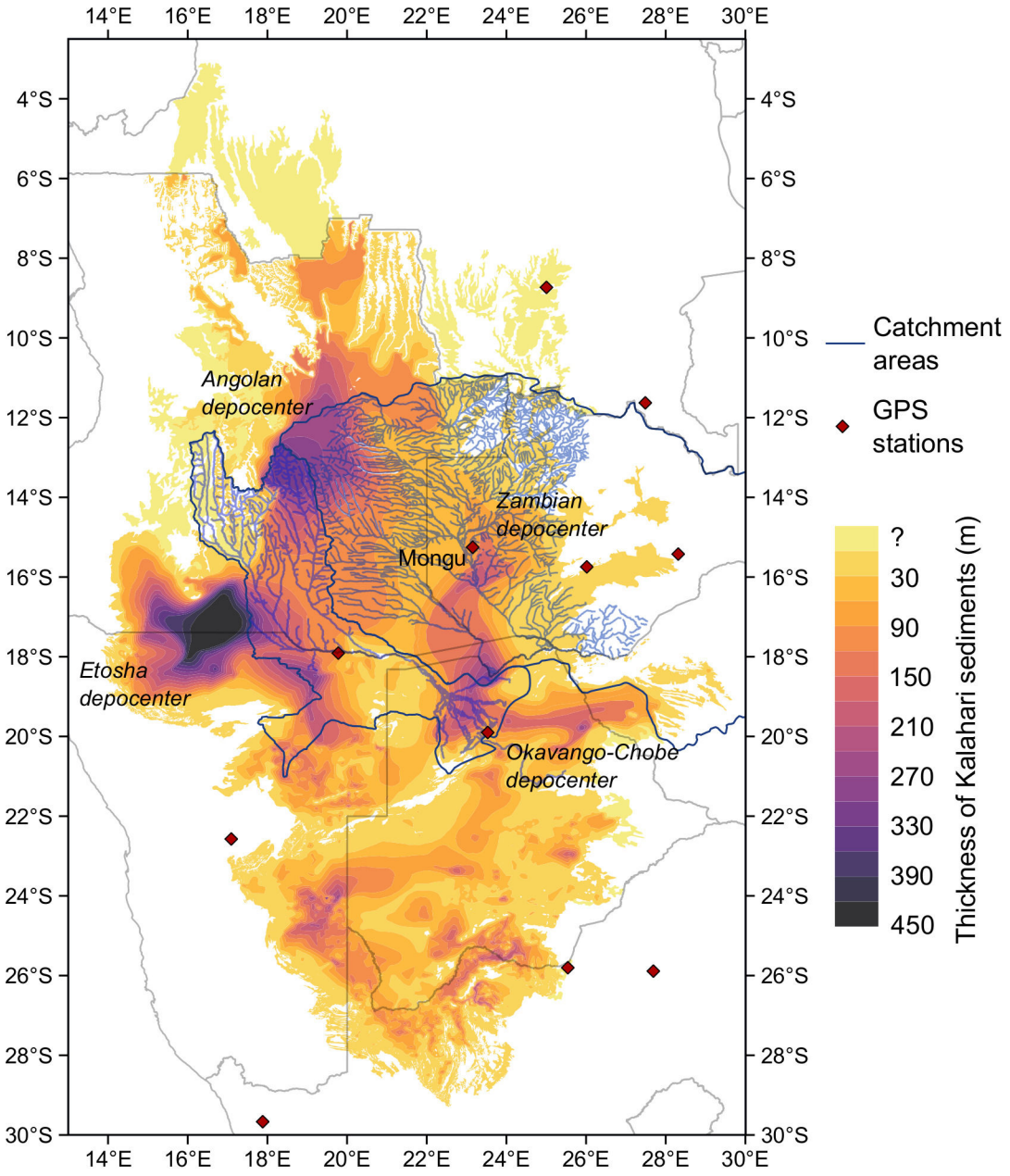

FIGURE 2.16 – Isopach map of the Kalahari sediments (modified from Haddon et al. 1999).

2.3.2 The Okavango Graben

Overview

The OG forms a gentle depression in the very flat local topography of the Kalahari basin, and is the second lowest part of the Kalahari depression after the Makgadikgadi pans (Figure 2.4). Only some faults exhibit a scarp in the topography, never exceeding a few tens of meters high (Figure 2.17). These subtle scarps are nevertheless sufficient to block the channels at the end of the system regarding the very low relief. The graben is seismically active (Scholz et al.,

1976; McCarthy et al., 1993) and was until very recently considered as the most seismic area of Botswana. The seismic activity is mainly focused in the southeastern part of the Delta. The normal bounding faults show downthrow up to about 500m (Kinabo et al., 2008; Shemang and Molwalefhe, 2011; Bufford et al., 2012).

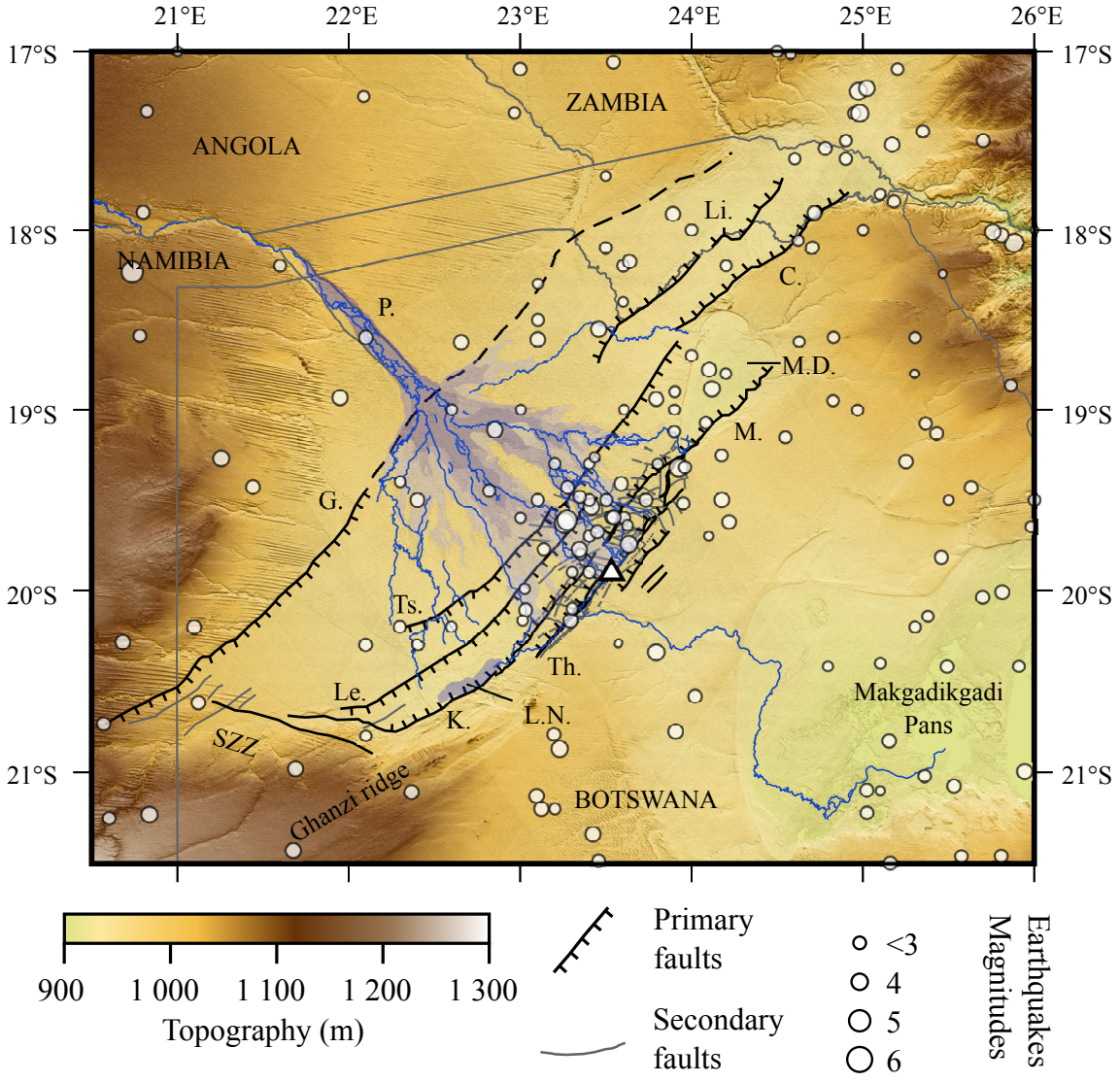

FIGURE 2.17 – Location of the primary and secondary fault sets (based on Modisi et al., 2000; Campbell et al., 2006; Kinabo et al., 2007) and recorded earthquake since 1950 (data from ISC unreviewed bulletin). Basemap shows topography from SRTM30 C : Chobe fault, G : Gumare fault, K. : Kunyere fault, Le : Lecha fault, Li : Linyanti fault, L.N. : Lake Ngami, M : Mababe fault, M.D. : Mababe Depression, P : Panhandle, SSZ : Sekaka Shear Zone, Th. : Thamalakane fault, Ts : Tsau fault.

Very few cores have been drilled in the protected Delta to overcome the blanket of KH sands, and even fewer reach the bedrock. The main data sets that brought insights on the OG structure are from the boreholes drilled by the Department of Water Affairs (Haddon et al., 1999) and Tsodilo Ressources (Linol, 2013), airborne aeromagnetic data (Modisi, 2000;

Campbell et al., 2006; Kinabo et al., 2008), MagnetoTelluric (MT) and Electrical Resistivity Tomography (ERT) (Bufford et al., 2012). As the faults of the OG cut the dykes of the ODS, the offset of their top due to downthrow along the faults allows computation of the total downthrow (Modisi, 2000; Kinabo et al., 2007; Shemang and Molwalefhe, 2011). Bufford et al. (2012) developed an ETM profile across the whole graben which provided a large scale picture of the tectonic geometry. These studies provide local insights to the graben structure, based on different observations, each with strengths and weaknesses.

The OG is a hemi-graben (Figures 2.15 and 2.18), formed by a series of normal, possibly strike-slip, faults showing downthrow up to about 500 m (Kinabo et al., 2008; Shemang and Molwalefhe, 2011; Bufford et al., 2012). The OG can be divided into three domains (Gumbricht and McCarthy, 2001) : 1) the most elevated northern block, supporting the Panhandle, 2) the least elevated central block, hosting the Delta, Lake Ngami and the Mababe Depression and comprising several normal faults and 3) the southern block, through which the Boteti river potentially flows.

The OG is formed by a primary 70°N fault set and a secondary NNW to NS fault set (Modisi, 2000; Campbell et al., 2006; Kinabo et al., 2007). Among these faults, only the isolated Gumare, the Kunyere, Thamalakane, Linyanti and Chobe faults exhibit a topographic scarp. The OG is comprised of three depocentres : 1) Lake Ngami in the SW is bounded by the Kunyere and Lecha faults, 2) the Mababe Depression in the east is bounded by the Mababe and Tsau faults and 3) the Linyanti-Chobe swamps bounded in the SE by the Chobe and Linyanti faults, and possibly in the NW by the extension of the Gumare fault. In the between, the Okavango Delta is bounded by the single Gumare fault in the NW and the Thamalakane and Kunyere faults in the SE. The OG is assymetric, hence a hemi-graben, with the several southeastern faults showing downthrows of up to 500 m (Kinabo et al., 2007; Bufford et al., 2012) and the single northwestern Gumare fault showing a downthrow at least 5 times smaller. According to Campbell et al. (2006) and Kinabo et al. (2008), some dykes show a dextral offset indicating some strike-slip component in the tectonic regime, which could be responsible for the secondary WNW-ESE fault set located in the interslip of the main fault set. The description of the deep crustal structure, physical properties of the crust and seismicity is to be found in Pastier et al. (2017), chapter 5.

Figure 2.18 shows a schematic cross-section in the southwestern part of the graben. The assessment of the respective downthrows differs amongst studies. Regarding the displacements calculated on the offset of the top of the dykes (Kinabo et al., 2008; Shemang and Molwalefhe, 2011), they actually record the global displacement on the faults since the Lower Jurassic. The primary preservation of sediments and igneous rocks of the Upper Karoo in the graben implies fault activity before or during the Cretaceous erosion phase. Thus a part of the recorded displacement is not to be attributed to recent tectonic activity. Moreover, the dykes intruded the pre-existing Karoo sediments and are hence, where Upper Karoo sediments are preserved, of higher elevation than the Precambrian bedrock. The overall tectonic structure revealed by Bufford et al. (2012) is thus a record of the tectonic deformation accommodated since the late phase of erosion of the Damara belt. Finally, a significant part of the interpreted thickness of sediments might actually consist in a weathering profile of the bedrock, resulting in an overestimation of sediment accumulation and fault displacement. The roundness of the grains, commonly interpreted in terms of sediment transport, could actually have been

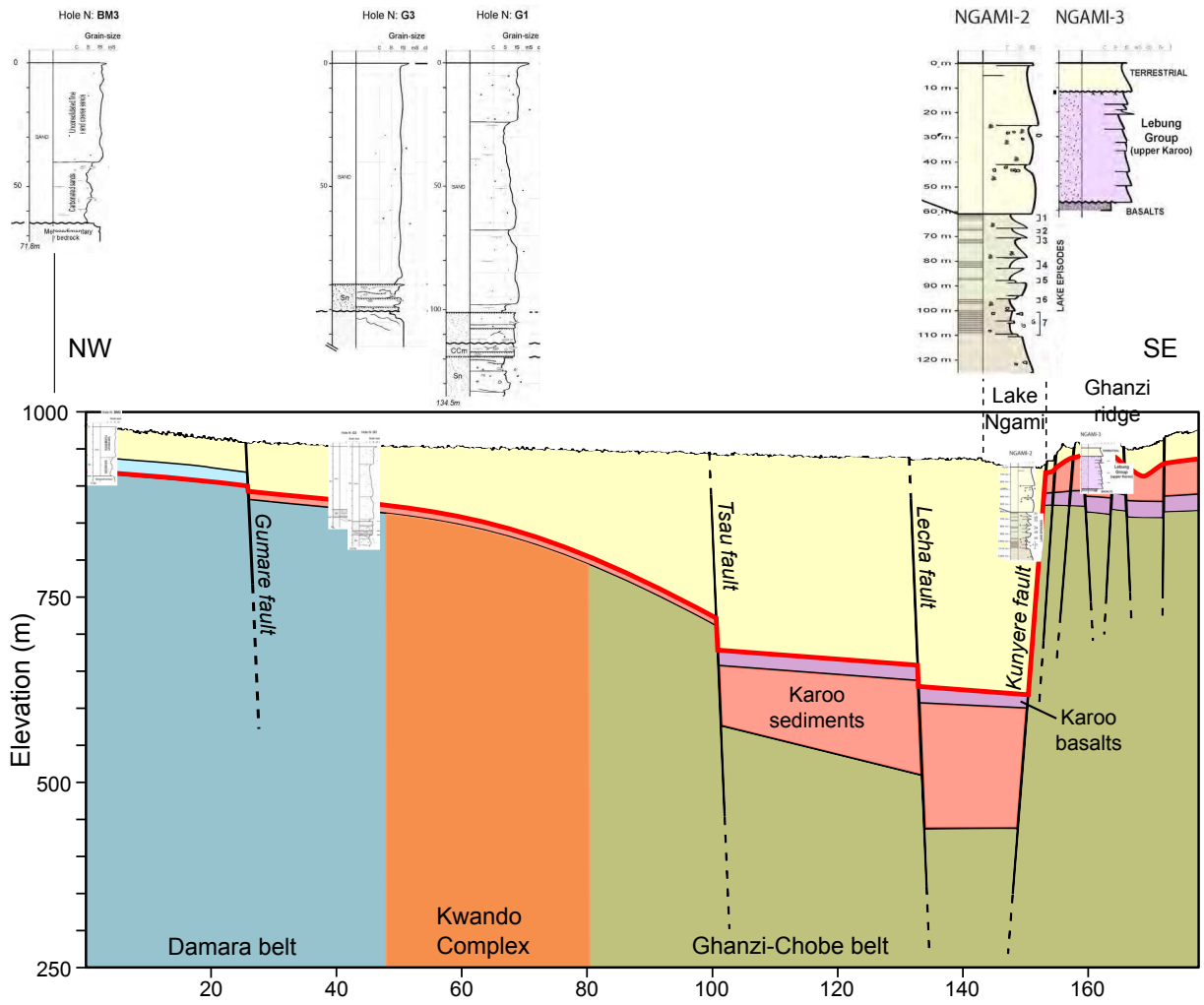

FIGURE 2.18 – Proposed schematic cross-section in the OG compiled from Haddon (2005); Kinabo et al. (2007); Shemang and Molwalefhe (2011); Bufford et al. (2012); Linol (2013), see location on figure 2.15. The Karoo dykes are located within the bedrock and Karoo sediments and basalts. The thick red line represents the theoretical top of the dykes, hence the fault displacements assessed with aeromagnetic data. Upper Karoo sediments and igneous rocks are preserved in the graben, at least between the Tsau and Kunyere faults. The Tsau and Lecha faults may be blind or inactive faults. The Ghanzi ridge hosts many small horsts and grabens. The slope formed by the top of the bedrock is higher than the topographic slope which could be partly due to minor faults rather than to a consistent slope. Rocks of the Damara belt, the Kawando complex and the Ghanzi-Chobe belt comprise the bedrock, visible in figure 2.19. Colors represent the geological units as in figure 2.15.

---

produced *in-situ* by repeated alteration (McFarlane et al., 2007).

Regarding the scarcity of data and the diversity of the studies, it is not a trivial task to propose a 3D model of the OG. Figure 2.19 proposes the first overall 3D reconstitution of the relief of the bedrock, revealing the downthrow and connections of the faults.

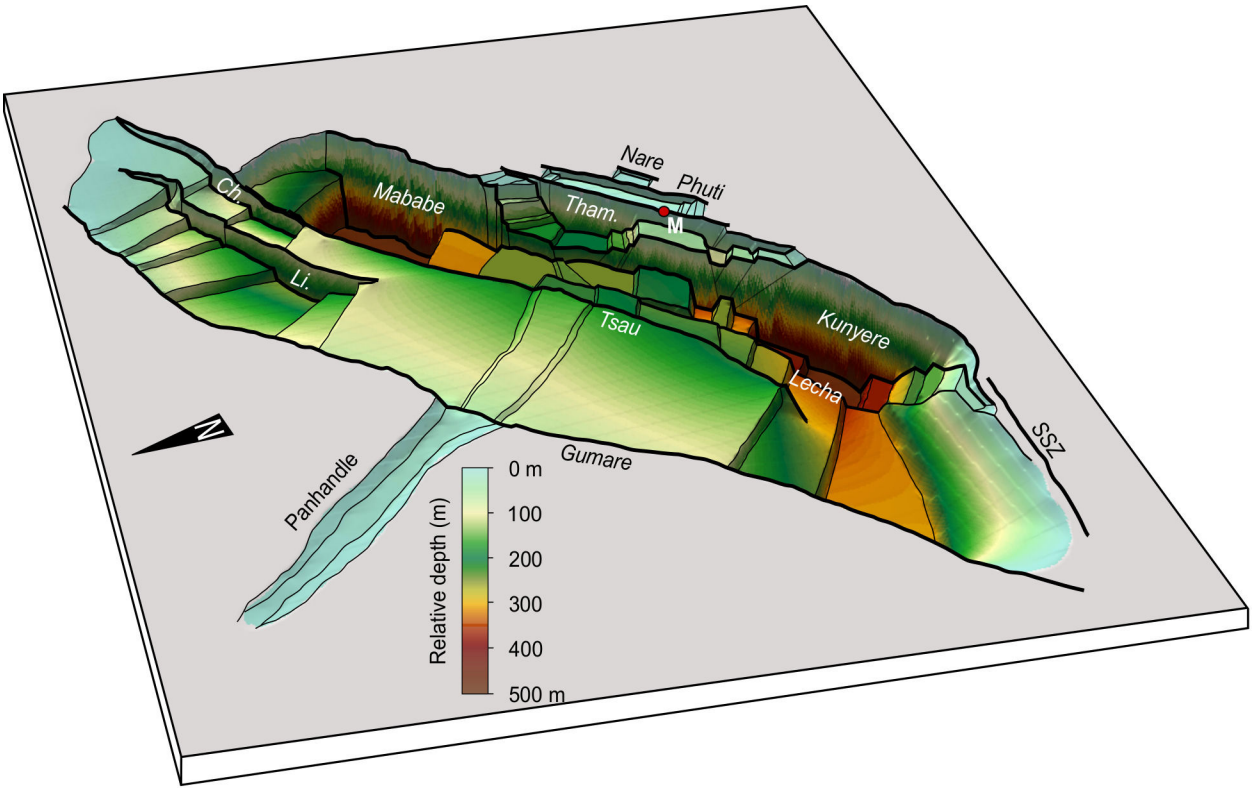

FIGURE 2.19 – Proposed reconstitution for the bedrock relief showing the geometry of the primary fault set, based on data from Modisi (2000); Haddon (2005); Campbell et al. (2006); Kinabo et al. (2008); Shemang and Molwalefhe (2011); Bufford et al. (2012); Linol (2013). The bedrock consist in the Damara belt, the Kwando complex and the Ghanzi-Chobe belt. Ch. : Chobe, Li. : Linyanti, M : Maun, SSZ : Sekaka Shear Zone, Tham. : Thamalakane.

Description of the faults

The Gumare fault is the single NW bounding fault of the graben responsible for the break-in-slope initiating the alluvial fan in the OG's central block. This fault is mainly defined geomorphologically by the intersection it creates with the NW Ngamiland paleo-dune field (Figure 2.2). Not only does the fault coincide with the sudden disappearance of the dunes, but the composition of the sand is also modified. Although the particle size distribution is similar on both sides of the fault, the sands composing the dune field is much richer in iron, providing a darker colour (Figure 2.1). The fault shows a scarp between 0 to 10m high (McFarlane et al., 2005), fading in the topography towards the Panhandle. No study has defined the exact extent of the fault at depth. As other faults play a role in the sedimentary basin but show no impact on the topography, this fault could actually extend further NE, under the Panhandle, as proposed by McCarthy (2013). It would then be responsible for the break in slope intiating the Linyanti swamps. The downthrow of the fault, as well as its lateral variability, is also poorly known. While the geophysical studies agree on a downthrow of 50 to 100 m (Modisi et al., 2000; Kinabo et al., 2007; Bufford et al., 2012) in the Delta area, cores drilled in the southwestern portion revealed a depth to bedrock of more than

280 m (Linol, 2013). Finally, while some earthquakes have been recorded in the vicinity of the Gumare fault, no significant cluster can be identified on its location (Figure 2.17). This lack of observed seismicity is paradoxical with the geomorphological impact of the fault. If displacement is occurring on this fault, either fault creep is at play, or the tectonic activity is episodic, with a period longer than the present seismic records.

The Kunyere fault extends from the SSZ in the SW to the Mababe fault in the NE. It is considered as the main bounding fault of the graben, due to its estimated mean downthrow, between 334 m in the south to 286 m in the north, the highest mean downthrow in the graben (Kinabo et al., 2008). Its scarp culminates in Lake Ngami at 35 m and fades to 0 along the SSZ in the west. In the NE, the fault scarp progressively fades in the surroundings of the Gomoti channel in the NE, with the main decrease located at the north-eastern end of the Ghanzi ridge. Its downthrow follows the same trend, with the highest estimates reaching 600 m along a sub-vertical fault plane in Lake Ngami (Bufford et al., 2012) to a null vertical displacement relative to the Thamalakane fault in its northern extent. The area between the Lecha and Kunyere faults hence shows the greatest total vertical displacement. The dykes exhibit a general lateral offset (Kinabo et al., 2008), possibly reaching 5 km right lateral displacement (Campbell et al., 2006). Detailed mapping of the area revealed the Kunyere fault as a fault zone with several parallel faults about 3 to 5 km wide from its southern extent (Shemang and Molwalefhe, 2009) to its northern end (Laletsang, 1995; Campbell et al., 2006). Bufford et al. (2012) noticed no low resistivity anomaly on the fault at depth in June 2007, when the Kunyere river was dry (*Atekwana, pers. comm.*). Earthquakes have been recorded in the neighbourhood of the fault, but exclusively on its northern portion. The southern portion, bordering Lake Ngami, shows no recorded seismic event. Kinabo et al. (2008) proposed that the Kunyere actually joins the Mababe fault. The Kunyere fault is thought to be one of the most active, thus having accommodated the highest deformation in the graben.

The Mababe fault is located on the alignment of the Kunyere fault and borders the whole Mababe Depression. Its scarp varies from 20 m at the entrance of the Depression through the Mababe river to 40 m in the heart of the Depression. This latter scarp is nevertheless subdivided into two 20 m stepped scarps. The Mababe Depression exhibits a significant seismicity but the lack of precision in the location of the epicentres, with a typical uncertainty of $\sim$50 km, does not allow the determination of the particular fault responsible for the earthquakes. The Mababe fault shows a downthrow of up to 500 m dipping NE (Kinabo et al., 2007) but only 90 m maximum of Kalahari beds are proposed by Haddon et al. (1999). The area recorded the strongest earthquake of the 2013-2014 seismic activity with a magnitude of 4.3. The Mababe and the Kunyere can now be considered as a single fault. The earlier distinction was based on their historical recognition but the aeromagnetic data showed a continuity between the two faults. Moreover, no detailed study has been done in the area of the connection to determine the depth of the basement between the Maun area and the Mababe Depression.

The Thamalakane fault extends from the junction of the Nhabe and Kunyere rivers in the south to north of the Gomoti channel. Its scarp varies from 20 m in the south to 2 m in the north. It is noteworthy that the Boteti river does not cross the Thamalakane fault either at the location of its lowest scarp, or at the lowest point of elevation along the fault. Like the Kunyere, the Thamalakane fault is a fault zone with several parallel faults a few km wide (Modisi, 2000; Campbell et al., 2006). The downthrow of the Thamalakane fault is

variable along strike (Campbell et al., 2006; Shemang and Molwalefhe, 2011) and averages 80 m (Kinabo et al., 2007), dipping NW. Campbell et al. (2006) noticed a general dextral offset of the dykes averaging 1 km. Bufford et al. (2012) portrayed the fault as a sub-vertical zone of low resistivity anomaly, possibly meaning that the fault is filled with fresh water. The Thamalakane fault is seismic, with events recorded during every period of seismic activity of the OG. The Thamalakane fault joins the Kunyere and Mababe faults respectively in the south and north, through a series of secondary faults oriented NNW-SSE to N-S (Modisi, 2000; Campbell et al., 2006) which are much denser in the north than in the southern junction with the Kunyere. Kinabo et al. (2008) proposed that the more moderate downthrow of the Thamalakane fault relative to the Kunyere fault indicates a younger reactivation consequent to a migration of the accommodation of the deformation southeastwards.

The Phuti and Nare faults seem to match such a model as they exhibit much lower downthrows, respectively 18 and 71 m, and are located SE of the Thamalakane fault.

The Lecha fault and **the Tsau fault**, previously unidentified, were only revealed by the aeromagnetic data (Modisi et al., 2000) as they exhibit no topographic fault scarp. They are conjugated to the Thamalakane and Kunyere faults as they are dipping SW. Their precise extent is not clearly defined. The Lecha fault initiates in the vicinity of the SSZ and fades in the area of Chief's Island in the north, while the Tsau fault could be initiated more in the northeast and continue further northeastwards to form the NW bording fault of the Mababe Depression. The Tsau fault shows a downthrow between 43 to 130 m, while the Lecha fault is considered as a major fault of the graben with a downthrow estimated between 232 and 334 m (Kinabo et al., 2008). The differential downthrows relative to the Gumare fault induce a higher slope of the bedrock between the Gumare and Tsau faults than the topographic slope. Other minor faults could be responsible for this progressive dipping. Both faults show some possible seismic activity in the Central Delta. The Tsau fault could be responsible for the few recorded earthquakes in the southern part of the central block. Bufford et al. (2012) revealed the presence of a fault zone conductor on these two faults from ETM data.

The Sekaka Shear Zone prevents the propagation of deformation in the southwest of the OG. It probably is inherited from the Damaran orogeny and no neotectonic activity is visible (Modisi et al., 2000).

The Linyanti fault and **the Chobe fault** extend the OG in the northeast. Both faults mark the topography, with scarps reaching only a maximum of 6 m high for the Linyanti fault, and up to 80 m high for the Chobe fault. Both faults are dipping NW, but estimations of downthrow are only available for the Linyanti fault, reaching between 56 and 163 m. Aeromagnetic data indicate that the Lynianti fault is actually composed of two faults related by a hook (Kinabo et al., 2008). A diffuse seismicity is located in the north of the Linyanti fault. With the Kwnado river, the Linyanti fault forms a small analogue of the Okavango Delta, called the Linyanti swamps. Once again, the several channels diverging from the main river are blocked by the topography resulting from tectonic activity. Apart from the Savuti offtake, the river is directed northeastwards until the scarp is low enough for the river to flow southwards. The Chobe fault finally steers the river to join the Zambezi.

The secondary fault set is found in the OG, mainly oriented 110°N (Modisi, 2000; Campbell et al., 2006). These normal faults are located in the interfault zones of the primary set, mainly between the Thamalakane and the Kunyere. They may actually extend further as no detailed study has been carried out outside this area. Their observed density is thus

biased by the better accuracy of the processing of the aeromagnetic data in the region of Maun (Campbell et al., 2006). Some of the subsidiary faults can be traced on each side of the primary faults. Some of the faults exhibit a dextral strike-slip displacement, such as the curvilinear fault in the lower Delta. This secondary fault set is thought to accommodate the deformation within the southeastern boundary of the graben and form an en-echelon pattern between the primary faults (Modisi, 2000). This pattern is visible in the topography between the Kunyere and Thamalakane faults and is responsible for the junction of the Nhabe and Kunyere rivers. A fault of similar orientation is most probably present between the Gumare and Tsau fault, explaining the difference in the thickness of Upper Karoo sediments observed between the close cores G1 and G3 (Figure 2.18). Given the locations of the recorded earthquakes, this last fault set is probably not active anymore.

2.3.3 Conclusion

To influence the decadal variation of the flood distribution, tectonics must induce either swift pluricentimetric offsets of the surface at the channel scale, to trigger channel avulsion, or more continuous deformation at the fan scale, high enough to counterbalance sedimentation rate and influence the topographic slope, and thus the direction of preferential flow (Pike, 1970; McCarthy et al., 1993; Bauer et al., 2006). This then raises a series of questions. **Is the tectonic activity high enough to significantly shift the overall topography in the Delta and influence the variation of the flood distribution ?** To answer this question, it is crucial to first answer the question : **what is the deformation rate across the graben ?**

To determine the effective influence of tectonics on the endorheism of the Delta at the geological time scale, it is crucial to know the long-term deformation rate. **How old is the graben ? Or, when did the current tectonic activity begin ? What is its long-term deformation rate ?** Different hypotheses have been proposed for the initiation of the current tectonic activity, from ∼27kyrs (Gamrod, 2009) to Miocene (McFarlane, *pers. comm.*). **Is the tectonic activity continuous or episodic ?** Such answers would bring precious insights to better constrain the geodynamic/structural model and to elucidate the bigger scale question : **Which geodynamic process is responsible for the tectonic activity in the OG ?** This answer would bring a strong constraint on the long-term deformation rate. **Is the deformation continuous or episodic ?** This answer is crucial to better interpret the sedimentary record in terms of endorheism, then climatic reconstructions.

2.4 A sedimentological system

Different types of sedimentation currently take place in the Delta, driven by hydrology, vegetation and wind, and driving them in return. Many studies have identified and tried to quantify the different processes currently at play and their influence on the variability of the flood distribution at the management time scale (e.g., McCarthy et al., 1988; Ellery et al., 1993; Garstang et al., 1998; Milzow et al., 2010; McCarthy et al., 2012). On the geological time scale, datings have been carried out on shallow sediments, yielding ages of 140 ky maximum within a few meters deep.

2.4.1 Current sedimentation

The processes responsible for sediment transport and accumulation have been qualitatively well studied since the 90's (e.g., McCarthy et al., 1991), with the first quantifications of inputs. Three types of sedimentation occur within the Delta and lead to the progressive aggradation of the fan (McCarthy, 2013) : the Okavango River is responsible for fluviatile clastic sedimentation and solute load precipitation, to which is added aeolian deposition.

Clastic fluviatile sedimentation

Clastic fluviatile sediments transported by the Okavango River mostly consist of well-sorted quartz grains originating from the surrounding Kalahari sands (McCarthy et al., 1991) and almost no clay enters the system (Stanistreet et al., 1993). The average grain-size at the entrance of the Delta, Mohembo, is 0.35 mm (McCarthy et al., 1991), similar to the grain-size observed in the surrounding dune fields (Stanistreet et al., 1993). According to Milzow et al. (2010), the average grain-size decreases downstream, along with flow velocity down to ∼0.2 mm in the vicinity of Maun. The main part of these sands is transported by bedload, estimated between 120 000 and 155 000 t/yr. The suspended load is still significant with an estimation of 30 000 t/yr (Table 2.2).

Clastic sediments are easily trapped by the roots of the aquatic vegetation and form, along with peat, the permeable levees of the channels. Unlike water, clastic sediments are thus exclusively transported in the channels. According to McCarthy et al. (1991), about 90% of the incoming fluviatile sand is trapped in the Panhandle. Once deposited, the sand can be remobilised in erosional phases of channels and transported downstream.

As fluviatile sediments are mainly transported by bed load, channels are primary sites for sediment deposition. Sand deposition can block a channel, and thus whole distributary systems, within a few years (Ellery et al., 1993). In decades to centuries, sedimentation coupled with vegetation can block major channels and lead to their avulsion (Ellery et al., 1993; McCarthy and Ellery, 1995a). When occurring in areas strategic for the distribution of water amongst the distributary systems, i.e. in the Panhandle or upper Delta, blockages can induce major permanent shifts in the flood regime of the systems, leading to dessication of hundreds of km^2 and strongly impact the spatial distribution of the flood. In doing so, sedimentation indirectly influences the flooding of the different outlets of the Delta.

Type	Annual amount (kt/yr)	Source(s)
Bed load	120 to 155	Milzow et al. (2010) and McCarthy et al. (1991)
Suspended load	30	McCarthy et al. (1991)
Solute load	106.9 to 247.4	Milzow et al. (2010) and McCarthy et al. (1991)
Aerosols	250	Garstang et al. (1998)

TABLE 2.2 – Quantification of sedimentary input

Solute load

Solute load is parent material for the precipitation of calcrete and silcrete, under islands (detailed in Section 2.1.4) and in the distal reaches of the Delta (McCarthy and Ellery,

1995b; Shaw and Nash, 1998). Layers of calcrete are common in the sub-surface, as calcite precipitates due to water table oscillations resulting from evapotranspiration. The amplitude of water table variations can thus form beds of calcrete in the order of meters thick. The average annual mass of solute load is estimated between 106 900 (Milzow et al., 2010) and 247 400 t/yr (McCarthy and Metcalfe, 1990).

Aeolian sedimentation

Aerosols deposits have been quantified by Garstang et al. (1998) at 250 000 t/yr, based on a comparison with estimations in the Etosha Pan. Unlike the fluviatile part, the aeolian grains are poorly sorted, revealing multiple origins (Humphries et al., 2014). Almost half of the dust load consists of organic matter and is therefore provided by erosion of floodplains soil mostly during the dry season. The inorganic fraction is mostly comprised of amorphous biogenic silica coming from the floodplain vegetation (Krah et al., 2004). The deposition of the dust load is heterogeneous both in space and time. Floodplains are vast open areas where winds have enough velocity to erode the surface when they are dry. Arriving at island fringes, winds decrease primarily due to the presence of trees, and dust is partly trapped amongst trees growing on the margins. This process contributes to the island topography and has been estimated to account for 40% of island mass. Dust load is also strongly seasonal with a deposition maximum between September and November. It shows a strong correlation with wind speed which peaks at the same season. It also depends on other environmental factors such as primary production and the annual flood but in a weaker and more indirect manner.

According to Krah et al. (2004), aeolian sedimentation hence seems to act mainly as a mass transfer within the Delta, eroding the floodplains to accumulate on islands, despite the significant amount of incoming aeolian particles from other regional sources. This is corroborated by the fact that 84% of the dust load is transported below 3 m high, implying that not many dust particles leave the Delta.

The current estimates for sedimentary inputs are essential order of magnitude values for estimation of sedimentation rate, but the high variability of the water velocity and the rare discrete measurements of sediment fluxes most probably imply an underestimation of the effective sediment input. Deposition of sediments at the apex of alluvial fan is responsible in general for the migration of channels. The superimposition of these successive migrations through time and across the fan provides their conical shape to such sedimentological features (Gumbricht and McCarthy, 2001; Hartley et al., 2010). Based on sediment mass balance and micro-topography, Gumbricht et al. (2005) proposed that all regions of the fan experience aggradation through channel migration within a period of 150 000 yr.

2.4.2 Long-term sedimentation

Many studies have been carried to date sediments in the Delta through ThermoLuminescence or OSL (e.g., Thomas and Shaw, 2002; Burrough et al., 2007; Ringrose et al., 2008; Linol, 2013) in the three termini as well as in the Delta's floodplains. Most of them dated shallow sediments, of a few meters deep only. Among the Delta's termini, Lake Ngami is the most documented. Its paleo-shorelines have been dated in many studies and synthesised in

Burrough et al. (2007) and in figure 2.20.

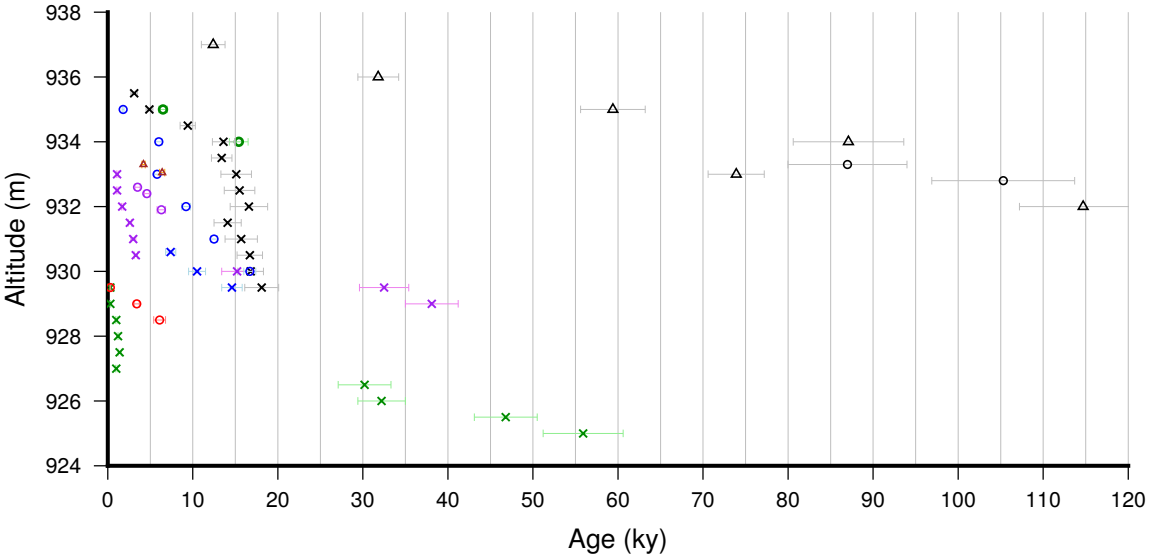

FIGURE 2.20 – Age and absolute elevation of the dated samples in the paleo-shorelines of Lake Ngami synthetised in Burrough et al. (2007), revealing the variable sedimentation rates. Each coloured symbol represents samples from a single core. Note the variability visible in a single core (green crosses) with a low sedimentation rate of about 4 x 10^{-5} m/yr between 55 and 30 ky BP, the hiatus between 30 ky and ∼3 ky, followed by the fastest sedimentation rate of the whole record, 8.3 x 10^{-4}.

A striking feature is the variability of the sedimentation rates calculated from these datings, from 4 x 10^{-5} to 8.3 x 10^{-4} m/yr. This variability is first observed between the different cores. It obviously depends on the location of the core relative to the most active part of the former lake and reveals the spatial variability of sedimentation within the lake. But the rate of accumulation can also vary within a single core, revealing the variability of the Delta regime on a time scal of thousands of years.

Deeper sediments have not been dated, and even the initiation of the Kalahari sand deposition is poorly constrained, estimated as more recent than 80 My (Linol, 2013). It is thus risky to extrapolate current sedimentation to the long-term in order to compare it to the subsidence rate within the graben.

2.4.3 Erosion

As an endorheic system, the Okavango Delta is considered not to be subject to erosion at the global scale. Fluviatile erosion is at play within the fan, but only locally in the Delta and the sand deposited during a previous flood is only remobilised to be deposited further downstream. In the short term, water flow in meandering channels erodes the external banks and deposits sand on the inner edge of meanders (see figure 2.21). In doing so, erosion helps the migration of the channel and erases previous landmarks. Erosion is also responsible for the establishment of new channels. Moreover, erosion can degrade islands, partially or totally.

In the long term, erosion may be invoked as a hypothesis for hiatus in the sedimentary record, for instance the datings at Lake Ngami. The spatial separation of the cores, as well as the datings within cores, does not permit the discrimination between a phase of non-deposition and erosion at present. Determination of long-term sedimentation rates can thus be biased.

Conclusion Sedimentation has a strong control on both short and long wavelength topography and is probably one of the most documented process in the Delta at the management time scale. It is responsible for channel avulsion, which can permanently impact a distributary system. When occurring in an area critical for attribution of water, such as the upper Delta, it can strongly impact the distribution of the flood at the scale of the Delta.

At the geological time scale, sedimentation fills the graben and reduces the topographic depression. This long-term sedimentation is poorly constrained as very few cores are accessible in the Delta and even fewer reach the bedrock. While the variations of sedimentary input are interpreted in terms of climatic variations, other factors, such as the hydrographic network can be at play. Assessing the short-term variability of sedimentary processes is not the aim of this study, but determining its long-term variability is essential to estimate the ratio between sedimentation and subsidence rates controlling the endorheism. **How variable are the sedimentation rates ? What is causing sedimentation rates variations, at different time scales ? How does erosion/sedimentation impact the print of tectonic deformation in the landscape ?** Although it is not the aim of this study to answer all these questions, they provide critical context while trying to disentangle the controls on the system.

FIGURE 2.21 – Sandy cliff formed by channel erosion in an island, at the end of the Panhandle.

2.5 A pristine and interactive ecosystem

A particularity of the Okavango Delta is that it is a vegetated alluvial fan (Hartley et al., 2010) hosting a flourishing biota. The biotic component of the ecosystem exerts a significant influence on the small scale topography, mainly in three ways : 1) the highly productive aquatic vegetation, 2) the foraging termites and 3) the big herbivores. Apart from the influence of tree growth (see details in Section 2.1.4), vegetation strongly influences water flow in the floodplains and channels. It is mostly comprised of *Cyperus papyrus* (Figure 2.22A) and *Miscanthus, Phragmites spp* in perennially inundated floodplains, while seasonal floodplains are covered by smaller emergent grasses and sedges. The primary production in the floodplains is intense and the dense roots, combined with accumulating peat and trapped sands form the permeable levees confining rapid flow. Peat accumulation on the edges of channels also forces water to flow on topographic highs in some channels (McCarthy et al., 1991; Tooth and McCarthy, 2004).

This high primary production is moderated over decades by the occurrence of fires. While peat can accumulate to thicknesses of 3 to 4 m, the frequent fires occurring in the Delta level previous organic sedimentation by removing about 90% of accumulated peat (Ellery et al., 1993; Heinl et al., 2006). The other organism responsible for the primary production removal is the termites, mainly representated by *Macrotermes michaelseni* (Dangerfield et al., 1998). Termite mounds (Figure 2.22C) are ubiquitous in the Delta. They can reach 4 m high, 2 m deep, with a 50 m^2 base. Termite mounds not only create local topographic highs allowing island initiation (McCarthy et al., 1998), but also redistribute sediments between the floodplains to the islands to form their mounds. Mounds are built by concentrating clays. New and old abandoned mounds are much more resistant to flow-driven erosion, and these concentrations of clay in the sedimentary pile are often involved in flow path control. Finally, termites play a crucial role as a sink for nutrients, as they forage grass and woody litter so efficiently that they are competitors with wild and domestic herbivores (Dangerfield and Schuurman, 2000). Termites are landscape architects in the Delta.

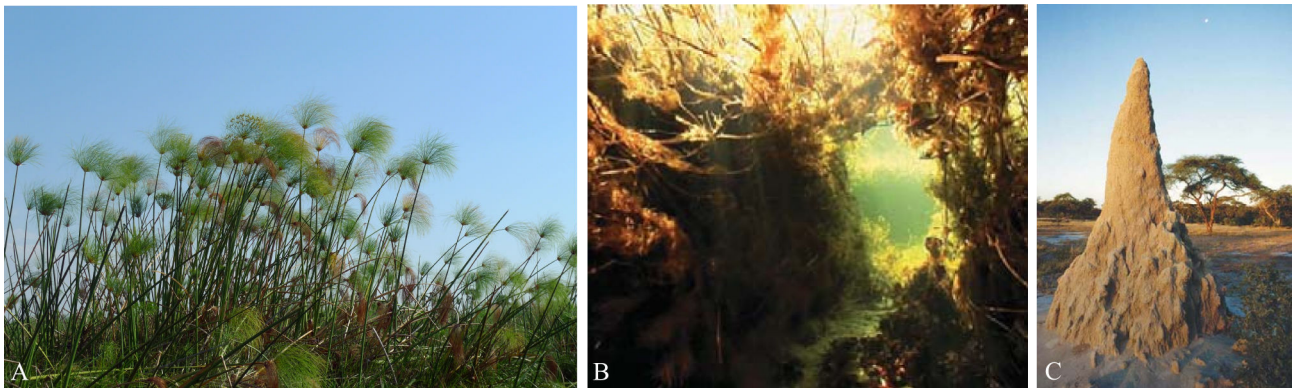

FIGURE 2.22 – Influence from the flourishing ecosystem. A : Papyrus host the edges of channels. B : Hippopotamus path under floodplain. C : Termite mound. (Source : `www.earth-touch.com` in Mendelsohn et al. 2010 for B and C).

The movements of big herbivores, mainly elephant paths and hippopotamus tunnels (Figure 2.22B), disturb the floodplains. Repeated movement to feeding grounds maintain pathways devoid of vegetation in the floodplains. These paths of preferential flow can encourage channel avulsion by initiating new channels, act as nodes between distinct channels or even lead to lake formations (McCarthy et al., 1998).

Unlike the other processes, the influence of the ecosystem is only significant at a decadal to multi-centennial time scale, but due to the repeated peat fires removing all traces of organic matter stored in the ground, not much organic matter is conserved. Obviously, while the ecosystem exerts a certain influence on the flood, it is completely dependent on the distribution of water, and particularly, on the maximum extent of the flood (Lindholm et al., 2007).

Chapitre 3

Origin of the signal of deformation of the ground surface

3.1 Introduction

Astride the Okavango Delta, the ground surface is currently deformed by two main processes : seasonal hydrological loading and tectonics, which impact the GPS signal differently (Figure 3.1). To discriminate the contribution of each process, it is necessary to understand in which manner they impact the deformation. The hydrological seasonal loading induces a vertical periodic annual signal, as the Earth's crust flexures during the rainy season under the pressure of the mass of water pouring into the basin (e.g., van Dam et al., 2007; Chanard et al., 2014). When water leaves the system during the dry season, through evapotranspiration in the Okavango basin, the surface relaxes and rises. This periodic signal is not only visible on the vertical component, where its amplitude can reach several centimeters, but also on the horizontal ones as the flexure of the surface displaces the stations towards the center of the loading. The direction of the observed horizontal displacement thus differs depending on the location of the station relative to the distribution of the loading. This horizontal displacement is nevertheless much lower than the vertical one. With variable rainfall and evapotranspiration over the years, the recharge or discharge of the aquifer implies inter-annual loading variations, hence a pluri-annual trend in the GPS signal. Tectonics impact the observed GPS signal in two possible ways : a linear trend revealing the overall deformation, and potentially sudden offsets induced by seismic activity.

To disentangle the contribution of each process, it is possible to model the crustal flexure consequent on seasonal hydrological loading (e.g., Tregoning et al., 2009; Fu and Freymueller, 2012; Wang et al., 2017). Indeed, GRACE satellites provide periodic data on the Earth's gravity field, which variations reveal integrated variations in the distribution of mass at all spatial scales. Variation in mass distribution occurring at the annual time scale can be interpreted as variations in storage of surface and groundwater (Tapley et al., 2004), i.e. TWS variations. These variations are observed to be surprisingly high in the Okavango-Zambezi basin, both in terms of annual amplitude and long-term accumulation over the past 15 years (Ramillien et al., 2008, 2014; Hassan and Jin, 2016). If this interpretation is valid, then the temporal variations of mass distribution provided by GRACE data products allow the modelling of the crustal flexure inducing ground surface deformation under the pressure of the

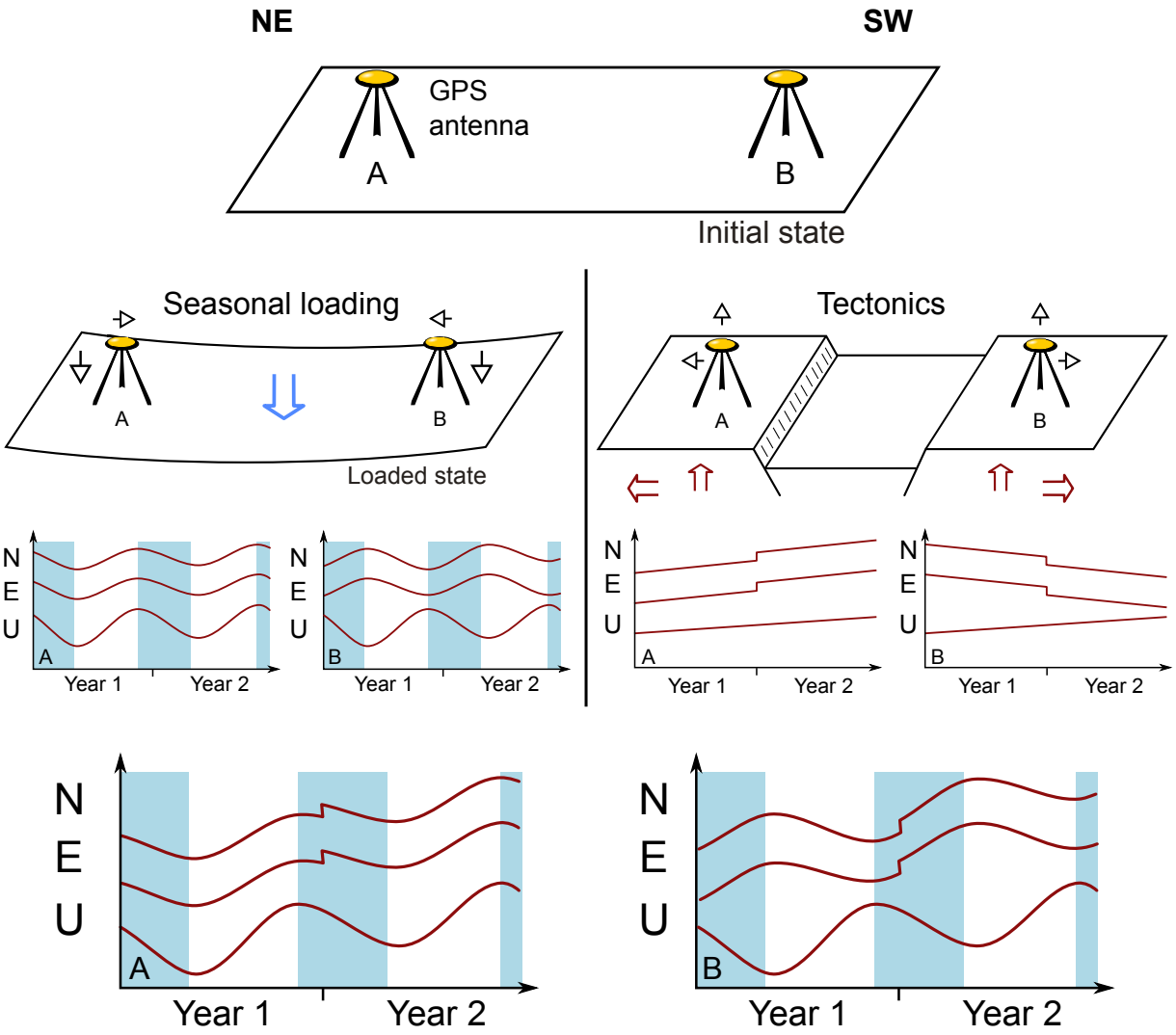

FIGURE 3.1 – Schematic principle of surface deformation under influence of both regional seasonal loading and tectonics, as seen in the GPS signal of two theoretical stations. Left : during the rainy season (blue bars), the excess of water flexures the crust, inducing a vertical and horizontal displacement of the GPS stations. They subside and move towards the center of the loading. The dry season allows the relaxation of the crust due to evapotranspiration in the basin. In case of complete relaxation, the stations move backwards to their initial position. Right : tectonics can provide steady displacement through fault creep or vertical displacement. Earthquakes of high enough magnitude can induce sudden offset. Bottom graphs : resulting signal observed at the GPS stations. N : North, E : East, U : Up

---

hydrological seasonal loading. As no other process is expected to induce a surface deformation in the area, the residual signal after removal of the crustal flexure consequently potentially reveals the tectonic component of the deformation observed in the GPS time series. To provide Equivalent Water Height (EWH) variations, processing of GRACE data products is subjected to several models and interpretations, thus hypotheses. GRACE solutions therefore

require better constraints to validate the amplitude and origin of the final interpretation. Such constraints are available through the surface deformation observed in the GPS time series.

3.2 Data and Methods

3.2.1 Surface deformation monitoring : GPS time series

The deformation of the surface is monitored in the area by three permanent GPS stations from the UNAVCO/AfricaArray (data available on the UNAVCO's server or on the AfricaArray's server : `afrefdata.org`), located in Maun, Botswana (MAUA), Rundu, Namibia (RUND) and Mongu, Zambia (MONG, see locations on figure 2.10). All stations were set up in August 2010 and are still active, but RUND and MONG are not connected to the Internet and downloads of the data can be intermittent. The MAUA station is located slightly SE of the Thamalakane fault, thus on the edge of the upthrown block of the graben. The RUND and MONG stations are located on the northern block, as no additional major fault has been determined between the Gumare fault and these two GPS stations. While the MAUA and RUND stations are located in the Okavango basin, the MONG station lies along the Upper Zambezi. 26 permanent stations from the International GNSS Services (IGS) or UNAVCO/AfricaArray are used to complete the network (see complete network configuration in Pastier et al. 2017 in Section 5.1).

The *gamit/globk* 10.61 processing software (Herring et al., 2015) was used to compute daily solutions in ITRF14 (Altamimi et al., 2016) for the stations, adjusting IGS final orbits and estimating tropospheric parameters (1 tropospheric zenith delay/2 h, 2 couples of horizontal gradients/day). The VMF1 Mapping function (Boehm et al., 2006), the ocean loading model FES2004 (Lyard et al., 2006), atmospheric loading according to Tregoning and van Dam (2005), and the absolute antenna phase center variation model IGS08 were used. The Kalman filter GLOBK was used with the "real-sigma" strategy (Reilinger et al., 2006) to determine final velocities for the stations for the horizontal components and first order velocities for the vertical rates. The reference frame is set up by constraining 19 IGS stations to their ITRF14 velocities.

The time series provided by GPS monitoring are unique continuous and quantified insights to the evolution of the surface through time. The accuracy henceforth available reveals small scale displacements, of only a few millimeters. But certain facets of this method require careful attention. The actual parameter of GPS is the travel time between the satellites and the GPS antenna. As mentioned above, the interpretation of the observed signal is not straightforward. Rigorous and accurate processing of the data is extremely model-dependent. Consequently, although similar at first order, solutions may vary depending on the processing software used, the set-up of the processing, models used for tropospheric delay, ocean and atmospheric loading, etc. These considerations are of great significance in areas of tenuous deformation.

Moreover, the final solution is also dependent on the geometry of the station network. 29 stations is not a very dense geodetic network for GPS computing, but Africa is not as densely instrumented as Europe or North America. As South Africa is much more instrumented than

the other countries in southern Africa, the least continuous South African stations were not taken into account so as not to bias the signal with too many stations in the south. This selection process permits a satisfactory distribution of stations for this study.

3.2.2 GRACE data products

The Gravity Recovery And Climate Experiment (GRACE) is a space mission jointly run by the National Aeronautic and Space Administration (NASA) and the Deutschen Zentrum für Luftund Raumfahrt (DLR). It consists of two satellites recording the Earth's gravity field variations periodically, about every 10 days (Tapley et al., 2004). Launched in 2002, the GRACE gravity satellite mission has revolutionized the way large mass changes can be detected on Earth by monitoring the temporal variations of Earth's gravity field through the variation of the distance between the two satellites despite their following the same orbit. GRACE is the first temporally (semi-)continuous record of the Earth's gravity field, and thus brings brand new insights into many processes. Moreover, the accuracy of the measurements of the gravity field by the satellites is higher than any previous gravimeter, allowing the quantification of the subtle variations produced by temporal variations of TWS for the first time. It also allowed the production of models for the Earth's gravity field with unprecedented accuracy, up to 1 cm for the geoid elevation (e.g., Tapley et al., 2005). The mission was decommissioned in October 2017, due to a battery failure in GRACE-2. A new pair of satellites, GRACE Follow-On, is scheduled for launch in boreal spring 2018.

The temporal variations of the distance separating the satellites and their effective orbits (Level 0 data product) can then be interpreted in terms of variations of the Earth's gravity field (Level 1 data product) and finally in terms of continental EWH (Level 2 data product). The spatial resolution of the final data set approaches 300 km. Different laboratories produce their own solution : The Center for Space Research (CSR), Austin, Texas, the Jet Propulsion Laboratory (JPL), Pasadena, California and the Helmholtz Centre (GPZ), in Potsdam, Germany are official centers. Other laboratories develop their own solutions, as the Centre National des Etudes Spatiales (CNES) and the Groupe de Recherche en Géodésie Spatiale (GRGS), in Toulouse, France (Figure 3.2).

The GRACE Level 2 product also consists of a set of Stokes coefficients, which are dimensionless coefficients of the spherical harmonic (SH) expansion of the gravity field. The final products provided by the different laboratories can be classified as unconstrained solutions, such as CSR, GFZ, JPL (see Bettadpur, 2012), or constrained solutions such as CNES/GRGS (Bruinsma et al., 2010). Changes in Stokes coefficients from month to month allow computation of maps of spatial water mass variations (Wahr et al., 1998).

Globally, seasonal to long-term variations are similarly captured by different GRACE solutions (Sakumura et al., 2014). However, significant differences occur at the regional scale (e.g., Farinotti et al., 2015). Such differences reflect the varying computational strategies and are related to : 1) the use of different background models to compute and remove the contribution of atmospheric and oceanic mass changes, 2) the inversion method used to estimate the Stokes coefficients and 3) the associated spectral content (maximum degree n) and signal to noise ratio. Furthermore, unconstrained solutions generally show prominent North-South striping related to the amplification of uncertainties in the background models,

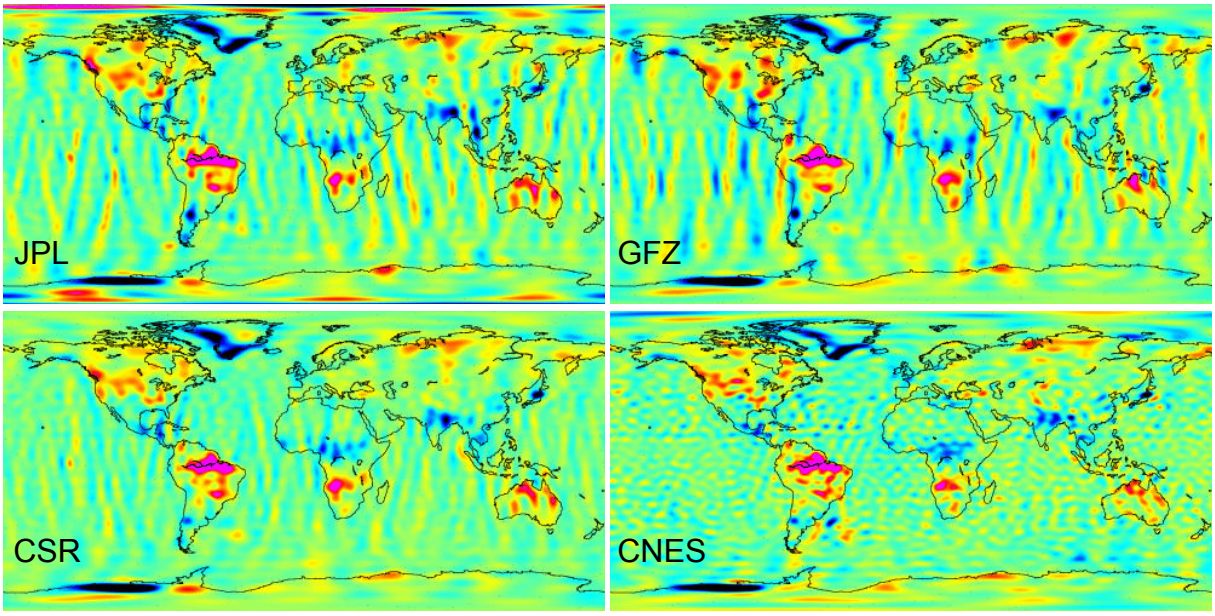

FIGURE 3.2 – Maps for the four GRACE solutions used in the study, after the intensive rainy season of 2010-2011, May 2011. All solutions show a major accumulation of water for the Okavango-Zambezi basin. Note the stripes on the unconstrained solutions (CSR, JPL, GFZ) opposite to the constrained solution (CNES/GRGS). Maps were made with `www.thegraceplotter.com`, courtesy of CNES/GRGS.

---

and the increasing noise with increasing degree (e.g., Save et al., 2012). Post-processing is therefore required, with the dual goal of noise suppression and conservation of spatial resolution (Longuevergne et al., 2010).

Two pairs of data sets of GRACE solutions are used in this study to evaluate the impact of processing and post-processing strategies on the estimation of vertical displacement :

- CSR products of SH degree 60, on a monthly basis, with different filtering strategies to remove the stripes :
  - the widely used Gaussian isotropic filter (Jekeli, 1981) in combination with a data-adaptative decorrelation filter as in Duan et al. (2009) (CSR5-60-gaussian)
  - the DDK-4 anisotropic filter, according to Kusche et al. (2009) (CSR5-60-dd4)
- GRGS release 3 (RL3v3) products, which provide gravity variations at 10-day time scale and high spatial resolution. In this product, a stabilization method is applied to avoid the creation of spurious stripes (Bruinsma et al., 2010). Two different SH degrees are tested :
  - degree 80, the maximum provided for this solution (GRGS-80)
  - degree 60, a smoother version to focus on the coefficients with the best signal to noise ratio (GRGS-60)

The JPL and GFZ solutions have been assessed as too strongly striped to be the most pertinent in such a regional study.

Low degree coefficients cannot be measured accurately by GRACE. Degree 1 coefficients,

describing the relative motion between the Earth's center of mass and a crust-fixed terrestrial reference frame, are therefore substituted following Rietbroek et al. (2012). Degree 2 coefficients, linked to the Earth's oblateness are also updated following Cheng and Tapley (2004). Finally, the time series are corrected from the Glacial Isostatic Adjustment (GIA) to focus on surface mass redistribution. GIA is the ongoing viscoelastic relaxation of the Earth in response to the presence of large ice masses in the past. The model ICE-5G is used herein (Geruo et al., 2012), although the impact of GIA is negligible over the Okavango and Zambezi basins, below ∼1 mm/yr EWH or 0.05 mm/yr in terms of vertical deformation.

The unprecedented insight GRACE brings to large scale studies of hydrological systems must, however, be validated. Two methodologically demanding consecutive inversions are at play in the retrieval of the variations of EWH, based on several hypotheses. Another potential source of error lies in the multiple potential sources of gravity field, from the core to the atmosphere. Other influences can come from sediment accumulation, or crustal displacement related to strong earthquakes (Mikhailov et al., 2013). Like GPS time series, GRACE data products are strongly model-dependent, and their interpretation as water height variation should not be straightforward. As GRACE data products are global large-scale products, quite recently available, they are still not strongly constrained particularly at the regional scale. Gradually, studies over precisely delineated, monitored basins progressively validate the data sets and strengthen GRACE inversions. In the Okavango-Zambezi basin, GRACE solutions have yet to be validated.

3.2.3 Vertical deformation modelling from GRACE data products

The loading theory describes how surface mass distribution impacts different kind of geodetic variables (Farrell, 1972), and how these variables are linked. The vertical displacement u of the Earth's surface can be computed by summing the GRACE Stokes coefficients C_{nm} and S_{nm} :

$$u(\theta,\lambda,t) = a\sum_{n=0}^{n_{max}}\sum_{m=0}^{n}\frac{h'_n}{1+k'_n}P_{nm}(cos\theta)(C_{nm}(t)cosm\lambda + S_{nm}(t)sinm\lambda) \tag{3.1}$$

where a is the mean radius of the Earth, P_{nm} are the fully normalized Legendre functions, n and m are degree and order, θ and λ being the colatitude and longitude of the point of interest, n_{max} is the maximum degree described by the GRACE solution. The Love numbers h'_n and k'_n describe the elastic response of the Earth's to the surface load for each degree n. They have been derived from the PREM model by Guo et al. (2004).

3.3 Results and discussion

3.3.1 GPS time series

Figure 3.3 shows the time series for daily solutions of the MAUA, MONG and RUND stations surrounding the Okavango graben. The horizontal components are plotted detrended relative to the MAUA station in order to highlight the intra-continental displacement across

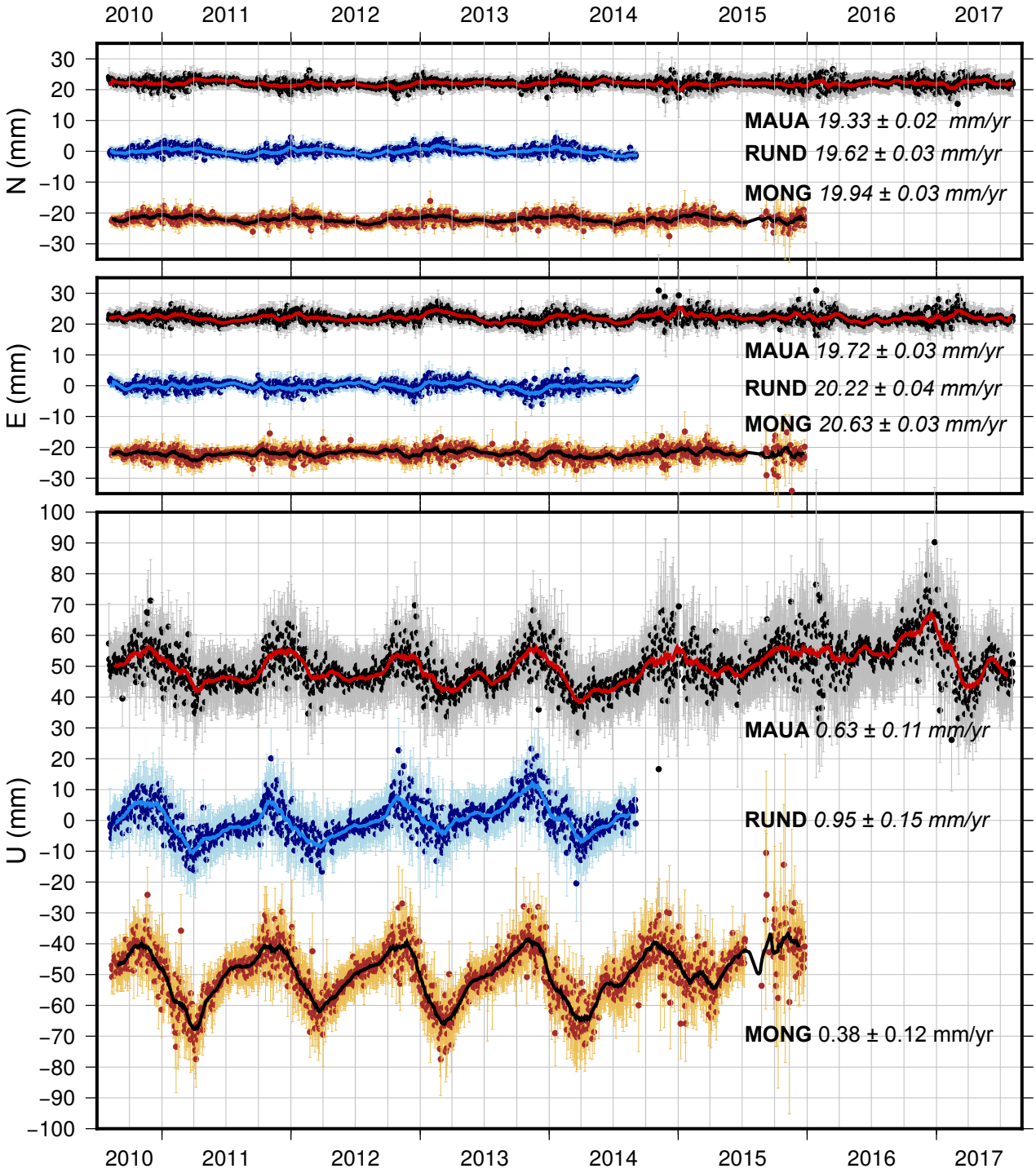

FIGURE 3.3 – GPS time series for the three AfricaArray stations surrounding the Okavango graben, with velocities provided by *gamit/globk* for each component. Horizontal components for RUND and MONG are detrended relative to MAUA.

the graben. As anticipated, all time series show both a periodic annual signal, principally in the vertical component, and a long-term trend. In the horizontal components, the influence of inter-annual variations of the hydrological loading can be considered as negligible on the linear trend. The annual displacement rate provided by *globk* for the north and east components can thus directly be attributed to the tectonic deformation and are discussed in Section 5.1.

In contrast, the vertical component is highly impacted by the annual periodicity, the amplitude of which is far greater than the long-term trend. The vertical long-term trend is thus a combination of tectonic deformation and inter-annual variation of hydrologic loading. The peak-to-peak amplitude of the GPS signal is approximately 2 to 3 cm, slightly inferior to the seasonal deformation occurring in Nepal (Fu and Freymueller, 2012) or in the Amazon basin (Davis et al., 2004). This amplitude varies between both stations and years. MAUA shows the least amplitude with the highest occurrence in 2013-2014, a year of massive rainfall in the basin, reaching 2 cm. RUND's signal is less smooth as its peaks are more visible. The highest amplitude is also reached in 2013-2014, with 2.5 cm. MONG shows the highest amplitude, reaching 3.3 cm in 2010-2011. The difference in the amplitude of the response of the GPS stations of the two hydrological basins reveals the greater variations of TWS in the Zambezi basin compared to the Okavango.

The highest elevation is reached for all three stations in October-November, corresponding at the beginning of the rainy season. The surface then subsides by approximately 20 to 30 mm in 4 to 5 months. At the end of the rainy season (∼April), the surface rises due to the relaxation of the crust from unloading with water evaporating. The seasonal rise is slower than the subsidence phase and less steady, as all three stations slow down around July, or even sometimes stabilize or subside (as MAUA in 2013). This slowing down in the rate of rise is in phase in all three stations, but is more visible in MONG than in RUND. Such slowdowns can also be found in the phase of subsidence, as in 2013-2014, but are less frequent and conspicuous. The phase of uplift ends with a sudden rise of the stations of a few millimeters, along with an increase of the noise of the GPS signal.

The annual frequency is not always visible in the horizontal components. Their amplitudes only reach a few millimeters (see enlarged graph for horizontal components in Appendix A.1). Their semi-annual shifts are not in phase with the inversions of the vertical displacements, but exhibit a regular delay of three months. This behaviour is unexpected as horizontal displacements associated with crustal flexure are conventionally thought to occur simultaneously with the vertical ones (Chanard et al., 2014). However, the almost systematic slowdown during the period of rise is phased with an annual horizontal inversion.

3.3.2 Validation of GRACE interpretation

Figure 3.4 shows the comparison between the vertical displacement observed in the GPS time series and the vertical displacement estimated from the Stokes coefficients revealing the potential hydrologic loading provided by GRACE solutions. The RMS gives a relative indication of the difference of amplitude between two signals, while the correlation coefficient (CC) evaluates the co-evolution of the signals through time. A biased signal can thus have a good correlation coefficient, but a significant RMS. RMS and CC are calculated over the longest time span of data recovery, independently of hydrological years. The correlation is high between the observed and modelled deformation, with correlation coefficients up to 0.94

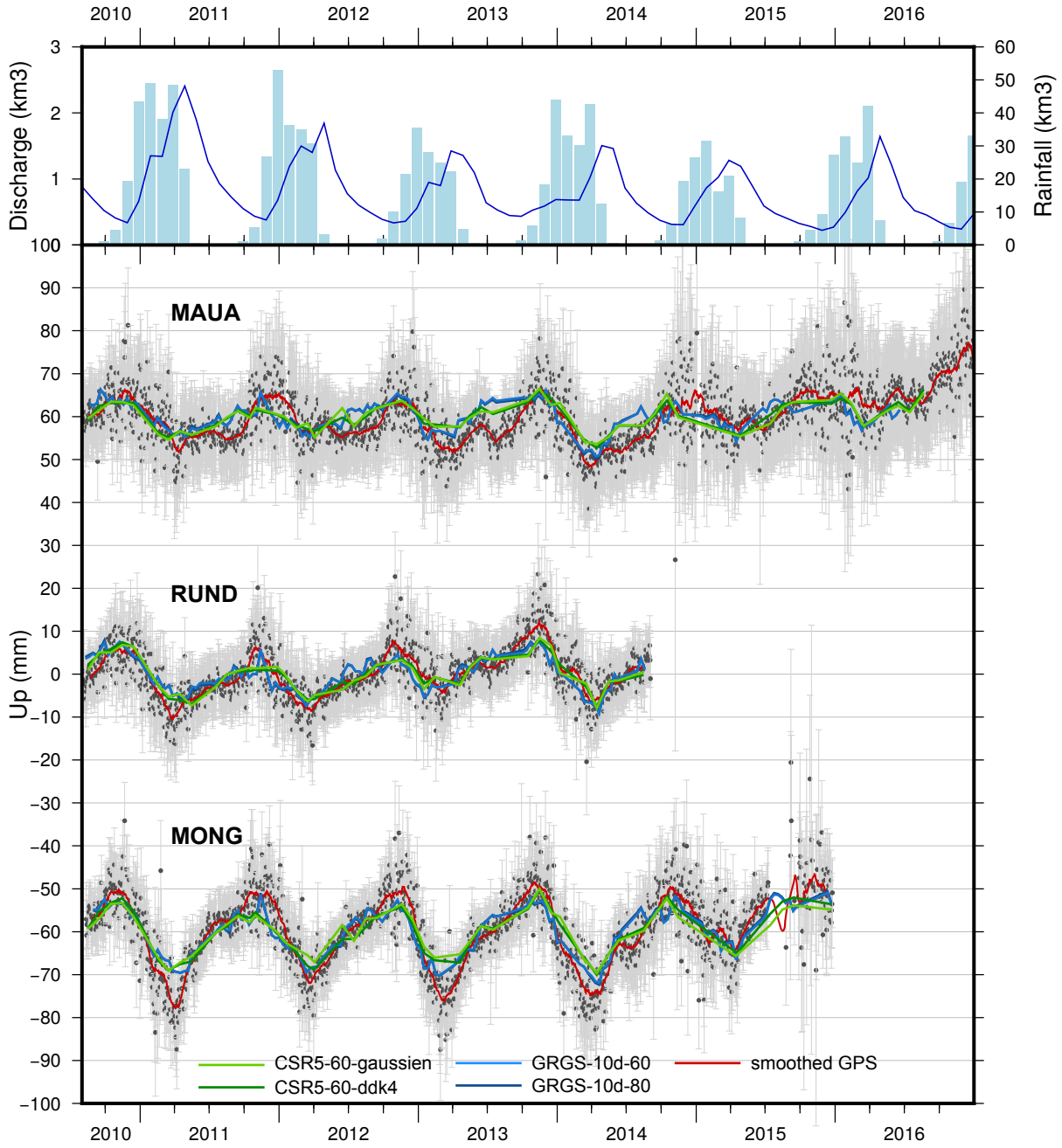

FIGURE 3.4 – Comparison between the GPS signal, the deformation modelled from GRACE data and the hydrological regime. Bottom plots show the surface deformation at the three GPS sites along with deformation modelled from GRACE data products for the four tested solutions. Top plot shows monthly integrated rainfall over the Okavango catchment area (moderated CHIRPS, see Section 4 for details about the data, light blue bars) and discharge in Mohembo (DWA, blue line).

(Root Mean Squares and Correlation Coefficients are summarized in Table A.1 in Appendix A.2). The correlation is very high for the stations in the Okavango basin (0.70 to 0.84) and satisfactory in the Zambezi basin (0.61 to 0.70). Stations in South Africa exhibit much lower, to negative, correlation coefficients, but these stations are also far less affected by seasonal hydrological loading due to lower precipitation.

The correlation is also high between the signals of deformation and the hydrological regime. The annual subsidence systematically occurs during the rainy season. The subsidence usually starts on the second or third month of rain, once more regular and heavy rains occur, for MONG and RUND. The signal is more noisy for the MAUA station which usually starts subsiding after three to four months of rain, at the peak of the rainy season. The subsidence stops precisely at the end of the rainy season for all three stations. RUND and MONG then abruptly rise, revealing the return of the domination of the evapotranspiration flux on the water balance, while MAUA can even stabilize for a few month. TWS decreases and the Earth's crust relaxes. The annual frequency observed in the GPS signal thus corroborates the GRACE hypothesis of an important aquifer with annual variations of high amplitude.

The correlation of the annual vertical deformation of the surface observed in the GPS time series in southern Africa with the hydrological regime is finally supported by the subtle inverse vertical displacements of the HNUS station. HNUS is located in a different climatic area, with a maximum of precipitation occurring in September (Nicholson, 2000). The highest elevation is reached for the station in March-April, opposite to November-December for the other stations, and the lowest elevation is reached at the end of the year, after the most humid month of September (see GPS time series and precipitation in Appendix A.1).

The four signals of deformation derived from the GRACE data products show very similar trends. Either the different SH degrees used for the GRGS solution or the different filtering methods used for the CSR solution do not provide significant differences in both RMS and correlation coefficients. In contrast, the difference is more visible between the CSR and GRGS solutions, with highest correlation coefficients (respectively 0.54 and 0.43) and lower RMS (respectively 2.93 and 3.34) for the CSR than for the GRGS solution. This difference may actually be due to the different time step of the two solutions. The 10 days period of the GRGS solution also induces more variations in the signal. In contrast, the temporal resolution of the GRGS solution allows a better observation of variation in the rate of relaxation than the monthly resolution of the CSR solution, partly reproducing some years the vertical slowdowns impact the phase of uplift. All signals are phased, with the highest elevation reached in November-December, and the lowest one in March-April.

Nevertheless, all the deformation signals derived from the four GRACE solutions used in this study globally underestimate the annual amplitude of the GPS signal. Figure 3.5 shows the mean annual amplitude of the deformation signals, computed over complete hydrological years. Despite lower correlation coefficients, GRGS solutions better reproduce the high amplitude of seasonal loading. Four hypotheses should be explored to explain this difference in amplitude :

— The GPS signal possibly overestimates the amplitude of the annual vertical displacements. The sudden increase in elevation occurring at the beginning of the rainy season (Figure 3.4) could be due to the arrival of the ITCZ. Masses of water vapor are carried in the troposphere, and possibly delay the GPS signal (Heleno et al., 2010). The

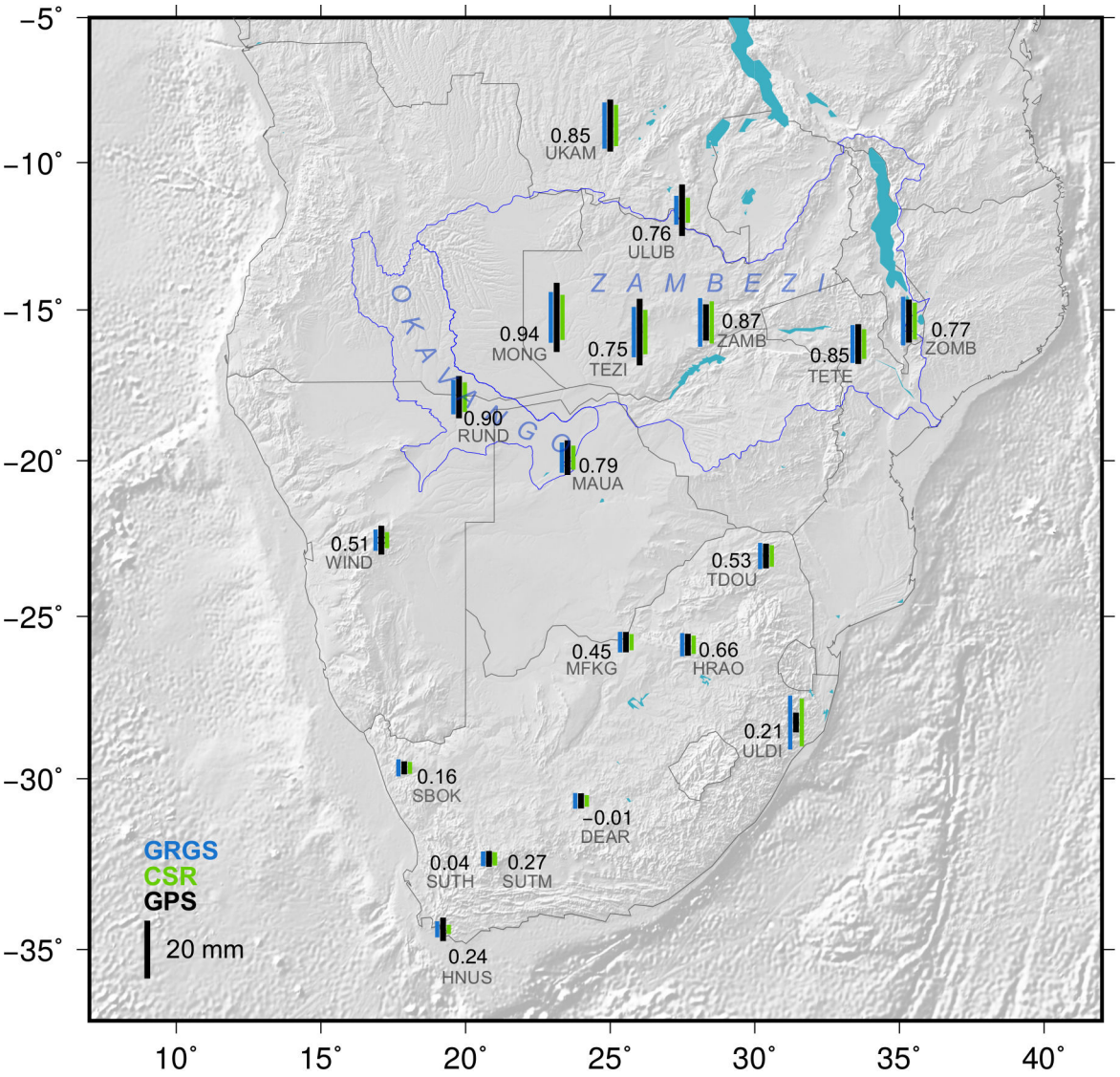

FIGURE 3.5 – Map of mean annual amplitudes of vertical surface displacements for the GPS signal (black) and the modelled deformation based on CSR-60-ddk4 (green) and GRGS-60 (blue) solutions. Correlation coefficients between the GPS signal and the CSR solution are indicated in black above each station's name. Annual amplitudes are globally well reproduced, but generally underestimated by the GRACE solutions.

---

increase in water vapor is also responsible for the increase of noise in the GPS signal.

— GRACE may underestimate the TWS variations. The final solutions depend on several hypotheses or computation processes, still requiring further development : models, such as the Earth's geoid, the precise determination of the satellites' orbits, based on GPS, the corrections for ranging variations unrelated to the Earth's gravity field, like the influence of the Sun and the Moon (e.g., Dahle et al., 2013), or spatial smoothing.

— Imprecision in the modelling of the deformation is another possible source of minimizing the crust flexure modelled from GRACE Stokes coefficients, notably the estima-

tion of the Earth's elastic modulus. The PREM structure used for the modelling of the flexure from GRACE solutions may not correspond to the actual locally thicker and colder crust and lithosphere. Moreover, the PREM structure does not reproduce the lateral variability of the Earth's structure in the study area (see Section 5). Moreover, the poor spatial resolution of GRACE does not allow the distribution of water masses heterogeneously in the basin. The flexure modeled from a homogeneous distribution of mass in the basin is thus different from the observed deformation, due to heterogeneous masses, possibly mobile. This hypothesis could be tested by using different crustal models, like CRUST1.0 in Chanard et al. (2014).

— Due to the nature of the substrate, poro-elastic deformation due to the recharge of TWS, either soil moisture or aquifer, is unlikely. Lenses of clay could locally provide a vertical deformation opposite to the loading flexure, but all three stations are impacted, revealing a large scale process.

Figure 3.5 shows a good validation of the GRACE signal for all the stations tested in southern Africa, as weak correlation coefficients are related to low annual amplitude, thus to an absence of seasonal loading. A few stations do not show good agreement between the GPS and GRACE signals. Apart from the very discontinuous GPS stations, which do not provide a reliable constraint to correlate the observed and modelled deformations (WIND, ULUB), two stations clearly exhibit significant differences in the annual period between the observed and modelled signals : ULDI and DEAR (Figure 3.6).

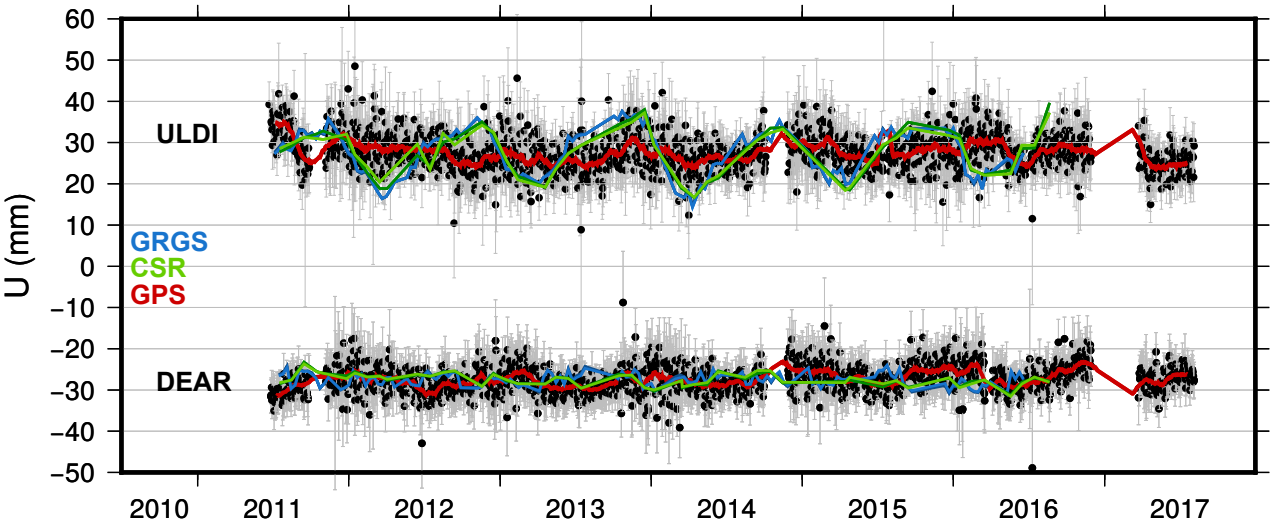

FIGURE 3.6 – Time series of vertical displacements for two stations showing divergence in the annual signal between the observed (GPS) and modelled (GRACE) displacements. Location of the stations is given in figure 3.5.

These stations exhibit a very tenuous annual signal in the GPS time series. Regarding ULDI, located near the South African eastern coast, GRACE predicts a seasonal vertical displacement with an annual amplitude of ∼20 mm for both CSR and GRGS solutions. Such an amplitude is not predicted for stations located closer to the Zambezi-Okavango basin

(HRAO, TDOU, MFKG). GRACE solutions tend to extend the area of important annual amplitude in the region of ULDI. The GPS time series from ULDI infirm this hypothesis. In contrast, the DEAR station shows a vertical annual signal, which is not predicted by GRACE. Two dams are located at 100 km NE and 150 km E of the GPS station, which are most probably responsible for local seasonal loading at a geographical scale too small for GRACE resolution. The seasonal flexure is not visible on the horizontal displacements time series.

The observed GPS signal and the deformation modelled from the GRACE solutions are in phase. Their periodicity is directly related to the hydrological regime. This correlation validates the annual variation of TWS seen by GRACE in the Okavango-Zambezi, in both terms of amplitude and phase. Hence, it is therefore possible to retreive the residual displacement due to potential tectonic activity.

3.3.3 Residual vertical displacement

Determination of residual vertical displacement

The vertical displacements modelled from GRACE solutions are subtracted from the GPS time series in order to remove the influence of the seasonal hydrological variations on the signal of the ground surface deformation and possibly retreive the tectonic deformation. The different temporal resolutions of the time series require the transformation of one series. The processing strategy used in this study is to degrade the GPS signal to match the GRACE temporal resolutions. Indeed, interpolating the GRACE solutions to subtract daily positions from the GPS signal not only preserves noise from the GPS, but also provides a greater residual annual amplitude. The GPS signal is first smoothed with a one month sliding average, consistent with GRACE resolution, and then resampled for each date comprising the GRACE signal.

Figure 3.7 shows the residual signal for each GPS station located in southern Africa. Due to the strong similarity between the different computational strategies for each laboratory, only two solutions are further tested : CSR-60-ddk4 and GRGS-60. The seasonality is still obvious in the remaining signal, which is mainly due to differences in the peak-to-peak amplitudes with GRACE deformation showing lower amplitude, as observed in the preceding section.

For all time series (GPS, GRACE and residual), final displacement rates are computed by linear least square regression. Time series are resampled to cover exclusively complete years, in order to address the seasonal variability. Interpolation is required to overcome the uneven temporal resolution of GRACE data products and the possible discontinuity of the GPS time series. The bias induced by the interpolation of the GPS time series is considered acceptable as long as the discontinuity does not cover an overly long period including a break in the slope of the vertical displacement. The influence of this process (interpolation and resampling over complete years) is visible in the different rates provided for the GPS stations, by *gamit/globk* over raw time series or by linear regressions over processed series (Table 3.1 and Figure 3.8).

Uncertainties

Retreiving the residual deformation signal despite the seasonal deformation due to hydrological loading from the GRACE data products is a method validated in dynamic contexts showing vertical rates of several mm/yr (Fu and Freymueller, 2012; Wang et al., 2017). In a more stable context, such as the interior of the Nubian plate, rates of deformation are expected to be lower. The uncertainty is crucial for further interpretation of final residual vertical rates close to 0 mm/yr. Low errors can then lead to misinterpretation of subsidence or uplift, and hence to great errors in terms of geodynamic interpretation.

The final minimum uncertainties associated to the residual vertical velocities (see last column of table 3.1) result from the association of the uncertainties related to the GPS time series, provided by *gamit/globk*, and the modelled deformation based on the GRACE solutions. In this study, the uncertainty associated with the modelled deformation based on GRACE solutions is defined by the difference between the two solutions. These uncertainties are for the most part greater than the residual vertical rates, especially for the CSR solution which provides lower final rates. Other possible sources of errors, not always quantifiable, must be taken into account along with these minimum quantifiable uncertainties. They can originate from differences in : 1) the processing of the GPS time series, 2) the modelling of the deformation from GRACE solutions or 3) the time span used for the computation of velocities.

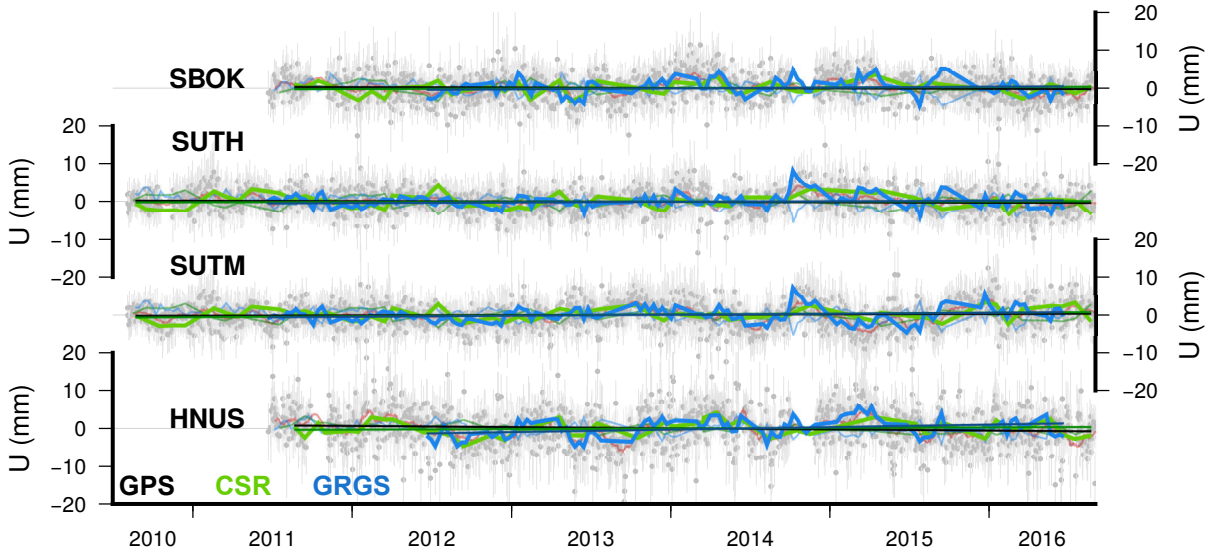

FIGURE 3.7 – Residual displacement after removal of vertical deformation modelled from GRACE data products to the GPS signal. Transparent lines are for GPS (black dots and red curve), GRACE-CSR (green) and GRACE-GRGS (blue) initial signals. Solid broken lines show the residual time series for each GRACE solution, straight lines show linear regressions for these time series. Stations are plotted from south (bottom graph this page) to north (top graph, last page), representing the increasing deformation due to seasonal hydrological loading.

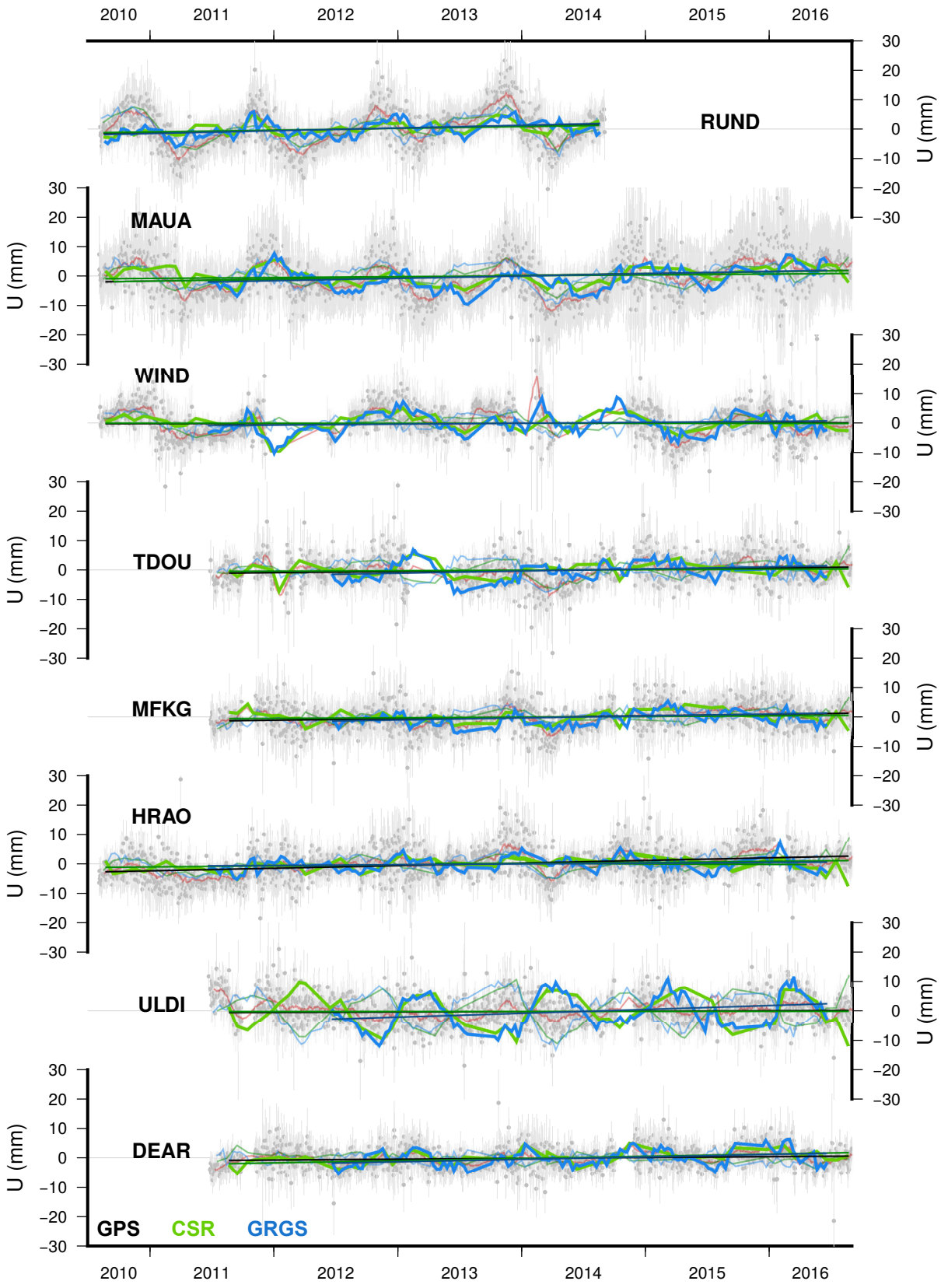
2010
2011
2012
2013
2014
2015
2016
RUND
MAUA
WIND
TDOU
MFKG
HRAO
ULDI
DEAR
U (mm)
30
20
10
0
−10
−20
−30
GPS
CSR
GRGS

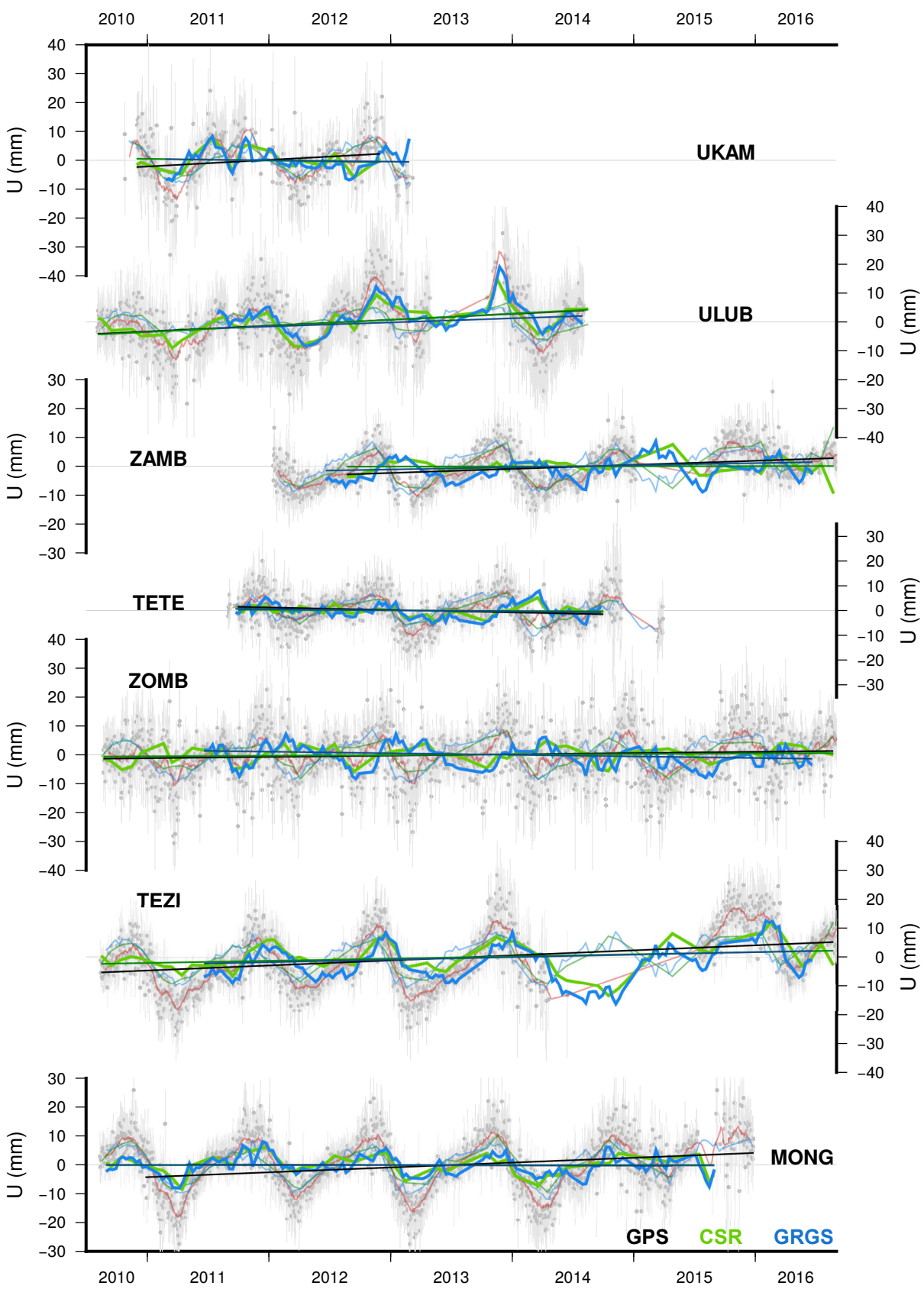
2010
2011
2012
2013
2014
2015
2016
U (mm)
UKAM
ULUB
ZAMB
TETE
ZOMB
TEZI
MONG
GPS
CSR
GRGS

Regarding the GPS processing, the difference in the vertical velocities between the SUTH and SUTM stations highlights the underestimation of the uncertainty provided by *globk*. The two stations are located at the same site, 135 m away from each other (see locations and time series for all GPS stations in Appendix A.1). The difference between their respective vertical displacement rates, over complete years, is greater (0.19 mm/yr) than the highest uncertainty provided by *globk* (0.13 mm/yr). As the stations are located in a particularly stable area, both tectonically and hydrologically, this difference provides a more realistic minimum uncertainty for the vertical displacement rates based on GPS time series.

Moreover, an important source of error initially lies in the definition of the reference frame used to define the GPS daily solutions and stations velocities. A new version of the ITRF, ITRF2014 (Altamimi et al., 2016), has been released recently. According to Altamimi et al. (2016), differences in vertical rates relative to the precedent reference frame, ITRF2008 (Altamimi et al., 2012), can reach 1 mm/yr. This value should thus be considered as a realistic error on the vertical rates defined in the ITRF2014. In the study area, the impact of the choice of the ITRF on the vertical rates is highlighted by the difference in vertical rates for the three stations, MAUA, RUND and MONG, which vertical rates have decreased by respectively 1 mm/yr, 0.52 mm/yr and 0.14 mm/yr from the ITRF2008 to the ITRF2014 (see solutions in ITRF08 in Pastier et al., 2017 in Section 5.1).

GRACE solutions are not only subject to uncertainty, but may also not be realistic, as the difference visible in the ULDI station time series, between the strong annual amplitude predicted by GRACE and the very low amplitude signal observed by GPS, indicates. Another source of error in the GRACE solutions relates to the spatial distribution of TWS over the basins, poorly defined by the satellites. This is revealed by the relatively homogeneous distribution of annual amplitudes in the GRACE solutions over the Zambezi basin, while the GPS stations clearly show higher amplitudes in the western part of the basin (MONG), relative to the eastern part (TETE, ZOMB). This lack of accuracy within the basin may also impact the estimation of the inter-annual trend. Then, the low spatial resolution of the GRACE satellites does not allow the recording of local variations of masses, as in the DEAR station. The modelled deformation then does not compensate these local effects. Due to this uncertainty, it is not possible for stations impacted by local effects to confirm that the residual displacement rate is free of inter-annual hydrological loading variations without further modelling and local hydrological data.

Finally, the time span used for the computation of the velocities also impacts the final residual rates especially for the stations showing the strongest annual amplitude. MONG shows the highest difference with a vertical rate up to 1.54 mm/yr if computed over the latest period (12/2010 to 12/2015, see Figure 3.7). This issue is particularly important for time series covering only a few years. In this study, the initial dates for the computation of linear regressions depend only on the availability and reliability of the GPS time series and vary among stations. These dates should ideally be constant within time series, but it was found preferable to preserve as many years as possible due to the relative shortness of the GPS time series.

Station	GPS *glob*k	Error *glob*k	Processed GPS	CSR	Residual (CSR)	GRGS	Residual (GRGS)	Error GRACE	Final error
HNUS	-0.06	0.07	-0.29	-0.43	0.14	-0.94	0.65	0.51	0.58
HRAO	0.84	0.17	0.63	0.77	-0.14	0.38	0.25	0.39	0.56
MAUA	0.63	0.11	0.63	0.34	0.29	-0.16	0.79	0.50	0.61
MFKG	0.95	0.25	0.50	0.29	0.21	-0.17	0.67	0.45	0.71
MONG	0.38	0.12	-0.10	0.36	-0.46	-0.02	-0.08	0.38	0.50
RUND	0.95	0.15	0.79	0.20	0.59	-0.14	0.93	0.34	0.49
SBOK	-0.06	0.06	-0.11	-0.24	0.13	-0.34	0.23	0.10	0.16
SUTH	-0.18	0.04	-0.09	-0.13	0.04	-0.24	0.15	0.11	0.15
SUTM	0.10	0.13	0.09	-0.13	0.22	-0.18	0.27	0.05	0.18
TDOU	0.34	0.09	0.40	0.24	0.16	-0.32	0.72	0.56	0.65
TETE	-0.89	0.22	-0.96	-0.75	-0.21	-0.51	-0.45	0.24	0.46
TEZI	2.69	0.08	1.73	0.99	0.75	0.87	0.86	0.12	0.20
UKAM	-0.24	0.70	2.26	2.87	-0.61	2.71	-0.45	0.16	0.86
ULUB	1.19	0.31	2.02	-0.11	2.13	0.61	1.41	0.72	1.03
ULDI	-0.30	0.08	0.15	0.13	0.02	-1.14	1.28	1.26	1.34
WIND	-0.07	0.07	0.05	0.07	-0.02	-0.26	0.31	0.33	0.40
ZAMB	1.02	0.07	1.40	1.35	0.05	0.67	0.72	0.68	0.75
ZOMB	0.63	0.10	0.44	0.23	0.20	0.97	-0.54	0.74	0.84

TABLE 3.1 – Vertical displacement rates provided by *gamit*/*glob*k for the GPS time series, and recomputed over complete years for the GPS permanent stations, the deformation modelled from GRACE solutions and the residual signal after removal of the GRACE based signal, provided in mm/yr. Corresponding linear regressions are plotted in figure 3.7.

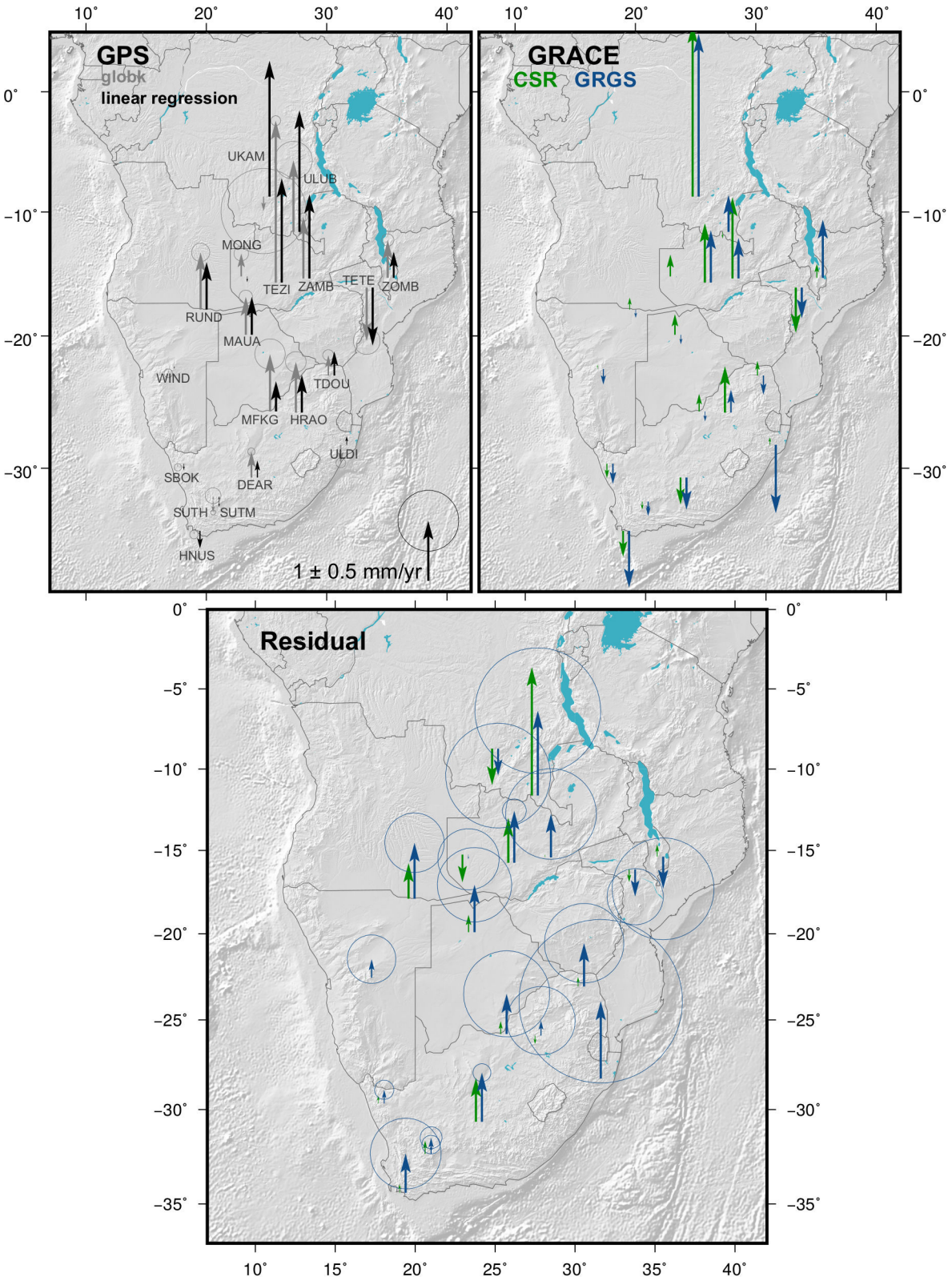
GPS
globk
linear regression
GRACE
CSR GRGS
Residual
UKAM
ULUB
MONG
TEZI
ZAMB
TETE
ZOMB
RUND
MAUA
WIND
TDOU
MFKG
HRAO
ULDI
SBOK
DEAR
SUTH
SUTM
HNUS
1 ± 0.5 mm/yr
10°
20°
30°
40°
0°
−10°
−20°
−30°
−5°
−15°
−25°
−35°
15°
25°
35°

FIGURE 3.8 – Vertical inter-annual displacement rates in southern Africa. Top maps show the rates provided by *gamit/globk* (grey), and recomputed over complete years for the observed GPS time series (black), the rates provided by the deformation modelled from GRACE solutions (green for CSR and blue for GRGS). Bottom map shows the residual displacement rates obtained for each GRACE solution. The associated uncertainty is for both solutions but is only plotted relative to the GRGS solution for a better readability.

Discussion

Figures 3.7 and 3.8 show a good fit between the deformation of the surface observed by the GPS and the deformation modelled from GRACE solutions. All low correlation coefficients affect stations with a very low annual signal. This is corroborated by the fact that the lowest RMS is associated with these stations. The high correlation coefficients as well as the validation of the annual vertical amplitude support the confidence of the modelling of the ground surface deformation based on GRACE solutions to reproduce the impact of inter-annual evolution of TWS.

Yet some divergences between the two signals appear. Due to its low sensitivity to the spatial distribution of the mass anomaly, GRACE predicts similar annual amplitude of vertical deformation for all the stations in the Zambezi basin. In contrast, the GPS time series exhibit more variable annual amplitude. The annual vertical amplitude is maximum at the westernmost MONG station (24 mm), decreases eastward to reach a minimum at the central ZAMB station (12.5 mm) and increases again towards the Indian Ocean coast (14.9 mm at ZOMB).

Many stations, notably in the Zambezi basin, are also impacted by local effects. The high annual vertical amplitude visible at the TEZI station may partly result from the seasonal recharge of the neighbour Itezhi-Tezhi dam (see location of the GPS station in Appendix A.1). In a similar way, it is possible that the explanation of the increase in the annual vertical amplitude from ZAMB to TETE and ZOMB lies in the seasonal loading of lake Malawi. Further examination of the GPS time series, including the horizontal displacements can help to discriminate these local effects. It is then possible to better constrain the spatial distribution of TWS variation (see Section 4.2).

Vertical velocities derived from the GPS time series show a global uplift over the Okavango-Zambezi, extending as south as the north of South Africa. Velocities derived from the vertical deformation based on GRACE data products reveal that this uplift is at least partly due to the discharge of TWS over the past six years, especially in the eastern part of the Zambezi basin. The two GRACE solutions provide overall similar inter-annual trends, but differ on particular stations, especially on the edge of the basin, with maximum differences obtained for ZOMB and ULDI with $\sim$1 mm/yr of difference. GRGS solution also generally provides more subsiding vertical rates.

The residual vertical rates visible in figure 3.8 consequently differ. In agreement with the higher correlation coefficients, the CSR solution provides inter-annual vertical displacement rates closer to the GPS ones than the GRGS solution. Consequently, modelling the seasonal hydrological loading based on this solution tends to smooth residual vertical displacements,

with the exception of the two DRC stations, UKAM and ULUB, and the locally impacted DEAR station. Residual rates then show a globally stable sub-continent, relatively to the uncertainty of the GPS, but with uplift at most stations located between Lake Tanganyika and MAUA, up to ∼2 mm/yr at ULUB. In contrast, the GRGS solution provides globally higher residual vertical rates. The difference is mostly visible in the southeastern part of the continent, and produces an overall uplift of the sub-continent exceeding 0.5 mm/yr. Implications in terms of tectonics and geodynamics are discussed in Section 5.2.

The differences between the GRACE solutions combined with the uncertainties of the GPS processing and the short time span of the GPS time series provide final uncertainties generally greater than the residual vertical rates. Yet this study highlights the predominant influence of seasonal hydrological loading on the vertical deformation of the surface in southern Africa. Although the final residual rates exhibit great uncertainty, this study validated that correcting the vertical displacements of GPS time series with the surface deformation modelled from the GRACE solutions is a necessary prerequisite to further investigations regarding the vertical deformation of the surface in southern Africa.

The method is promising in the study area, despite the present uncertainties, notably due to the constant improvement of the Earth's reference frame. Another perspective of improvement lies in a better constraint of GRACE solutions based on a more detailed examination of the GPS time series. The distribution of vertical deformation, as well as the amplitude and phase of the annual signal impacting the horizontal components, allows a better determination of the distribution of the loading in the basins (see Section 4.2), which could allow in turn a better modelling of the consequent deformation.

3.3.4 GPS time series peculiarities

The GPS time series of the stations located in the Okavango-Zambezi basin show two systematic peculiarities, particularly visible in figure 3.9 for the MONG station. First, the inflexions visible on the horizontal components are out-of-phase relative to the inflexions on the vertical components by ∼3 months. Then, the horizontal displacements exhibit a systematic slowdown during the period of rise, possibly leading to transitory subsidence. Such a slowdown is also visible during the subsidence period, but is less pronounced and does not occur in a systematic manner.

Different hypotheses can explain one or both these peculiarities. Climatic variations can be responsible for non-linear variations of TWS during the rainy and dry seasons, with bimodal distribution of rainfall in the rainy season and temporary drastic decrease of ET during the dry season. The 10 day resolution of the GRGS solution for GRACE data products allows the recording of such variations (Figure 2.12), which also appear in some years in the modelled deformation (Figure 3.4), especially during the dry season. But temporal variations in the rates of accumulation and discharge of TWS would not affect the phase of the horizontal annual deformation signal. Thus, while this climatic hypothesis alone cannot explain all the peculiarities of the GPS time series, it is at least partly responsible for the non-linear rates of subsidence and uplift on the vertical component.

Two hydrological hypotheses can also be proposed to complete the climatic one. First, circulation of surface and groundwater within the basins could be responsible for temporal

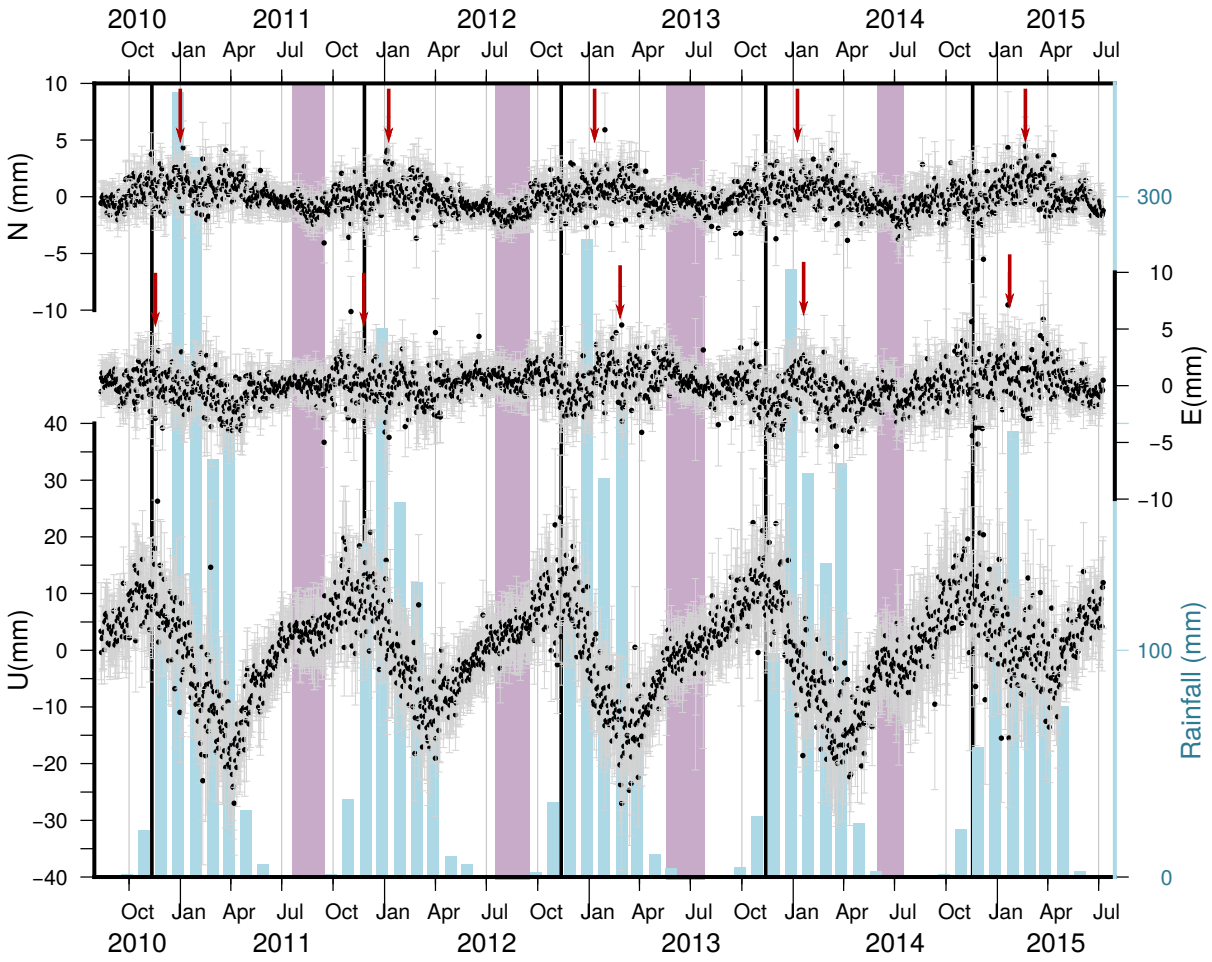

FIGURE 3.9 – Peculiarities in the GPS time series for the MONG station and monthly precipitation from CHIRPS for the location of the GPS station. Purple areas indicate periods of vertical slowdowns, corresponding to semi-inflexion of the horizontal components. The red arrows indicate the other semi-annual inflexion of the horizontal components.

---

variations in the distribution of TWS. Such circulation would not only disturb the vertical rates but also the phase of the horizontal components. Indeed, a water body passing by a GPS station during the dry season would 1) slow down the relaxation of the crust in its vicinity while getting closer and 2) shift the horizontal displacement from the direction of arrival of the water body to the direction of removal. These climatic and hydrologic hypotheses are discussed in Section 4.2. Temporal variations in the spatial distribution of TWS could also occur in the basins without any circulation of water, but under the influence of the distribution of rainfall. The stations could be under the influence of two areas of main TWS accumulating and discharging at slightly different paces over the rainy season. While the areas of TWS accumulation would jointly participate to the vertical deformation, they would compete on the horizontal components. Different rates of TWS increase and decrease could shift the main influence on horizontal displacements from one area of main TWS variations to the other.

Finally, a rheological hypothesis can be proposed, due to the particularly long and complex tectonic history of the subcontinent. The presence of a belt of younger crust and lithosphere of Damaran age between two Archean thick cratons (see Section 5.1) provides a strong rheological contrast. The particularities of the WIND station, showing a possible extension of the crustal flexure further than modelled could possibly be explained with different rheological parameters. Moreover, according to Chanard et al. (2014), the phase of the horizontal components are strongly related to the rheological properties. This hypothesis suggests that there is much to be learned from modelling the horizontal displacements due to the seasonal hydrological loading, which has not been realised in this study.

3.4 Conclusion

The GPS time series in southern Africa are impacted by both seasonal hydrological loading and long-term tectonics. The inter-annual trend of the horizontal components can be directly interpreted in terms of tectonics (see Section 5.1). But the vertical displacements exhibit a strong annual signal revealing the strong influence of hydrological loading. The gravity field variations provided by GRACE satellites allow the modelling of the crustal flexure due to this loading, which shows a very good fit with the observed GPS time series. The consistency between the GPS and GRACE-derived time series validates the GRACE observations regarding important TWS occurring in the Okavango-Zambezi with high annual amplitudes of variation.

GRACE data products thus provide a new proxy for one of the main unknowns of the hydrological systems, TWS. Its poor spatial resolution only provides an overall overview of the storage variations, smoothed over the two basins, but this overview is the first of its kind. This new proxy is not only crucial to a better understanding of the system, but also provides a new constraint for hydrological models (see Section 4.1).

Modelling the deformation from GRACE's gravity field variations shows that the seasonal hydrological loading and its inter-annual variations are responsible for an important part of the vertical deformation observed in southern Africa, apart from most of the stations located in the south of South Africa, where precipitation is much lower. Hence, this process cannot be ignored for the interpretation of vertical GPS displacements in southern Africa regarding other processes (tectonic movements, GIA), especially since it impacts a very large area comprising almost the entire width of the continent.

The GPS time series provide constraints to discriminate between the GRACE solutions. The CSR solution delivers the best fit in terms of annual and inter-annual variations. On the other hand, the temporal resolution of the GRGS solution allows improved recording of short time scale TWS variations. This latter solution also provides a slightly better annual amplitude. As a conclusion, in agreement with Sakumura et al. (2014) revealing that the ensemble of GRACE data is stronger than a single solution, both solutions are kept in this study. But, opposite to Sakumura et al. (2014), the two solutions are conserved independently and not averaged in order to preserve their respective advantages.

Finally, more detailed examination of the GPS time series can further constrain the GRACE solutions by determining the spatial distribution of water masses, and its potential temporal variability. The anomalies of the GPS time series, such as the phase shift

between the horizontal and vertical components and the vertical slowdowns may turn out to be critical evidence to better constrain the hydrological cycle (see Sections 4.2 and 4.3).

Chapitre 4

Hydrology

Once validated by the surface deformation recorded by the GPS stations, GRACE data products provide a very useful proxy to monitor variations in Terrestrial Water Storage in the Okavango basin. In order to properly use them as a tool for decision making regarding the management of water resources in the basin, it is necessary to understand the forcings on these variations. This can usually be done through a water balance, by estimating the inputs (precipitation) and outputs (evapotranspiration and outflow). The lack of data in the broad remote catchment area has not allowed a satisfactory ground-based constrained water balance assessment in the Okavango basin so far. Monitoring is all the more complicated by the high variability of the hydrological system in both space and time, which does not allow scarce single measurements, as continuous as they might be, to account for an average value over a large area. Along with monitoring, there is a need for a hydrological model able to reliably predict effects of climate or land use change, as in Andersson et al. (2006).

In order to forecast the flood distribution and predict the impact of future changes, numerical hydrological models have been developed for the Okavango Delta, as early as Dincer et al. (1987). Gieske (1997) was the first to take into account groundwater in the hydrological system, resulting in much better results, by allowing constant hydrological parameters through time. Recently, Wolski and Murray-Hudson (2008) developed a coupled GIS-reservoir model for the Delta obtaining a good reproducibility of the outflow in the different outlets. In contrast, the catchment area remained un-modelled for a long time, mainly due to the lack of data. Hughes et al. (2006) were the first ones to apply a rainfall-runoff model to the basin, the same year as Folwell and Farqhuarson (2006). More recently, Milzow et al. (2011) developed a new hydrological model in order to capture the consequence of small scale changes in land use in the basin. But most of these attempts remained poorly constrained, only validated by the outflow (Wilson and Dincer, 1976; Gieske, 1997; Hughes et al., 2006; Wolski and Murray-Hudson, 2008). GRACE data now represents a supplementary and reliable data set available to monitor water storage in the whole basin. This new proxy can be used to validate hydrological models with a second state variable, TWS, as in Milzow et al. (2011). In this study, GRACE data products are used to validate the calibration of the Pitman model for the Okavango basin of Hughes et al. (2006).

However, the Okavango Delta itself may be too small for GRACE spatial resolution ($\sim$ 300 km). Unlike in the catchment area, a few piezometric records are available in the Delta and can be compared to GRACE data products. Two sites were discretely monitored by ORI

between 1997 and 2014, which records permit the comparison with GRACE data products. For this study, 4 piezometers were installed in selected sites in the Delta and equiped with pressure probes to continuously record the elevation of the water table during the rainy season.

The contribution of the deformation of the surface to a better understanding of the hydrological is not limited to the validation of GRACE solutions. The distribution of the observed vertical and horizontal deformation can be used to determine more accurately the location of the area of main TWS variations, while GRACE smoothes these variations over a large area. Careful examination of the GPS time series can also better constrain the temporal evolution of the TWS spatial distribution. Finally, by better constraining the spatial and temporal evolution of TWS in the Okavango-Zambezi basin, it is possible to better constrain the meteorological data sets used for water balances.

4.1 Validation of the Pitman model for the Okavango basin

4.1.1 The Pitman model

Principle

The monthly hydrological model used in this study (here refered to as the Pitman model) is actually a coupling between a rainfall-runoff model and a reservoir model, related by functions corresponding to the relevant hydrological processes : infiltration, interception, evapotranspiration, etc. The actual Pitman (1973) model is the rainfall-runoff component, developed especially for southern African catchment areas. It attributes precipitation fallen during a rainfall event in order to predict the consequent variations in the different hydrological reservoirs : runoff, atmosphere, soil moisture/aquifer. Details of the processing are given in figure 4.1.

The original Pitman model was modified for the Okavango basin by Hughes et al. (2006), with particular attention to ground and surface water interactions (groundwater recharge/discharge, channel transmission losses). The basin is subdivided into 24 sub-basins, to address the spatial heterogeneity of the system. The hydrological parameters of the model were calibrated for the Okavango River on the basis of the outflow of 18 gauged sub-basins over the period 1960-1972, when rain-gauge data and water level were available in the Angolan catchment area. These parameters comprise summer and winter soil absorption rates (minimum, mean and maximum), the maximum storage capacity, the storage-recharge curve, the storage-runoff curve and the maximum groundwater recharge, among others. As discharge in Mohembo has been monitored since 1933, the parameters defined during the most tightly constrained period were verified over the last three decades, to validate the use of satellite-derived data. The validation of the model calibration is limited in two aspects. First, the time span of rainfall and outflow chronicles used to validate the parameterisation is not long enough. The 12 year long chronicle, from 1960 to 1972, does not even cover the 18 years of the supposed cycle controlling regional rainfall. Second, the calibration is based on only one surface state

variable, the outflow. The supplementary state variable provided by GRACE (TWS) allows a more robust validation of calibration of the relationship between the atmosphere and surface and groundwater in the hydrological model.

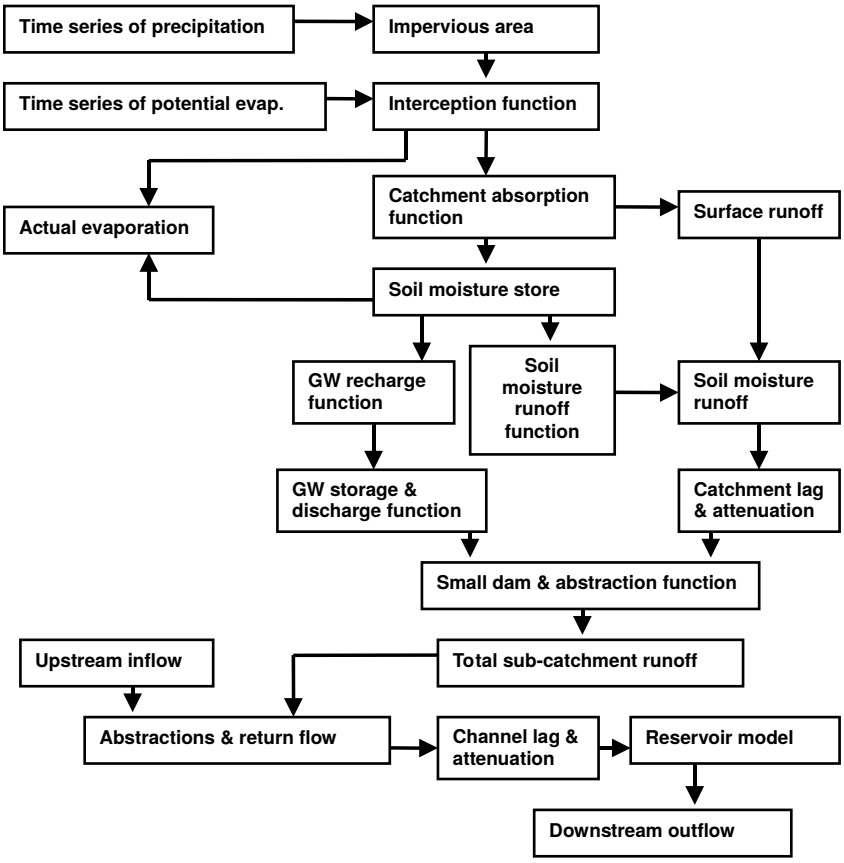

FIGURE 4.1 – Flow diagram of the modified Pitman model as defined by Hughes et al. (2006) for each sub-basin.

Model inputs

It is necessary to provide the model with different inputs, such as the spatial definition of the 24 sub-basins forming the spatial variability of the catchment area. Values for interception of rainfall by vegetation are provided in January and July and extrapolated throughout the year. The soil distribution is provided by FAO, the topography and geology by the USGS (Persits et al., 2002) and the GLC2000 land cover map is derived to retreive forest cover. Drainage density, ground water transmissivity and ground water storativity are not calibrated, but estimated based on available information about the catchment characteristics. However, due to a lack of information on aquifer properties, some calibration was necessary.

The Pitman model also needs monthly time series for two of its boundary conditions : rainfall and evapotranspiration. Both are critical for the assessment of the water balance, and exhibit a great variability depending on the chosen data set. All available data sets for

the two variables have advantages and disadvantages which may differ among basins. The reasons for the choice for each data set are detailed in the next sections.

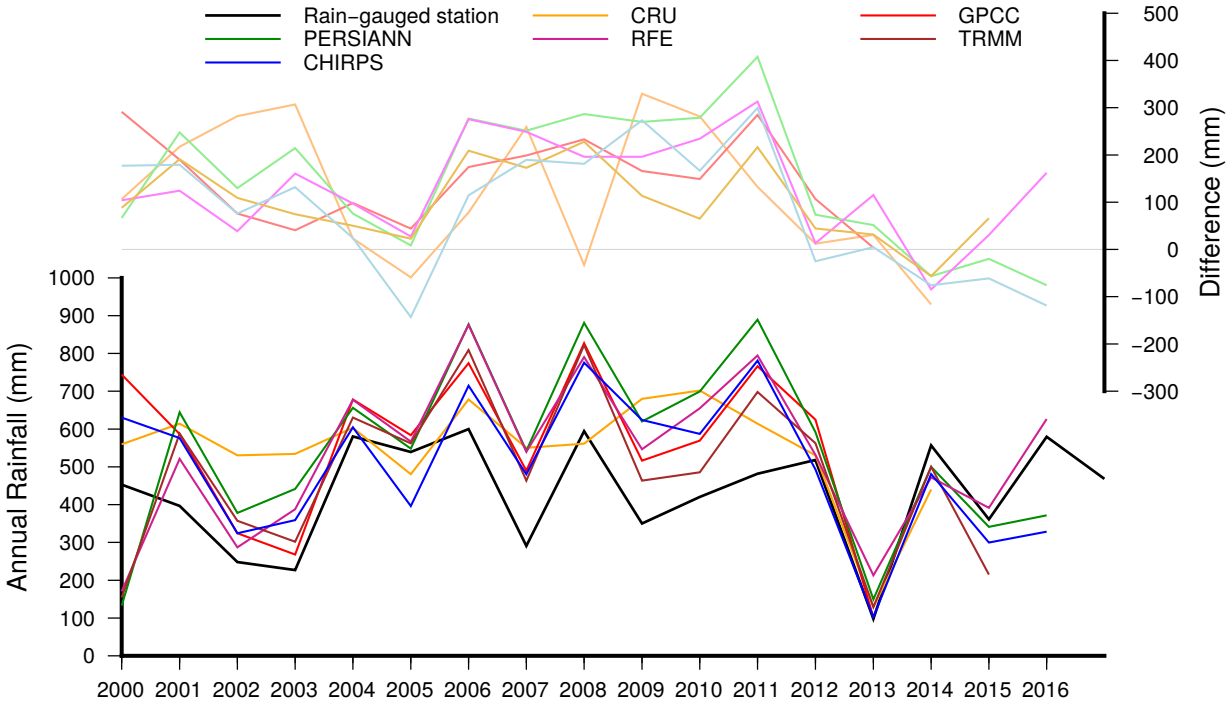

FIGURE 4.2 – Comparison of annual rainfall between rain-gauge records at the Shakawe station (location in figure 2.3) and the different continuous rainfall data sets. Bottom plot shows annual rainfall for each data set (ground-based station in black), top plot shows difference between data set and the station records. The low value of 2013 is due to a discontinuity in the data of the weather station, consequently subtracted from the other data set.

Rainfall Many different data sets are available for precipitation, based on remote sensing (PERSIANN), rain-gauged stations (GPCC, CRU) or both (CHIRPS, TRMM, RFE). The only three weather stations currently available in the Angolan catchment area, with only few months of discontinuous records, make it impossible to choose among current data sets on the basis of ground-based data for the whole basin. The comparison is more easily feasible in the Delta, where the Department of Meteorological Services (DMS) and DWA records rainfall. Figure 4.2 shows the example of the Shakawe station (data available at `http://leutra.geogr.uni-jena.de/obis/metadata/start.php`), which highlights the variability among rainfall data sets. All the spatially continuous data sets overestimate annual rainfall at this station, up to 100 %, which is revealing a general trend observed in the region. This general overestimation is due to the predominantly convective rainfall. Wilk et al. (2006) calculated that the TRMM data sets overestimate rainfall in the basin by 20%. This overestimation is the result of a double bias. While satellites tend to underestimate the precipitation falling during massive storms, they also estimate occurrence of lower rainfall too often. This second bias is greater than the first one, and results in monthly overestimation of rainfall. Finally, all the proposed data sets regularly exhibit significant differences in the spatial distribution of

rainfall through the rainy season. This distribution has a strong influence on the hydrological system, due to the variable nature of the subsurface.

To get around this problem, the Pitman model can be used to test the different data sets, which provide very different runoff generation. Wilk et al. (2006) concluded that rainfall data need to be moderated by rain-gauged measurements to be more realistic. More recently, the Climate Hazards InfraRed Precipitation with Stations (CHIRPS), computed by the Climate Hazards Group, has been found to be the data set providing the best fit between modelled and observed outflow (Wolski[1], pers. comm.). CHIRPS, moderated by the Pitman model in the Okavango basin, is thus the data set used in this study for assessment of precipitation.

Evapotranspiration Assessment of evapotranspiration is even more debatable. Opposite to rainfall, it is first complicated to actually quantify evapotranspiration through weather stations. Integral weather stations (SASSCAL Weather Net), recording parameters necessary to assessment of evapotranspiration (temperature, wind speed, humidity, etc.) are still rare in the basin and have only been recording for a few years at best. Available continuous data sets are fewer than for rainfall (MODIS16, GLEAM, MPI), and even show a higher variability. The strategy chosen in the Pitman model is to compute evapotranspiration for each month and sub-basin, based on the Eddy covariance (e.g., Aubinet et al., 2012). The Eddy covariance is a method to assess vertical turbulent fluxes in the surface boundary layer of the atmosphere. The method requires meteorological parameters (temperature, wind speed, etc.) and time series for potential evapotranspiration (PET), herein provided by GLEAMv3 data sets (Martens et al., 2017). GLEAM provides estimates of PET based on the equation of Priestley and Taylor (1972) and using surface net radiation and near-surface temperature provided by satellite data. A comparison between the data sets is presented in Section 4.3.

4.1.2 Validation based on GRACE solutions

The new proxy provided by GRACE on TWS in the Okavango basin allows further testing the hydrological model of Hughes et al. (2006), with a constraint on an additional state variable to discharge characterising the system. To do so, monthly mass balance for TWS is assessed through both GRACE and the Pitman model, and compared (Figure 4.3). TWS from the Pitman model is represented by the total of three reservoirs, runoff, soil moisture and groundwater, monthly integrated over the whole basin upstream of Mohembo. In this manner, the output from the Pitman model is comparable with the integrated EWH estimations provided by GRACE. Given the satellites' spatial resolution, estimation of TWS from GRACE solutions is here based on the time series obtained for the central part of the basin (18°E, 15.5°S) on `thegraceplotter.com`. Values of EWH variations are then extrapolated to the surface area of the whole basin. TWS time series are finally resampled with linear interpolation to provide monthly balances, comparable to the time step of the Pitman model.

The overall mass variations are well correlated between the Pitman model and the GRACE signals, all three exhibiting an annually periodic signal and an inter-annuel trend. TWS from

1. P. Wolski is a researcher at the Climate Systems Analysis Group (CSAG), University of Cape Town

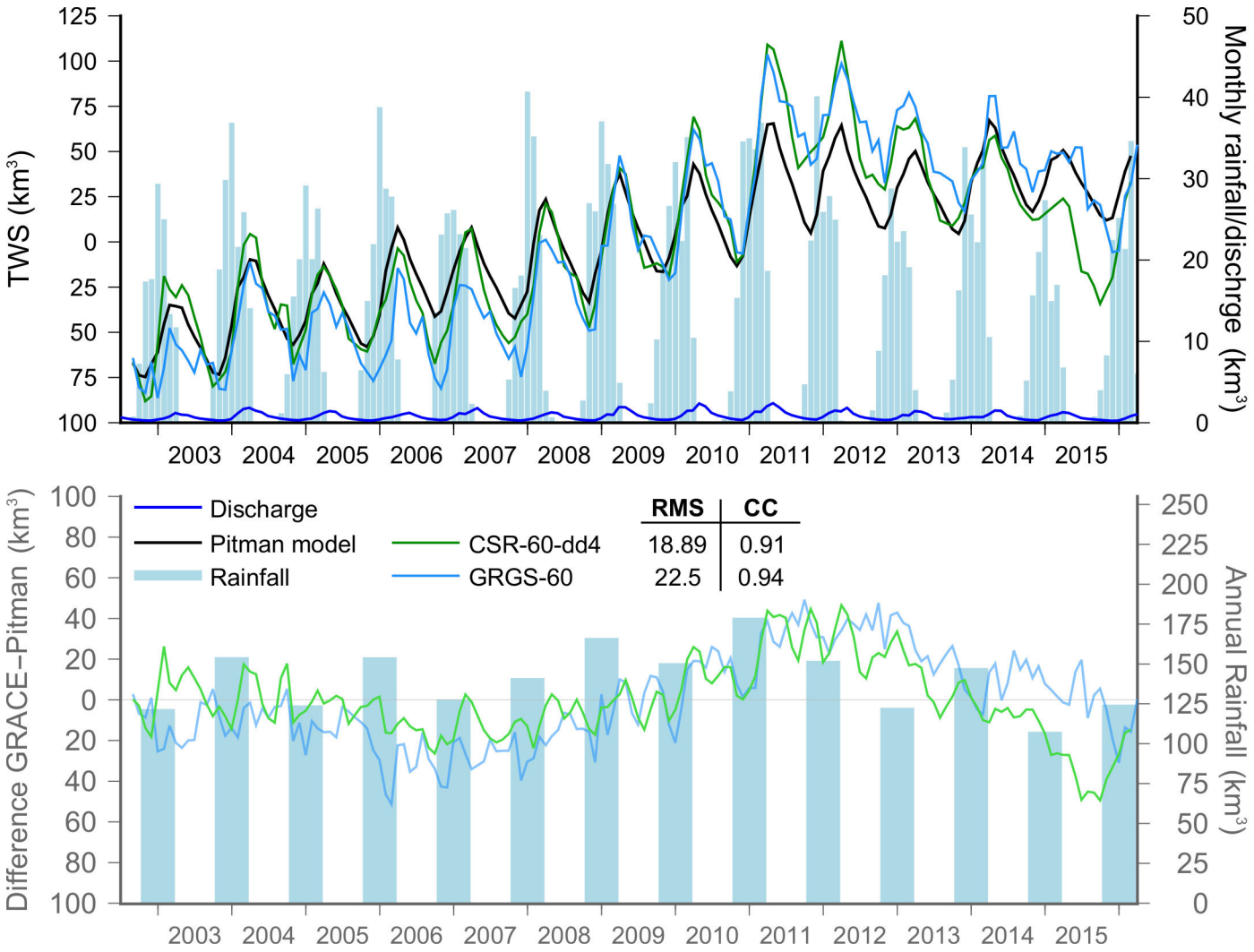

FIGURE 4.3 – Comparison between output from the Pitman model for TWS (groundwater and runoff) and different solutions for GRACE data products Level 3. Top graph : black line shows monthly variation in TWS from the Pitman model, colored lines show GRACE solutions, blue histogram shows monthly rainfall (CHIRPS moderated by Pitman model) and darker blue line, the monthly discharge measured at Mohembo (DWA). Top graph shows difference between GRACE solution and output from the Pitman model (TWS), along with annual rainfall. All values, except rainfall and discharge, are shown relative to their mean value.

the Pitman model show correlation coefficients of 0.91 and 0.94 respectively with the CSR and GRGS solutions. All the main characteristics of the GRACE signal are well reproduced : the phase and amplitude of the annual periodicity and the inter-annual trend.

Annually, both GRACE signals and Pitman model prediction are in phase, showing the recharge of TWS in the catchment area occurring during the rainy season, but starting after one month (2005-2006) to three months of rain (2012-2013), depending on the intensity of rainfall. The seasonal recharge of TWS, both in the Pitman output and the GRACE signals,

is almost linear until the end of the rainy season. TWS then suddenly declines as soon as rainfall stops. This decline can even begin sooner, in case of moderate rainfall in the last month(s) of the rainy season. While most of the years show an abrupt change, some years exhibit a step in the water balance at the end of the rainy season, depending on the rate of decrease of rainfall (2003, 2004, 2014).

The large amplitude of TWS variations seen by GRACE satellites is almost reproduced by the model, although GRACE shows slightly higher variations. In case of underestimation of TWS variations by GRACE, as proposed in the preceding chapter, the underestimation of TWS by the Pitman model would then be greater. The model also reproduces well the inter-annual variability of the amplitude of TWS variations. The smallest amplitude occurred in 2004-2005 ($\sim$50 km^3), while 2010-2011 exhibits the highest variation ($\sim$ 75 km^3 for the Pitman model and almost 125 km^3 for GRACE).

Finally, the Pitman model reproduces the inter-annual trend very well, with an increase in average TWS from 2002 to reach a maximum in 2011-2012. The difference in the minimum of discharge in the years 2006 to 2008 may not be significant as it only represents 20% of the variation, and occurred in a period of groundwater recharge. On the other hand, the difference between GRACE and the Pitman model in the 2011-2012 maximum clearly shows an understimation of TWS recharge in the Pitman model, with a mean difference of about 50 km^3. The recharge in the Pitman model is a little too early, around 2006-2007, resulting in a negative difference. After 2009, the difference turns positive as the increase seen by GRACE is faster than the one predicted by the model. This more constant regime predicted by the model also results in a stabilisation of average TWS since 2011, while GRACE data describe a decrease in TWS.

The Pitman model does not manage to reproduce the vertical slowdowns in TWS discharge visible in the GRGS solution signal. As the monthly resampling of the 10 days solution of the GRGS solution still allows the detection of the slowdown, the conspicuously linear rate of TWS in the model cannot be attributed to its low temporal resolution. It may instead reveal a secondary bias in the model.

The Pitman model from Hughes et al. (2006) shows a better fit to the GRACE data than the rainfall-runoff model proposed by Milzow et al. (2011), which hardly manages to reproduce half of the TWS amplitude of variation visible in the GRACE data. As mentioned by the authors, a comparison between the models may reveal differences in the data sets used as inputs for rainfall rather than model performance. But the range of difference cannot rely exclusively on the differences between rainfall data sets, which, although highly variable, do not exhibit such strong variations.

The Pitman model as calibrated by Hughes et al. (2006) thus accurately anticipated the very large variations of TWS in the Okavango basin, its high amplitude of annual variations, as well as the annual phase of maximum recharge. Hence, it is relevant to use it as a tool to understand not only the functioning of the hydrological system, but also to predict changes due to climate change or anthropic development. Runoff is the most important reservoir for human activity, but according to both the Pitman model and GRACE solutions, it represents less than 1% of the mass budget (Figure 2.12). TWS is consequently highly controlled by the degree of saturation of the groundwater reservoir.

4.2 Distribution of the water bodies in the Okavango-Zambezi basin

GRACE solutions are not sensitive to the spatial variability within major gravity anomalies such as the one in the Okavango-Zambezi basin. This is highlighted by the homogeneous amplitudes of the GRACE signal within the Zambezi basin, opposite to the variability observed in the GPS time series (Figure 3.5). A careful examination of the GPS time series can help to retreive the distribution of the mass of water, by virtue of 1) the spatial distribution of the amplitude of the annual vertical displacement, 2) the amplitude and phase of the annual horizontal displacements and 3) the ratio between the vertical and horizontal displacements. Indeed, the highest vertical displacements occur at the centre of the flexure, thus at the location of the main TWS variation (Figure 3.1). Horizontal periodic displacements are expected to be centripetal towards the area of maximum TWS variation during the period of loading and indicate the same location. As this area is also the location of the lowest horizontal displacements, the ratio of vertical displacement over horizontal displacement increases with the proximity of the station to main TWS variation.

4.2.1 Determination of the spatial variability of TWS through the hydrological cycle

The inter-annual climatic variability, encapsulating for the date of initiation of the rainy season, the amount of total precipitation, the spatial and temporal distribution of the precipitation and the intensity of evapotranspiration, induces a significant inter-annual variability in the surface deformation signal. Despite these variations, and in order to comprehend the relationships between the different components, the amplitude and direction of the displacements of the surface in the three spatial dimensions can be summarized into eight stages (Figure 4.4). The horizontal annual amplitudes are determined by the average of measurable amplitudes. As the horizontal time series exhibit significant noise, the accuracy of the amplitudes are to be taken with care. The phase shift in the horizontal displacements relative to the vertical ones is visible in all the stations of the Okavango-Zambezi basin.

The spatial distribution of the annual vertical amplitudes of the GPS signals, the spatial and temporal distribution of the horizontal displacements as well as the vertical/horizontal ratio all indicate a similar area of major annual deformation. This area is located in the Upper Zambezi, in the southern vicinity of MONG, possibly straddling the boundary between the Okavango and Zambezi catchment areas. Indeed, MONG shows the greatest vertical annual amplitude and the second highest vertical/horizontal ratio. TEZI shows the highest vertical/horizontal gradient, but its signal is most probably impacted by the water level in the nearby dam (see location in Appendix A.1). This hypothesis is supported by the southwestwards horizontal displacements of the MONG station between January to August, indicating the direction of the location of the area of main TWS variation. The horizontal displacements of the MAUA station are the only ones deviating from this pattern, with a norteastward displacement during the loading. In contrast to the eastern one, the northern component of the MAUA station is very noisy, and the interpreted signal may not be significant.

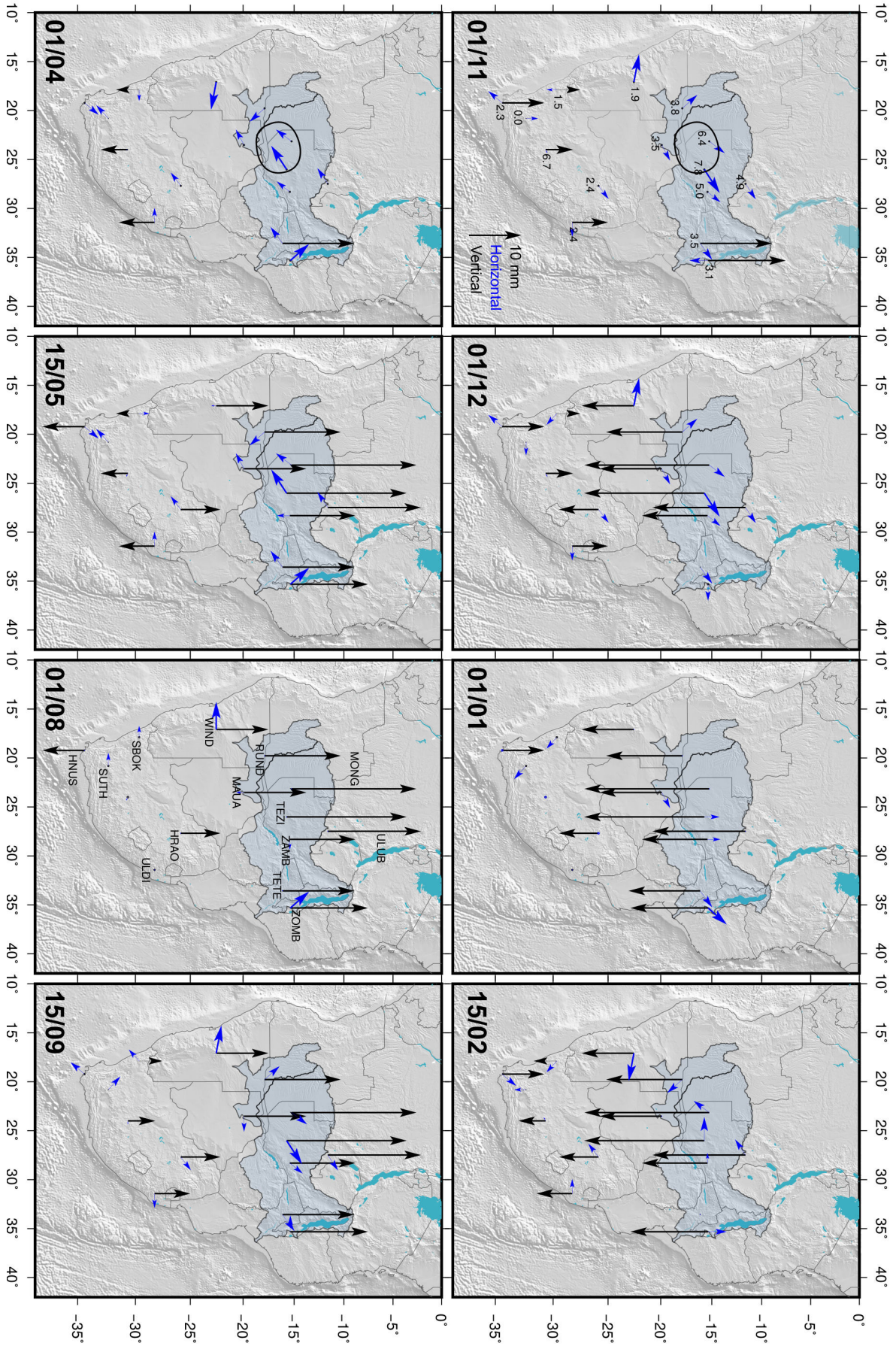
01/11
01/12
01/01
15/02
01/04
15/05
01/08
15/09
10 mm
Horizontal
Vertical
MONG
ULUB
TEZI
ZAMB
TETE
ZOMB
RUND
MAUA
WIND
HRAO
ULDI
SBOK
SUTH
HNUS

FIGURE 4.4 – Maps of the schematic evolution of the vertical (black) and horizontal (blue) displacements over the hydrological year. Arrow length represents the mean half-amplitude of annual displacement ; absence of arrows represents inflexion of the displacement direction. The area of maximum loading variation is circled in black (01/11 and 01/04). Coefficients (01/11) indicate the ratio of vertical amplitude over horizontal amplitude. Loading flexure in the Okavango-Zambezi basin is initiated at the beginning of the rainy season (01/11) and is maintained until the end of rainfall (01/04). The expected horizontal displacements related to this flexure are delayed and only begin in mid-February. As soon as the rainy season stops, vertical displacements invert and relaxation begins (01/04).

The southernmost station (HNUS) shows vertical displacements inversely correlated with the displacements in the Okavango-Zambezi basin. This reveals the different climatic regime as HNUS is located in the winter rainfall zone, providing a maximum in precipitation in August-September (Nicholson, 2000).

The decreasing gradient of seasonal deformation from the main area of TWS variation differs between the western Okavango basin and the eastern Middle and Lower Zambezi basins. The western gradient is higher, with vertical/horizontal ratio decreasing to $\sim$3.5 at RUND and MAUA stations and 1.9 at the WIND station. Despite this high gradient, the deformation due to the seasonal loading in the Okavango-Zambezi basin could extend as far as the WIND station. The annual vertical amplitude of the deformation modelled based on GRACE solutions is lower than the amplitude observed in the discontinuous GPS signal for this last station (Appendix A.1), like many stations in the sub-continent. Local effects, such as loading due to the local aquifer, could explain the difference in amplitude. But the horizontal displacements of the GPS station reject this hypothesis. The Windhoek aquifer is mainly located south and south west of the GPS station (Tredoux et al., 2009). The observed GPS horizontal displacements mainly show an annual periodicity on the eastern component, up to 7 mm of amplitude, while the northern component only exhibits 1 to 2 mm of annual amplitude.

Although the northern component could indicate a balance between the two loading sources, the eastern component clearly indicates a remote impact of the Okavango-Zambezi basin. The eastern component of the GPS time series shows an exception for the 2010-2011 massive rainy season, especially significant in the region of Windhoek. The deviation of the eastern component during this important local event of aquifer recharge supports the impact of remote loading during dryer years. Moreover, the vertical annual amplitude shown by the GPS station (10 mm) is almost similar to MAUA's (12 mm) and higher than HRAO's (7.6 mm), more distant from the area of main TWS, but receiving more annual rainfall.

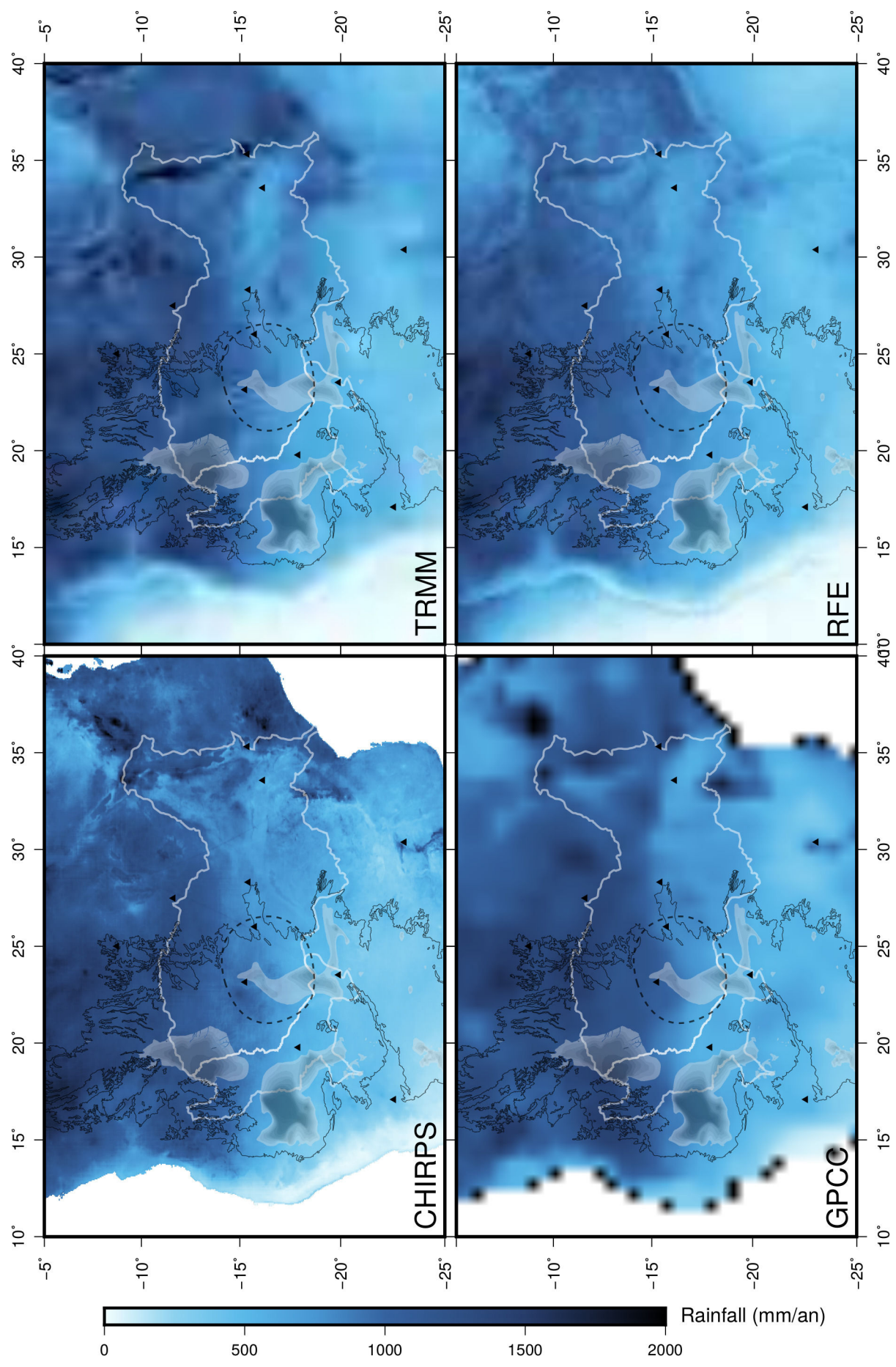
TRMM
RFE
CHIRPS
GPCC
Rainfall (mm/an)
0
500
1000
1500
2000

FIGURE 4.5 – Maps of average annual precipitation for four different data sets. Time span for average differs relative to the availability of data over the GPS record : CHIRPS, 2010-2016, TRMM : 2011-2014, GPCC : 2009-2012. The location of the area of main TWS variation is indicated in dashed line. Kalahari deposits are delineated by thin black line ; Kalahari beds exceeding 120 m thick are indicated in grey areas, with darker shades up to 420 m thick. Catchment areas are delineated in white.

Eastward, the gradient of observed deformation is much lower, with vertical annual amplitude reamining higher than 12.5 until the most remote ZOMB station. Similarly, the vertical/horizontal ratio remains higher than 3. This lower gradient is consistent with the distribution of annual rainfall (Figure 2.9). Several GPS stations are nevertheless influenced by their direct environment, such as TEZI and ZOMB. Thus direct interpretation of the differential displacements within the basin should not be straightforward. The distribution of GPS stations across the basin is nevertheless promising, and a decreasing gradient in TWS is still visible downstream. As the broad Zambezi basin is not the area of this study, perspectives are only developed for this basin (Section 6.2).

4.2.2 Interpretation of TWS variability

Location of the area of maximum TWS variation

The area of highest surface deformation, defined in figure 4.4, thus represents the area of highest variation in TWS. Accumulation of TWS occurs with 1) important precipitation, 2) lower evapotranspiration, and 3) capacity of storage in the subsurface. As assessment of ET, temporally and spatially, cannot be reliably constrained, this parameter is not examined hereafter.

Figure 4.5 shows the distribution of average annual rainfall in the Okavango-Zambezi basin according to four different data sets : CHIRPS, TRMM, RFE and GPCC. All data sets agree on a concentration of precipitation in the upper catchment areas, north of the area of main TWS variation. None of the data sets shows a contrast in the precipitation revealing a particular concentration of rainfall in the area of maximum TWS variation. Estimation from GPCC is the most generous in this area. CHIRPS exhibits a restricted area of high precipitation repeated in many years, but not of significant spatial extent. The hypothesis of particularly important concentration of rainfall is thus rejected.

The explanation may lie in the nature of the subsurface, forming the substrate of potential aquifers. There are few porous subsurface sediments in the entire middle and lower Zambezi basin (CGMW-BRGM, 2016), which could host important groundwater during the dry season. In the western Okavango basin, the decreasing gradient of precipitation may not allow an accumulation of TWS in the Etosha depocenter as significant as in the vicinity of MONG.

More specifically, the sedimentary layer forming the most adequate substrate for water storage is the most recent unconsolidated sands with their porosity of 33% (Obakeng and

Gieske, 1997). A significant volume of such sediments may lie in the area of maximum TWS variation as it coincides with a region of extensive wetlands and pans (Figure 4.6). In the vicinity of Mongu, the Zambezi river is indeed comprised of a wide floodplain named the Barotse floodplain, extending over 180 km long and to a maximum of ∼50 km wide. Downstream this floodplain narrows progressively until the Ngyone Falls, delineating the boundary between the upper and middle Zambezi. This floodplain exhibits a very low topographic gradient and shallow slowly flowing water. It is flooded between January and June, along with all lower sections of the Zambezi tributaries (Moore et al., 2008).

The area is mainly covered with Kalahari sands, while these are regularly breached downstream of the Ngonye Falls, where rocks of the lower Kalahari, sandstones and quartzites, outcrop (Money 1972, in Thomas and Shaw 1991). This upper sedimentary unit, named the Mongu sand member, can reach 200 m thick, but also shows an important spatial variability in the logs provided by Money (1972) (in Thomas and Shaw 1991). Given the large amplitude of TWS in the area, it is possible that this upper Kalahari sand unit is more significant than previously thought.

Other geomorphological features reveal a significant influence of the groundwater in the area. The flanks of the upper Zambezi are dotted with numerous pans, some of which are perennial (Figure 4.6). These pans are fed by groundwater or margin springs (Thomas and Shaw, 1991). Most of these pans extend on a belt crossing the Zambezi at a latitude of -15.2°. They are more or less connected to each other and to the Zambezi by grassy narrow valleys named dambos (Moore et al., 2008). Dambos are characterized by a high elevation of the water table all through the year, which declines only in case of severe drought. This persistent elevated groundwater prohibits tree growth due to the consequent anaerobic soils. According to Wolski (1998), these pans-dambos play a critical role in the hydrological system of the upper Zambezi.

Peculiarities in the GPS time series

The explanation of the non-linearity of the vertical displacements, particularly visible during the phase of crustal relaxation, at least partly relies on non-linear variations of TWS. Indeed, GRGS 10 days solution for GRACE data products exhibits similar variations in the estimation of EWH. The longer temporal resolution of the CSR solution does not exhibit the same variations. During the period of loading, the occasional decrease of the subsidence rate is related to a significant double peak of precipitation which occur during some rainy seasons. In the Okavango basin, it is particularly visible in 2013-2014, with relaxation even beginning at RUND. The same process occurs in the Zambezi basin.

If the presence of thick beds of Kalahari sediments is responsible for preferential TWS, then the depocenter located in Angola, astride the Cuito and Upper Zambezi catchments, and receiving the most important precipitation, could represent a major area of TWS variation too. Indeed, it is thought to progressively discharge groundwater to provide the smooth Cuito discharge (Andersson et al., 2006). But such an influence is not visible in the time series of the GPS stations in the basins, all of which point south in periods of loading. In the case of loading due to the northernmost depocenter, then it probably is too far from the stations to be dominating. Such an influence could nevertheless account for the phase shift

FIGURE 4.6 – Satellite views of the region of Mongu (Zambia). Bottom image shows the numerous geomorphological features of important groundwater storage with the extensive Barotse floodplain hosting the Upper Zambezi surrounded by seasonal to perennial pans and fed by several dambos. Top image shows a detailed view of pans and dambos (Source : Landsat/Copernicus by Google Earth).

between the horizontal and vertical components. As the rainy season begins earlier in the upper catchments, loading in the northermost Angolan depocenter could initiate subsidence in November, while maintaining the horizontal displacements northward at RUND station. Such a hypothesis could also explain the difference in phase for the two horizontal components at MONG station. Later in the rainy season (∼January-February), the closer influence of the Okavango-Chobe depocenter prevails, and horizontal components all point towards this area.

During the phase of relaxation, interpreting the systematic decrease of vertical displacement rate in terms of TWS variability, during the dry season, leads to the assessment of ET. Periods of vertical slowing down seem to be correlated to the minimum of ET estimated through Eddy covariance. While the phase of the ET cycle provided by the Pitman model is validated by the phase of the GRACE and GPS vertical signals, its amplitude may be revealed to be too low. Moreover, the Pitman model does not predict the systematic slowdown of vertical displacement. In order to produce a variation in the decrease of TWS leading to a possible stagnation, it is necessary that ET decreases much more than predicted, to reach a possibly null value. To do so, the required order of magnitude of ET variations is more similar to the one provided by the MODIS16 data products. Such a higher annual amplitude of ET could also palliate the lack of annual amplitude of TWS predicted by the Pitman model. More detailed examination of the different data sets for ET is to be found in Section 4.3.

Another hypothesis to explain both vertical slowdowns and the phase shift between the horizontal and vertical components is the displacement of a significant mass of water. Such a displacement could occur for instance if groundwater circulation accompanied the surface annual flood. It would explain both vertical slowing down and shift of the horizontal components during the rainy season. But no temporal offset is visible between RUND and MAUA, for the Okavango basin. All the horizontal inversions are in phase, as well as the vertical slowing downs. Similar phasing is also observed across the broad Zambezi basin. Such phasing therefore indicates the rejection of the hypothesis of displacement of significant masses of water within the basins.

The climatic hypothesis of TWS non-linear variations explains satisfactorily the slowing down of the vertical displacement during both periods of loading and relaxation. It is also the only hypothesis conforming with the variations of gravity field revealed by the GRGS solution for GRACE. Although the displacement of significant water bodies is shown to be unlikely, the hydrological hypothesis of different areas of major TWS variations, corresponding to the depocenters of the Kalahari beds should be further examined. Finally, as these two hypotheses may not fully explain the phase shift between the horizontal and vertical components, the hypothesis of a different rheology than the PREM model should also be taken into account. The possibility of a crustal flexure extending as far as WIND also calls into question the rheological parameters used for this study.

4.3 Improved constraint of evapotranspiration estimates for the Okavango basin

Evapotranspiration exerts a great forcing on the maximum depth of the water table at the end of the dry season. Now that the Pitman model is robustly validated, the com-

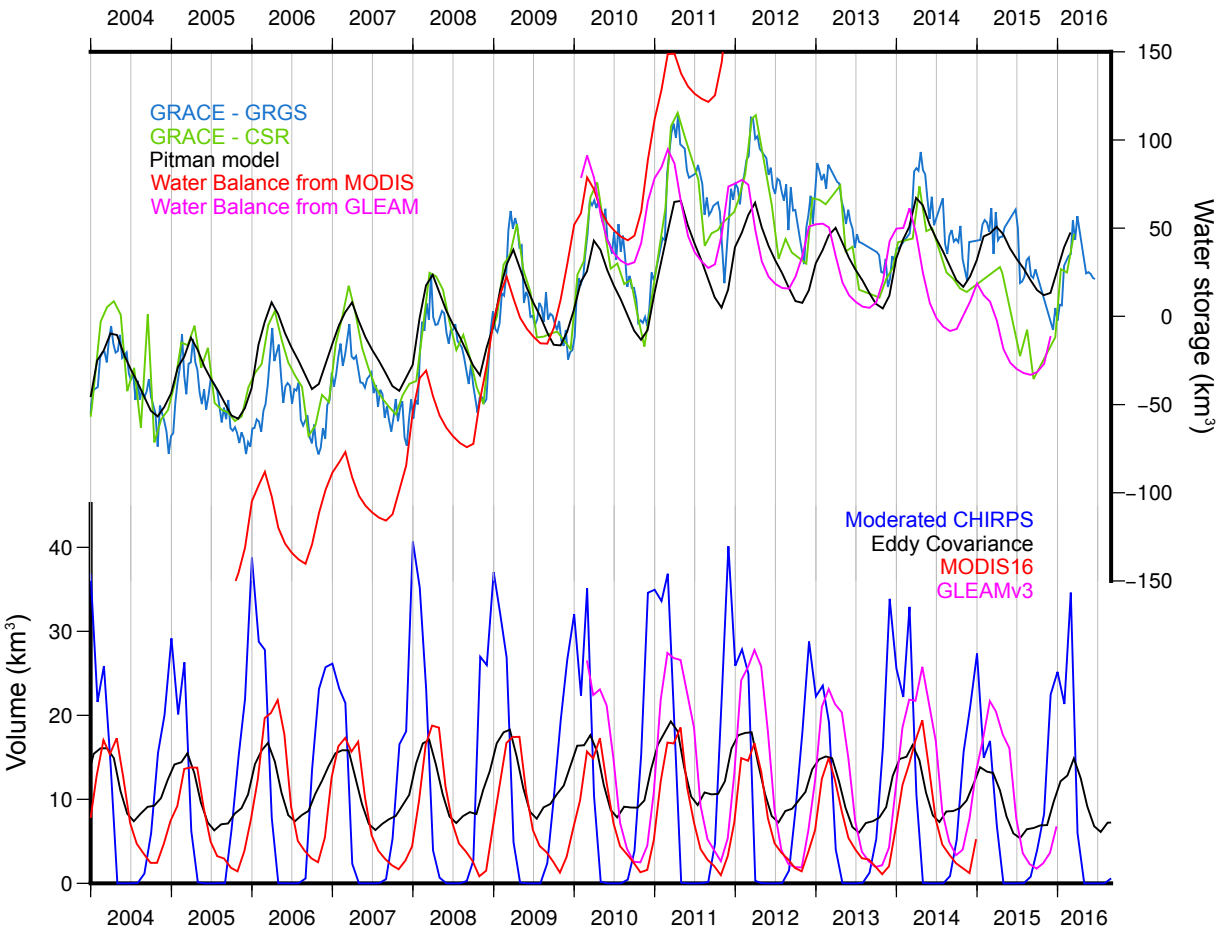

FIGURE 4.7 – Bottom graph shows a comparison of ET estimated by GLEAMv3, MODIS16 and Eddy Covariance in the Pitman model, along with precipitation from moderated CHIRPS. Top graph shows the variation of TWS from GRACE solutions along with water balances from the Pitman model (black), the difference between rainfall from moderated CHIRPS and MODIS16 (red) and GLEAMv3 (magenta). Unlike the other balances, the water balance from MODIS16 does not exhibit a decrease of TWS after 2010.

---

parison between its ET estimation based on Eddy covariance and classical water balance from gridded data sets can help constrain evapotranspiration assessment. Figure 4.7 shows a comparison between different data sets available for ET : MODIS16 (Mu et al., 2011), GLEAMv3.1(Martens et al., 2017), the ET from Eddy Covariance computed in the Pitman model. Different variations of TWS for the Okavango basin are assessed, depending on the data set used for ET, based on rainfall from CHIRPS moderated by the Pitman model. GLEAM and MODIS products show a generally similar trend and phase, with a major difference in the amplitude of the annual periodicity, with GLEAM reaching almost twice the value proposed by MODIS16 products. Their estimation of ET is maximum around March, up to ∼90 mm/month for MODIS16 and ∼120 mm/month for GLEAM, and reaches a very low minimum value, possibly less than 5 mm/month for MODIS16 and 10 mm/month for GLEAM, in October. The ET assessed with Eddy covariance shows a slightly different

pattern, with a lower annual amplitude. The maximum value is reached a little earlier in January-February, with values similar to those generated from MODIS. But the minimum ET is reached earlier, in July, and does not fall below 20 mm/month. This low value is more or less maintained until the end of the rainy season, before to rise gently with arrival of the rain.

Both amplitude and phase of the GRACE signal are better reproduced by TWS variations assessed by the Eddy covariance in the Pitman model. Both MODIS16 and GLEAM exhibit minima occurring two to three months too early. Maintaining a moderate ET all through the dry season assures a decrease in TWS as late as the arrival of the rainy season and assures the consistency between the phases of the GRACE signal and the TWS variations in the Pitman model. The phase of ET provided by Eddy covariance also reproduces the sudden inversion in TWS occurring at the beginning of the rainy season. On the opposite, the progressive decrease visible in MODIS and GLEAM products produces a smooth curved inflexion.

The inter-annual evolution of TWS based on MODIS16 products increases far too much and does not even stabilize after 2011-2012. This continuous increase highlights the general underestimation of ET by MODIS16 products. It is well reproduced by both Eddy covariance and GLEAM. The latter has the benefit of reproducing the decrease of TWS in the recent years better than the Pitman model. Both data sets provide similar annual estimations, respectively 603 and 665 mm/yr for Eddy covariance and GLEAM, while MODIS16 provides an insufficient average annual value of only 412 mm/yr.

Finally, the regular slowing down in the decrease of TWS visible in the GRGS solution for GRACE is not reproduced in the water balance from the Pitman model. As this slowing down occurs in the dry season, only a variation in ET can be responsible for it. The intensity of the slowdown in the discharge of TWS, possibly reaching a complete stop, implies a drastic decrease in ET during one to two months around July. As this slowdown in TWS decrease is limited in time, ET probably increases again with the increasing temperature of the austral spring. Such an increase is visible in the Eddy covariance time series, but a greater amplitude would be required to recover from a preceding drastic decrease, while maintaining an annual amount falling somewhere between the Eddy covariance and GLEAM values.

4.4 Groundwater in the Okavango Delta

The validation of the Pitman model, along with the GRACE data products, demonstrates the predominance of groundwater in the hydrological Okavango basin, with runoff representing less than 1% of TWS. The co-evolution of TWS recorded by GRACE and the discharge measured at Mohembo, entrance of the Delta (Figure 2.12), suggests the importance of the saturation of the aquifer in the production of runoff in the catchment area. In the Delta, the saturation of the aquifer is also thought to exert a great influence on the propagation of the flood pulse, and thus on the extent of inundated areas (Wolski and Murray-Hudson, 2008).

In order to investigate this hypothesis, the determination of the evolution of the aquifer along the hydrological cycle, and the forcings responsible for this evolution is required. To do so, it is necessary to collect data about this evolution. As useful as GRACE data products might be in the broad catchment area, they may not be used in such a straightforward manner in the Delta. While the validation of GRACE proved useful across the catchment,

the spatial resolution of GRACE satellites, of about 300 km, is a strong limitation for a similar application in the Delta. In such a spatially variable area, the GRACE signal could be influenced either by the variations of the nearby area of main TWS variation, or by the dryness of the southwestern Kalahari.

Very few piezometric records are available in the Delta. ORI regularly measured the depth to the water table at two monitoring sites, Weir and Observation island, south west of Chief's island (see locations on figure 2.3). Although these records are discontinuous and local, thus influenced by their immediate environment, they constitute the most complete records of groundwater elevation in the study area through more than a decade. Figure 4.8 shows a comparison between these records and water table variations based on GRACE data products for EWH. A porosity of 33% for the Kalahari sand has been determined by Obakeng and Gieske (1997) and is used to convert EWH variations from GRACE to variations of elevation of the water table. As the proportion of soil moisture relative to groundwater is not known, the variations of this last reservoir are thus comprised in the variations of water table elevation modelled from GRACE. Finally, piezometers equipped with continuous pressure probes were installed in the Delta from spring 2016 to fall or winter 2017 (location on Figure 2.3, records on Figure 4.9).

4.4.1 Evolution of the goundwater level through the hydrological cycle

Piezometric records for the oldest two sites are very similar (Figure 4.8). Although not far away from each other they are located in different environments. The piezometer at Observation island is located in an island, while the Weir piezometer is located in a floodplain. Their similarity thus supports at first order the non-specificity of each site and the correspondance with a general trend for the water table in the whole Delta. Their annual variations are in phase and exhibit the same amplitudes, between 1 to 3 m.

They show a systematic maximum elevation of the water table in July-August, most generally after a very fast episode of recharge of the aquifer, consequent on the propagation of the flood pulse. But the piezometric time series often show an initiation of the recharge of the aquifer during the rainy season. If so, the recharge starts at best at the peak of the rainy season (2000-2001, 2008-2009, 2011-2012), but can also only begin at the end of the rainy season, when precipitation is lower (2006-2007, 2013-2014). The only years not showing any elevation of the water table during the rainy season (2002-2003, 2004-2005, 2012-2013) were years of very low rainfall in the Delta.

The winter recharge of the aquifer, consequent on the propagation of the flood, is most generally the main episode of recharge of the aquifer. Exceptions are made in the years of peculiarly important rainfall (2005-2006, 2007-2008), when the maximum elevation of the water table is almost reached at the peak of local rainfall.

The recharge of the aquifer during the rainy season is also visible in the more recent piezometric records (Figure 4.9). These latest records also depict different environments (islands, seasonal floodplain, occasional floodplain). All the time series show a recharge of the aquifer during the rainy season. These results have to be regarded with care as 2016-2017 has been a

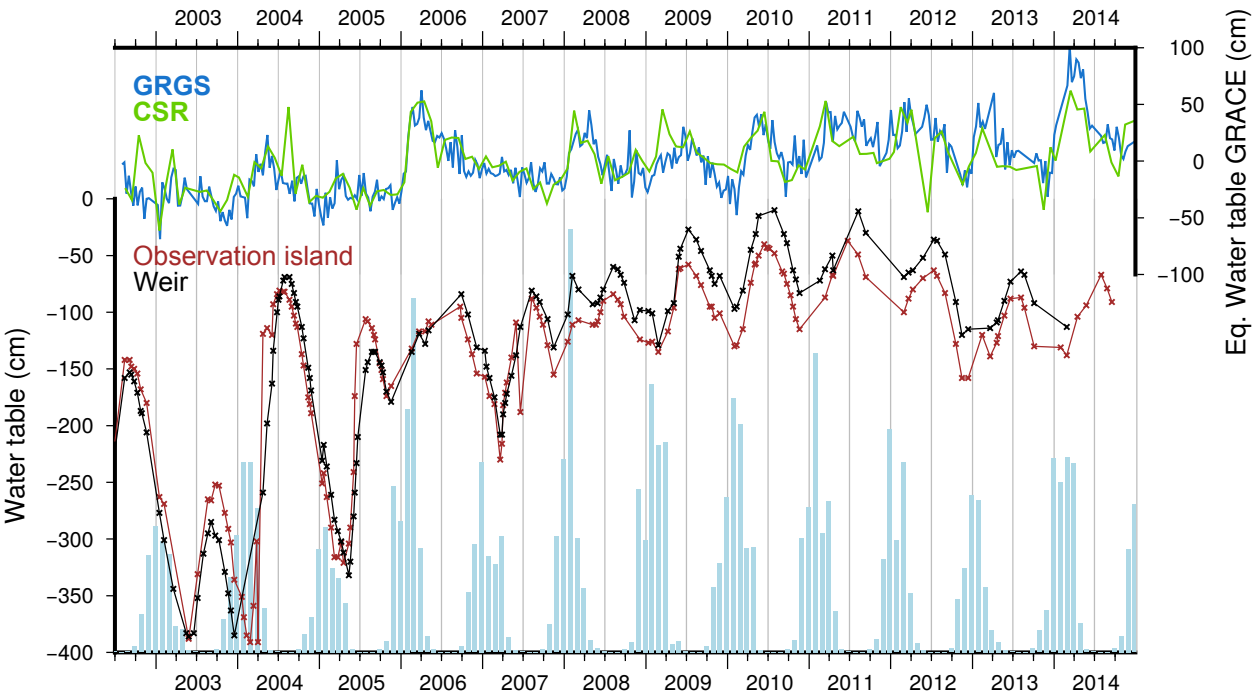

FIGURE 4.8 – Piezometric records in the Delta (location of sites on figure 2.3, data from ORI) along with variations of water table elevations from GRACE data products : GRGS and CSR solutions. Rainfall is plotted for temporal distribution, from chirps integrated over the Delta, same data as in Figure 2.12.

---

year of exceptionally high rainfall over the Delta. Moreover, they are for now only descriptive and should be coupled to detailed small scale hydrological modelling to capture the processes responsible for the different response of each site. Nevertheless, the water level in the channels rose only under the influence of the local rainy season, with almost no contribution of the flood, due to intense rainfall the preceding summer in the Delta. But these results are supported by the previous piezometric records showing possible recharge during the rainy season.

All the sites show different amplitudes of recharge from $\sim$ 50 cm at KUNY to 175 cm at JAOI and FMMH. The recharge mainly occurs with sudden increases due to large rain storms, especially in the northern JAOI and middle XUDU stations. This behaviour is less frequent in the southern stations. KUNY only exhibits one main episode of recharge. FMMH shows increases of recharge with large rain events, but the main recharge occurs progressively through lateral loss from the channel. This can be seen from the water level in the nearby channel, the Thamalakane river, increasing faster than the elevation of the water table. Three months after the last rainfall event at this site, equilibrium is reached between the channel and the aquifer.

The relationship between rain events and aquifer recharge is not systematic. The XUDU piezometer indicates sudden rises of the water table while no precipitation was recorded on site. These are most probably due to rain events occurring in the vicinity of the station and impacting a broader area. On the other hand, many rain events did not induce a shift in the

water table elevation. This can be seen at KUNY, where CHIRPS indicates two episodes of rain which do not appear to affect the water table. It can also be seen in the FMMH station in late February, where important rains did not disturb the slow and steady rise of the water table.

The absence of influence of massive rainfall on the elevation of the water table is mainly obvious at the beginning of the rainy season. Records at JAOI shows no influence of the first moderate rains, until several consecutive days of more important rains in January. The elevation of the water table then suddenly rose of ∼50 cm within a few days. FMMH also shows almost no influence of local rainfall on the elevation of the water table until February, when this influence is also visible in the water level on the Thamalakane river.

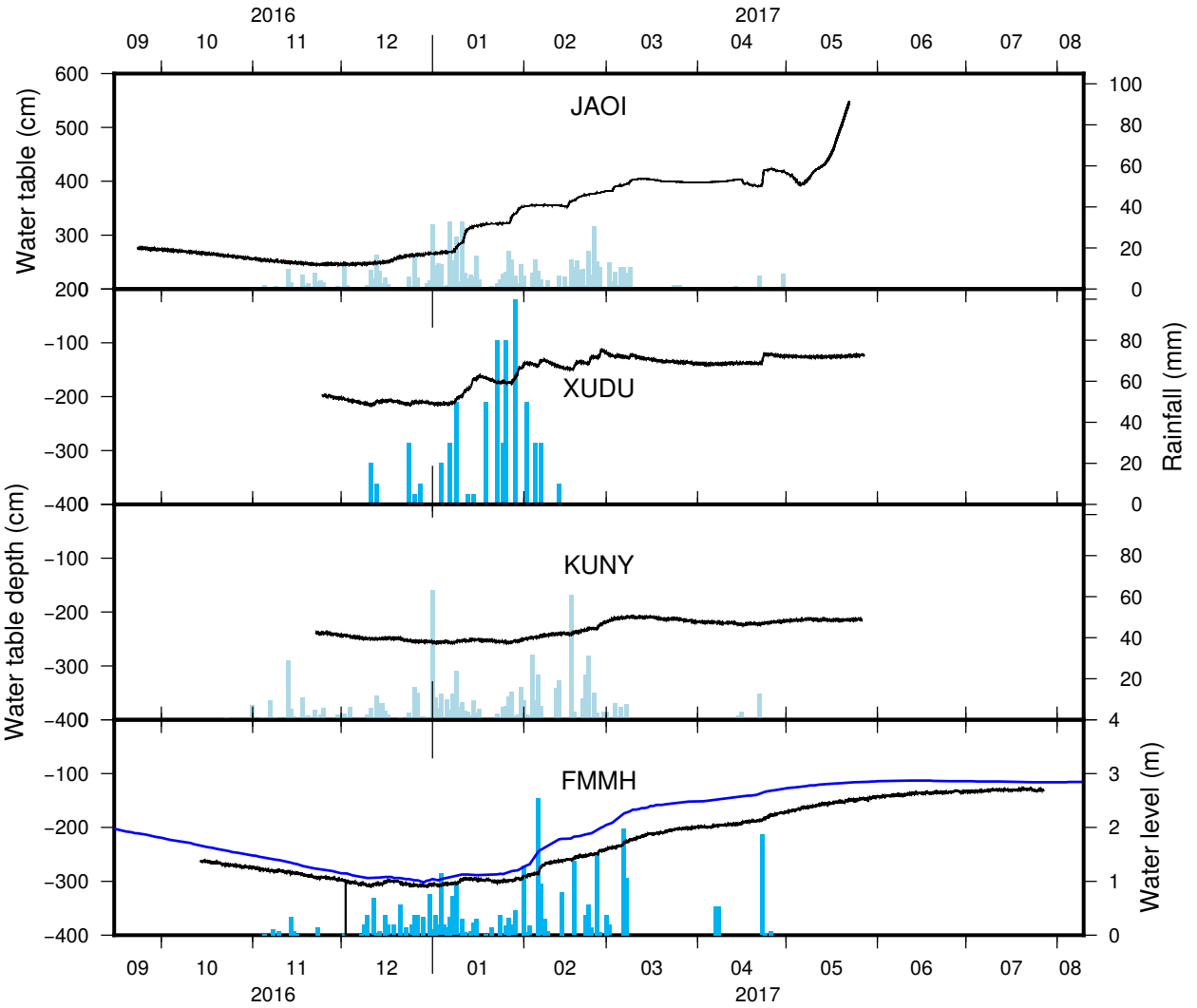

FIGURE 4.9 – Continuous piezometric records in the Delta (black line), along with local precipitation (data from rain-gauge are in darker blue, lighter blue shows time series extracted from CHIRPS). Only the southeastern FMMH station has records for water level in the neighbour Thamalakane river (blue line). See location of the piezometers in Figure 2.3.

4.4.2 Testing GRACE in the Okavango Delta

Time series for EWH were extracted from `www.thegraceplotter.com` at 19.5°S, 23°E, approximately locating the centre of the Delta, for the two GRACE solutions used in this study. The variations of TWS predicted by GRACE (Figure 4.8) show a lesser annual amplitude of variation than in the catchment area, as expected, providing a lower signal-to-noise ratio. The annual amplitude of variation of water table elevation predicted by GRACE (∼50 to 100 cm) is comparable to the amplitude of variations observed in the piezometers between 2006 and 2012 (∼ 75 to 125 cm). But the maximum recharge predicted by the GRACE generally occurs around March-April, shift-phased relative to the maximum in the piezometers occurring in July-August. This phase-shift reveals that GRACE is therefore still under the influence of the variations of the important aquifer in the Okavango-Zambezi in the middle of the Delta, although moderated by the dry and close Kalahari desert.

However, two anomalies in the GRACE signal extracted in the Delta, compared to the GRACE signal extracted in the catchment area, reveal that the Delta may exert a minor influence on the GRACE signal. First, in 2005 and 2007, while the GRACE annual signal exhibits its usual amplitude in the catchment area (Figure 4.3), the GRACE signal in the Delta, for both GRGS and CSR solutions, does not show any annual variation. As these years brought peculiarly low rainfall in the Delta, their deviation relative to the signal in the catchment area may reveal an influence of the variations of the Delta's groundwater on the variations of gravity field recorded by GRACE.

Then, 2009 and 2010 show, particularly in the GRGS solution of better spatial resolution, a maximum in TWS occurring in July. This difference in the phase of the signal is typically indicating a possible strong of the Delta in the GRGS solution, as the Delta is the only hydrological system in the broad basin exhibiting such a phase.

Thus, the GRACE data products cannot be used as a monitoring proxy for TWS in the Okavango Delta for now, due to the modest extent of the Delta (∼ 150 km wide) relative to the poor spatial resolution of GRACE satellites (∼ 300 km). But the differences between the GRACE signals in the catchment area and in the Delta, revealing a partial but possible influence of the Delta, encourages the current improvement of the spatial resolution of GRACE data products. Moreover, the spatial resolution could be further improved by integrating the better constraint on the distribution of TWS variations within the Okavango-Zambezi determined in this study.

4.4.3 Discussion

Several studies have been carried out to determine the impact of the flood arrival on the recharge of the groundwater, but far less studies have been carried out during the rainy season. Apart from the piezometric records from ORI (Figures 4.8 and 4.9), no record of the water table over several complete hydrological cycles is available in the literature. Only a few records of the water table variations during the rainy season are available over the 1996-1997 (McCarthy, 2006) and 1997-1998 (Ramberg et al., 2006) rainy seasons. Ramberg et al. (2006) did not notice any influence of local rainfall and concluded to the very little or no influence of local rainfall on the elevation of the water table. Studies based on assessment of water balance, led to the conclusion of groundwater recharge occurring exclusively with the flood

propagation (Dincer et al., 1976; McCarthy, 2006). But McCarthy (2006) also noticed the rise of the water table after events of massive rainfall and concluded that local rainfall can participate to the propagation of the flood by doing so.

The ORI piezometric records, covering several years of variations of the water table, show the regular influence of the local rainy season on the elevation of the water table, possibly rising of several decimeters during the rainy season. But the relationship between the occurrence of rainfall and infiltration is not steady, neither in time over the rainy season, nor in space, among the different stations (Figure 4.9). A threshold seems to control the recharge of the aquifer, requiring a certain amount of initial precipitation to initiate groundwater recharge. This threshold hypothesis is supported by the JAOI time series, where several days of rainfall finally triggered the recharge of groundwater. The following rain events, although less important, are then regularly impacting the water table elevation.

On these detailed records, the threshold effect of the first rains before recharge of groundwater is more visible. JAOI, XUDU and FMMH stations show a slow decrease of the water table elevation until the arrival of the first rains, which stop the decrease and at least maintain a stable level of groundwater. The threshold is reached at the same period for JAOI and XUDU (mid-January), while it happens later in the FMMH station. The occurrence of this threshold reveals the saturation of the soil moisture necessary to further aquifer recharge, necessary for the local rainfall to impact surface water level. FMMH shows an exclusive feature with the rise of the water table continuing after the end of the rainy season. This recharge occurs now through lateral flow between the neighbour channel and the aquifer. This is revealed by the almost perfect correlation between the water table and surface water elevations. Unfortunately, FMMH is the only station where surface water level is available in the neighbour channel.

Such a threshold in the recharge of the aquifer would explain the absence of influence of local precipitation during the years of low rainfall (2002-2003, 2004-2005). This threshold seems to be more related to a rate of precipitation rather than a global amount. Massive rain storms seem to be good triggers for the recharge, as visible in the FMMH time series. This is consistent with the winter recharge generally initiating at the peak of rainfall. If no important rainfall occurs, the initiation of recharge can be still be triggered after the peak of rainfall, but would then require more months of rain (2006-2007).

Such a threshold could be explained by the saturation of soil moisture in the unsaturated zone. At the arrival of the rainy season, this reservoir has been emptied while it represents the connection between the surface and the aquifer. It is thus required that rain regenerates soil moisture before the water table can rise. Massive rain storms provide more efficient infiltration. As the regeneration of soil moisture is challenged by evapotranspiration, too low rain events will not exert a sufficient influence. Finally, such a threshold would also explain why almost no visible influence has been recorded in the late 1990's, when rainfall was lower.

4.5 Conclusion

The examination of the deformation of the surface in the Okavango basin, coupled with GRACE data products, validated the presence of an important aquifer in the catchment area, showing a high annual amplitude of variation. GRACE data product for EWH can hence be

used as a monitoring proxy for global TWS in the Okavango-Zambezi basin. This new proxy allowed the validation of the hydrological Pitman model calibrated by Hughes et al. (2006) for the Okavango basin, providing a reliable tool to assist decision makers in the development of the three concerned countries.

The detailed examination of all the time series available in the Okavango and Zambezi basins permitted the first order determination of the area of maximum TWS in the basins, correlated to the presence of thick Kalaharii beds, although the horizontal components of the signal of ground surface deformation suggests that different areas could be at play. It also determined that the water body responsible for this major variation is not migrating along the hydrological cycle, or in proportions not significant to be observed by surface displacements. Thus, the migration of the flood wave, although crucial for life support in the Delta, affectively represents an unsignificant proportion of the hydrological system, as proposed by Hughes et al. (2006).

The anomalies of the GPS signal regarding the theoretical smooth displacement observed in case of crustal flexure, i.e. the slowdowns during the phase of crust relaxation, permitted a much better constrain on the hardly quantifiable forcing on the aquifer : evapotranspiration. Finally, forcings on the aquifer in the Delta have also been better defined, with the demonstration of the regular influence of local rainfall on the water table in case of sufficient rain.

This study thus permits a better understanding of the functionning of the hydrological system, notably by confirming the role of buffer of the aquifer in the catchment area, modulating climatic variations proposed by Hughes et al. (2006). Such an influence may be at play in the Delta, as proposed by Wolski and Murray-Hudson (2008). This buffer effect is thought to be partly responsible for the non-linear response of the catchment to climatic variations, as well as for the non-linear of response of the flood propagation to variations of inflow at Mohembo. The recharge in the Delta seems to occur after a initial threshold of rainfall. These two effects could induce a strong non-linear behaviour of the Delta to inflow variations (see Section 6.1.1).

This study opened promising perspectives to monitor TWS variations in the Okavango-Zambezi. The deployment of new permanent GPS in the area would not only bring a more continuous insight into the deformation in the area, but would also densify the network, hence mathematically improve the uncertainties associated with the GPS time series. Finally, given the importance of the data provided by GRACE in the largely poorly monitored basins, the future launch of GRACE-Follow On is of great importance to maintain the durability of the records.

Chapitre 5

Tectonics and geodynamics

Quantifying the fault activity with the rate of deformation across the OG is a critical point to assess the impact of tetonics on the inter-annual variability of the distribution of the flood. It is also useful to constrain the rate of tectonic deformation at the geological time scale. As the ages commonly proposed for the tectonic activity responsible for the endorheism of the Okavango basin are very young, they impose the high rate of deformation so high, with a subsidence of $\sim$1 cm, that current tectonic deformation is necessarily important.

Determining the deformation rate also allows to better constrain the processes at play in the tectonic activity. The OG is conventinally assumed to represent an early stage of continental rifting, but this hypothesis has not been revisited since Scholz et al. (1976). New data are now available regarding the thickness of the crust and lithosphere in the study area, which complete the new geodetic data set. Section 5.1 reexamines the geodynamic context of the OG regarding all the data sets now available.

While horizontal displacements have been proved to be reliable and consistent at the continental scale to assess tectonic deformation or plate motion (e.g., Saria et al., 2013), vertical displacements are too strongly impacted by seasonal hydrological loading to be used without the procedure detailed in Section 3. The GRACE data products for EWH variations allow the modelling of the seasonal loading, but the uncertainties associated with this correction provides a wide range of value for the residual displacements. The two GRACE solutions used in this study provide different residual vertical displacement rates, which can be exposed to geological evidence (Section 5.2).

5.1 Horizontal displacements

The GPS time series provided by the permanent stations of the AfricaArray/UNAVCO finally quantified and orientated the current deformation related to the activity of the OG faults. This new data set can therefore help to determine the influence of the fault activity on the variability of the flood distribution in the Okavango Delta. This question is discussed in Section 6.1.1. It can also help to better constrain the tectonic history of the OG at the geological time scale, at least by constraining the age of the tectonic structure. As the rate of deformation is much lower than expected, the age of 41 kyr proposed by Kinabo et al. (2008) for the initiation of fault activity in the Delta is called into question. The long-term

fault activity in the OG and its impact on the endorheism of the Delta is discussed in section 6.1.2.

Since Scholz et al. (1976), it is generally stated the OG is an incipient rifting zone, similar to the first stage of mature rifts such as Lake Albert (Modisi et al., 2000; Bufford et al., 2012). In the following section, the low deformation rate determined across the graben is examined in a geodynamic perspective. All the criteria defining a rifting zone are submitted to the recently published geophysical surveys providing new data on the crust and lithosphere in the area. The seismicity is re-assessed and revealed to be observationally biased by the inconsistent seismological networks. Finally, in order to open the debate again on the origin of the tectonic activity in the OG.

Tectonophysics 712-713 (2017) 469–481

Contents lists available at ScienceDirect

Tectonophysics

journal homepage: www.elsevier.com/locate/tecto

Is the Okavango Delta the terminus of the East African Rift System? Towards a new geodynamic model: Geodetic study and geophysical review

Anne-Morwenn Pastier[a,*], Olivier Dauteuil[a], Michael Murray-Hudson[b], Frédérique Moreau[a], Andrea Walpersdorf[c], Kaelo Makati[b]

[a] UMR6118-Géosciences Rennes, Univ. Rennes 1, Beaulieu Campus, Rennes 35042, France
[b] Okavango Research Institute, Univ. of Botswana, Maun P/Bag 285, Botswana
[c] ISTerre, Univ. Grenoble Alpes, CNRS, BP 53, Grenoble 38041, France

ARTICLE INFO

Article history:
Received 6 December 2016
Received in revised form 25 May 2017
Accepted 29 May 2017
Available online 8 June 2017

Keywords:
Intraplate tectonics
Okavango
Geodesy
East African Rift System

ABSTRACT

The Okavango Graben (OG) has been considered as the terminus of the southwestern branch of the East African Rift System (EARS) since the 1970s based on fault morphology and early seismic and geophysical data. Thus it has been assumed to be an incipient rifting zone, analogous to the early stage of mature rifts in the EARS. Recent geodetic data and geophysical studies in the area bring new insights into the local crust and lithosphere, mantle activity and fault activity. In this study, we computed the velocities for three permanent GPS stations surrounding the graben and undertook a review of the new geophysical data available for the area. The northern and southern blocks of the graben show an exclusively low strike-slip displacement rate of about 1mm/year, revealing the transtensional nature of this basin. The seismic record of central and southern Africa was found to be instrumentally biased for the events recorded before 2004 and the OG may not represent the most seismically active area in Botswana anymore. Moreover, no significant lithosphere and crustal thinning is found in the tectonic structure nor any strong negative Bouguer anomaly and surface heat flux. Thus the OG does not match the classical model for a rifting zone. We propose a new geodynamic model for the deformation observed west of the EARS based on accommodation of far-field deformation due to the differential extension rates of the EARS and the displacement of the Kalahari craton relative to the Nubian plate.

1. Introduction

The East African Rift System (EARS) is a major geodynamic feature which has been splitting the African continent since the late Eocene-Oligocene (e.g., Macgregor, 2015). It propagates from the northern Afar Depression and Main Ethiopian Rift to the southern diverging branches (Fig. 1): the eastern branch from the Kenyan rifts to central Tanzania and the western branch from Lake Albert to Lake Malawi. The tectonic functioning of the termini, and thus the initiation stages for continental rifting are poorly understood. Some authors (e.g., Scholz et al., 1976; Modisi et al., 2000; Bufford et al., 2012) propose that a third branch of the EARS extends southwestwards from Lake Tanganyika (named the southwestern branch) and postulate that the most remote feature is the Okavango Graben (OG).

Located in northern Botswana, the Okavango Delta is an extensive wetland (12,000 km^2) confined in the OG. Its NE-SW trending faults, which match the orientation of the Lake Kariba valley, and the localized seismic activity led many authors since the late 1960s to consider it to be the final extension of this southwestern branch of the EARS and therefore an incipient rifting zone (Scholz et al., 1976; Modisi et al., 2000; Bufford et al., 2012). Scholz et al. (1976) first postulated this OG EARS extension hypothesis in the current terms from their seismic study in the area. Apart from fault orientation and morphology, proponents of this hypothesis use the first geophysical studies to infer that rifting is at play in the OG in a similar way to that observed in the EARS (Fairhead and Girdler, 1969; Scholz et al., 1976; Wilson and Dincer, 1976; Girdler, 1975; Ballard et al., 1987). Few geological data are available due to the extensive cover of Kalahari sands of varying thickness (Haddon, 2005) but several recent geophysical studies bring new insights into the crustal and lithospheric structure, and mantle activity of the area (e.g., Forte et al., 2010; Khoza et al., 2013; Yu et al., 2015a) that call into question the

* Corresponding author.
E-mail address: anne-mouwenn.pastier@univ-rennes1.fr (A.-M. Pastier).

http://dx.doi.org/10.1016/j.tecto.2017.05.035
0040-1951/

rifting hypothesis for the OG. Other deformation models have been proposed (McCarthy, 2013; Yu et al., 2015a) and are supported by newly available data.

In order to interrogate this problem, it is important to define criteria for a rifting zone, and to gather geophysical and geological data and points of view. In the framework of continental break-up, a rifting zone can be defined by thinning lithosphere and crust which is revealed by shallow depth to the Moho (Sengör and Burke, 1978; Allen and Allen, 2013). The upwelling asthenosphere may be manifested by a strong negative Bouguer anomaly and an increased surface heat flow. The consequent surface deformation is characterized by significant seismic activity with predominantly extensional focal mechanism solutions and bounding faults which can exhibit important scarps. This morphology is mainly valid for active rifts initiated by mantle upwelling, and is rarely observed in passive rifting due to crustal stretching. Volcanic activity is also expected but may only happen at an evolved stage. Kinematically, rifting zones are defined by crustal extension, marginal uplift and inner subsidence, but may appear with strike-slip displacements in accommodation zones. The order of appearance of these displacements (horizontal before vertical or vice versa) can help to characterize the process initiating the rifting. Indeed, active rifting due to mantle upwelling will induce early uplift leading to secondary crustal extension whereas passive rifting due to crust stretching will primarily show horizontal extension followed by uplift due to the consequent mantle upwelling (Allen and Allen, 2013).

This study brings new results from a geodetical study based on 5 years of records from permanent GPS stations to monitor slow displacements on the tectonic structure. Since rifting kinematics are associated with extension, the kinematics of the area then help to discriminate the processes at play in the graben deformation. We also reexamine available geophysical data in the area in order to construct an alternative model of the OG and compare it with the EARS characteristics. We propose a new kinematic model based on far-field accommodation of the deformation due to both EARS opening and differential movements between the Kalahari and Congo cratons impacting a wide region from Lake Upemba in the north to the central Kalahari in Botswana. We thus propose to re-open the debate on the OG EARS extension hypothesis.

1.1. Geological setting

1.1.1. EARS

South of the Main Ethiopian Rift, the EARS separates into two distinct branches extending from north to south through a series of

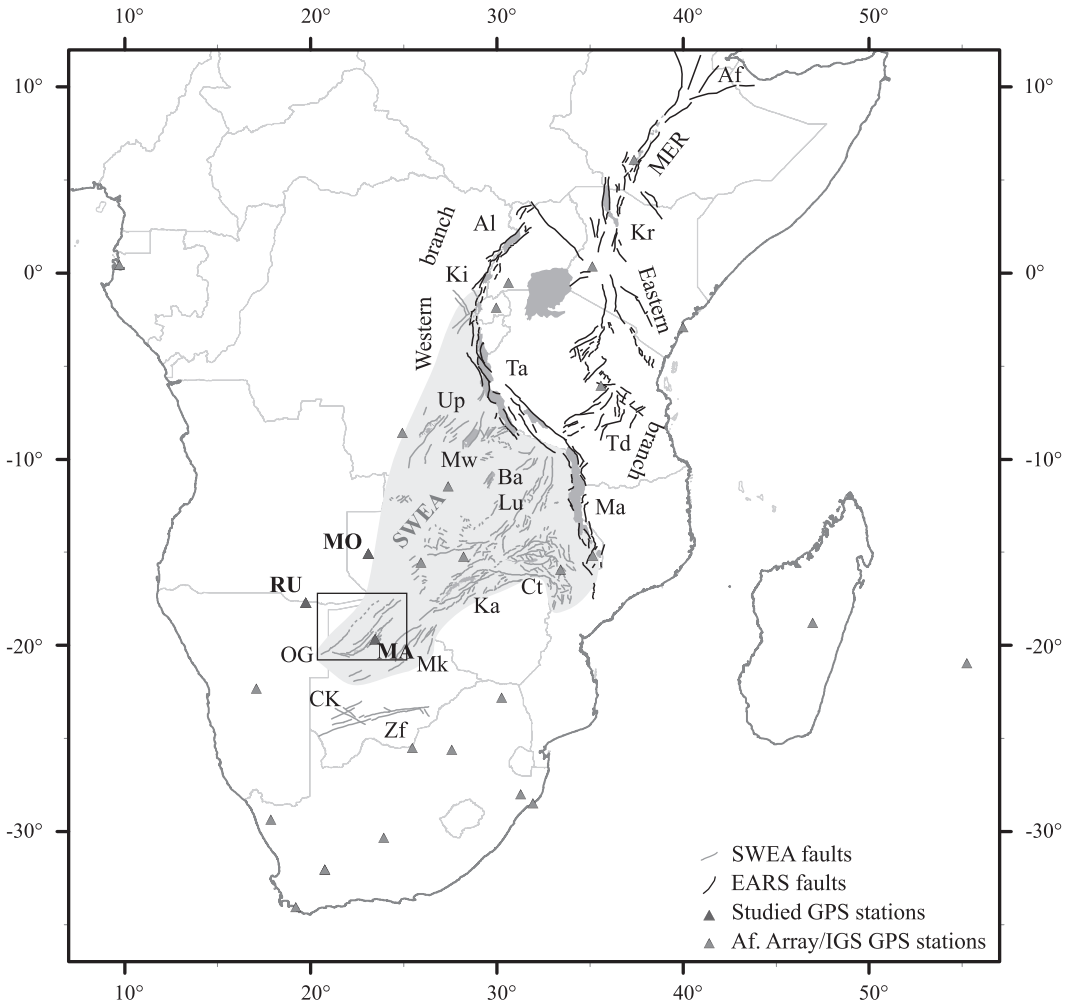

Fig. 1. Location of the Okavango Graben and the three studied permanent AfricaArray GPS stations (MA: MAUA, MO: MONG, RU: RUND). 26 GPS stations complete the network. The EARS and SWEA (South Western Extension Area) main faults are compiled from Lepersonne (1974), Reeve et al. (1981), Pinna et al. (1987), Stagman (1991), Haddon (2005), Kinabo et al. (2007), and Milesi et al. (2010). The SWEA extent is filled with light grey. Af: Afar Depression, Al: Lake Albert, Ba: Lake Bangweulu, Ct: Chicoa trough, CK: central Kalahari, Ka: Lake Kariba, Ki: Lake Kivu, Kr: Kenyan rifts, Lu: Luangwa Valley, Ma: Lake Malawi, MER: Main Ethiopian Rift, Mk: Makgadikgadi Pans, Mw: Lake Mweru, Ta: Lake Tanganyika, Td: Tanzanian divergence, Up: Upemba trough, Zf: Zoetfontein fault.

rift basins (Fig. 1). The older (>25 My) eastern branch extends continuously from the Afar Depression to Kenya and central Tanzania. It is characterized by signifcant volcanism but shallow (5–15 km), low-magnitude earthquakes. The younger (>15 My) western branch extends from Lake Albert to Lake Malawi in a discontinuous series of rift basins related by transform zones in varying orientations. It is nearly amagmatic, characterized by high-magnitude (>6.5), deep (30–40 km) earthquakes and deeper rifts, and is considered as less evolved (e.g., Chorowicz, 2005; Macgregor, 2015). Overall, the EARS has propagated southwards at the rate of between 2.5 and 5 cm/year (Chorowicz, 2005). Extension rates in those rifts vary from 5.2 mm/year in the northern Afar Depression to less than 1 mm/year in the south (Saria et al., 2014).

The EARS termini, and the characteristics of its propagation in the continental crust, are poorly known. The eastern branch bifurcates and dissipates in the Tanzanian divergence, an area of numerous faults oriented from NE-SW to WNW-ESE. The western branch ends in central Mozambique. Authors agree on a southwestern extension of the western branch but several grabens seem to diverge from this branch in a NE-SW orientation, from north to south: the Upemba trough, Lake Mweru, Lake Bangweulu, Luangwa Valley and the Chicoa trough (Fig. 1). While most of these tectonic structures show no evident extension, the Luangwa Valley and Chicoa trough converge towards Lake Kariba. Some authors add the OG as the terminus of the southwestern extension branch (e.g. Scholz et al., 1976; Modisi et al., 2000; Leseane et al., 2015). As this southwestern extension branch is poorly defined, we name the region from the EARS in the east, Lake Upemba in the north and the OG in the southwest, the South-Western Extension Area (SWEA). This area exhibits a gradient in fault density from north to south (Lake Upemba to the Chicoa trough) and from east to west (OG to Chicoa trough).

Du Toit (1927) first proposed a relationship between the OG and the EARS, followed by Fairhead and Girdler (1969) who proposed an EARS extension in Botswana, but oriented N-S. Then Reeves (1972a) proposed an extension of the EARS along a NE-SW axis but in the central Kalahari, 250 km south from the OG. It seems to be finally Scholz et al. (1976) who postulated the OG EARS extension hypothesis in its current form. This hypothesis has consensually led to the name of "Okavango Rift Zone" for the area, thus implying a genetic connotation for the deformation of the area.

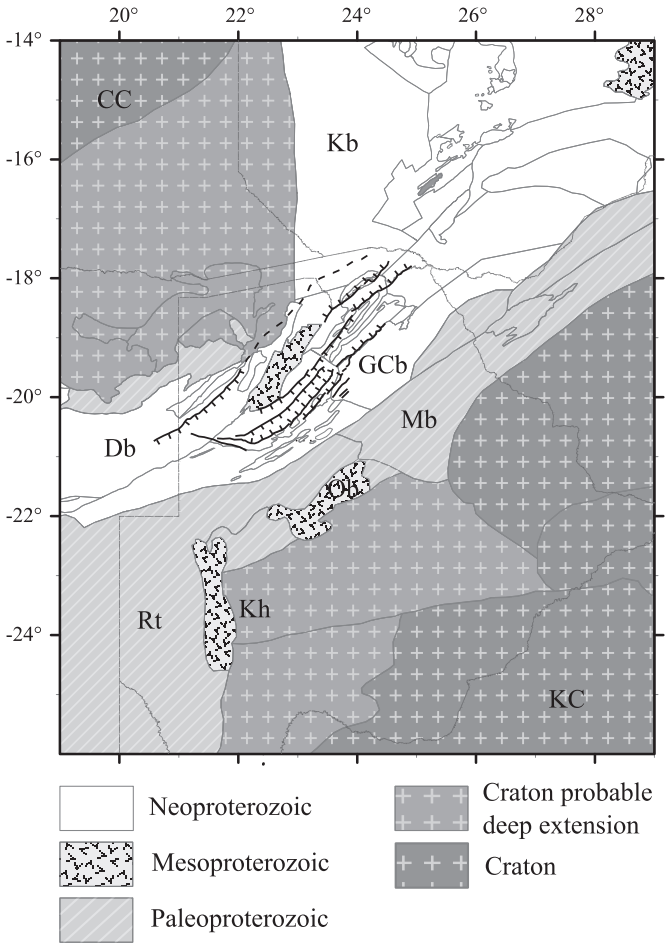

Fig. 2. Structural crust model compiled from Singletary et al. (2003), Haddon (2005), Kinabo et al. (2007), Muller et al. (2009), Begg et al. (2009), Miensopust et al. (2011), Khoza et al. (2013), and Youssof et al. (2013). Archean thick cratons surround younger weaker orogenic belts. CC: Congo Craton, Db: Damara belt, GCb: Ghanzi-Chobe belt, Kb: Kibarian belt, KC: Kalahari Craton, Kh: Kheis belt, Mb: Magondi belt, Ob: Okwa block, Rt: Rehoboth terrane.

1.1.2. Study area

The OG is located between two cratons joined by a series of Paleo to Neoproterozoic belts (Fig. 2). Bedrock outcrops are scarce in the area as it is almost entirely covered with tens to hundreds of meters of Kalahari sands, occasionally directly overlying the Karoo basalts (Haddon, 2005). But recent geophysical studies bring new insights on the distribution and importance of the main units in the area.

To the north lies the Archean Congo craton. Its southern limit was originally thought to lie in central Angola, but has subsequently been redefined further south underneath the Damara Belt in northern Botswana (Singletary et al., 2003; Begg et al., 2009; Khoza et al., 2013). Its associated lithosphere is estimated to reach a thickness of up to 250 km. To the south lies the Kalahari craton, comprised of the Kaapvaal and Zimbabwe cratons joined by the Archean Limpopo belt. This craton may extend further north beneath the Okwa block and its associated lithosphere may reach up to 220 km (Muller et al., 2009; Miensopust et al., 2011). These cratons are joined together along the Neoproterozoic Pan-African Damara belt. This last orogeny led to the deformation of the Ghanzi formation sediments into the Ghanzi-Chobe fold belt. This Precambrian assemblage leads to belts of different lithospheric rheology with a central younger (thus thinner and weaker) lithosphere zone surrounded by older thus thicker and more rigid belts and cratons.

The Karoo period (~300 My–~178 My) was characterized by intense rifting, which resulted in intensive sedimentation and concluded with expansive basalt flows (~180 My), in particular in central and northern Botswana, and the emplacement of the ENE-WSW Okavango Dyke Swarm dated at ~178 My (Le Gall et al., 2002). In northern Botswana, the Karoo deposition was controlled by NE-SW syn-sedimentary tectonic and paleotopographic structures. In the southwestern part of the OG, the remaining basalts and dolerites are clearly delimited by the Sekaka Shear Zone (SSZ) and the current Lecha, Kunyere and Thamalakane faults (cf. Fig. 3 for faults location). During the Permian, a major shear zone, the Southern Trans-Africa Shear System (STASS) is thought to have developed between the Congo and Kalahari blocks to accommodate differential displacements of plates astride the current African continent, and thus controlled sedimentary deposition (De Wit et al., 1995).

During the Cretaceous, continental break-up on both sides of the African continent (South America at ca. 129–121 My, and Madagascar between 150 and 112 My.) was responsible for transform faults, which formed a series of grabens across southern Africa (Haddon, 2005) and possibly reactivated the STASS. Karoo Supergroup rocks may have subsided into NE-SW grabens preserving them from erosion. Southeast of the OG, rifting reactivated the Passarge basin structures as far south as the Zoetfontein fault (up to 300 m downthrow). Generalized uplift affected the whole of southern Africa at

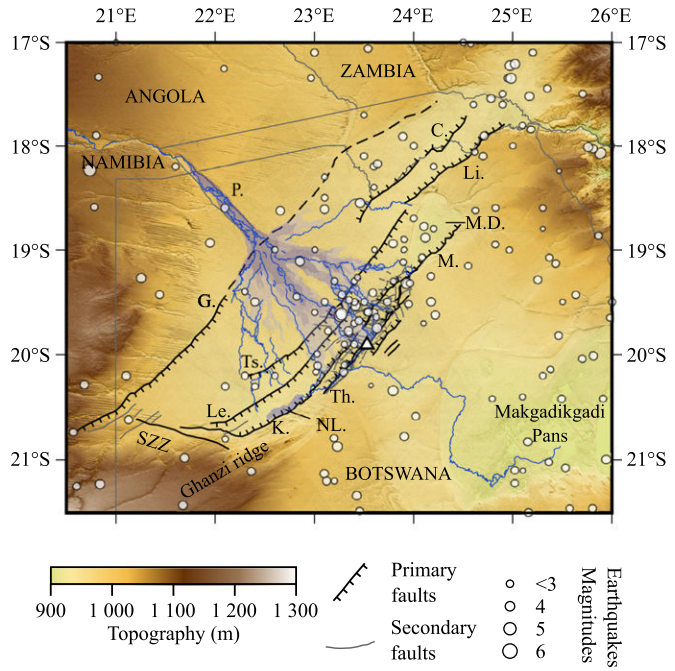

Fig. 3. Topographical map (SRTM30) showing location of the main faults (modified from Campbell et al., 2006; Kinabo et al., 2007), seismic activity and inundated areas. C.: Chobe fault, G.: Gumare fault, K.: Kunyere fault, Le.: Lecha fault, Li: Linyanti fault, M.: Mababe fault, M.D.: Mababe Depression, N.L.: Lake Ngami, P.: Panhandle, SSZ: Sekaka Shear Zone, Th.: Thamalakane fault, Ts.: Tsau fault.

that time, leading to an extensive period of erosion in the Cretaceous, locally forming red sandstone beds like those near Etosha pan (Miller et al., 2010) or in the OG (Linol, 2013).

In the OG, Kalahari sediments overlie these red beds unconformably. The erosion surface between the two periods is marked by pedogenesis and is constrained between 80 and 40 My (Linol, 2013). According to Haddon (2005), Kalahari sedimentation may have been initiated mainly by Late Cretaceous inner southern Africa downwarping, as well as relative uplift of the edges as a minor contribution. This would have led to the rivers back-tilting into the basin and the appearance of inner basin lakes. This hypothesis is supported in the northern part of the OG by stratigraphy showing a southward tilting between the possibly Jurassic-Cretaceous red beds and the Kalahari sediments (Linol, 2013). Vertical movements within the Kalahari basin occurred throughout the Cenozoic and shaped the Kalahari basin, notably along the Kalahari-Zimbabwe axis. The continuous or episodic nature of these uplifts is still in debate.

1.1.3. The Okavango Graben

The OG is a tectonic structure consisted of a series of normal to dextral strike-slip faults (Fig. 3) forming a hemi-graben with the most active faults concentrated in the southeastern part (Modisi et al., 2000; Campbell et al., 2006; Bufford et al., 2012). They are distributed along a NE-SW zone from the SSZ and the Gumare fault in the SW to the Linyanti and Chobe faults in the NE.

The OG can be divided into three domains (Gumbricht and McCarthy, 2001): (1) the northern block containing the Panhandle, (2) the central block which hosts the Delta and (3) the southern block where the Ghanzi ridge isolates the Makgadikgadi pans. Focal mechanisms identified by Scholz et al. (1976) showed normal mechanisms, and many studies based on borehole logs (Haddon, 2005; Linol, 2013), aeromagnetic data (Modisi, 2000; Campbell et al., 2006) and electromagnetic data (Podgorski et al., 2015) have shown downthrow on the main faults (Tsau, Lecha, Kunyere, Thamalakane) and, depending on interpretation, up to 600 m of sediments in the OG inner part (Lake Ngami, Bufford et al., 2012). A slight dextral strike-slip component is revealed by an offset in the dykes (Modisi et al., 2000; Campbell et al., 2006). Both studies revealed complex fault zones (branching and en-echelon faulting) for the Kunyere and Thamalakane faults rather than single faults, which could form smaller grabens and hemi-grabens within the OG. These faults are structures inherited from the underlying Proterozoic basement, occurring along the same NE-SW orientation as the Ghanzi-Damara belt, and could have been initiated during the Pan-African orogenesis. They have possibly been reactivated several times: during the STASS accommodation, the Karoo rifting and post-Karoo faulting, and the Cenozoic uplifts. Campbell et al. (2006) proposed a secondary normal fault set, as indicated in Fig. 3, highlighted by lateral offset in the dykes. According to Modisi et al. (2000), these faults could be responsible for lineaments at the surface of the Okavango Delta.

Thus, the OG lies upon a zone of lithospheric weakness relative to the adjacent thick and cold cratons, affected by ancient tectonic structures, which have been reactivated several times. Vertical and sometimes strike-slip displacements have a long and complex history and a great influence on the area.

1.2. Geophysical settings

1.2.1. Seismicity

The seismicity associated with the OG is a major argument for the rifting hypothesis. Plate boundaries and continental rifting such as the EARS are associated with regular seismicity revealing the deformation consequent to crustal extension. Knowledge of the OG seismicity mostly relies on studies carried out in the 1970s that revealed a local concentration of seismic activity. Seismic data are here reexamined with regard to the more recent data available on the International Seismological Center (ISC) website.

The OG seismicity was first officially described by Gane and Oliver (1953) who recorded a series of earthquakes in 1951–1953 thanks to the four first South African seismographs. From May 1952 to May 1953, 33 events were recorded, mostly exceeding magnitude 5, with a maximum of 6.7 clustering in the Okavango Delta. Until the mid-1960s, seismicity in Africa was poorly documented, mostly based on anecdotal evidence. From 1959 to 1965, the Rhodesia Meteorological Services deployed the first network of seismographs in Zimbabwe revealing the seismic activity of the OG. The closest seismic station was at Bulawayo, Zimbabwe, 400 km away from the OG. This equipment led to the founding works of Reeves (1972a) and Scholz et al. (1976), who both identified elevated earthquake activity in the OG and proposed a relation between the seismicity in Botswana and the EARS. But their data differ slightly: although the article of Scholz et al. (1976) is later, it shows fewer earthquakes in the central Kalahari than Reeves (1972a). This seems to be mostly due to the different time-spans they studied (1969–1973 and Sept. 1965–Aug. 1971 respectively). Consequently their conclusions differ. While Reeves (1972a) proposed the Kalahari axis, a line 250 km south of the OG, for the EARS extension and proposed no solution for the OG seismicity, Scholz et al. (1976) suggested that the OG is an extension of the EARS and did not mention the seismic activity in the central Kalahari. More recently, Haddon (2005) used the data available from the ISC from 1071 to 1996 and suggested three distinct parallel NE-SW earthquake alignments in the SWEA, with the southern one ending in the OG. Between 2005 and 2008, at least 26 seismic stations were deployed through the EARS and southern Africa by the AfricaArray (Nyblade and Dirks, 2006), leading to a very large increase in the number of recorded seismic events available from the ISC database (Fig. 4). No reexamination of the seismicity in the SWEA has been made since then.

In this study, we use the unreviewed data set from the ISC (downloaded in February 2016), which gathers records from many different

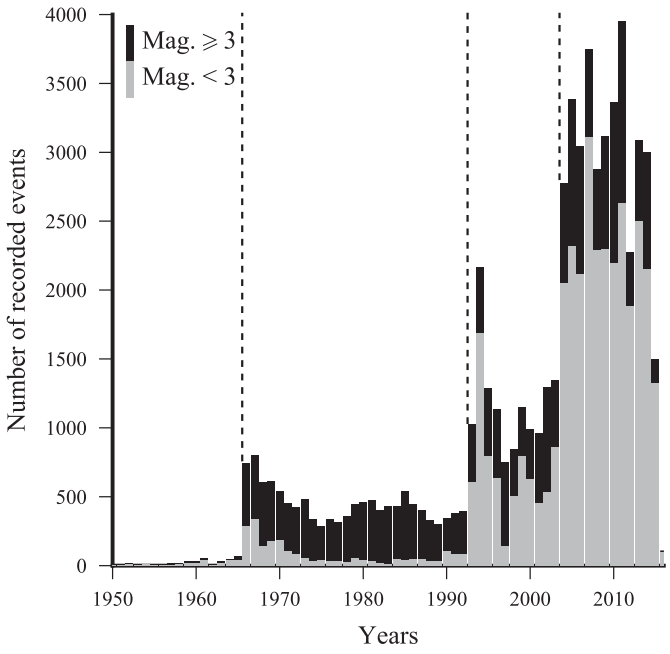

Fig. 4. Number of recorded earthquakes per year from ISC database (from 0°E, 18.7°N to 51.7°E, 38°S and from the 16/03/1901 to the 06/02/2016). Dotted lines mark the dates of significant improvements in seismic instrumentation in Africa.

seismological networks in Africa. The deployment of seismic instrumentation in the EARS took place in four stages (Fig. 4). Prior to the mid-1950s, records are scarce and mostly based on anecdotes. Then the first network of seismometers arrived, which brought the initial insights into African seismicity. The third phase began in 1993. The increase in the number of recorded events seems to be mostly due to the addition of minor earthquakes (magnitude < 3), with the number of powerful events remaining constant. The current phase with a denser network began in 2004, and has led to at least double the number of recorded events for both high and low magnitudes.

These new data highlight an instrumental bias in the previous seismic studies due to the paucity of seismometers on the continent. This bias is corroborated by the historical seismicity (1952–1953 seismic series and prior) recovered from anecdotal evidence in a country mostly comprised of desert, and thus sparsely inhabited. Reeves (1972b) introduced his study with these biases. The overall larger number of seismic events with magnitude over 3 recorded since 2004 compared to the 1966–2003 period indicates that this instrumental bias had an impact not only on microseismic records. Some earthquakes greater than magnitude 3 may well have remained invisible to the previous network. Due to the low density of seismic stations, some earthquakes may be recorded by only one seismological network. The ISC review procedure requires each earthquake to be recorded by at least two networks. This procedure cannot readily be applied in Africa, justifying our usage of the unreviewed data set, although it prevents any quantitative approach. In order to get rid of this instrumental bias, data before 2004 were excluded in this study at the scale of the central and southern Africa.

In Botswana, this instrumental bias seems to have hidden or obscured major areas of seismic activity. While the OG represented a major proportion of the seismicity in Botswana before the 2004 instrumentation, it now appears to represent a minor part of it (Fig. 5). This change is due to both a decrease in the Delta seismic activity and an increase of the records in remote parts of the country because of the improved coverage of the seismic network. Seismic data since 2004 show many more earthquakes with magnitude over 3 which suggest that some areas remained invisible to the previous network, one of which is the central Kalahari.

North and west Botswana experienced a dense series of more than 400 earthquakes from August 2013 to December 2014 with a majority of magnitudes ranging from 3 to 5.6. About half of these events were located in the central Kalahari, south of the Ghanzi ridge. This area corresponds to a ENE striking Karoo failed rift filled with Karoo sediments from Permian to Jurassic, capped by Karoo basalts (Haddon et al., 1999). No particular earthquake concentration can be identified on the Zoetfontein fault. Furthermore, the seismic

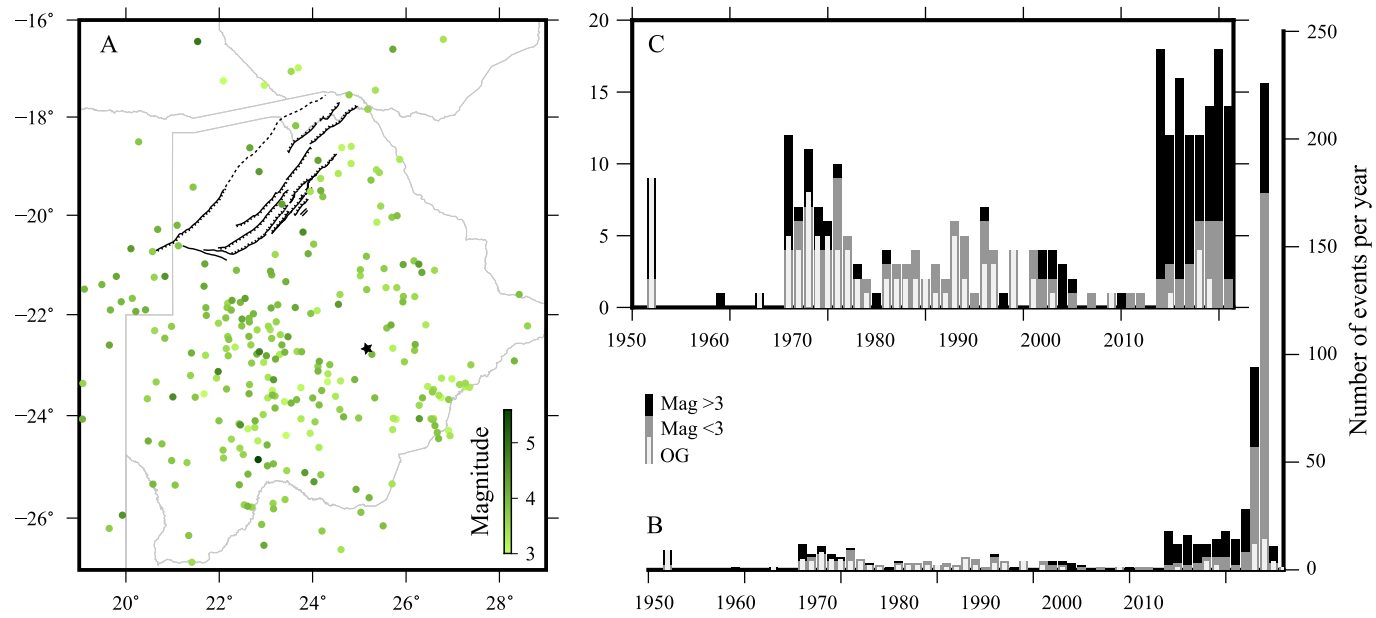

Fig. 5. Seismicity in Botswana. A: Location of earthquakes from August 2013 to December 2014. The black star shows location of the recent M6.5 earthquake. B: Number of events per year in Botswana and the OG (International Seismological Centre, 2016). C: Zoom on previous graph, note the expanded scale.

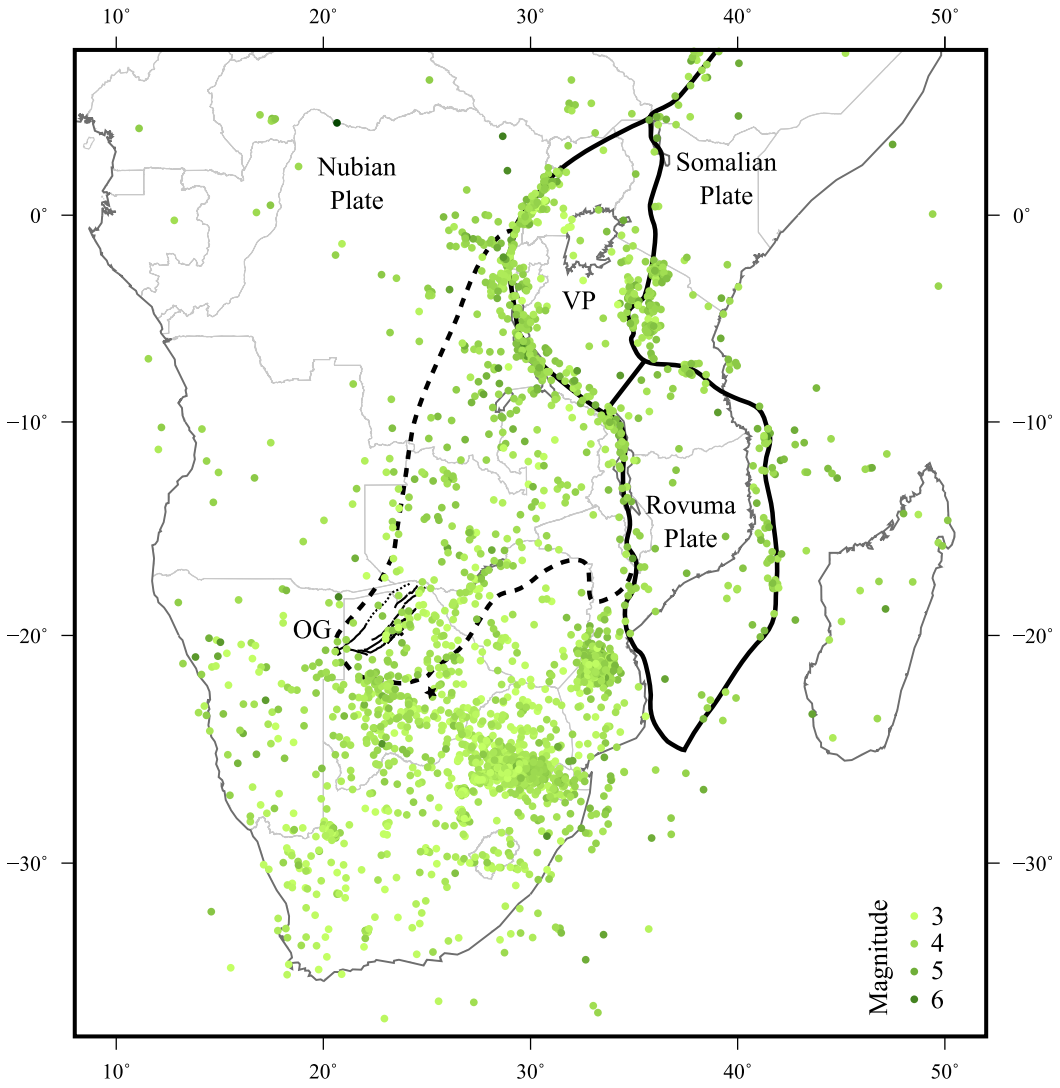

Fig. 6. Recorded earthquakes from 2004 to 2016, with magnitude over 3 (International Seismological Centre, 2016). The black star indicates the location of the recent M6.5 earthquake. Plate boundaries are from Saria et al. (2014).

province shows a NW-SE orientation superimposed on a topographic ridge. During this 2013–2014 seismic series in Botswana, only 26 events were recorded in the OG, one magnitude of 4.4 occurring in the Mababe Depression.

In Fig. 6, only events after 2004 were plotted. Moreover, only events with a magnitude exceeding 3 have been retained, to prevent any earthquake induced by human activity such as mining. In this data set, the SWEA is seismically less defined, as the earthquakes in the central Kalahari induce a spatial continuity between the seismicity of the SWEA and South Africa. Most of the seismic stations deployed in 2004/2005 were installed in South Africa. This heterogeneity leads to a better detection of earthquakes in southern Africa, relative to the SWEA, and thus an apparent higher seismic activity.

Within the SWEA, three striking spatial features appear. (1) Whereas former data showed three distinct potential extension branches with a NE-SW orientation through the SWEA, data from between 2004 and 2016 reveal a much more dispersed seismicity in the whole SWEA. While seismic events with magnitude over 3 are indeed more dense on the three NE-SW branches described by Haddon (2005), axes of earthquake clusters are also visible on the NW-SE orientation (from mid-Congo to northern Malawi, from eastern Angola through Zambia and Zimbabwe and from eastern Namibia through central Kalahari to northeastern South Africa). Microseismicity is present throughout the grid pattern defined by these axes. (2) The Luangwa/Kariba axis shows the longest and most continuous alignment, and extends across the entire African continent as far as the Namibian atlantic coast, in continuity with the Damara belt. (3) Some areas reveal particular seismic activity, like the Loma river in eastern Congo, the previously assumed aseismic Ghanzi Ridge and the central Kalahari.

Given that the OG has been quite well-monitored since the late 1960s, we considered all recorded events for our analysis of local seismicity (Fig. 3). Within the graben, seismic activity is concentrated on the SW faults between the Tsau and Thamalakane faults on a NW-SE axis ending at MAUA in alignment with the Panhandle. To the northeast the Mababe depression shows significant seismicity whereas the southwestern Lake Ngami seems to be relatively aseismic. No activity has been recorded on the Gumare fault, where it is clearly defined, but some appears on its presumptive extension northeast of the Delta up to the northern part of the Linyanti swamps. Most of the earthquakes are confined to the central distal part of the Delta, close to the current outlets. The northern block of the graben is

stable relative to the activity in the central block. Unlike the central block, the southern block shows greater seismic activity in its southwestern part than in its northeastern part between the Delta and the Makgadikgadi pans.

This seismologic reexamination reveals an historic instrumental bias in the seismic records in southern Africa. The seismicity of the SWEA area is more homogeneously distributed over the numerous tectonic structures than previously thought and extends to the southwestern African coast. This may reveal a wider distribution of the deformation in the SWEA. Some seismically active areas were invisible to the previous network, especially the southern Karoo failed rift, reducing the significance of the seismicity in the OG relative to the rest of Botswana. This hypothesis was very recently supported by the occurrence of one of the most powerful recent earthquakes in Southern Africa, south of the Makgadikgadi pans (M>6, https://earthquake.usgs.gov). Thus the OG does not seismologically conform to the strict definition of a rifting zone. There appear to be discrepancies between the distributions of events in previous studies and those derived from the current ISC database, which call for further investigation.

1.2.2. From the crust to the mantle

Crust models for the OG area are proposed by two local studies based on seismic receiver functions (Yu et al., 2015b) and aeromagnetic and gravity data (Leseane et al., 2015). Both studies indicated a thinned crust beneath the OG relative to the adjacent crust although they suggest different magnitudes for the thinning (4 to 5 km and 10 to 12 km respectively). Within the same seismic study, the estimate of crust thickness at Maun varies from 37.5 and 38 km to 43.6 and 44.2 km (respectively for the station B06OR of the temporary SAFARI Network, Yu et al. (2015b), and the station MAUN of the temporary Congo Craton Network, Kachingwe et al. (2015)), depending on the seismic rays sampled. The wide range of values highlights the uncertainty intrinsic to the interpreted thickness, and in fact this range exceeds the proposed thinning.

Various values for the OG Moho depth are found in continental scale studies; they lie between 37 km as reported by Tugume et al. (2013) to 43 to 45 km in the Earth crustal model CRUST1.0 (Laske et al., 2013). Both studies show a crustal thinning in the OG relative to the thick adjacent Congo (45 km and 46 km respectively) and Kalahari (45 km and 48 km respectively) cratons. 38 km is a thickness commonly found in the (globally relatively thick) African crust. Such a value is found at Rundu (Kachingwe et al., 2015) and even in the Congo craton, areas in which rifting is commonly assumed to be absent. This latter study found an average crustal thickness of 39 $+/-2$ km for southern Africa.

In the EARS, crustal thickness varies from north to south, from 25 ± 3 km in the Afar Depression, to 30 to 35 km beneath the Kenyan rift (Dugda et al., 2005) and 35 to 40 km for the eastern branch end in Tanzania. In the western branch, the Moho is at a depth of 30–35 km (Bram and Schmeling, 1975), 38 to 42 km beneath Lake Tanganyika (Dugda et al., 2005; Kachingwe et al., 2015), but differences of up to 4 km are found within the same rifts (southern Kenyan rifts for instance) showing strong lateral variability. Gummert et al. (2015) developed a high-resolution Moho topography across the Albertine rift and showed that the crustal depth varies from up to 39 km at the rift shoulders to a minimum of 22 km within the rift shoulders. The wide range of values and the associated uncertainties for depth to Moho in southern Africa make it difficult to infer a direct relationship between rifting and crustal thinning in the OG.

The lithosphere thickness in the area was determined by local magnetotelluric studies at about 160 km for the Damara belt, 180 km for the Ghanzi-Chobe belt, at least 250 km for the Congo craton, and 220 km for the Kalahari craton (Muller et al., 2009; Begg et al., 2009; Miensopust et al., 2011; Khoza et al., 2013). The proposed Kalahari craton lithospheric thickness is supported by kimberlite pipe studies, which show a thickness of at least 200 km south of the Makgadikgadi pans (Griffin et al., 2003). It is worthwhile to note that 160 km does not represent thin lithosphere. According to Begg et al. (2009), these lateral variations in lithosphere indicate the different tectonothermal ages for the three different units in the area (Congo craton, Damara/Ghanzi-Chobe belt, Kalahari craton). Moreover, this relative thinning of the lithosphere falls short of values given for more evolved features in the EARS: from 50 km thick in the western branch (Lake Edward, Lake Kivu) to less than 40 km in the more evolved Kenyan rift (Simiyu and Keller, 1997).

At greater depth, Yu et al. (2015a) found no perturbations in the d410 and d660 discontinuities between the deeper Congo craton (ca. 410 km) and the shallower Kalahari craton (ca. 390 km). The Mantle Transition Zone shows no significant thinning and thus no evidence for thermal perturbation beneath the OG. These observations are corroborated by seismic tomography revealing the African plume at much greater depth (Forte et al., 2010; Steinberger et al., 2010). All these models conclude on null to positive anomalies for S-waves velocity, revealing relatively colder material, down to at least 800 km in the mantle, thus precluding any mantle influence on the OG activity.

The EARS extension hypothesis for the OG was supported by the first gravity anomaly surveys (Girdler, 1975). The currently available Bouguer anomaly data (The International Gravimetric Bureau, 2012) show a great negative Bouguer anomaly tightly correlated with the EARS (from ~ -260 to $<\sim -90$ mGal). The strongest is located on the northern part of the EARS, the Afar Depression, and corresponds to the well-established section of the EARS. This negative anomaly is due to the shallow asthenosphere beneath the rift. It extends along the eastern branch. The western branch is characterized by weaker but still significant negative anomalies. An extensive area of discontinuous moderate negative anomaly extends southwestwards from Lake Tanganyika through the southern Congo, Zambia, northwestern Botswana, Angola and as far as Namibia. The strongest anomaly is found beneath lakes Mweru and Bangweulu. Beneath the OG, the average Bouguer anomaly (−112 mGal) is not significant enough to support the hypothesis of uplifted lithosphere.

Direct measurements of heat flow in the study area are scattered and inhomogeneous. Ballard et al. (1987) found greater heat flow values for sites on the Damara belt (from 50 and 80 mW/m^2 towards the inner belt) than on the Kalahari craton (60 to 30 mW/m^2 towards the inner craton). But they explain this distribution in terms of fundamental difference in thermal structure between the craton and the belt thus indicating the difference of lithospheric history and this does not necessarily imply a rift system in the area. Recently, Davies (2013) provided a global Earth surface heat flow by combining direct measurements and geology and showed no significant heat flow beneath the OG. This conclusion is supported by the absence of significant delays in teleseismic P- and S-wave traveltime residuals (Yu et al., 2015a), which are commonly found beneath rifting zones. This lack of pronounced heat flow further supports the absence of rifting in the area.

Thus, we can not conclude that crustal and lithospheric thinning can be attributed to recent rifting from seismic and magnotelluric tomographies, gravity anomalies and heat flow measurements. The observed thinning in the Damara belt relative to its surrounding cratons is as likely to be inherited from long tectonic history, as to be acquired by recent continental rifting. Mantle activity cannot have caused the OG tectonic activity as it has beneath the EARS.

2. Geodetic study

In the framework of the fault morphology and normal focal mechanisms proposed by Scholz et al. (1976), the displacement field across the OG would be expected to be extensional, as proposed

in the World stress map (Heidbach et al., 2010). In order to constrain the OG model better, we generated three time series of precise positioning from permanent GPS stations.

2.1. Data and methods

We used Global Navigation Satellite System (GNSS) data from three permanent stations (MAUA, MONG and RUND, Fig. 1) belonging to the AfricaArray (data downloadable at http://afref-data.org) available on the UNAVCO website (https://www.unavco.org/data/gps-gnss/gps-gnss.html). They were set up in August 2010. MAUA is still active whereas MONG and RUND were interrupted in 2015 and 2014 respectively. MAUA is located on the edge of the graben southern block, southeast of the Thamalakane fault. RUND and MONG are located on the northern block, on the Cubango and upper Zambezi rivers respectively. 26 International GNSS Service (IGS) or AfricaArray permanent GNSS stations completed the network.

Daily solutions for station positions in ITRF08 were computed with the GAMIT/GLOBK 10.6 processing software (Herring et al., 2015), adjusting IGS final orbits and estimating tropospheric parameters (1 tropospheric zenith delay/2 h, 2 couples of horizontal gradients/day). The VMF1 Mapping function (Boehm et al., 2006), the ocean loading model FES2004 (Lyard et al., 2006), atmospheric loading according to Tregoning and van Dam (2005), and the absolute antenna phase center variation model IGS08 were used. Velocities were computed by the Kalman filter GLOBK with the "real-sigma" strategy. The reference frame is set up by constraining 19 IGS stations to their ITRF08 velocities (Altamimi et al., 2012).

The horizontal velocities of the stations MONG and RUND were then computed relative to MAUA to generate relative velocities for both sides of the graben.

2.2. Results

Time series of daily solutions for the three stations (Fig. 7) show linear tendencies modulated by a strong annual frequency. In this study we focus on the long-term linear trends and particularly on the horizontal components which reflect displacement within the Nubian plate. The annual signal is related to seasonally pulsed surface and groundwater levels, which reflect surface response to the periodic hydrological loading as modeled in areas subject to similar variations (Tregoning et al., 2009; Chanard et al., 2014). The vertical component is particularly impacted; the observed long-term trend is thus under the influence of both tectonics and hydrology and is therefore not used in this study as it will be discussed in another article (Pastier et al., in preparation).

All three stations move northeastwards but their rates differ slightly. The northern block on which RUND and MONG are located shows a very slow and steady NE to ENE displacement relative to the southern one, i.e. to MAUA (respectively 1.16 ± 0.09 mm/year and 1.33 ± 0.1 mm/year, Fig. 8). Within the northern block, MONG moves slightly faster and in a more northerly direction than RUND. In the vertical component, the elevations of all stations are increasing but the Okavango stations (RUND and MAUA) show a higher rate than the Zambezi station (MONG). Within the Okavango system, the rate of MAUA is higher than that of RUND.

The horizontal inner-plate displacements between the OG northern (RUND and MONG) and southern blocks (MAUA) show no extension perpendicular to the main trend of the graben during the past 5 years (Fig. 8), but do show a low dextral strike-slip displacement. These displacements are in the ranges of standard error reported by Saria et al. (2014), which used GAMIT/GLOBK with another wider network centered on the EARS. Our velocities correspond still better with the MIDAS automatic computation using GIPSY OASIS II software (Blewitt et al., 2016). These results are also consistent with the predictions of Reeves (1972b) and McCarthy (2013) for a very low deformation rate in the structure.

Movement within the northern block (between RUND and MONG) appears to be a very slow (≈0.4 mm/year) sinistral strike-slip displacement. This slight deformation could be accommodated on the supposed faults controlling the Panhandle, the Kwando and/or the Upper Zambezi.

The observed deformation rate is very low (1 mm/year) and restricted to a dextral strike-slip displacement in agreement with the dyke offset observed by Campbell et al. (2006). Surprisingly, no extensional component perpendicular to the OG main trend is observed. This may be a result of the relatively short period of record of the GPS time series, but the fact that it includes in its entirety one of the major seismic episodes in the area gives strength to our results. No significant displacement can be associated with the 2013–2014 high seismic activity for the MAUA GPS station located on the Thamalakane fault (supposedly one of the most active). The only earthquake inducing a very slight shift on the GPS time series happened on the 4th June, 2015, in the Mababe Depression. This low deformation rate is supported by the apparently very stable surface morphology of the Delta (McCarthy, 2013). The long-term strike-slip displacement observed on the GPS time series confirms the findings of Modisi (2000) and Campbell et al. (2006) in their tectonic model for the OG. The strike-slip dominated deformation is in contrast with the extensional EARS rifts, which exhibit higher rates of extension (from 1.2 to 2.8 mm/year in the Western Branch).

3. Discussion

3.1. Okavango Graben structural model

This geodetic study brings new constraints on the OG showing only strike-slip displacement on the tectonic structure. This movement is supported by the dextral displacement of the Karoo dykes from 1 km on the Thamalakane fault to 5 km on the Kunyere fault (Campbell et al., 2006). The strike-slip displacement could also be accommodated by the arcuate central strike-slip fault (Fig. 3). Seismic activity in the OG shows the major deformation currently occurs mostly between the Thamalakane and the Tsau faults in the vicinity of MAUA. Amongst the three depocenters described by Kinabo et al. (2007), the Mababe Depression and the Linyanti swamps show significant seismic activity, but Lake Ngami (i. e., the southern part of the Kunyere fault) shows no earthquake activity in the ISC data set. Thus deformation is mainly accommodated in the OG northeastern part. The very steady deformation rate, even during the 2013–2014 period of high seismic activity, supports the hypothesis that water may act as a lubricant in the upper part of the faults (Bufford et al., 2012). Extension within the basin could be responsible for the NW-SE geomorphologic features described by Modisi et al. (2000).

Based on its kinematics and geometry, it is still challenging to determine which model of a strike-slip basin the OG fit best: pull-apart or transtensional basin, as allowed by the uncertainty associated with horizontal displacement rates (cf. Fig. 9). Indeed, the structural heritage is so influential that it controls the fault orientation and potential activity. The SSZ can act as a lock, which can explain the lack of seismic activity SW of the OG and constrain the geometry of the current structure. Thus no direct relationship between fault orientation and activity and the regional stress can be precisely established. Based on the basin morphology, the width of the OG (≈150 km), its sediment thickness (600 m at its very maximum) and the number of depocenters (3) foster the transtensional type (Wu et al., 2009). The low observed deformation rate strengthens the assumption of low subsidence based on the morphology of the surface of the Okavango Delta (McCarthy, 2013), which also supports the transtensional basin model. This observation, as well as the

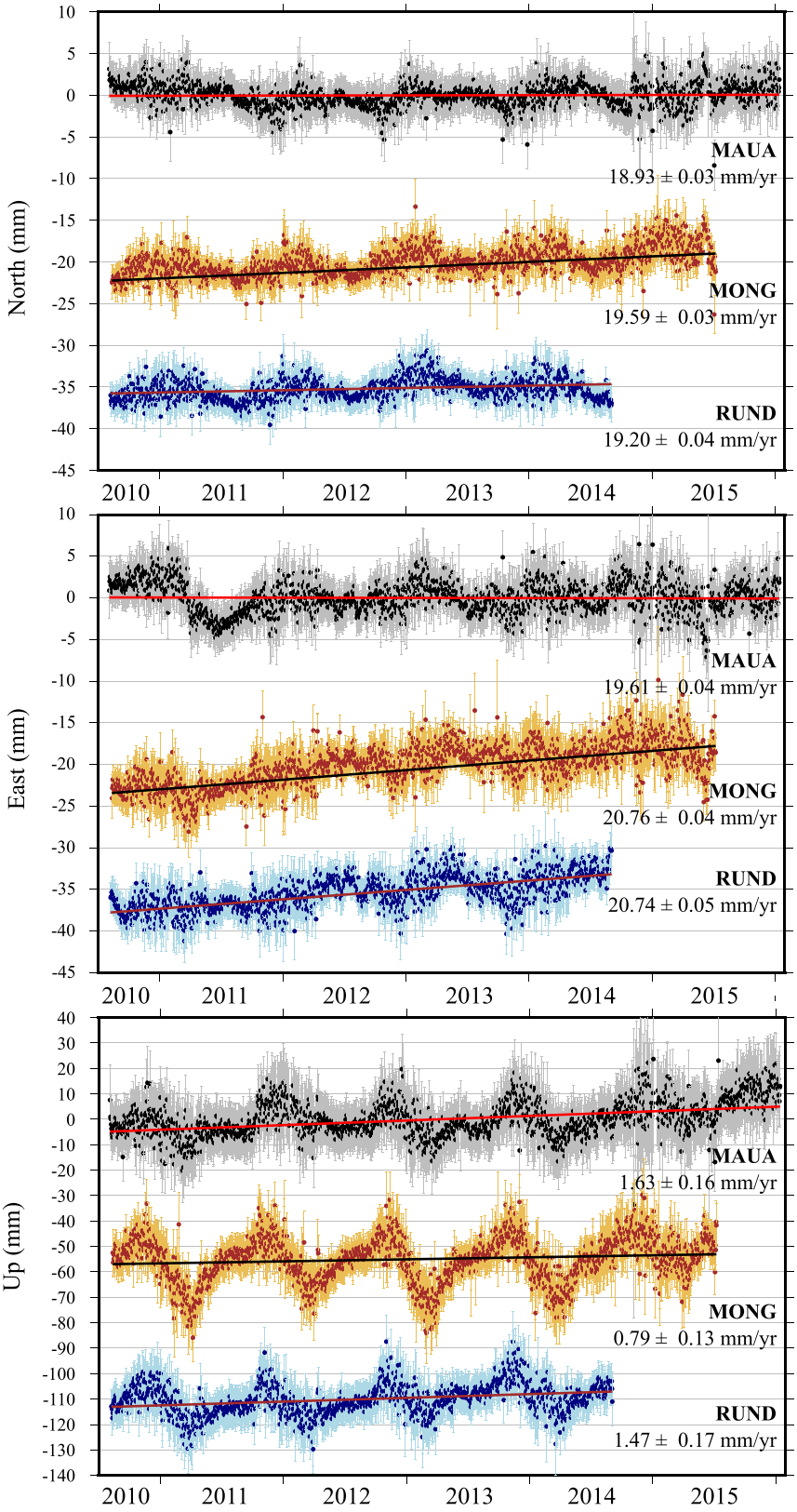

Fig. 7. Time series from the AfricaArray permanent GNSS stations records. Raw rates calculated by GLOBK are indicated under station name for each component; linear trends are drawn with straight lines. North and east components are shown detrended with MAUA's rate, vertical positions are plotted without correction.

NW-SE extension visible in the moment tensor of the recent M6.5 earthquake in central Kalahari, is in contradiction with the stress regime defined in the World Stress Map (Heidbach et al., 2010).

As a strike-slip initiation is not precluded in a rift system, the insights brought by this review allow us to re-open the debate on the rifting nature of the OG in the context of the criteria defining a rifting

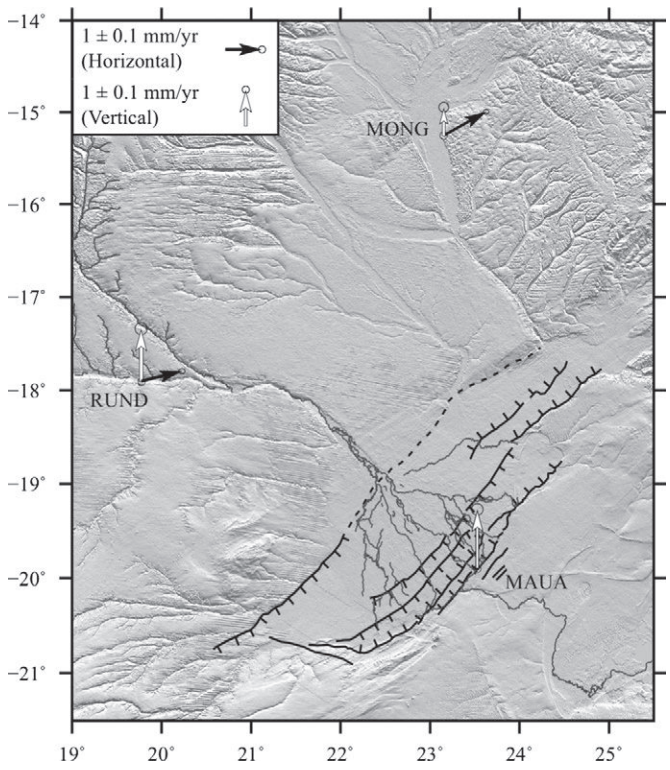

Fig. 8. Displacements of the three permanent GNSS stations. Horizontal rates are shown in black arrows, relatively to MAUA. Vertical rates are shown in white arrows. Background shows hillshade based on SRTM30.

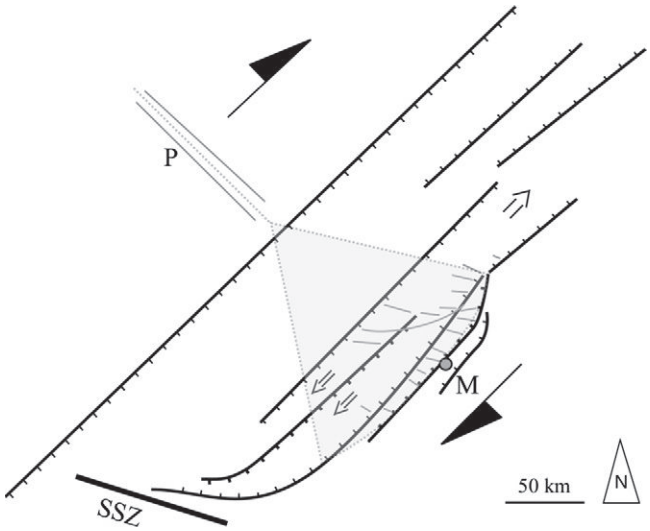

Fig. 9. Synthetic structural model for the OG showing strike-slip displacement astride the graben and extension on the secondary fault set, in the interslip of the primary fault set. The grey area shows the extent of the Okavango Delta. M: Maun, P: Panhandle. The grey area represents the extent of the Okavango Delta.

zone. The lithosphere and possibly the crust show a thinning relative to the adjacent blocks. This may be explained by the relative younger age of the Damara and Ghanzi-Chobe belts (Begg et al., 2009). Thus there is no substantive evidence to determine if this thinning was acquired recently through rifting or is inherited from the long and complex tectonic history of the area. No significant heat flow seems to rise to the surface and there is no strong Bouguer gravity anomaly to indicate an upwelling asthenosphere. Once the observational bias is removed from the record, the OG is not the most prominent center of seismic activity in the area, contrary to earlier observations, which led to the EARS hypothesis. Further, the lack of an anomaly in seismic waves observed beneath the graben suggests no influence from the mantle on the observed deformation. This re-examination of the evidence shows that the OG does not conform to the current definition of a rift system, although the possibility that it may develop into a rift system in the future cannot be ruled out. Consequently, we propose to re-name the system the Okavango Graben instead of the Okavango Rift Zone, to avoid any unfounded implications about genesis.

3.2. Regional contextualization

Our conclusion that the OG is not a rifting zone and hence cannot be considered as an analogue of the EARS rifts is in agreement with Khoza et al. (2013), McCarthy (2013) and Yu et al. (2015a) who questioned the dynamics of the tectonic activity. Both latter studies proposed new deformation models based on accommodation of differential far-field plate movements, consequent to the EARS dynamics according to McCarthy (2013) or to Kalahari craton displacement relatively to the central to northern Nubian plate in the case of Yu et al. (2015a). We propose to reconcile these two models to explain the strike-slip displacement in the OG and more generally the deformation observed in the whole SWEA (Fig. 10). Rather than rifting features, we suggest that the numerous horsts and grabens present in the SWEA compose an extensive area accommodating two distinct plate or block displacements. (1) The differential displacements between the diverging Victorian and Rovuma plates and the Nubian plate exhibit a gradient in extension rates, with higher rates at Lake Tanganyika decreasing northwards and southwards (Saria et al., 2014). The differences in seismic activity on each side of the EARS western branch show that the consequent deformation is mainly accommodated in the Nubian plate. Differential displacements leading to differential deformation could cause an extensive shear zone in the far-field. (2) The displacement between the Kalahari craton and the relatively stable central and northern Nubian plate was found to be clockwise relative to the Nubian plate and to reach 0.5 to 2 mm/year (Malservisi et al., 2013). NW-SE secondary fault sets are found in many SWEA grabens. These observations support the hypothesis for at least partial strike-slip displacements in the SWEA.

The distribution of SWEA faults appears to be strongly controlled by preexisting structures. Ancient faults are reactivated in Pan-African belts, and thus most of them exhibit the Proterozoic NE-SW strike. In the northern SWEA, faults appear not to propagate far from the EARS, which may reveal the influence of the Congo craton, the crust being too old to be broken-up. On the other hand, in the southern SWEA, Pan-African belts traverse the whole continent and offer a pathway of lithospheric weakness to accommodate far-field deformation. The distribution of faults exhibits two gradients with fault density increasing from north to south and from ESE to WNW. These gradients may reveal the differential stress distribution due to the two distinct sources of displacement. In the northern SWEA, the accommodated deformation only corresponds to the EARS differential opening rates. Southwards the influence of the Kalahari craton displacement increases to reach a maximum fault density in the Luangwa Valley and Chicoa trough. In the same way, the SWEA southwestern part is under the influence of only the Kalahari craton displacement, while the influence of the EARS opening increases northeastwards. These kinematics could then induce a transtensional stress regime in the whole SWEA. Such a distributed deformation model would also better fit the diffusion observed in the geophysical parameters (seismicity and Bouguer anomaly) than a model based on localized EARS extension branches.

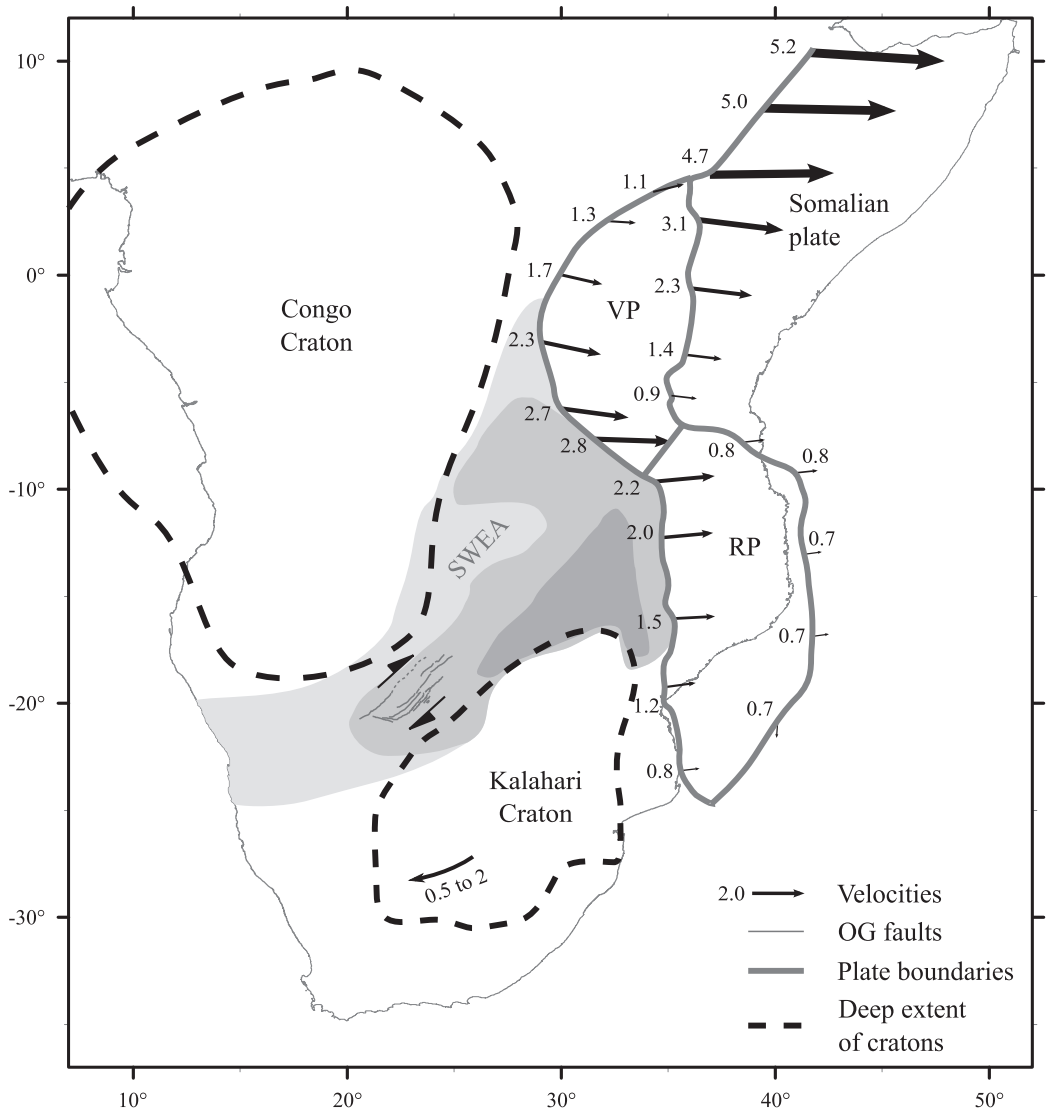

Fig. 10. EARS block limits and velocities (in mm/year, relative to adjacent blocks) from Saria et al. (2014), South Africa velocity relative to the Nubian plate from Malservisi et al. (2013). In the SWEA, increasing saturation represents observed fault density and hence probably increased deformation, revealing the distribution of the lithospheric weakness and conjugated influences of the southern Africa displacement and the EARS opening. RP: Rovuma plate, VP: Victoria plate.

4. Conclusion

The present geodetic study shows a very low strike-slip displacement on the entire OG at a rate about 1 mm/year. This deformation, as well as recent geophysical data, does not support the OG EARS extension hypothesis. The processes at play regarding the activity of the OG faults are called into question, as the tectonic structure better fits a transtensional basin model. The OG does not conform well with the classical definition of a rift system. Neither horizontal extension nor lithosphere thinning is found in the area, nor is there evidence of pronounced seismicity. Therefore, the OG should not be regarded as an incipient rifting zone. Several other tectonic structures diverge from the EARS western branch. These horsts and grabens are distributed in the extensive SWEA. We propose that this area is a deformation zone accommodating differential movements between the Nubian and Somalian, Victoria and Rovuma plates on one side and between the rigid Congo and Kalahari cratons within the somewhat less stable Nubian plate on the other side. Coupling these two deformations leads to a maximum deformation on the Chicoa-Luangwa-Kariba branch, which decreases and disperses west of the Botswana border to disappear through Namibia. In Botswana, the OG may not be the most active area as the seismicity in the central Kalahari has been obscured by instrumental bias in the African seismic network until 2004. We thus propose to change the commonly used but genetically loaded name “Okavango Rift Zone” to a more geologically neutral, descriptive, “Okavango Graben”.

Acknowledgments

We wish to thank the Okavango Research Institute and the Research Services Team for their precious support and warm hospitality. We thank the AfricaArray and UNAVCO for the availability of their data, as well as the critical view of its members. We also thank the reviewers for their constructive comments. Finally, we thank the INSU,CNRS and the University of Rennes 1 for the grants that funded our study.

Appendix A. Supplementary data

Supplementary data associated with this article can be found in the online version at http://dx.doi.org/10.1016/j.tecto.2017.05.035.

These data include the Google map of the most important areas described in this article.

References

Allen, P.A., Allen, J.R., 2013. Basin Analysis: Principles and Application to Petroleum Play Assessment. Third ed., John Wiley & Sons.

Altamimi, Z., Métivier, L., Collilieux, X., 2012. Itrf2008 plate motion model. J. Geophys. Res. Solid Earth 117, 1–14. http://dx.doi.org/10.1029/2011JB008930. b07402.

Ballard, S., Pollack, H.N., Skinner, N.J., 1987. Terrestrial heat flow in Botswana and Namibia. J. Geophys. Res. Solid Earth 92, 6291–6300. http://dx.doi.org/10.1029/JB092iB07p06291.

Begg, G., Griffin, W., Natapov, L., O'Reilly, S.Y., Grand, S., O'Neill, C., Hronsky, J., Djomani, Y.P., Swain, C., Deen, T., Bowden, P., 2009. The lithospheric architecture of Africa: seismic tomography, mantle petrology, and tectonic evolution. Geosphere 5, 23–50. http://geosphere.gsapubs.org/content/5/1/23.abstract. http://dx.doi.org/10.1130/GES00179.1. arXiv:http://geosphere.gsapubs.org/content/5/1/23.full.pdf+html.

Blewitt, G., Kreemer, C., Hammond, W.C., Gazeaux, J., 2016. MIDAS robust trend estimator for accurate GPS station velocities without step detection. J. Geophys. Res. Solid Earth 121, 2054–2068. http://dx.doi.org/10.1002/2015JB012552. 2015JB012552.

Boehm, J., Werl, B., Schuh, H., 2006. Troposphere mapping functions for GPS and very long baseline interferometry from European Centre for Medium-Range Weather Forecasts operational analysis data. J. Geophys. Res. Solid Earth 111, http://dx.doi.org/10.1029/2005JB003629. b02406. n/a–n/a.

Bram, K., Schmeling, B.D., 1975. Structure of crust and upper mantle beneath the Western Rift of East Africa, derived from investigations of near earthquakes. Afar between continental and oceanic rifting 2, Schweizerbart, Stuttgart, Germany., pp. 138–143.

Bufford, K.M., Atekwana, E.A., Abdelsalam, M.G., Shemang, E., Atekwana, E.A., Mickus, K., Moidaki, M., Modisi, M.P., Molwalefhe, L., 2012. Geometry and faults tectonic activity of the Okavango Rift Zone, Botswana: evidence from magnetotelluric and electrical resistivity tomography imaging. J. Afr. Earth Sci. 65, 61–71. http://www.sciencedirect.com/science/article/pii/S1464343X12000167. http://dx.doi.org/10.1016/j.jafrearsci.2012.01.004.

Campbell, G., Johnson, S., Bakaya, T., Kumar, H., Nsatsi, J., 2006. Airborne geophysical mapping of aquifer water quality and structural controls in the Lower Okavango Delta, Botswana. S. Afr. J. Geol. 109, 475–494. http://sajg.geoscienceworld.org/content/109/4/475. http://dx.doi.org/10.2113/gssajg.109.4.475. arXiv:http://sajg.geoscienceworld.org/content/109/4/475.full.pdf.

Chanard, K., Avouac, J.P., Ramillien, G., Genrich, J., 2014. Modeling deformation induced by seasonal variations of continental water in the Himalaya region: sensitivity to Earth elastic structure. J. Geophys. Res. Solid Earth 119, 5097–5113. http://dx.doi.org/10.1002/2013JB010451.

Chorowicz, J., 2005. The East African Rift System. J. Afr. Earth Sci. 43, 379–410. http://www.sciencedirect.com/science/article/pii/S1464343X05001251. http://dx.doi.org/10.1016/j.jafrearsci.2005.07.019. phanerozoic Evolution of Africa.

Davies, J.H., 2013. Global map of solid Earth surface heat flow. Geochem. Geophys. Geosyst. 14, 4608–4622. http://dx.doi.org/10.1002/ggge.20271.

De Wit, M., Vitali, E., Ashwal, L., 1995. Gondwana reconstruction of the East Africa-Madagascar-India-Sri Lanka-Antarctica fragments revised. Centennial Geocongress, Extended Abstracts 1, , pp. 218–221.

Du Toit, A., 1927. The Kalahari and some of its problems. S. Afr. J. Sci. 24, 88–101.

Dugda, M.T., Nyblade, A.A., Julia, J., Langston, C.A., Ammon, C.J., Simiyu, S., 2005. Crustal structure in Ethiopia and Kenya from receiver function analysis: implications for rift development in eastern Africa. J. Geophys. Res. Solid Earth 110, http://dx.doi.org/10.1029/2004JB003065. b01303. n/a–n/a.

Fairhead, J., Girdler, R., 1969. How far does the rift system extend through Africa? Nature 221, 1018–1020. http://dx.doi.org/10.1038/2211018a0.

Forte, A.M., Quéré, S., Moucha, R., Simmons, N.A., Grand, S.P., Mitrovica, J.X., Rowley, D.B., 2010. Joint seismic-geodynamic-mineral physical modelling of African geodynamics: a reconciliation of deep-mantle convection with surface geophysical constraints. Earth Planet. Sci. Lett. 295, 329–341. http://www.sciencedirect.com/science/article/pii/S0012821X10001883. http://dx.doi.org/10.1016/j.epsl.2010.03.017.

Gane, P., Oliver, H., 1953. South African earthquakes–1949 to December 1952. Trans. Geol. Soc. S. Afr. 61, 21–35.

Girdler, R.W., 1975. The great negative Bouguer gravity anomaly over Africa. Eos Trans. Am. Geophys. Union 56, 516–519. http://dx.doi.org/10.1029/EO056i008p00516.

Griffin, W., O'Reilly, S.Y., Natapov, L., Ryan, C., 2003. The evolution of lithospheric mantle beneath the Kalahari Craton and its margins. Lithos 71, 215–241. http://www.sciencedirect.com/science/article/pii/S0024493703001142. http://dx.doi.org/10.1016/j.lithos.2003.07.006. a Tale of Two Cratons: The Slave-Kaapvaal Workshop.

Gumbricht, T., McCarthy, T., 2001. The topography of the Okavango Delta, Botswana, and its tectonic and sedimentological implications. S. Afr. J. Geol. 104, 243–264. http://sajg.geoscienceworld.org.biblioplanets.gate.inist.fr/content/104/3/243.abstract. http://dx.doi.org/10.2113/1040243.

Gummert, M., Lindenfeld, M., Wölbern, I., Rümpker, G., Celestin, K., Batte, A., 2015. Crustal structure and high-resolution Moho topography across the Rwenzori region (Albertine rift) from P-receiver functions. Geol. Soc. Lond., Spec. Publ. 420, http://sp.lyellcollection.org/content/early/2015/02/09/SP420.4.abstract. http://dx.doi.org/10.1144/SP420.4. arXiv:http://sp.lyellcollection.org/content/early/2015/02/09/SP420.4.full.pdf+html.

Haddon, I.G., 2005. The Sub-Kalahari Geology and Tectonic Evolution of the Kalahari Basin, Southern African.Ph.D. thesis. Faculty of Science, University of the Witwatersrand.

Haddon, I.G., Erasmus, D.M., Roos, H.M., 1999. Isopach Map of the Kalahari Group.

Heidbach, O., Tingay, M., Barth, A., Reinecker, J., Kurfeß, D., Müller, B., 2010. Global crustal stress pattern based on the world stress map database release 2008. Tectonophysics 482, 3–15. http://www.sciencedirect.com/science/article/pii/S0040195109004132. http://dx.doi.org/10.1016/j.tecto.2009.07.023. frontiers in Stress Research.

Herring, T., King, R.W., Floyd, M., McClusky, S., 2015. Introduction to GAMIT/GLOBK, Release 10.6. Department of Earth, Atmospheric and Planetary Sciences, Massachusetts Institute of Technology.

International Seismological Centre, 2016. On-line Bulletin. International Seismological Center, Thatcham, United Kingdom. Http://www.isc.ac.uk.

Kachingwe, M., Nyblade, A., Julià, J., 2015. Crustal structure of Precambrian terranes in the southern African subcontinent with implications for secular variation in crustal genesis. Geophys. J. Int. 202, 533–547. http://gji.oxfordjournals.org/content/202/1/533.abstract. http://dx.doi.org/10.1093/gji/ggv136. arXiv:http://gji.oxfordjournals.org/content/202/1/533.full.pdf+html.

Khoza, T.D., Jones, A.G., Muller, M.R., Evans, R.L., Miensopust, M.P., Webb, S.J., 2013. Lithospheric structure of an Archean craton and adjacent mobile belt revealed from 2-D and 3-D inversion of magnetotelluric data: example from southern Congo craton in northern Namibia. J. Geophys. Res. Solid Earth 118, 4378–4397. http://dx.doi.org/10.1002/jgrb.50258.

Kinabo, B.D., Atekwana, E.A., Hogan, J.P., Modisi, M.P., Wheaton, D.D., Kampunzu, A.B., 2007. Early structural development of the Okavango rift zone, NW Botswana. J. Afr. Earth Sci. 48, 125–136. http://www.sciencedirect.com/science/article/pii/S1464343X07000258. http://dx.doi.org/10.1016/j.jafrearsci.2007.02.005.

Laske, G., Masters, G., Ma, Z., Pasyanos, M., 2013. Update on CRUST1.0 - A 1-degree global model of Earth's crust. EGU General Assembly Conference Abstracts. pp. EGU2013–EGU2658. http://igppweb.ucsd.edu/gabi/rem.html.

Le Gall, B., Tshoso, G., Jourdan, F., Féraud, G., Bertrand, H., Tiercelin, J., Kampunzu, A., Modisi, M., Dyment, J., Maia, M., 2002. $^{40}Ar/^{39}Ar$ geochronology and structural data from the giant Okavango and related mafic dyke swarms, Karoo igneous province, northern Botswana. Earth Planet. Sci. Lett. 202, 595–606. http://www.sciencedirect.com/science/article/pii/S0012821X0200763X. http://dx.doi.org/10.1016/S0012-821X(02)00763-X.

Lepersonne, J., 1974. Carte géologique du Zaïre, échelle 1:2.000.000.

Leseane, K., Atekwana, E.A., Mickus, K.L., Abdelsalam, M.G., Shemang, E.M., Atekwana, E.A., 2015. Thermal perturbations beneath the incipient Okavango Rift Zone, northwest Botswana. J. Geophys. Res. Solid Earth 120, 1210–1228. http://dx.doi.org/10.1002/2014JB011029.

Linol, B., 2013. Sedimentology and Sequence Stratigraphy of the Congo and Kalahari Basins of South-central Africa and Their Evolution During the Formation and Break-up of West Gondwana.Ph.D. thesis. Nelson Mandela Metropolitan University.

Lyard, F., Lefevre, F., Letellier, T., Francis, O., 2006. Modelling the global ocean tides: modern insights from fes2004. Ocean Dyn. 56, 394–415. http://dx.doi.org/10.1007/s10236-006-0086-x.

Macgregor, D., 2015. History of the development of the East African Rift System: a series of interpreted maps through time. J. Afr. Earth Sci. 101, 232–252. http://www.sciencedirect.com/science/article/pii/S1464343X14003240. http://dx.doi.org/10.1016/j.jafrearsci.2014.09.016.

Malservisi, R., Hugentobler, U., Wonnacott, R., Hackl, M., 2013. How rigid is a rigid plate? Geodetic constraint from the TrigNet CGPS network, South Africa. Geophys. J. Int. 192, 918–928. http://gji.oxfordjournals.org/content/192/3/918.abstract. http://dx.doi.org/10.1093/gji/ggs081. arXiv:http://gji.oxfordjournals.org/content/192/3/918.full.pdf+html.

McCarthy, T., 2013. The Okavango Delta and its place in the geomorphological evolution of Southern Africa. S. Afr. J. Geol. 116, 1–54. http://sajg.geoscienceworld.org/content/116/1/1.abstract. http://dx.doi.org/10.2113/gssajg.116.1.1. arXiv:http://sajg.geoscienceworld.org/content/116/1/1.full.pdf+html.

Miensopust, M.P., Jones, A.G., Muller, M.R., Garcia, X., Evans, R.L., 2011. Lithospheric structures and Precambrian terrane boundaries in northeastern Botswana revealed through magnetotelluric profiling as part of the Southern African Magnetotelluric Experiment. J. Geophys. Res. Solid Earth 116, 1–21. http://dx.doi.org/10.1029/2010JB007740.

Milesi, J.P., Frizon de Lamotte, D., De Kock, G.S., 2010. Carte tectonique de l'afrique. http://www.sudoc.fr/160194628. 1:10 000 000.

Miller, R.M., Pickford, M., Senut, B., 2010. The geology, palaeontology and evolution of the Etosha pan, Namibia: implications for terminal Kalahari deposition. S. Afr. J. Geol. 113, 307–334. http://sajg.geoscienceworld.org/content/113/3/307. http://dx.doi.org/10.2113/gssajg.113.3.307. arXiv:http://sajg.geoscienceworld.org/content/113/3/307.full.pdf.

Modisi, M., 2000. Fault system at the southeastern boundary of the Okavango Rift, Botswana. J. Afr. Earth Sci. 30, 569–578. http://www.sciencedirect.com/science/article/pii/S0899536200000397. http://dx.doi.org/10.1016/S0899-5362(00)00039-7. 50th Anniversary of the Geological Survey.

Modisi, M., Atekwana, E., Kampunzu, A., Ngwisanyi, T., 2000. Rift kinematics during the incipient stages of continental extension: evidence from the nascent Okavango rift basin, northwest Botswana. Geology 28, 939–942. http://geology.gsapubs.org/content/28/10/939.abstract. http://dx.doi.org/10.1130/0091-7613(2000)28<939:RKDTIS>2.0.CO;2. arXiv:http://geology.gsapubs.org/content/28/10/939.full.pdf+html.

Muller, M., Jones, A., Evans, R., Grütter, H., Hatton, C., Garcia, X., Hamilton, M., Miensopust, M., Cole, P., Ngwisanyi, T., Hutchins, D., Fourie, C., Jelsma, H.,

Evans, S., Aravanis, T., Pettit, W., Webb, S., Wasborg, J., 2009. Lithospheric structure, evolution and diamond prospectivity of the Rehoboth Terrane and western Kaapvaal Craton, southern Africa: constraints from broadband magnetotellurics. Lithos 112, Supplement 1, 93–105. http://www.sciencedirect.com/science/article/pii/S0024493709002631. http://dx.doi.org/10.1016/j.lithos.2009.06.023. Proceedings of the 9th International Kimberlite Conference.

Nyblade, A., Dirks, P., 2006. AfricaArray Newsletter. http://africaarray.psu.edu/publications/newsletters/2006_Web.pdf.

Pastier, A.-M., Murray-Hudson, M., Wolski, P., Makati, K., Longuevergne, L., Ramillien, G., Moreau, F., Walpersdorf, A., Dauteuil, O., New insights on the hydrological regime in the Okavango Basin, reciprocal validation from surface deformation, numerical modelling and satellite data (in preparation).

Pinna, P., Marteau, P., Becq-Giraudon, J.F., Manigault, B., 1987. Carta Geológica. República Popular de Moçambique. 1/1.000.000.

Podgorski, J.E., Green, A.G., Kalscheuer, T., Kinzelbach, W.K., Horstmeyer, H., Maurer, H., Rabenstein, L., Doetsch, J., Auken, E., Ngwisanyi, T., Tshoso, G., Jaba, B.C., Ntibinyane, O., Laletsang, K., 2015. Integrated interpretation of helicopter and ground-based geophysical data recorded within the Okavango Delta, Botswana. J. Appl. Geophys. 114, 52–67. http://www.sciencedirect.com/science/article/pii/S0926985115000051. http://dx.doi.org/10.1016/j.jappgeo.2014.12.017.

Reeve, W., Thieme, J., Johnson, R., 1981. Geological Map of Zambia. 1:1,000,000.

Reeves, C., 1972a. Earthquakes in Ngamiland. Botswana Notes Records 4, 257–261.

Reeves, C.V., 1972b. Rifting in the Kalahari? Nature 237, 95–96. http://dx.doi.org/10.1038/237095a0.

Saria, E., Calais, E., Stamps, D.S., Delvaux, D., Hartnady, C.J.H., 2014. Present-day kinematics of the East African Rift. J. Geophys. Res. Solid Earth 119, 3584–3600. http://dx.doi.org/10.1002/2013JB010901.

Scholz, C.H., Koczynski, T.A., Hutchins, D.G., 1976. Evidence for incipient rifting in Southern Africa. Geophys. J. Int. 44, 2135–2144. http://gji.oxfordjournals.org/content/44/1/135.full.pdf+html. http://dx.doi.org/10.1111/j.1365-246X.1976.tb00278.x.

Sengör, A.M.C., Burke, K., 1978. Relative timing of rifting and volcanism on Earth and its tectonic implications. Geophys. Res. Lett. 5, 419–421. http://dx.doi.org/10.1029/GL005i006p00419.

Simiyu, S.M., Keller, G.R., 1997. An integrated analysis of lithospheric structure across the East African plateau based on gravity anomalies and recent seismic studies. Tectonophysics 278, 291–313. http://www.sciencedirect.com/science/article/pii/S0040195197001091. http://dx.doi.org/10.1016/S0040-1951(97)00109-1.

Singletary, S.J., Hanson, R.E., Martin, M.W., Crowley, J.L., Bowring, S.A., Key, R.M., Ramokate, L.V., Direng, B.B., Krol, M.A., 2003. Geochronology of basement rocks in the Kalahari Desert, Botswana, and implications for regional Proterozoic tectonics. Precambrian Res. 121, 47–71. http://www.sciencedirect.com/science/article/pii/S0301926802002012. http://dx.doi.org/10.1016/S0301-9268(02)00201-2.

Stagman, J., 1991. Provisional geological map of Zimbabwe. Original map from 1977 revised in 1991.

Steinberger, B., Buiter, S., Medvedev, S., Tetreault, J., 2010. The mantle under Africa: an overview of global and regional tomography models, lithosphere thickness models and their effect on present-day and past dynamic topography.

The International Gravimetric Bureau, 2012. Iag geodesist's handbook. J. Geod. 86, 946–950.

Tregoning, P., van Dam, T., 2005. Effects of atmospheric pressure loading and seven-parameter transformations on estimates of geocenter motion and station heights from space geodetic observations. J. Geophys. Res. Solid Earth 110, http://dx.doi.org/10.1029/2004JB003334. b03408. n/a–n/a.

Tregoning, P., Watson, C., Ramillien, G., McQueen, H., Zhang, J., 2009. Detecting hydrologic deformation using GRACE and GPS. Geophys. Res. Lett. 36, http://dx.doi.org/10.1029/2009GL038718. l15401. n/a–n/a.

Tugume, F., Nyblade, A., Julià, J., van der Meijde, M., 2013. Precambrian crustal structure in Africa and Arabia: evidence lacking for secular variation. Tectonophysics 609, 250–266. http://www.sciencedirect.com/science/article/pii/S0040195113002825. http://dx.doi.org/10.1016/j.tecto.2013.04.027. moho: 100 years after Andrija Mohorovicic.

Wilson, B., Dincer, T., 1976. An introduction to the hydrology and hydrography of the Okavango Delta.. In: Society, B. (Ed.), Symposium on the Okavango Delta, Gaborone, Botswana. pp. 33–48.

Wu, J.E., McClay, K., Whitehouse, P., Dooley, T., 2009. 4d analogue modelling of transtensional pull-apart basins. Mar. Pet. Geol. 26, 1608–1623. http://www.sciencedirect.com/science/article/pii/S0264817208001177. http://dx.doi.org/10.1016/j.marpetgeo.2008.06.007.

Youssof, M., Thybo, H., Artemieva, I., Levander, A., 2013. Moho depth and crustal composition in Southern Africa. Tectonophysics 609, 267–287. http://www.sciencedirect.com/science/article/pii/S004019511300543X. http://dx.doi.org/10.1016/j.tecto.2013.09.001. moho: 100 years after Andrija Mohorovicic.

Yu, Y., Liu, K., Moidaki, M., Reed, C., Gao, S., 2015a. No thermal anomalies in the mantle transition zone beneath an incipient continental rift: evidence from the first receiver function study across the Okavango Rift Zone, Botswana. Geophys. J. Int. 202, 1407–1418. http://gji.oxfordjournals.org/content/202/2/1407.abstract. http://dx.doi.org/10.1093/gji/ggv229. arXiv:http://gji.oxfordjournals.org/content/202/2/1407.full.pdf+html.

Yu, Y., Liu, K.H., Reed, C.A., Moidaki, M., Mickus, K., Atekwana, E.A., Gao, S.S., 2015b. A joint receiver function and gravity study of crustal structure beneath the incipient Okavango Rift, Botswana. Geophys. Res. Lett. 42, 8398–8405. http://dx.doi.org/10.1002/2015GL065811. 2015GL065811.

5.2 Vertical displacement

The residual vertical displacement rates provided by the two tested GRACE solutions converge for many stations, but diverge significantly in the eastern part of the subcontinent (Figure 3.8). As the GRGS predicts a lower reduction in TWS, or higher storage, the residual vertical rates are generally higher than the residual rates obtained with the CSR solution. They are also more consistent and present an uplift of more than 0.5 mm/yr for most of the stations.

The CSR provides the most stable vertical rates close to the coasts. This solution is in better agreement with Pedoja et al. (2011), who proposed uplift rates between 0.1 and 0.2 mm/yr based on a compilation of elevations of marine terraces and uplifted beach deposits dated from the sea level highstand of MIS 5e ($\sim$125 ky).

The different velocity fields provided by the two GRACE solutions show differences in the vertical displacement of the SWEA relative to southern Africa which are too large to be useful in discriminating between the different models proposed in the literature. Subswells are regularly invoked to explain the evolution of the drainage areas in the Kalahari basin, or rivers beds incising topographic highs, like the Zambezi river between the Chobe fault and the Victoria Falls. The density of the GPS network combined with the uncertainties of the ITRF14 and the GRACE solutions does not presently permit the confirmation or rejection of any of these hypotheses.

Although tested in more dynamic areas (Fu and Freymueller, 2012; Wang et al., 2017), the method used in this study to discriminate the signals does not yet provide accurate enough residual rates in such a tectonically stable context.

Chapitre 6

Discussion

A key question in the Okavango Delta is to identify and quantify the drivers responsible for 1) the inter-annual to centennial variability of the flood distribution and 2) the millennial to mega-annual variability of the endorheic regime. This study brings crucial new information on two of these forcings. First, the presence of a very extensive aquifer previously predicted by hydrological modelling (Hughes et al., 2006) and GRACE records (Ramillien et al., 2014) is confirmed, as well as its high variability at the management time scale, both seasonally and inter-annually. Secondly, the current tectonic activity of the graben is lower than expected, as are the long-term tectonics, possibly lower and more complex than previously thought by some authors (Modisi et al., 2000; Kinabo et al., 2007). From these new observations, added to the many previous studies, it is possible to draw some general conclusions on the processes driving the evolution of the Delta, at both management and geological time scales. Finally, this work opens many perspectives in different domains, from hydrology to geodynamics.

6.1 Who's the boss ?

As detailed in chapter 2, the influence of the different drivers can vary with time scales. For instance, the ecosystem may be very influential at the decadal to centennial time scale, but probably not at the geological time scale. It is thus necessary to examine each time scale separately.

6.1.1 Inter-annual to decadal time scale

The underground influence of hydrology

All surface deformation, GRACE data products and Pitman model indicate the presence of a very large pulsing groundwater reservoir (soil moisture and aquifer) over the whole basin, even possibly bigger than the most generous prior estimations (Hughes et al., 2006). The saturation of groundwater is a major parameter for the intensity of the flow at Mohembo, as illustrated by the major floods of 2010 and 2011 (Figure 2.12 and 6.1), consequent to the intense rainfall of the previous years allowing the progressive recharge of the aquifer. Regarding the ratio between runoff and groundwater storage ($<1\%$), runoff can be considered as a very thin layer flowing on a very large buffering aquifer.

This study also clarified the strengths and weaknesses of each data set, allowing a more rigorous mechanism for choice in all the available solutions for different variable (precipitation, TWS, ET), depending on the constraints and resolution of each question (summarized for the catchment area in figure 6.1). When direct and continuous observations are available, they should always be preferred, but only the discharge measured at Mohembo posses these characteristics. Rainfall in the catchment area seems to be better defined by the CHIRPS data set moderated by the Pitman model, as well as ET based on the Eddy covariance method. TWS in the catchment area, while well estimated by the Pitman model, may be better described by the GRACE data products regarding the lack of amplitude in the signal of vertical surface deformation. On the other hand, the spatial resolution of GRACE data products does not allow a quantification of TWS in the Delta at present.

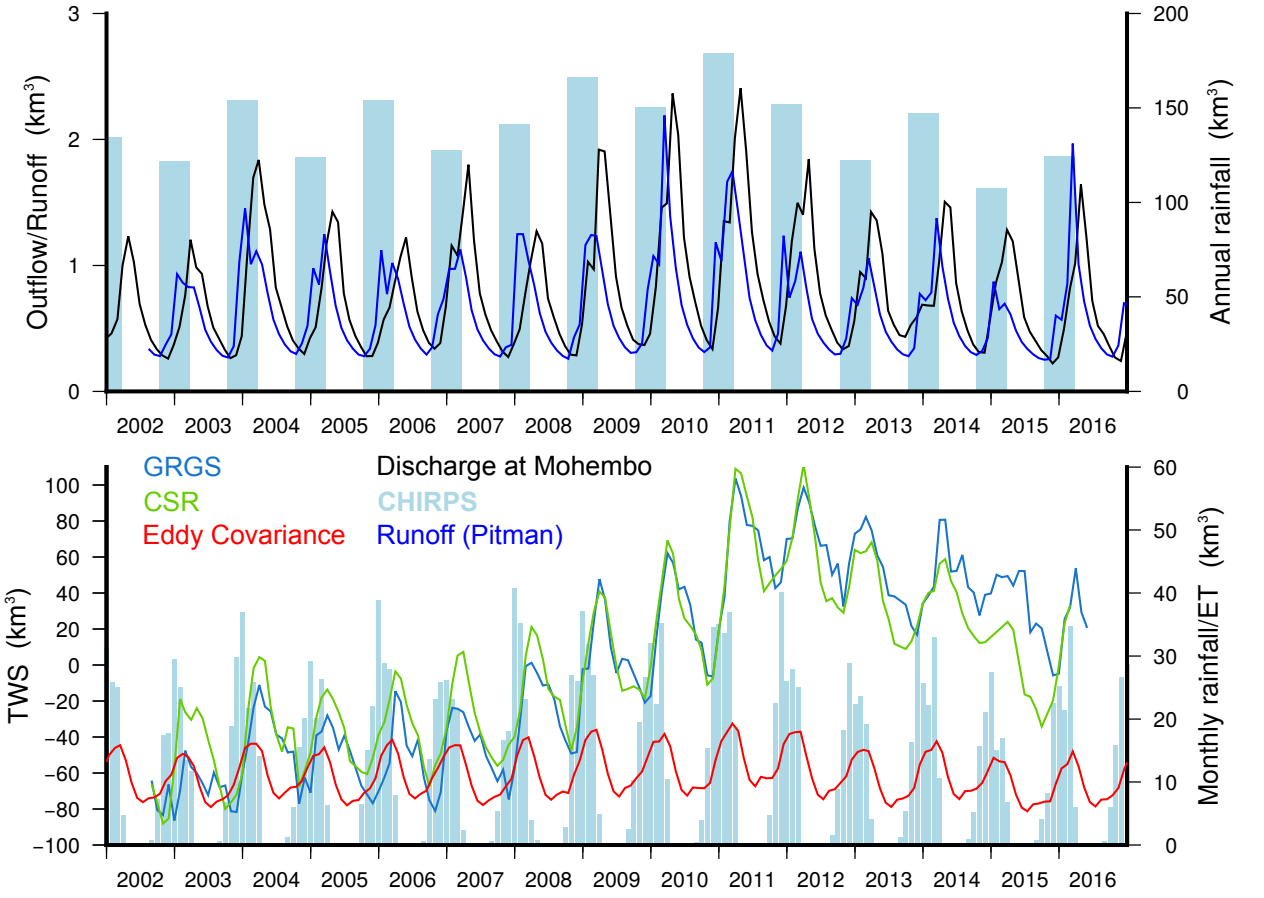

FIGURE 6.1 – Most reliable hydrological data sets for the Okavango basin. Rainfall is provided by CHIRPS, moderated by the Pitman model ; ET is computed by Eddy covariance, based on the GLEAM PET ; TWS by both CSR and GRGS solutions as they are complementary, discharge is measured at Mohembo by DWA ; Runoff generated in the catchment area is provided by the Pitman model.

In the catchment area, TWS is recharged each year during the rainy season, and discharged progressively during the dry season through evapotranspiration and possibly groundwater discharge to surface water. The extensive aquifer acts as a buffer in the hydrological system, delaying and smoothing the response of runoff to climatic variations, in agreement with Mazvimavi and Wolski (2006). This effect is illustrated by the difference in the regime of the Cuito and Cubango headwaters, depending on the presence of thick Kalahari beds (Hughes et al., 2006).

But the response of TWS to water budgets variations is not linear neither. Figure 6.1 shows that the peaks of recharge of TWS and runoff generation are in phase, and generally occur at the end of the rainy season. In a similar way, recharge of TWS and runoff generation occur after 1 to 3 months of rain, depending on the intensity of the first rainstorms. This delay indicates a threshold in the response of groundwater, increasing its recharge after a few months of rain, and maintaining this rate even through less intense precipitation. This threshold is similar to the one observed in the high-resolution piezometric time series in the Delta.

The non-linearity of the aquifer recharge is also visible in the relative amplitudes of runoff and TWS variations. The year 2012-2013 for instance shows a greater amount of runoff for a relatively lower recharge of TWS while the previous and wetter year 2011-2012 encouraged TWS recharge over runoff generation (Figure 6.1).

The buffering effect of groundwater, along with the dependence of the groundwater recharge threshold on precipitation rate, thus contribute to the non-linear response of the outflow from the catchment area to regional climatic variations. These two effects could at least partly explain the difference between the 18 yr cycle in regional rainfall variations and the proposed 70-80 yr cycle in the outflow variations (Mazvimavi and Wolski, 2006). According to both GRACE data products and Pitman model, it takes several years of increased rainfall to significantly increase outflow, once the aquifer is recharged enough. Consequently, the inter-annual trend in TWS variations observed in the GRACE time series not only supports the cyclicity proposed by Mazvimavi and Wolski (2006), but also brings elements of response to explain this cyclicity.

In the Delta, the shallow aquifer most probably plays a crucial role of buffer too, thus influencing the propagation of the flood. Indeed, water infiltrates during the propagation of the flood and recharges the aquifer. The more saturated the aquifer is, the less water infiltrates and the further, and faster, the flood will spread. Piezometric records in the Delta in the decade preceding the major flood of 2011 show an inter-annual recharge of the aquifer synchronous with the recharge of the aquifer in the catchment area, as rainfall increased along in the two areas. Given the porosity of the Kalahari sands, approximately 4 km^3 of water are required to increase the elevation of the water table of 1 m in the 12 000 km^2 of permanent to occasional wetlands of the Delta, without taking the intense ET into account.

This volume represents about the half of the annual inflow, and between half to 2/3 of local rainfall, depending on estimations. These proportions reveal how the presaturation of the groundwater can influence the amount of infiltrated water, thus the extent of the flood propagation, and at least participate in the non-linear response of the distributary systems in the Delta to inflow variations. Unfortunately, the superposition of the influences of the presaturation of the aquifer and increasing inflow on the maximum extent of the flood, both

providing larger floods mask their respective influence. Further hydrological modelling is required to discriminate these effects, by testing for instance if a lower ET, providing a more elevated water table at the arrival of the flood, manages to compensate for a lower inflow at Mohembo. On the opposite, it would be interesting, in the context of climate change to predict if higher inflow, consecutive to more intense rainfall events, could compensate an increasing ET, as will happen with global warming.

The observed spatial variations of the water table depth range within a few meters in the Delta (Figure 4.8 and 4.9, McCarthy, 2006). Given the influence of the antecedent elevation of water table on the flood propagation, it is likely that the spatial distribution of the water table elevation in the Delta prior to the arrival of the flood influences the spatial distribution of the flood amongst the distributary chanels (Wolski and Murray-Hudson, 2008). Groundwater would then act as a positive feedback, with a repeatability of flooding in a distributary channel, due to antecedent regular recharges during the previous flood.

The controls on the aquifer in the Delta are 1) the infiltration during the propagation of the flood, providing the primary (often sole) source of recharge, 2) the evapotranspiration, controlling the decline of the water table elevation and drying of the soil and 3) the local rainfall, recharging soil moisture and possibly the aquifer. The minimum water table level is reached in the rainy season and depends on the ratio between ET and infiltration, thus local rainfall. The temporal and spatial variability of the previous flood, the local rainfall and the ET may provide a great spatial and temporal variability in the elevation of the water table, and thus could account for variability of the flood extent and spatial distribution by controlling the phreatic water level. In contrast, such a spatial variation in the water table elevation in the Delta may be smoothed by lateral flow in the highly transmissive unconsolidated sands of the Kalahri, as visible in detailed piezometric records (Figure 4.9).

Hydrology, expressed as the system responding to climatic variations, thus strongly constrains the spatial and temporal variability of the flood, but all the changes mentioned above are transient. Hydrology also exerts another kind of influence, sometimes providing major floods capable of shifting the distribution of water amongst the distributary channels (Wolski and Murray-Hudson, 2008). Years of exceptional inflow can for instance precipitate channel avulsion by opening new channels. Historical evidence shows that major shifts in the flood distribution followed major inundations (Wilson, 1973). Such shifts are permanent changes, and debate is still open regarding the origin of such changes in the Delta, between tectonics, sedimentation, hydrology and vegetation.

Hydrology thus strongly drives the inter-annual variability of the flood through the saturation of the aquifer. Although it may actually be one of the most important reservoirs of the hydrological system, it is presently almost unmonitored. While plans for surface water monitoring are being developed by the intergovernmental organisation OKACOM, it is crucial to initiate a monitoring program of the groundwater in the catchment area. Indeed, although the Pitman model can now be used as a predictive tool for management, new data will always be required to monitor changes in the system. GRACE data products bring a new proxy for TWS in the catchment area. Such indirect data still need ground-based validation, possibly in combination with the deformation of the surface monitored by GPS. Moreover, the

spatial resolution TWS of GRACE data products cannot provide information either on the specificity of the sub-basins, or on the different reservoirs comprising TWS. Finally, GRACE data products cannot at present be used as a monitoring proxy for TWS in the Okavango Delta, for the same reasons as its limited applicability to the river basin (ie, coarse spatial resolution).

In order to accurately capture the impact of the changes to come on the vital groundwater, it is necessary to develop a groundwater monitoring network over the whole basin. While general conclusions cannot be drawn from particular cases, aggregating single cases can facilitate accommodating the variabilty of ground-based observations. Ground-based data can then be used to constrain remote sensing data sets, in order to eventually reach a global but satisfatory overview of the hydrological system. In the Delta, increasing the number of groundwater monitoring sites, and maintaining the records through the whole hydrological cycle, would bring new insights into different kinds of configuration (floodplains, islands) and on the spatial variability of the drivers, such as local rainfall.

Finally, the global account for all integrated TWS variations provided by GRACE solutions does not allow a proper understanding of the relationships between the different hydrological reservoirs responsible for TWS variations. It is for instance necessary to know if the recharge of TWS occurs mainly via soil moisture or in the aquifer, in order to better quantify the threshold in rainfall for the rise of the water table, as these two reservoirs do not have the same influence on the hydrological cycle and on available water resources. Monitoring these two reservoirs would permit the quantification of the threshold of preliminary rainfall before groundwater recharge. Such an understanding, as well as predictions of variations due to modification of land use, are necessary to avoid previous examples of dramatic of abuse of major aquifers for agricultural and/or industrial development (e.g., Scanlon et al., 2012; Voss et al., 2013).

Can tectonics still influence the decadal evolution of the flood distribution with a low deformation rate ?

The influence of tectonics on the inter-annual evolution of the spatial distribution of the flood in the Delta has so far been mostly speculative, as no deformation rate had ever been measured. While many authors proposed the possible responsibility of seismic events for sudden shifts in the flood distribution (Pike, 1970; Bauer et al., 2006) or channel blockages (McCarthy et al., 1993), none was ever able to demonstrate it, as argued by Wilson and Dincer (1976). After decades of speculation on the tectonic deformation, this study provides quantitative and qualitative (orientation) data about the current tectonic deformation.

The tectonic activity is shown to be considerably lower than expected. The age for the initiation of the tectonic activity in the OG proposed by Kinabo et al. (2008), based on datings from Ringrose et al. (2008), implies an inner subsidence of the graben of $\sim$1 cm/yr ($\sim$400 m in $\sim$40 ka). Although no GPS station records the deformation within the graben, such a subsidence cannot be reached with an overall strike-slip displacement of only 1 mm/yr.

The observed tectonic deformation is also very steady. No sudden displacements have been observed in the GNSS time series of MAUA, located on the upthrown block of supposedly the most active fault of the graben, even during the 2013-2014 period of relative high

seismic activity. This supports the hypothesis of more or less continuous displacement on the faults occurring not only during particularly seismic periods, but also through continuous microseismicity and possibly creep due to reduction of shear strength from fault lubrication (Shemang and Molwalefhe, 2011; Bufford et al., 2012). Based on the records of the seismic activity, extrapolation of tectonic deformation rate can be done for the last decades with quite good confidence. A pluricentimetric vertical shift occurring during an earthquake, as tested in Bauer et al. (2006), in the past decades is unlikely. Displacements on the order of meters could not have happened.

Consequently, the probability that tectonics are implicated in major rapid shifts of the flood distribution or channel blockage, either by local relief formation or global topographic gradient variation, is very low. If any exists, this influence is most probably insignificant in relation to the other processes operating on the evolution of the flood regime at the management time scale.

The conclusion that the distribution of the flood in the Okavango Delta is not related to the tectonic activity in the OG is finally supported by field evidence, namely the differences between two main outlets : Lake Ngami and the Mababe Depression. The lower and more seismically active Mababe Depression has not been significantly flooded in the past two centuries (Shaw, 1984), while the aseismic Lake Ngami is regularly and currently flooded. If a relationship existed between the seismically-induced possible subsidence in the OG and the propagation of water, distribution of water between the outlets would be reversed.

Another example can be found in the shift in the flood regime of the Boro and the Thamalakane river between 1951 and 1953. The only seismic event which could be responsible for an observable shift in the flood distribution occurred in September 1952. While Pike (1970) (in Wilson, 1973) proposes the influence of this M6.5 earthquake, Wilson (1973) maintains that there is no evidence to support this scenario. He argues that the change in the flood regime could also result from the 1951 major floods which arrived after several dry years. The flood pulse thus found a dry river bed, deprived of vegetation where it could easily flow.

The alluvial fan rules

Although hydrology most probably exerts the greatest influence on the flood distribution in the Okavango Delta, particularly on the extent of the flood, the variability of the spatial distribution of water among the distributary systems is also strongly controlled by the other processes at play in the system, i.e. the sedimentation and the ecosystem. Indeed, blockages by vegetation and sand, opening of new channels by big herbivores or the role of buffer for surface water played by the peat generating floodplains in the Panhandle and the Upper Delta modulate, disturb, or even counter hydrological variations.

The main process driving the whole Delta is actually revealed by its conical shape, as concluded by Stanistreet and McCarthy (1993) and Gumbricht and McCarthy (2001). The Delta is an alluvial fan, and like all other alluvial fans, depocenters migrate. As the Delta is a very flat and highly vegetated fan, there is not a unique depocenter, but deposition over the broad upper and middle Delta mainly. Yet this broad inundated area is not homogeneous and it is possible that the major portion of inundation oscillates from one side to the other, as postulated by Gumbricht et al. (2005). This latter study estimated that 150 000 yr were

necessary for the whole surface of the fan to have been subjected to aggradation.

Sedimentation and vegetation not only affect water flow in the upper parts of the Delta, but also in the lower parts. While more water reaches the middle part of the Thamalakane river, NE of Maun, and while the topographic global gradient should direct water into the Mababe Depression, the Thamalakane river counterintuitively flows towards the center of the system, where sediments are supposed to be accumulated. Moreover, the alluvial fan, its variability in the flood distribution and the variability of sediment transport among distributary systems provide temporally uneven distribution of water flow and sediment load in the graben. It is particularly understandable with the example of Lake Ngami, which was fed in the 1850's by the Thaoge system directly from the Okavango. Current supply by the pulse-fed Xudum and Boro systems, through the Kunyere river, brings water filtered through the floodplains, and the lake now receives far less sediments.

6.1.2 Geological time scale

On a longer time scale, endorheism is a consequence of concave continental topography, which results from the balance between tectonic activity creating relief and sedimentation filling the depression. Neither this ratio, nor its temporal evolution, have been quantified in the Okavango Graben. Consequently, it is not known if the system is currently balanced, filling, or rejuvenating available space for a future perennial megalake similar to lakes in the African Rift Valley. The new insights brought by this study on the deformation rate can help to constrain the long-term evolution of the Delta, directly related to the evolution of the Okavango graben. On the other hand, long-term sedimentation rate remains undetermined.

Long-term extrapolation of tectonic deformation

To extrapolate from the short-term process observations to the geological time scale is risky. The structure of the OG and the evolution of its sedimentary environment call into question the possibility of a long-term continuity in the displacement. The stratigraphy of the graben (preservation of Karoo sediments, erosion surface, paleosoils) indicates several ancient reactivations rather than a single recent rifting initiation, as proposed in Modisi et al. (2000); Kinabo et al. (2007); Bufford et al. (2012). The sudden disruption of the flow of the Okavango dated at 41ky (Ringrose et al., 2008) is attributed by these authors to rifting initiation. But it could actually represent either the latest reactivation of the faults after a preceding complex tectonic history, or the inversion in the ratio between fault activity and sedimentary input, particularly as the datings have been carried out on sediments sampled in the Xudum distributary at a depth of 2.6 m (Ringrose et al., 2008). These sediments cannot represent the initiation of the fault activity in the graben, as they represent the very sub-surface of the sedimentary record reaching several hundreds of meters thick.

Yet the consistency between GPS velocities and the displacements in the dykes, encourages the trial of long-term extrapolation. Indeed, while the top of the dykes only exhibits offset of several hundreds of meters, the lateral dextral offset can sometimes reach 5 km (Campbell et al., 2006). Assuming a constant 1 mm/yr strike-slip displacement, it would take 5 My to reach the maximum offset of 5 km observed on the Kunyere fault. Given the 1/2 to 1/10 ratio between vertical and horizontal displacements on the dykes, the inner sub-

sidence of the graben would reach between 0.1 mm/yr to 0.5 mm/yr. According to Allen and Allen (2013), such rates agree with rifts, failed rifts or strike-slip basin models. This rate is far more moderate than the 1 cm/yr proposed by Kinabo et al. (2007), which exceeds every documented subsidence rate in basins, typically ranging between 0.01 and 1 mm/yr.

This quantification lends credibility to the old age hypothesis for the tectonic activity of the graben.

The linearity of the tectonic activity of the OG through time has not been determined yet. Proponents of a young rifting hypothesis imply a continuous tectonic deformation over the whole structure, with a migration of the fault activity within the primary fault set, from SW to NE (Kinabo et al., 2008). But plausible evidence for several reactivations since the Pan-African orogeny (reviewed in Pastier et al. (2017)) call into question this hypothesis of a single continuous episode of tectonic deformation over the last 40 ky. Reactivation of the ancient faults of the Ghanzi-Chobe fold belt comprising the southeastern part of the OG may have occurred several times since their formation. The OG is located in the regional younger lithosphere, between two rigid cratons, and could have been accommodating far-field deformation during the break-up of Gondwana, as well as during the Cretaceous. The origin of the tectonic activity is thought to relate to the same genesis as the EARS from early seismic and geophysical data.

Long-term sedimentation rate

In order to determine the ratio between sedimentation rate and relative subsidence within the graben, it is critical to quantify the long-term sedimentation rate in the OG. Although the basin has encountered major variations in climatic conditions, providing variations in sedimentary inputs, it is possible to provide an order of magnitude estimate of the long-term sedimentation by extrapolating the current estimates for aeolian and fluviatile sedimentation. Based on the highest available values (Milzow et al., 2010), a density of 2650 kg/m^3 for quartz and a porosity of 33% for the Kalahari sands (Obakeng and Gieske, 1997) distributed over 20 000 km^2 provides a very low sedimentation rate of 12 x 10^{-6} m/yr.

This low average estimate for current sedimentation is lower than the rates estimated from the datings in Lake Ngami, which were between 4×10^{-5} and $8.3\times10-4$ m/yr (Figure 2.20). But these higher values are found in aggrading geomorphological features, paleo-shorelines, which locally concentrate deposition of sediments.

Need for a global approach and implications for paleo-reconstructions

Endorheic systems can oscillate at the geological time scale between different regimes : lakes, wetlands, desert and even loose their endorheic characteristic and turn into a river discharging into the sea. As a proper endorheic system, the Okavango Delta area shows evidence for previous megalake regimes, joining the Lake Ngami, the Mababe Depression and sometimes even the Makgadikgadi pans (e.g., Thomas and Shaw, 2002; Burrough et al., 2009), and exorheism (Thomas and Shaw, 1988), or at least significant and permanent flow across the Thamalakane fault (Ringrose et al., 2008). The regime of the Okavango Delta is controlled in the graben by three parameters, illustrated on figure 6.2 : 1) the dip-slip rate on

the SE normal faults shaping the hemi-graben's depression, 2) the sedimentation rate filling the graben's depression and 3) the water inputs more or less inundating the area.

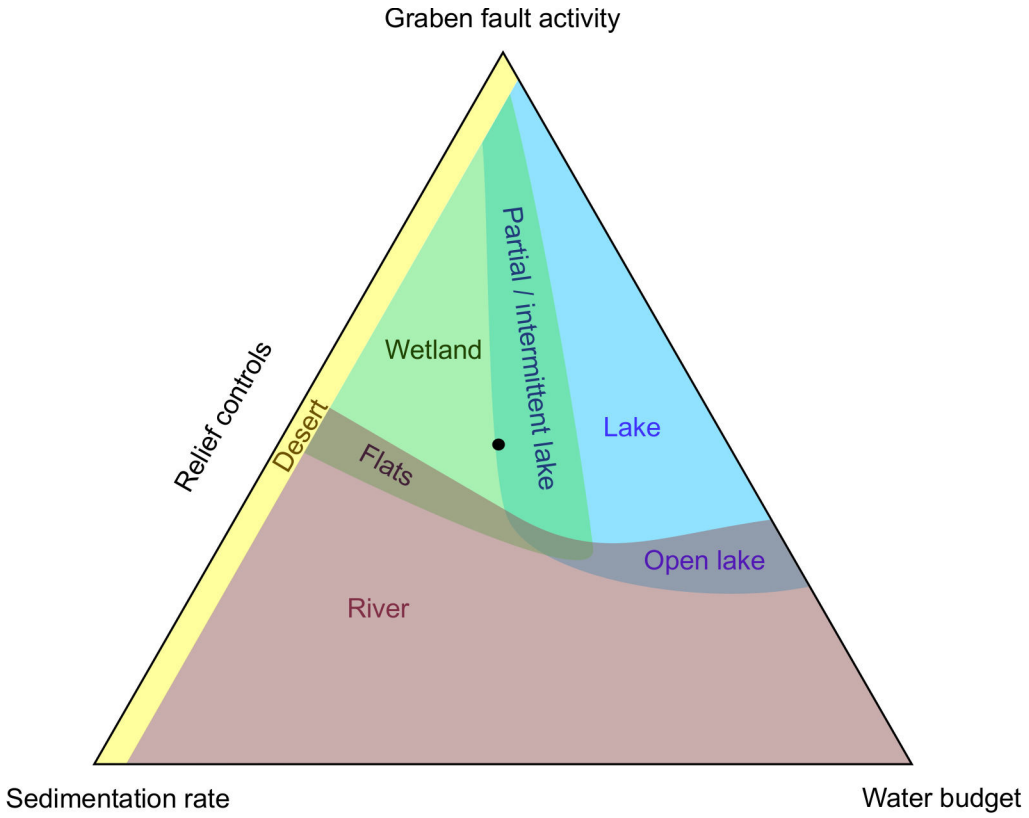

FIGURE 6.2 – Conceptual diagram representing the state variables controlling the regime of the Delta area. Endorheism is reached when the subsidence rate in the graben exceeds sedimentation rate, but exorheic regime may prevail in case of moderate uplift balanced with incision rate of a pre-existent river, or dominating water inputs (open lakes). The endorheic regime between wetlands and lakes is mainly driven by the ratio between the sedimentation rate and water budget. Obviously, insufficient water input leads to desertification. Intermediary stages are found between these three main regimes. Black dot shows the possible settings for the current Okavango Delta.

Ranges of value for these three parameters are quite low in the Delta compared to other similar systems and seem to be relatively balanced. On the cumulative ∼400 m of downthrow on the Thamalakane and Kunyere faults estimated by Kinabo et al. (2007), only a few meters to a few tens of meters separate the global thickness of sediments from the overall fault activity, revealed by the current topographic fault scarps. Due to the intense evapotranspiration, the overall water budget, although varying along with climatic variations, does not exhibit a global increase allowing to open the hydrological system. Thus, the current set of parameters controlling the endorheism of the Delta (Figure 6.2) seem to indicate control of the current endorheism by the fault activity of the OG. Indeed, the proposed sedimentation rate (0.12 x 10^{-6} m/yr) is exceeded by far by the proposed subsidence rate in the southeastern part of the inner graben (0.2 to 0.5 mm/yr). The difference between these rates does not currently

result in important topographic fault scarps because of 1) the low deformation rate and 2) the most probable discontinuous history of these two parameters. The current low rates of both sedimentation and tectonic activity imply that tiny changes in these parameters can easily induce a shift in their ratio and nudge the Delta into another regime, such as a lake, in the case of increased water inputs, or a river in the case of temporary cessation of fault activity or increased sedimentation rate.

At the geological time scale, the Delta should thus be viewed as a whole, i.e. as a hydro-sedimento-tectonic system. Consequently, records for state variables defining the Delta should not be directly related to a variation of a peculiar driver. This can be illustrated by the long-term sedimentation rate, showing variations and intermittence. The presence of sediment in the graben is commonly interpreted in terms of climatic variations (e.g., Burrough et al., 2007), but the presence of sediments does not only imply sufficient water to transport sediment to the depocenter. It also requires fault activity of sufficient magnitude to block the flow of water and allow definitive deposition. Regarding the processes at play within the OG, the sedimentation rate is finally locally controlled by the relationship between the feeding channel(s) and the Okavango river. The sedimentation rate is thus lower in Lake Ngami under the present input configuration, mainly fed by the Kunyere and Nhabe rivers, than it was in the late 1800's when it was fed by the Thaoge system, via a direct hydraulic connection to the Okavango mainstream.

Moreover, the forcings on sedimentation rate are actually more abundant at the regional scale. First, water inputs are not only controlled by climatic forcings, but also by tectonics, shaping drainage areas. This process could be responsible for a significant increase in water inputs about 4 My, with the capture of the Cubango, previously flowing to Namibia (Miller et al., 2010). Then, sediment inputs are even more strongly controlled by the tectonic regime upstream, as relief formation increases erosion.

Such a global approach of the system allows another interpretation of the evolution of the study area through time, and thus the reinterpretation of sediment datings, which are the only evidence constraining the age of the faulting. The low values for the three parameters controlling the Okavango Delta (Figure 6.2) make it easy to shift from one regime to another. Considering such a dynamic evolution of the Delta area, the age of 41 ky could actually represent the last episode of significant effect of tectonics on the alluvial fan. The Delta is thus potentially evolving along with the graben since its first activation, possibly a few millions of years ago. This hypothesis is corroborated by the hypothesis posited by Podgorski et al. (2015) of a paleofan at the bottom of the Kalahari sequence located exactly beneath the current Delta.

6.1.3 Conclusion

From this study, it can be concluded that, in a general way, and at both management and geological time scales, the Okavango Delta should be considered as a complex system, the controls of which are too tightly correlated to be studied completely separately. The integral perspective of the alluvial fan as an eco-hydro-sedimentological system at inter-annual to centennial time scale has already been perceived as necessary since the 1990's. But a similar global perspective of the alluvial fan as a hydro-sedimento-tectonic system at the geological

time scale is still not widely accepted.

This can be illustrated at the management time scale by the maximum extent of the flood, resulting from variations in inflow (due to climatic and groundwater variations in the catchment area), relationships between the channels and the river (due to sedimentation and vegetation), the antecedent elevation of the water table (due to previous floods, local rainfall and evapotranspiration, thus vegetation), among others.

The direct consequence of such global perspectives is that state variables defining the Delta, such as water level, flood extent, sedimentation rate, should not be directly translated into independent parameters of controlling processes. Variations of state variables are most likely to result from a combination of feedbacks between the different processes.

While many studies have brought crucial insights on the different processes, with more or less well determined quantification, independently. Very few attempts have been made to treat the Okavango Delta as an integral system (McCarthy, 2013). **How to comprehend the system in its entire complexity ?** While many unknowns remain, a global approach can allow the integration of the complexity of the system, by cross-cutting different data sets and perspectives, and attempting to improve the quantification of the feedbacks on the processes, as realised in this study between tectonics and hydrology, on the basis of the deformation of the surface.

6.2 Perspectives

6.2.1 Hydrology

Data, now and for ever

The lack of instrumentation in the Okavango basin has been mentioned a few times in this study. The increasing awareness of the need for reliable continuous time series of the state variables defining the hydrological system is increasing with the conspicuous land use change consequent to economic development in the region. The development of a transboundary monitoring network for surface is currently being pursued by the transgovernmental OKACOM. In its initial form, this network should comprise 9 stations : 4 in Angola, 2 in Namibia and 3 in Botswana. But this study confirms that the presently unmonitored and unquantified aquifer plays a major role in the water budget of the system in each three countries. Therefore, it is critical that groundwater monitoring joins this incipient network as soon as possible. Indeed, if realized, the plans of dams as well as the development of intensive cereal cultivation with irrigation in the Angolan catchment are surely going to drastically impact this important buffering component of the hydrological system. As developed by this study with &Beyond Safaris, and for years by ORI with other lodges, such as the Guma Lagoon Camp, partnerships with local actors, lodges, but also schools and farms, can help to overcome the difficulty in accessing to remote regions of the vast catchment area. Finally, to complete the monitoring of the different TWS reservoirs, soil moisture probe profiles can be installed along with piezometers. Indeed, this enigmatic reservoir (soil moisture) is often badly constrained, and may actually play a large role. The area is subjected to intense ET, and soil moisture could be the key reservoir. According to Milzow et al. (2011), this reservoir could actually comprise the majority of the total groundwater storage.

Now that the network of permanent GPS stations has been shown to be useful in the monitoring of TWS at the scale of the Okavango-Zambezi, increasing the number of permanent GPS staions would allow an improvement of spatial resolution for the deformaiton of the surface. It would also reinforce the reliability of the processing of the daily solutions.

Data acquisition is not the only issue, their curation and sharing is too. As mentioned during the development of the future surface water monitoring network in the basin, it is necessary to maintain a dedicated database, curating all kind of data regarding hydrology in a consistent way. ORI's website fills the mission regarding the Delta. Further implementation could be brought regarding the remote sensed data sets used in this study. Indeed, these data sets can be very helpful to complete records on a station, with their strengths and weaknesses. The collection of data sets and accompanying scripts could be implemented on ORI's website to provide time series for TWS from GRACE data products over the catchment area, time series for recent daily time series by RFE, or more accurate but later and only monthly from CHIRPS. Such an ease and freedom of use would give access to these data sets to researchers in other domains, such as biologists, or to decision makers.

Finally, increasing the spatial resolution of the GRACE data products is a challenge faced by every laboratory releasing GRACE solutions. The strong constraints brought through the deformation of the surface by this study on the spatial distribution of TWS in the Okavango open new perspectives to simultaneously improve the solutions for GRACE and the modelled deformation of the surface for seasonal hydrological loading. The improvement of the spatial distribution of TWS in the extensive Zambezi basin could also allow to further constrain hydrological models in this basin.

6.2.2 Geodynamics

Geodynamics in southern Africa suffers the same lack of instrumentation as hydrology in the Okavango basin. More than the 2013-2014 seismic activity, the recent M6.5 earthquake in the Central Kalahari, hitherto considered as aseismic, highlights the necessity to further develop the seismic network. Indeed, the seismicity of this area leads to the reconsideration of seismic hazard in the whole of southern Africa (R. Durheim, *pers. comm.*). In the same way, GPS measurements, as insights in the crustal deformation, are too scarce. Moreover, inreasing the density of the network would not only bring data on new locations, but would also strengthen the computation for the daily solutions. Monitoring networks are currently particularly sparse to non-existent in the vast neighbouring Angola and DRC.

The surface water monitoring network being currently developed by the OKACOM carries partnership with Angolan universities. Moreover, during this study, contacts have been made with different lodge or camp managers in the Central Kalahari, willing to help scientific research. One perspective of this study is thus to develop a joint proposal for the UNAVCO and AfricaArray, to instrument sites in these two areas. Such partnerships would provide safe areas for the equipment, and potentially power sources and Internet access.

Further detailed study of the seismicity in southern Africa requires a properly reviewed earthquakes catalogue, as begun by Mulabisana (2016). This begins with the definition of a review procedure for earthquakes adapted to the African continent. Indeed, the first criteria of the ISC to retain a seismic event in the final bulletin is to be recorded by at least two seismic networks. But the density of seismic stations sometimes is not dense enough to

record a remote event in two networks. Some governmental seismic networks do not always communicate their reports to the ISC, such as the Botswana or Namibia Geological Surveys. Moreover, earthquakes not fitting the recognised structural pattern of the area are susceptible to being removed from the database. The review procedure of the ISC is the reason why the concentration of seismic events in the Central Kalahari in 2013-2014 only appears in the unreviewed database.

Finally, many studies have provided crucial information about the model of the Earth's deep structure beneath Africa in the past years, especially regarding the thickness of the lithosphere. This could be used to precisely relocate epicentres and compute magnitudes. Such a detailed earthquake catalogue is a necessary prerequisite to study the tectonic regime more deeply. Precise locations of epicenters could help to decipher if the main current displacement is occurring on the main or secondary fault sets. The question of the distribution of the activity either on the Tsau or secondary curvilinear fault (...) would be solved, thus bringing insights on stress transfer within the structure as proposed by Kinabo et al. (2008); Bufford et al. (2012). Finally, such a precise catalogue would help to answer the questions of one of the possible feedbacks of hydrology on tectonics : **Is seasonal water loading triggering tectonic activity ? At the seasonal scale, is it visible in the micro-seismicity ? At the decadal time scale, with periods of seismic activity more or less corresponding to periods of higher inflow (50's, 70's, 2010's) ?**

Finally, to further validate or reject the alternative geodynamic context proposed in this study, two perspectives could be developed. First, the network of GPS stations is quite dense in the SWEA, compared to other areas in Africa, and other couples of GPS stations straddle seismically active grabens. These structures are potential additional actors of the far-field accommodation of the deformation consecutive to the opening of the EARS and the displacement of the Kalahari craton. If the model is valid, some strike-slip displacement should compose their tectonic regime. As in this study, examination of their kinematics should be accompanied by a review of all aspects concerning their deformation.

The second perspective is to use numerical and/or analogue modelling to verify the crustal deformation induced by the proposed stress regime. **Can far-field plate or sub-plate displacements alone manage to reproduce the observed dynamics without any mantellic influence ? Can they manage to reproduce the north-south and east-west gradients of deformation observed through geology ?** Many challenges would face analogue modelling. The differential opening rates of the EARS combined to lateral displacement of the Kalahari craton, possibly responsible for strike-slip regime, require differential compression rates not only between the different box boundaries, but also within one of the boundaries. Moreover, the strong influence of the prexistent structures, namely the belt of weaker lithosphere beneath the SWEA compared to the rigid cratons, requires an heterogeneous model of the crust.

Chapitre 7

Conclusion

This study brought quantified insights into two driving processes in the Okavango Delta through the examination of the deformation of the ground surface monitored by permanent GPS stations : hydrology and tectonics. The henceforth classical approach of modelling the seasonal hydrological loading based on GRACE products has been proved useful to validate GRACE data products in the basin and hence assess the importance of the aquifer in the Okavango basin. The new monitoring proxy thus provided for TWS allowed to reliably constrain the hydrological Pitman model for the Okavango river, and gave an overview of the behaviour of water storage over the hydrological cycle, as well as its inter-annual evolution.

Water storage, indifferently comprised of groundwater and soil moisture, is revealed as the most important reservoir, exceeding by far the surface water. The inter-annual variation in the recharge of TWS during the rainy season is confirmed as most probably responsible for the non-linear response of the outflow provided by the catchment area to climatic variations, as proposed by Hughes et al. (2006). Moreover, the phase of all GPS signal, GRACE signal and output from the Pitman model agree on a delay of TWS recharge after the beginning of the rainy season. This threshold is another responsible for the non-linear response of the basin.

In a similar way, the aquifer in the Delta modulates the inter-annual variations of inflow. The piezometers instrumented for this study permitted the first detailed records of the water table during the rainy season. This study revealed the influence of local rainfall on the water table, and quantified the strong impact of the elevation of the water table on the propagation of the annual flood. It also highlighted the threshold in rainfall necessary to further groundwater recharge, for which saturation of the soil moisture could be responsible.

Hydrology thus exerts a great control on the variability of the flood distribution at the management time scale, by modulating climatic variations at different levels of the hydrological cycle. In contrast, the tectonic activity in the OG is revealed too low to be likely to influence the propagation of water through topographic shifts. Beyond the influence of each process, the Okavango Delta is to be apprehend as a whole complex eco-hydro-sedimentary system in order to predict future changes in the fan due to climate change or anthropogenic impacts.

At the geological time scale, the OG should not be considered as an incipient structure as the current surprisingly low deformation rate is consistent with the stratigraphy, implying a longer and more complex tectonic history than previousy thought. The origin of the tectonic

deformation has been called into question as the recent geodetic and geophysical do not match the precedently conventionally admitted geodynamic model of an incipent rifting zone. The area is more likely to be submitted to the accommodation of far-field deformation due to the relative displacements of the neighbour sub-plates.

Regarding the data sets used in this study, further reciprocal constraints between the GPS and GRACE signals could be developed in the Okavango-Zambezi basin, notably through a more detailed study of the peculiarities of the GPS signals. Many perspectives are opened by this study, from developing not only groundwater but trans-disciplinary monitoring in order to better understand its drivers, to modelling of crustal deformation implied by far-field plate displacements in a rheologically heterogeneous crust in order to test the alternative geodynamic model.

Bibliographie

Allen, P. A. and J. R. Allen (2013). *Basin Analysis : Principles and Application to Petroleum Play Assessment* (Third edition ed.). John Wiley & Sons.

Altamimi, Z., L. Métivier, and X. Collilieux (2012). Itrf2008 plate motion model. *Journal of Geophysical Research : Solid Earth 117*(B7), 1–14. B07402.

Altamimi, Z., P. Rebischung, L. Métivier, and X. Collilieux (2016). Itrf2014 : A new release of the international terrestrial reference frame modeling nonlinear station motions. *Journal of Geophysical Research : Solid Earth 121*(8), 6109–6131.

Andersson, L., J. Wilk, M. C. Todd, D. A. Hughes, A. Earle, D. Kniveton, R. Layberry, and H. H. Savenije (2006). Impact of climate change and development scenarios on flow patterns in the Okavango River. *Journal of Hydrology 331*(1), 43 – 57. Water Resources in Regional Development : The Okavango River.

Aubinet, M., T. Vesala, and D. Papale (2012). *Eddy covariance : a practical guide to measurement and data analysis*. Springer Science & Business Media.

Barton, J. and D. van Reenen (1992). When was the Limpopo Orogeny ? *Precambrian Research 55*(1), 7 – 16. The Archaean Limpo Granulite Belt : Tectonics and Deep Crustal Processes.

Batumike, J., E. Belousova, and W. Griffin (2007). U-Pb Dating of Perovskite : Nxau-Nxau Kimberlites, Botswana. Confidential Report to Tsodilo Resources. Technical report, GEMOC Macquarie, University, Australia.

Bauer, P., T. Gumbricht, and W. Kinzelbach (2006). A regional coupled surface water/groundwater model of the okavango delta, botswana. *Water Resources Research 42*(4), n/a–n/a. W04403.

Bauer, P., R. Supper, S. Zimmermann, and W. Kinzelbach (2006). Geoelectrical imaging of groundwater salinization in the okavango delta, botswana. *Journal of Applied Geophysics 60*(2), 126 – 141.

Bauer, P., G. Thabeng, F. Stauffer, and W. Kinzelbach (2004). Estimation of the evapotranspiration rate from diurnal groundwater level fluctuations in the okavango delta, botswana. *Journal of Hydrology 288*(3), 344 – 355.

Bauer-Gottwein, P., T. Langer, H. Prommer, P. Wolski, and W. Kinzelbach (2007). Okavango delta islands : Interaction between density-driven flow and geochemical reactions under evapo-concentration. *Journal of Hydrology 335*(3–4), 389 – 405.

Begg, G., W. Griffin, L. Natapov, S. Y. O'Reilly, S. Grand, C. O'Neill, J. Hronsky, Y. P. Djomani, C. Swain, T. Deen, and P. Bowden (2009). The lithospheric architecture of Africa : Seismic tomography, mantle petrology, and tectonic evolution. *Geosphere 5*(1), 23–50.

Bettadpur, S. (2012). UTCSR Level-2 Processing Standards Document. Technical report, University of Texas, Center for Space Research.

Boehm, J., B. Werl, and H. Schuh (2006). Troposphere mapping functions for GPS and very long baseline interferometry from European Centre for Medium-Range Weather Forecasts operational analysis data. *Journal of Geophysical Research : Solid Earth 111*(B2), n/a–n/a. B02406.

Borg, G. (1988). The Koras—Sinclair—Ghanzi rift in southern Africa. Volcanism, sedimentation, age relationships and geophysical signature of a late middle proterozoic rift system. *Precambrian Research 38*(1), 75 – 90.

Bruinsma, S., J.-M. Lemoine, R. Biancale, and N. Valès (2010). CNES/GRGS 10-day gravity field models (release 2) and their evaluation.

Bufford, K. M., E. A. Atekwana, M. G. Abdelsalam, E. Shemang, E. A. Atekwana, K. Mickus, M. Moidaki, M. P. Modisi, and L. Molwalefhe (2012). Geometry and faults tectonic activity of the okavango rift zone, botswana : Evidence from magnetotelluric and electrical resistivity tomography imaging. *Journal of African Earth Sciences 65*(0), 61 – 71.

Bumby, A. and R. Guiraud (2005). The geodynamic setting of the Phanerozoic basins of Africa. *Journal of African Earth Sciences 43*(1), 1 – 12. Phanerozoic Evolution of Africa.

Burrough, S. and D. Thomas (2008). Late quaternary lake-level fluctuations in the mababe depression : Middle kalahari palaeolakes and the role of zambezi inflows. *Quaternary Research 69*(3), 388 – 403.

Burrough, S. L., D. S. Thomas, and R. M. Bailey (2009). Mega-lake in the kalahari : A late pleistocene record of the palaeolake makgadikgadi system. *Quaternary Science Reviews 28*(15), 1392 – 1411.

Burrough, S. L., D. S. Thomas, P. A. Shaw, and R. M. Bailey (2007). Multiphase quaternary highstands at lake ngami, kalahari, northern botswana. *Palaeogeography, Palaeoclimatology, Palaeoecology 253*(3–4), 280 – 299.

Cahen, L., N. Snelling, J. Delhal, J. Vail, M. Bonhomme, and D. Ledent (1984). *The geochronology and evolution of Africa*. Oxford : Clarendon Press.

Campbell, G., S. Johnson, T. Bakaya, H. Kumar, and J. Nsatsi (2006). Airborne geophysical mapping of aquifer water quality and structural controls in the Lower Okavango Delta, Botswana. *South African Journal of Geology 109*(4), 475–494.

Carney, J., D. Aldiss, and N. Lock (1994). The geology of botswana.

CGMW-BRGM (2016). Geological Map of Africa, 1 :10 million scale.

Chanard, K., J. P. Avouac, G. Ramillien, and J. Genrich (2014). Modeling deformation induced by seasonal variations of continental water in the himalaya region : Sensitivity to earth elastic structure. *Journal of Geophysical Research : Solid Earth 119*(6), 5097–5113.

Cheng, M. and B. D. Tapley (2004). Variations in the Earth's oblateness during the past 28 years. *Journal of Geophysical Research 109*(B9), B09402.

Dahle, C., F. Flechtner, C. Gruber, D. König, R. König, G. Michalak, and K. Neumayer (2013). Gfz grace level-2 processing standards document for level-2 product release 0005 : revised edition. Technical report, GeoForschungsZentrum, Potsdam.

Dangerfield, J., T. Mccarthy, and W. Ellery (1998). The mound-building termite macrotermes michaelseni as an ecosystem engineer. *Journal of Tropical Ecology 14*(4), 507–520.

Dangerfield, J. M. and G. Schuurman (2000). Foraging by fungus-growing termites (isoptera : Termitidae, macrotermitinae) in the okavango delta, botswana. *Journal of Tropical Ecology 16*(5), 717–731.

Davis, J. L., P. Elósegui, J. X. Mitrovica, and M. E. Tamisiea (2004). Climate-driven deformation of the solid earth from grace and gps. *Geophysical Research Letters 31*(24), n/a–n/a. L24605.

Dieppois, B., B. Pohl, M. Rouault, M. New, D. Lawler, and N. Keenlyside (2016). Interannual to interdecadal variability of winter and summer southern African rainfall, and their teleconnections. *Journal of Geophysical Research : Atmospheres 121*(11), 6215–6239. 2015JD024576.

Dieppois, B., M. Rouault, and M. New (2015, Nov). The impact of ENSO on Southern African rainfall in CMIP5 ocean atmosphere coupled climate models. *Climate Dynamics 45*(9), 2425–2442.

Dincer, T., S. Child, and B. Khupe (1987). A simple mathematical model of a complex hydrologic system — okavango swamp, botswana. *Journal of Hydrology 93*(1), 41 – 65.

Dincer, T., H. Heemmsra, and D. Kraatz (1976). The study of hydrological conditions in an experimental area in the seasonal swamp. tech. Technical Report 20, United Nations Development Programme/Food and Agricultural Organization.

Duan, X., J. Guo, C. Shum, and W. V. D. Wal (2009). On the postprocessing removal of correlated errors in GRACE temporal gravity field solutions. *Journal of Geodesy 83*(11), 1095–1106.

Duncan, R. A., P. R. Hooper, J. Rehacek, J. S. Marsh, and A. R. Duncan (1997). The timing and duration of the karoo igneous event, southern gondwana. *Journal of Geophysical Research : Solid Earth 102*(B8), 18127–18138.

Ellery, W., K. Ellery, K. H. Rogers, and T. S. McCarthy (1995). The role of cyperus papyrus l. in channel blockage and abandonment in the northeastern okavango delta, botswana. *African Journal of Ecology 33*(1), 25–49.

Ellery, W. N., K. Ellery, K. H. Rogers, T. S. McCarthy, and B. H. Walker (1993). Vegetation, hydrology and sedimentation processes as determinants of channel form and dynamics in the northeastern okavango delta, botswana. *African Journal of Ecology 31*(1), 10–25.

Farinotti, D., L. Longuevergne, G. Moholdt, D. Duethmann, T. Mölg, T. Bolch, S. Vorogushyn, and A. Güntner (2015). Substantial glacier mass loss in the Tien Shan over the past 50 years. *Nature Geoscience 8*(9), 716–722.

Farrell, W. (1972). Deformation of the Earth by surface loads. *Reviews of Geophysics 10*(3), 761–797.

Folwell, S. and F. Farqhuarson (2006). The impacts of climate change on water resources in the okavango basin. In *Climate Variability and Change—Hydrological Impacts*, Volume 308, pp. 382.

Fu, Y. and J. T. Freymueller (2012). Seasonal and long-term vertical deformation in the nepal himalaya constrained by gps and grace measurements. *Journal of Geophysical Research : Solid Earth 117*(B3), n/a–n/a. B03407.

Fynn, R. W. S., M. Murray-Hudson, M. Dhliwayo, and P. Scholte (2015, Aug). African wetlands and their seasonal use by wild and domestic herbivores. *Wetlands Ecology and Management 23*(4), 559–581.

Gall, B. L., G. Tshoso, F. Jourdan, G. Féraud, H. Bertrand, J. Tiercelin, A. Kampunzu, M. Modisi, J. Dyment, and M. Maia (2002). 40ar/39ar geochronology and structural data from the giant okavango and related mafic dyke swarms, karoo igneous province, northern botswana. *Earth and Planetary Science Letters 202*(3–4), 595 – 606.

Gamrod, J. L. (2009). *Paleolimnological records of environmental change preserved in Paleolake Mababe, northwest Botswana*. Ph. D. thesis, Oklahoma State University.

Garstang, M., W. Ellery, T. McCarthy, M. Scholes, R. Scholes, R. Swap, and P. Tyson (1998). The contribution of aerosol- and water-borne nutrients to the functioning of the okavango delta ecosystem, botswana. *South African Journal of Science 94*(5), 223–229.

Geruo, A., J. Wahr, and S. Zhong (2012, 11). Computations of the viscoelastic response of a 3-D compressible Earth to surface loading : an application to Glacial Isostatic Adjustment in Antarctica and Canada. *Geophysical Journal International 192*(2), 557–572.

Gieske, A. (1996). Vegetation driven groundwater recharge below the okavango delta (botswana) as a solute sink mechanism - an indicative model. *Botswana Journal of Earth Sciences 3*, 33–37. In : Botswana Journal of Earth Sciences, 3(1996)12, pp. 33-37.

Gieske, A. (1997). Modelling of surface outflow from the okavango delta. *Botswana Notes &amp ; Records 28*(1), 165–192.

Gray, D. R., D. A. Foster, B. Goscombe, C. W. Passchier, and R. A. Trouw (2006). 40ar/39ar thermochronology of the pan-african damara orogen, namibia, with implications for tectonothermal and geodynamic evolution. *Precambrian Research 150*(1), 49 – 72.

Gumbricht, T. and T. McCarthy (2001). The topography of the Okavango Delta, Botswana, and its tectonic and sedimentological implications. *South African Journal of Geology 104*(3), 243–264.

Gumbricht, T. and T. McCarthy (2003). Spatial patterns of islands and salt crusts in the okavango delta, botswana. *South African Geographical Journal 85*(2), 164–169.

Gumbricht, T., T. S. McCarthy, and P. Bauer (2005). The micro-topography of the wetlands of the Okavango Delta, Botswana. *Earth Surface Processes and Landforms 30*(1), 27–39.

Guo, J. Y., Y. B. Li, Y. Huang, H. T. Deng, S. Q. Xu, and J. S. Ning (2004). Green's function of the deformation of the earth as a result of atmospheric loading. *Geophysical Journal International 159*(1), 53–68.

Haddon, I. G. (2005). *The Sub-Kalahari Geology and Tectonic Evolution of the Kalahari Basin, Southern Africa.* Ph. D. thesis, Faculty of Science, University of the Witwatersrand, Johannesburg.

Haddon, I. G., D. M. Erasmus, and H. M. Roos (1999). Isopach Map of the Kalahari Group.

Haggerty, S. E., E. Raber, and C. W. Naeser (1983). Fission track dating of kimberlitic zircons. *Earth and Planetary Science Letters 63*(1), 41 – 50.

Hartley, A. J., G. S. Weissmann, G. J. Nichols, and G. L. Warwick (2010). Large distributive fluvial systems : Characteristics, distribution, and controls on development. *Journal of Sedimentary Research 80*(2), 167–183.

Hassan, A. and S. Jin (2016). Water storage changes and balances in Africa observed by GRACE and hydrologic models. *Geodesy and Geodynamics 7*(1), 39 – 49. Special Issue : GNSS Applications in Geodesy and Geodynamics.

Heinl, M., A. Neuenschwander, J. Sliva, and C. Vanderpost (2006, Jul). Interactions between fire and flooding in a southern African floodplain system (Okavango Delta, Botswana). *Landscape Ecology 21*(5), 699–709.

Heleno, S., C. Frischknecht, N. d'Oreye, J. Lima, B. Faria, R. Wall, and F. Kervyn (2010). Seasonal tropospheric influence on SAR interferograms near the ITCZ – the case of fogo volcano and mount cameroon. *Journal of African Earth Sciences 58*(5), 833 – 856. Active Volcanism and Continental Rifting in Africa1st AVCOR International Workshop.

Herring, T., R. W. King, M. Floyd, and S. McClusky (2015, 6). *Introduction to GAMIT/GLOBK, Release 10.6.* Department of Earth, Atmospheric and Planetary Sciences, Massachusetts Institute of Technology.

Hughes, D. A., L. Andersson, J. Wilk, and H. H. Savenije (2006). Regional calibration of the pitman model for the okavango river. *Journal of Hydrology 331*(1), 30 – 42. Water Resources in Regional Development : The Okavango River.

Hughes, D. A., D. G. Kingston, and M. C. Todd (2011). Uncertainty in water resources availability in the okavango river basin as a result of climate change. *Hydrology and Earth System Sciences 15*(3), 931–941.

Humphries, M., T. McCarthy, G. Cooper, R. Stewart, and R. Stewart (2014). The role of airborne dust in the growth of tree islands in the okavango delta, botswana. *Geomorphology 206*(0), 307 – 317.

Jekeli, C. (1981). Alternative methods to smooth the Earth's gravity field. Technical Report 327, Department of Civil and Environmental Engineering and Geodetic Science, Ohio State University.

Jourdan, F., G. Féraud, H. Bertrand, A. Kampunzu, G. Tshoso, B. L. Gall, J. Tiercelin, and P. Capiez (2004). The karoo triple junction questioned : evidence from jurassic and proterozoic 40ar/39ar ages and geochemistry of the giant okavango dyke swarm (botswana). *Earth and Planetary Science Letters 222*(3–4), 989 – 1006.

Kamo, S. L., R. M. Key, and L. R. M. Daniels (1995). New evidence for neoarchaean, hydrothermally altered granites in south-central botswana. *Journal of the Geological Society 152*(5), 747–750.

Key, R. M. and N. Ayres (2000). The 1998 edition of the national geological map of botswana. *Journal of African Earth Sciences 30*(3), 427 – 451. 50th Anniversary of the Geological Survey.

Khoza, T. D., A. G. Jones, M. R. Muller, R. L. Evans, M. P. Miensopust, and S. J. Webb (2013, AUG). Lithospheric structure of an Archean craton and adjacent mobile belt revealed from 2-D and 3-D inversion of magnetotelluric data : Example from southern Congo craton in northern Namibia. *Journal of Geophysical Research-Solid Earth 118*(8), 4378–4397.

Kinabo, B., E. Atekwana, J. Hogan, M. Modisi, D. Wheaton, and A. Kampunzu (2007). Early structural development of the Okavango rift zone, NW Botswana . *Journal of African Earth Sciences 48*(2–3), 125 – 136. The East African Rift System : Dynamics, Evolution and Environment The East African Rift System : Development, Evolution and Resources.

Kinabo, B. D., J. P. Hogan, E. A. Atekwana, M. G. Abdelsalam, and M. P. Modisi (2008). Fault growth and propagation during incipient continental rifting : Insights from a combined aeromagnetic and shuttle radar topography mission digital elevation model investigation of the okavango rift zone, northwest botswana. *Tectonics 27*(3), n/a–n/a. TC3013.

Krah, M., T. S. McCarthy, H. Annegarn, and L. Ramberg (2004). Airborne dust deposition in the okavango delta, botswana, and its impact on landforms. *Earth Surface Processes and Landforms 29*(5), 565–577.

Kusche, J., R. Schmidt, S. Petrovic, and R. Rietbroek (2009, 3). Decorrelated GRACE time-variable gravity solutions by GFZ, and their validation using a hydrological model. *Journal of Geodesy 83*(10), 903–913.

Laletsang, K. (1995). Groundwater investigations using geophysical techniques at Marophe, the Okavango Delta, Botswana . Master's thesis, Memorial University of Newfoundland.

Lindholm, M., D. O. Hessen, K. Mosepele, and P. Wolski (2007, 12). Food webs and energy fluxes on a seasonal floodplain : The influence of flood size. *Wetlands 27*(4), 775–784.

Linol, B. (2013). *Sedimentology and Sequence Stratigraphy of the Congo and Kalahari Basins of South Central Africa and Their Evolution During the Formation and Break-up of West Gondwana*. Ph. D. thesis, Nelson Mandela Metropolitan University, Port Elizabeth.

Linol, B., M. J. de Wit, F. Guillocheau, M. C. de Wit, Z. Anka, and J.-P. Colin (2015). Formation and collapse of the Kalahari duricrust ['African Surface'] across the Congo Basin, with implications for changes in rates of Cenozoic off-shore sedimentation. In *Geology and Resource Potential of the Congo Basin*, pp. 193–210. Springer.

Lithgow-Bertelloni, C. and P. G. Silver (1998). Dynamic topography, plate driving forces and the African superswell. *Nature 395*(6699), 269.

Longuevergne, L., B. R. Scanlon, and C. R. Wilson (2010, 11). GRACE Hydrological estimates for small basins : Evaluating processing approaches on the High Plains Aquifer, USA. *Water Resources Research 46*(11), 1–15.

Lyard, F., F. Lefevre, T. Letellier, and O. Francis (2006). Modelling the global ocean tides : modern insights from fes2004. *Ocean Dynamics 56*(5), 394–415.

Martens, B., D. G. Miralles, H. Lievens, R. van der Schalie, R. A. M. de Jeu, D. Fernández-Prieto, H. E. Beck, W. A. Dorigo, and N. E. C. Verhoest (2017). Gleamv3 : satellite-based land evaporation and root-zone soil moisture. *Geoscientific Model Development 10*(5), 1903–1925.

Mazvimavi, D. and P. Wolski (2006). Long-term variations of annual flows of the okavango and zambezi rivers. *Physics and Chemistry of the Earth, Parts A/B/C 31*(15), 944 – 951. Water for Sustainable Socio-Economic Development, Good Health for All and Gender Equity.

McCarthy, T. (2006). Groundwater in the wetlands of the okavango delta, botswana, and its contribution to the structure and function of the ecosystem. *Journal of Hydrology 320*(3), 264 – 282. Groundwater - surface water interactions in wetlands for integrated water resources management.

McCarthy, T. (2013). The Okavango Delta and its place in the geomorphological evolution of Southern Africa. *South African Journal of Geology 116*(1), 1–54.

McCarthy, T. and W. Ellery (1994). The effect of vegetation on soil and ground water chemistry and hydrology of islands in the seasonal swamps of the okavango fan, botswana. *Journal of Hydrology 154*(1), 169 – 193.

McCarthy, T. and W. Ellery (1995a). The failure of the nqoga channel between hamoga and letenetso islands, northeastern okavango delta. *Botswana Notes & Records 27*(1), 129–150.

McCarthy, T. and W. Ellery (1998). The okavango delta. *Transactions of the Royal Society of South Africa 53*(2), 157–182.

McCarthy, T., W. Ellery, and J. Dangerfield (1998). The role of biota in the initiation and growth of islands on the floodplain of the okavango alluvial fan, botswana. *Earth Surface Processes and Landforms 23*(4), 291–316.

McCarthy, T., W. Ellery, and K. Ellery (1993). Vegetation-induced, subsurface precipitation of carbonate as an aggradational process in the permanent swamps of the okavango (delta) fan, botswana. *Chemical Geology 107*(1), 111 – 131.

McCarthy, T., W. Ellery, and I. Stanistreet (1992). Avulsion mechanisms on the okavango fan, botswana : the control of a fluvial system by vegetation. *Sedimentology 39*(5), 779–795.

McCarthy, T., R. Green, and N. Franey (1993). The influence of neo-tectonics on water dispersal in the northeastern regions of the okavango swamps, botswana. *Journal of African Earth Sciences (and the Middle East) 17*(1), 23 – 32.

McCarthy, T., M. Humphries, I. Mahomed, P. L. Roux, and B. Verhagen (2012). Island forming processes in the okavango delta, botswana. *Geomorphology 179*(0), 249 – 257.

McCarthy, T., J. McIver, and B. Verhagen (1991). Groundwater evolution, chemical sedimentation and carbonate brine formation on an island in the okavango delta swamp, botswana. *Applied Geochemistry 6*(6), 577 – 595.

McCarthy, T. and J. Metcalfe (1990). Chemical sedimentation in the semi-arid environment of the okavango delta, botswana. *Chemical Geology 89*(1–2), 157 – 178.

McCarthy, T., I. Stanistreet, B. Cairncross, W. Ellery, K. Ellery, R. Oelofse, and T. Grobicki (1988). Incremental aggradation on the okavango delta-fan, botswana. *Geomorphology 1*(3), 267 – 278.

McCarthy, T. S., A. Bloem, and P. A. Larkin (1998). Observations on the hydrology and geohydrology of the okavango delta. *South African Journal of Geology 101*(2), 101–117.

McCarthy, T. S., G. R. Cooper, P. Tyson, and W. N. Ellery (2000). Seasonal flooding in the okavango delta, botswana-recent history and future prospects. *South African Journal of Science 96*(1), 25–33.

McCarthy, T. S. and W. N. Ellery (1995b). Sedimentation on the distal reaches of the okavango fan, botswana, and its bearing on calcrete and silcrete (ganister) formation. *Journal of Sedimentary Research 65*(1a), 77–90.

McCarthy, T. S., W. N. Ellery, and A. Bloem (1998). Some observations on the geomorphological impact of hippopotamus (hippopotamus amphibius l.) in the okavango delta, botswana. *African Journal of Ecology 36*(1), 44–56.

McCarthy, T. S., I. G. Stanistreet, and B. Cairncross (1991). The sedimentary dynamics of active fluvial channels on the okavango fan, botswana. *Sedimentology 38*(3), 471–487.

McFarlane, M., F. Eckardt, S. Coetzee, and S. Ringrose (2010, 09). An African surface weathering profile in the Kalahari of North West Ngamiland, Botswana : processes and products. *Zeitschrift für Geomorphologie, NF 54*(3), 273–303.

McFarlane, M., F. Eckardt, S. Ringrose, S. Coetzee, and J. Kuhn (2005). Degradation of linear dunes in northwest ngamiland, botswana and the implications for luminescence dating of periods of aridity. *Quaternary International 135*(1), 83 – 90. Geochronology and Environmental Reconstruction : a Tribute to Glenn A. Goodfriend.

McFarlane, M. J., S. H. Coetzee, J. R. Kuhn, C. H. M. Vanderpost, and F. D. Eckardt (2007, 09). In situ rounding of quartz grains within an African surface weathering profile in North West Ngamiland, Botswana. *Zeitschrift für Geomorphologie 51*(3), 269–286.

Mendelsohn, J., C. van der Post, L. Ramberg, M. Murray-Hudson, P. Wolski, and K. Mosepele (2010). Okavango delta : floods of life.

Mikhailov, V., V. Lyakhovsky, I. Panet, Y. van Dinther, M. Diament, T. Gerya, O. deViron, and E. Timoshkina (2013). Numerical modelling of post-seismic rupture propagation after the sumatra 26.12.2004 earthquake constrained by grace gravity data. *Geophysical Journal International 194*(2), 640–650.

Miller, R. M. (1983). The Pan-African Damara Orogen of South West Africa/Namibia. In *Evolution of the Damara Orogen of South West Africa/Namibia*, pp. 431–515. Johannesburg (South Africa) : The Geological Society of South Africa.

Miller, R. M. and A. Burger (1983). U-Pb zircon age of the early Damaran Naauwpoort Formation. In *Evolution of the Damara Orogen of South West Africa/Namibia*, pp. 267–272. Johannesburg (South Africa) : The Geological Society of South Africa.

Miller, R. M., M. Pickford, and B. Senut (2010). The geology, palaeontology and evolution of the Etosha pan, Namibia : Implications for terminal Kalahari deposition. *South African Journal of Geology 113*(3), 307–334.

Milzow, C., P. E. Krogh, and P. Bauer-Gottwein (2011). Combining satellite radar altimetry, sar surface soil moisture and grace total storage changes for hydrological model calibration in a large poorly gauged catchment. *Hydrology and Earth System Sciences 15*(6), 1729–1743.

Milzow, C., O. Tshekiso, L. Kgotlhang, and W. Kinzelbach (2010, Jun). Sediment transport monitoring and short term modeling in the okavango delta, botswana. *Wetlands 30*(3), 417–428.

Modie, B. N. (2000). Geology and mineralisation in the meso- to neoproterozoic ghanzi-chobe belt of northwest botswana. *Journal of African Earth Sciences 30*(3), 467 – 474. 50th Anniversary of the Geological Survey.

Modisi, M. (2000). Fault system at the southeastern boundary of the okavango rift, botswana. *Journal of African Earth Sciences 30*(3), 569 – 578. 50th Anniversary of the Geological Survey.

Modisi, M., E. Atekwana, A. Kampunzu, and T. Ngwisanyi (2000). Rift kinematics during the incipient stages of continental extension : Evidence from the nascent okavango rift basin, northwest botswana. *Geology 28*(10), 939–942.

Money, N. (1972). An outline of the geology of western zambia. *Records of the Geological Survey, Republic of Zambia 12*(1972), 103–123.

Moore, A. E., F. P. D. w. Cotterill, M. P. L. Main, and H. B. Williams (2008). *The Zambezi River*, pp. 311–332. John Wiley & Sons, Ltd.

Mu, Q., M. Zhao, and S. W. Running (2011). Improvements to a modis global terrestrial evapotranspiration algorithm. *Remote Sensing of Environment 115*(8), 1781 – 1800.

Mulabisana, T. F. (2016). Compiling a homogeneous Earthquake Catalogue for Southern Africa. Master's thesis, School of Geoscience, University of Witwatersrand.

Nicholson, S. E. (2000). The nature of rainfall variability over Africa on time scales of decades to millenia. *Global and Planetary Change 26*(1), 137 – 158. Paleomonsoon variations and terrestrial environmental change.

Nicholson, S. E. and J. Kim (1997). The relationship of the el niño–southern oscillation to african rainfall. *International Journal of Climatology 17*(2), 117–135.

Nyblade, A. A. and S. W. Robinson (1994). The African Superswell. *Geophysical Research Letters 21*(9), 765–768.

Nyblade, A. A. and N. H. Sleep (2003). Long lasting epeirogenic uplift from mantle plumes and the origin of the Southern African Plateau. *Geochemistry, Geophysics, Geosystems 4*(12), n/a–n/a.

Oak Ridge National Laboratory Distributed Active Archive Center (2015). Oak ridge national laboratory distributed active archive center (ornl daac). FLUXNET Web Page.

Obakeng, O. and A. Gieske (1997). Hydraulic conductivity and transmissivity of a water-table aquifer in the boro river system, okavango delta. *Botswana Geological Survey Department bulletin series 46*, 191.

OKACOM (2010, May). Protocol on Hydrological Data Sharing for the Okavango River Basin.

Pastier, A.-M., O. Dauteuil, M. Murray-Hudson, F. Moreau, A. Walpersdorf, and K. Makati (2017). Is the Okavango Delta the terminus of the East African Rift System ? Towards a new geodynamic model : Geodetic study and geophysical review. *Tectonophysics 712*, 469 – 481.

Pedoja, K., L. Husson, V. Regard, P. R. Cobbold, E. Ostanciaux, M. E. Johnson, S. Kershaw, M. Saillard, J. Martinod, L. Furgerot, P. Weill, and B. Delcaillau (2011). Relative sea-level fall since the last interglacial stage : Are coasts uplifting worldwide ? *Earth-Science Reviews 108*(1), 1 – 15.

Persits, F., T. Ahlbrandt, M. Tuttle, R. Charpentier, M. Brownfield, and K. Takahashi (2002). Map showing geology, oil and gas fields and geologic provinces of Africa, Ver.2.0.

Pike, J. (1970). Iterim technical notes on the hydrology and water resources of the okavango river system. undp/fao/botswana government. surveys and training for the development of water resources and agricultural production, botswana. Technical report, Technical Note.

Pitman, W. (1973). *A mathematical model for generating monthly river flows from meteorological data in South Africa*. Ph. D. thesis, Hydrological Research unit, University of the Witwatersrand, Johannesburg, South Africa. Report No. 2/73.

Podgorski, J. E., A. G. Green, T. Kalscheuer, W. K. Kinzelbach, H. Horstmeyer, H. Maurer, L. Rabenstein, J. Doetsch, E. Auken, T. Ngwisanyi, G. Tshoso, B. C. Jaba, O. Ntibinyane, and K. Laletsang (2015). Integrated interpretation of helicopter and ground-based geophysical data recorded within the okavango delta, botswana. *Journal of Applied Geophysics 114*(0), 52 – 67.

Porter, J. and I. Muzila (1989). Aspects of swamp hydrology in the okavango. *Botswana Notes and Records 21*, 73–91.

Priestley, C. and R. Taylor (1972). On the assessment of surface heat flux and evaporation using large-scale parameters. *Monthly Weather Review 100*(2), 81–92.

Ramberg, L., P. Hancock, M. Lindholm, T. Meyer, S. Ringrose, J. Sliva, J. Van As, and C. Vander Post (2006, Oct). Species diversity of the okavango delta, botswana. *Aquatic Sciences 68*(3), 310–337.

Ramberg, L. and P. Wolski (2008). Growing islands and sinking solutes : processes maintaining the endorheic okavango delta as a freshwater system. *Plant Ecology 196*(2), 215–231.

Ramberg, L., P. Wolski, and M. Krah (2006, 09). Water Balance and Infiltration in a Seasonal Floodplain in the Okavango Delta, Botswana. *Wetlands 26*, 677–690.

Ramillien, G., S. Bouhours, A. Lombard, A. Cazenave, F. Flechtner, and R. Schmidt (2008). Land water storage contribution to sea level from GRACE geoid data over 2003–2006. *Global and Planetary Change 60*, 381–392.

Ramillien, G., F. Frappart, and L. Seoane (2014). Application of the Regional Water Mass Variations from GRACE Satellite Gravimetry to Large-Scale Water Management in Africa. *Remote Sensing 6*(8), 7379–7405.

Reilinger, R., S. McClusky, P. Vernant, S. Lawrence, S. Ergintav, R. Cakmak, H. Ozener, F. Kadirov, I. Guliev, R. Stepanyan, M. Nadariya, G. Hahubia, S. Mahmoud, K. Sakr,

A. ArRajehi, D. Paradissis, A. Al-Aydrus, M. Prilepin, T. Guseva, E. Evren, A. Dmitrotsa, S. V. Filikov, F. Gomez, R. Al-Ghazzi, and G. Karam (2006). GPS constraints on continental deformation in the Africa-Arabia-Eurasia continental collision zone and implications for the dynamics of plate interactions. *Journal of Geophysical Research : Solid Earth 111*(B5), n/a–n/a. B05411.

Rietbroek, R., M. Fritsche, S.-E. Brunnabend, I. Daras, J. Kusche, J. Schröter, F. Flechtner, and R. Dietrich (2012, 9). Global surface mass from a new combination of GRACE, modelled OBP and reprocessed GPS data. *Journal of Geodynamics 59-60*, 64–71.

Ringrose, S., P. Huntsman-Mapila, W. Downey, S. Coetzee, M. Fey, C. Vanderpost, B. Vink, T. Kemosidile, and D. Kolokose (2008). Diagenesis in okavango fan and adjacent dune deposits with implications for the record of palaeo-environmental change in makgadikgadi–okavango–zambezi basin, northern botswana. *Geomorphology 101*(4), 544 – 557.

Sakumura, C., S. Bettadpur, and S. Bruinsma (2014). Ensemble prediction and intercomparison analysis of grace time-variable gravity field models. *Geophysical Research Letters 41*(5), 1389–1397.

Saria, E., E. Calais, Z. Altamimi, P. Willis, and H. Farah (2013). A new velocity field for Africa from combined GPS and DORIS space geodetic Solutions : Contribution to the definition of the African reference frame (AFREF). *Journal of Geophysical Research : Solid Earth 118*(4), 1677–1697.

Save, H., S. Bettadpur, and B. D. Tapley (2012, 3). Reducing errors in the GRACE gravity solutions using regularization. *Journal of Geodesy 86*(9), 695–711.

Scanlon, B. R., C. C. Faunt, L. Longuevergne, R. C. Reedy, W. M. Alley, V. L. McGuire, and P. B. McMahon (2012). Groundwater depletion and sustainability of irrigation in the us high plains and central valley. *Proceedings of the National Academy of Sciences 109*(24), 9320–9325.

Schefusz, E., H. Kuhlmann, G. Mollenhauer, M. Prange, and J. Patzold (2011, 12). Forcing of wet phases in southeast Africa over the past 17,000 years. *Nature 480*, 509–512.

Scholz, C. H., T. A. Koczynski, and D. G. Hutchins (1976). Evidence for Incipient Rifting in Southern Africa. *Geophysical Journal International 44*(1), 2135–144.

Shaw, P. (1984). A historical note on the outflows of the okavango delta system. *Botswana Notes and Records 16*, 127–130.

Shaw, P. (1985a). The desiccation of lake ngami : An historical perspective. *The Geographical Journal 151*(3), 318–326.

Shaw, P. (1985b). Late quaternary landforms and environmental change in northwest botswana : The evidence of lake ngami and the mababe depression. *Transactions of the Institute of British Geographers 10*(3), 333–346.

Shaw, P. A., M. D. Bateman, D. S. Thomas, and F. Davies (2003). Holocene fluctuations of lake ngami, middle kalahari : chronology and responses to climatic change. *Quaternary International 111*(1), 23 – 35. Late Quaternary environmental change in African Drylands.

Shaw, P. A. and D. J. Nash (1998). Dual mechanisms for the formation of fluvial silcretes in the distal reaches of the okavango delta fan, botswana. *Earth Surface Processes and Landforms 23*(8), 705–714.

Shemang, E. and L. Molwalefhe (2009). Dc resistivity and seismic refraction survey across the se margin of lake ngami, nw botswana. *Acta Geophysica 57*(3), 728–742.

Shemang, E. and L. Molwalefhe (2011). Geomorphic landforms and tectonism along the eastern margin of the okavango rift zone, north western botswana as deduced from geophysical data in the area. In P. E. Sharkov (Ed.), *New Frontiers in Tectonic Research - General Problems, Sedimentary Basins and Island Arcs*. InTech.

Simmons, N. A., A. M. Forte, and S. P. Grand (2007). Thermochemical structure and dynamics of the African superplume. *Geophysical Research Letters 34*(2), n/a–n/a. L02301.

Stanistreet, I., B. Cairncross, and T. McCarthy (1993). Low sinuosity and meandering bedload rivers of the okavango fan : channel confinement by vegetated levées without fine sediment. *Sedimentary Geology 85*(1–4), 135 – 156.

Stanistreet, I. and T. McCarthy (1993). The okavango fan and the classification of subaerial fan systems. *Sedimentary Geology 85*(1–4), 115 – 133.

Stigand, A. G. (1923). Ngamiland. *The Geographical Journal 62*(6), 401–419.

Tapley, B., J. Ries, S. Bettadpur, D. Chambers, M. Cheng, F. Condi, B. Gunter, Z. Kang, P. Nagel, R. Pastor, T. Pekker, S. Poole, and F. Wang (2005, Nov). Ggm02 – an improved earth gravity field model from grace. *Journal of Geodesy 79*(8), 467–478.

Tapley, B. D., S. Bettadpur, J. C. Ries, P. F. Thompson, and M. M. Watkins (2004). Grace measurements of mass variability in the earth system. *Science 305*(5683), 503–505.

Tapley, B. D., S. Bettadpur, M. Watkins, and C. Reigber (2004). The gravity recovery and climate experiment : Mission overview and early results. *Geophysical Research Letters 31*(9), n/a–n/a. L09607.

Thomas, D. and P. Shaw (1990). The deposition and development of the Kalahari Group sediments, Central Southern Africa. *Journal of African Earth Sciences (and the Middle East) 10*(1), 187 – 197.

Thomas, D. and P. A. Shaw (1991). *The Kalahari Environment*. Cambridge University Press.

Thomas, D. S. and P. A. Shaw (1988). Late cainozoic drainage evolution in the zambezi basin : Geomorphological evidence from the kalahari rim. *Journal of African Earth Sciences (and the Middle East) 7*(4), 611 – 618.

Thomas, D. S. and P. A. Shaw (2002). Late Quaternary environmental change in central southern Africa : new data, synthesis, issues and prospects. *Quaternary Science Reviews 21*(7), 783 – 797. Interactions between arid and humid records of Quaternary change in drylands (IGCP 413).

Tooth, S. and T. S. McCarthy (2004). Controls on the transition from meandering to straight channels in the wetlands of the okavango delta, botswana. *Earth Surface Processes and Landforms 29*(13), 1627–1649.

Tredoux, G., B. Van Der Merwe, and I. Peters (2009). Artificial recharge of the windhoek aquifer, namibia : Water quality considerations. *Boletin Geologicoy Minero 120*(2), 269–278.

Tregoning, P. and T. van Dam (2005). Effects of atmospheric pressure loading and seven-parameter transformations on estimates of geocenter motion and station heights from space geodetic observations. *Journal of Geophysical Research : Solid Earth 110*(B3), n/a–n/a. B03408.

Tregoning, P., C. Watson, G. Ramillien, H. McQueen, and J. Zhang (2009). Detecting hydrologic deformation using grace and gps. *Geophysical Research Letters 36*(15), n/a–n/a. L15401.

Tyson, P. D., G. R. J. Cooper, and T. S. McCarthy (2002). Millennial to multi-decadal variability in the climate of southern Africa. *International Journal of Climatology 22*(9), 1105–1117.

van Dam, T., J. Wahr, and D. Lavallée (2007). A comparison of annual vertical crustal displacements from gps and gravity recovery and climate experiment (grace) over europe. *Journal of Geophysical Research : Solid Earth 112*(B3), n/a–n/a. B03404.

Voss, K. A., J. S. Famiglietti, M. Lo, C. de Linage, M. Rodell, and S. C. Swenson (2013). Groundwater depletion in the middle east from grace with implications for transboundary water management in the tigris-euphrates-western iran region. *Water Resources Research 49*(2), 904–914.

Wahr, J., M. Molenaar, and F. Bryan (1998). Time variability of the Earth's gravity field : Hydrological and oceanic effects and their possible detection using GRACE. *Research : Solid Earth (1978–) 103*, 205–229.

Wang, L., C. Chen, J. Du, and T. Wang (2017). Detecting seasonal and long-term vertical displacement in the north china plain using grace and gps. *Hydrology and Earth System Sciences 21*(6), 2905–2922.

Wilk, J., D. Kniveton, L. Andersson, R. Layberry, M. C. Todd, D. Hughes, S. Ringrose, and C. Vanderpost (2006). Estimating rainfall and water balance over the okavango river basin for hydrological applications. *Journal of Hydrology 331*(1), 18 – 29. Water Resources in Regional Development : The Okavango River.

Wilson, B. and T. Dincer (1976). An introduction to the hydrology and hydrography of the okavango delta. In B. Society (Ed.), *Symposium on the Okavango Delta*, Gaborone, Botswana, pp. 33–48.

Wilson, B. H. (1973). Some natural and man-made changes in the channels of the okavango delta. *Botswana Notes and Records 5*, 132–153.

Wolski, P. (1998). Remote sensing, land use and hydrotopes in western province, zambia. elements of a groundwater study. *Physics and Chemistry of the Earth 23*(4), 479 – 484.

Wolski, P. and M. Murray-Hudson (2008). An investigation of permanent and transient changes in flood distribution and outflows in the okavango delta, botswana. *Physics and Chemistry of the Earth, Parts A/B/C 33*(1), 157 – 164. Hydrological Assessment and Integrated Water Resources Management with Special Focus on Developing Countries.

Wolski, P., M. Murray-Hudson, P. Fernkvist, A. Liden, P. Huntsman-Mapila, and L. Ramberg (2005). Islands in the okavango delta as sinks of water-borne nutrients. *Botswana Notes & Records 37*(1), 253–263.

Wolski, P., M. Murray-Hudson, K. Thito, and L. Cassidy (2017). Keeping it simple : Monitoring flood extent in large data-poor wetlands using MODIS SWIR data. *International Journal of Applied Earth Observation and Geoinformation 57*, 224 – 234.

Wolski, P., H. Savenije, M. Murray-Hudson, and T. Gumbricht (2006). Modelling of the flooding in the okavango delta, botswana, using a hybrid reservoir-gis model. *Journal of Hydrology 331*(1), 58 – 72. Water Resources in Regional Development : The Okavango River.

Wolski, P., M. Todd, M. Murray-Hudson, and M. Tadross (2012). Multi-decadal oscillations in the hydro-climate of the okavango river system during the past and under a changing climate. *Journal of Hydrology 475*, 294 – 305.

Annexe A

GPS time series

A.1 GPS Time series

The following pages show the complete time series for the stations used in chapter 3 and 4. The time series for monthly rainfall are plotted along daily positions and are extracted from CHIRPS for each station's coordinates.

DEAR

Location: De Aar, South Africa
23.9926°E, 30.6652°S, 1321.71 m

Network: IGS
Antenna on a concrete beacon on bedrock

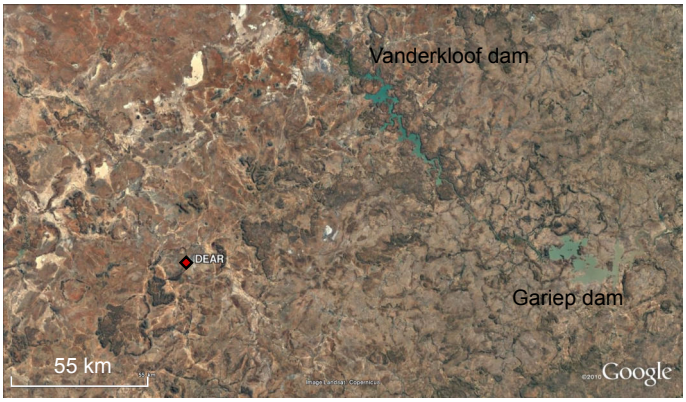

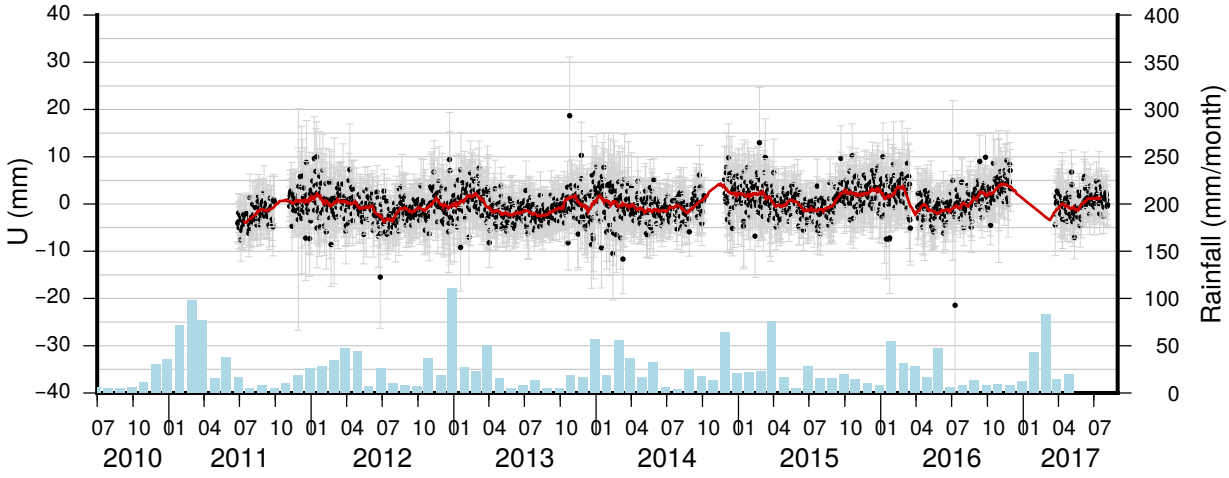

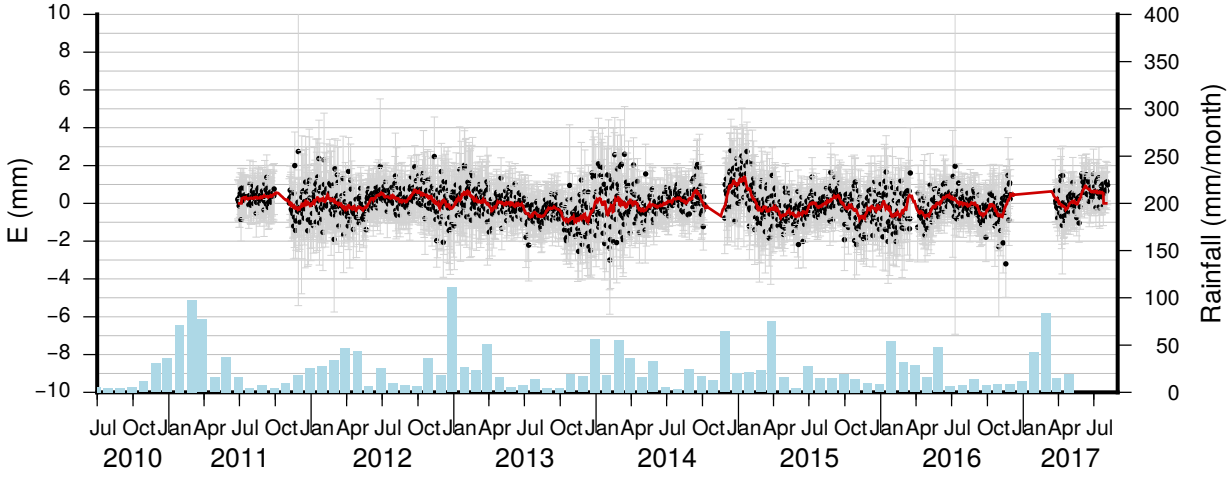

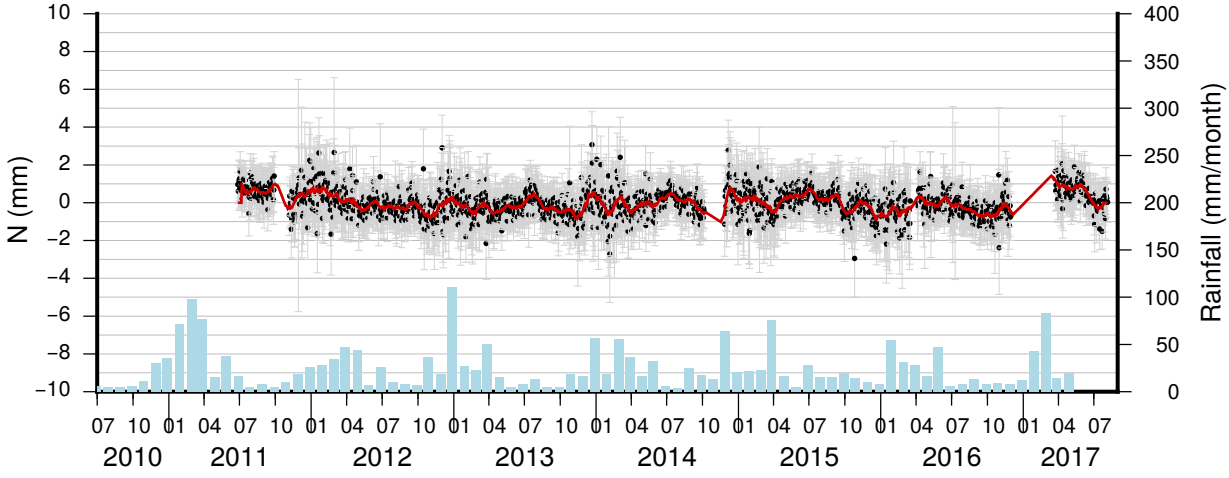

HNUS

Location: Hermanus, South Africa
19.2231°E, 34.4246°S, 63.05 m

Network: IGS
Antenna on a concrete beacon on bedrock

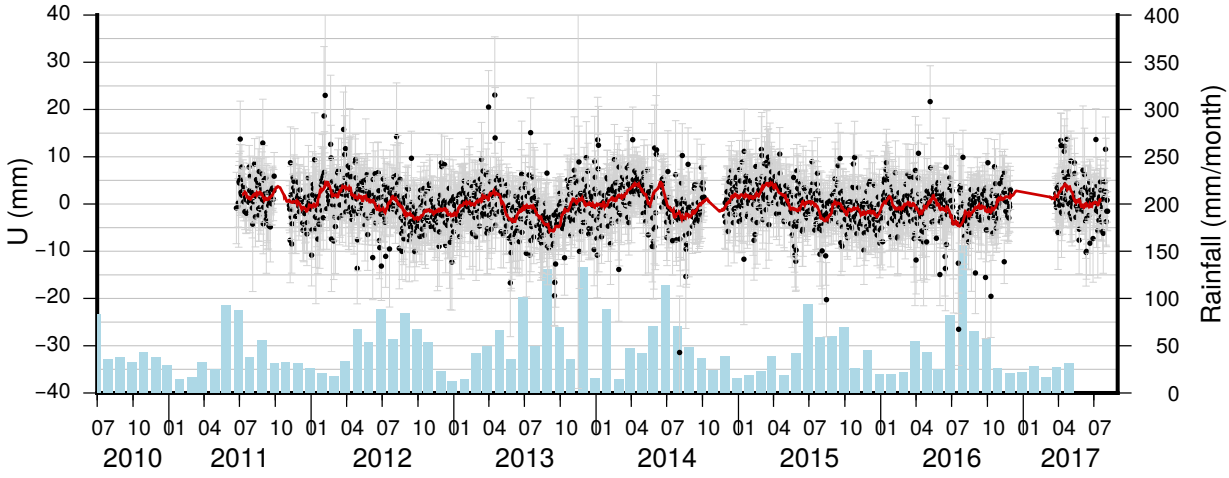

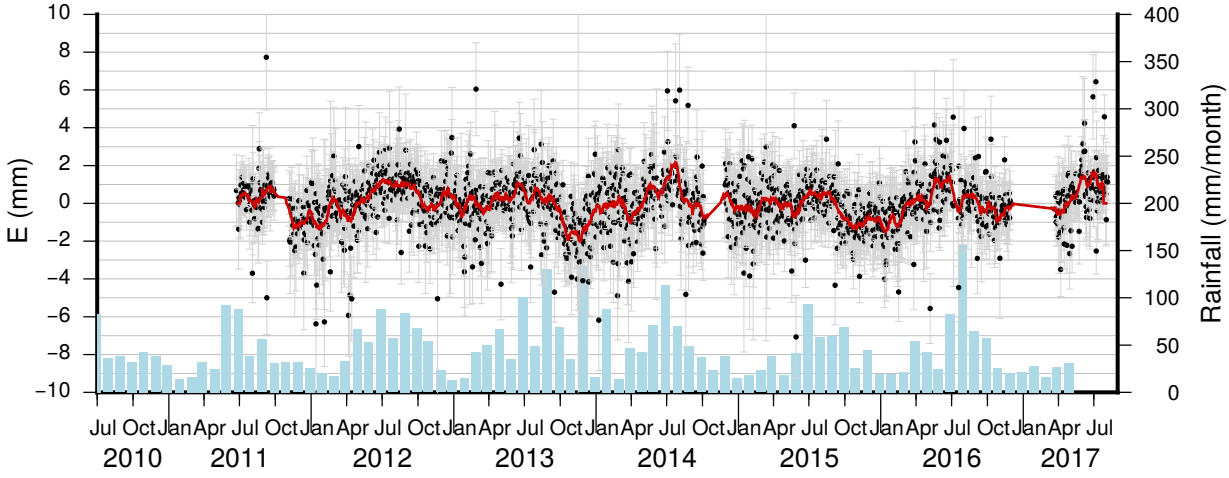

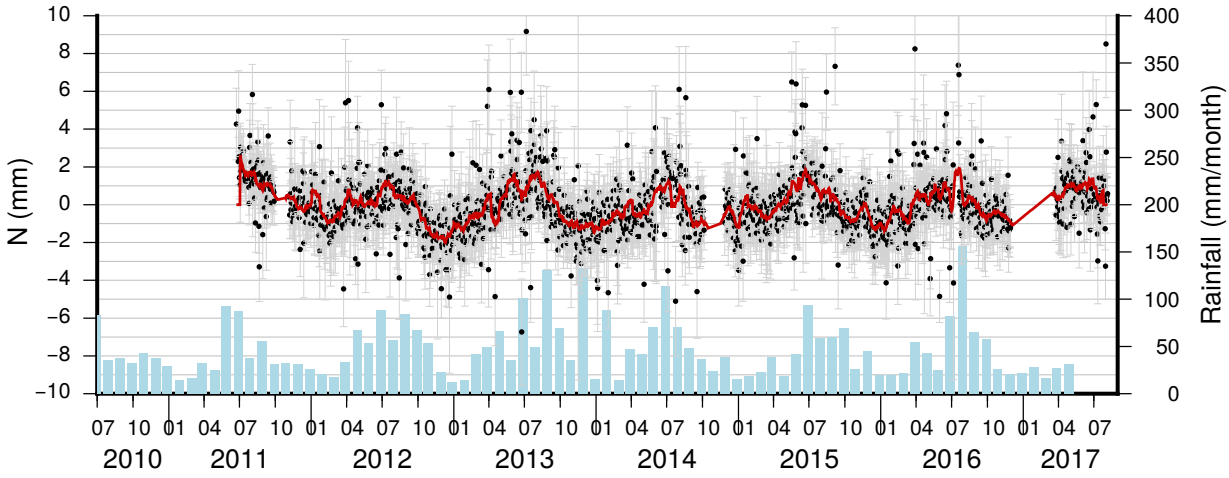

HRAO

Location: Hartebeesthoek, South Africa
27.687°E, 25.8901°S, 1414.14 m

Network: IGS
Antenna on a cement filled steel pipe/pillar
Hartebeesthoek Radio Astronomy Observatory

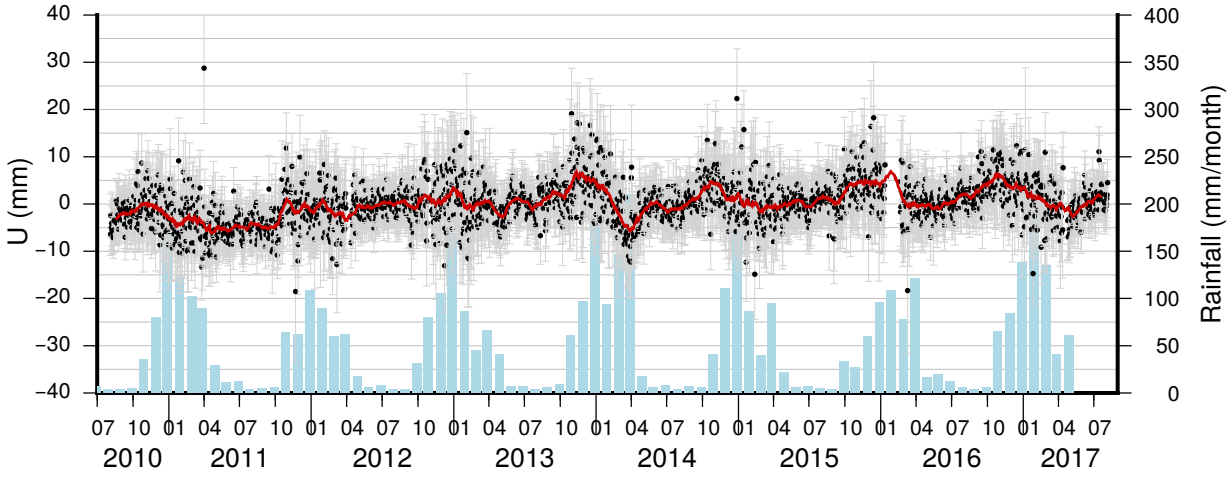

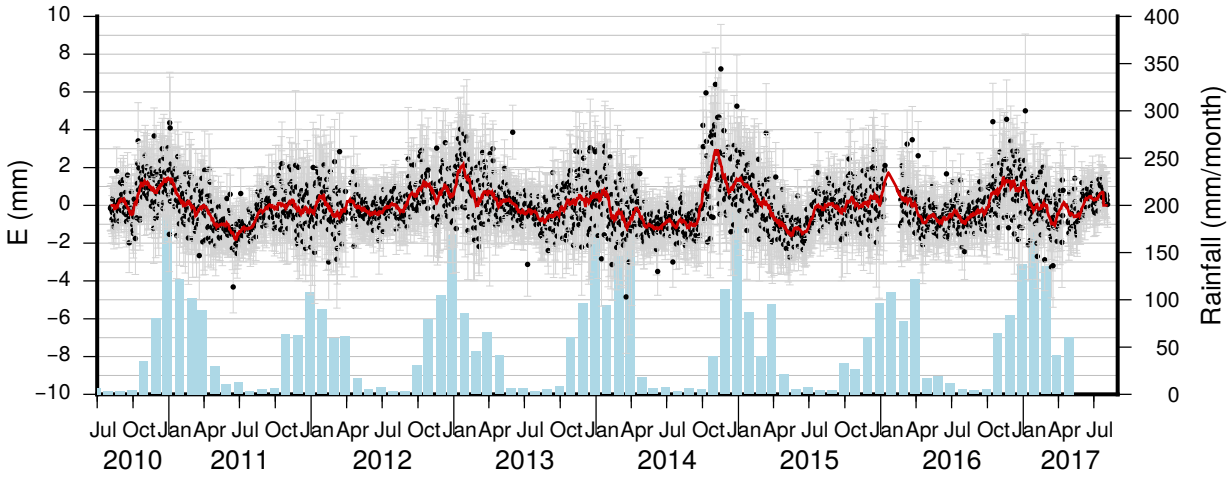

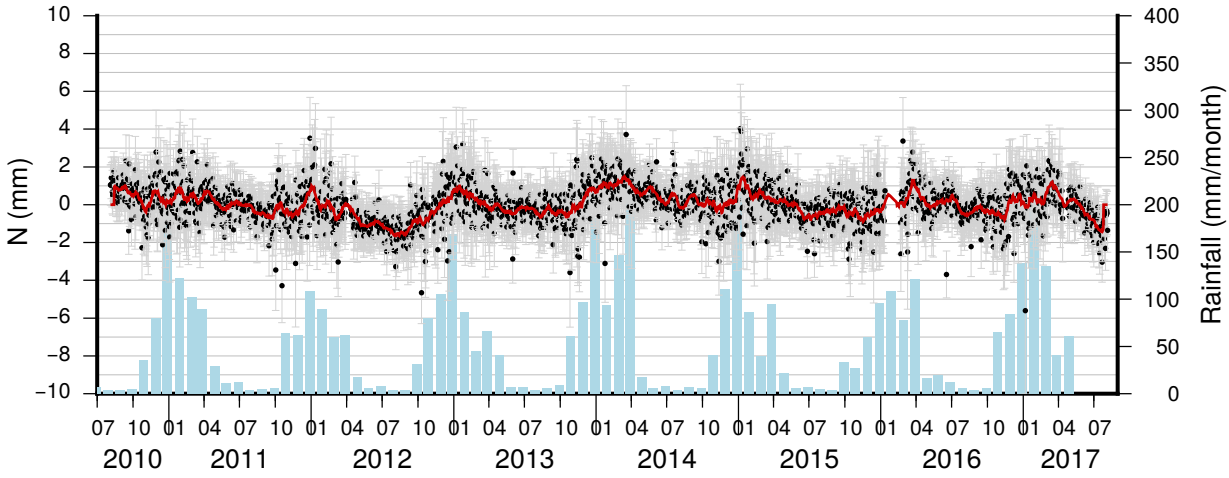

MAUA

Location: Maun, Botswana
23.5283°E, 19.9022°S, 960.75 m

Network: UNAVCO/AfricaArray
Antenna on a building roof of the Okavango Research Institute

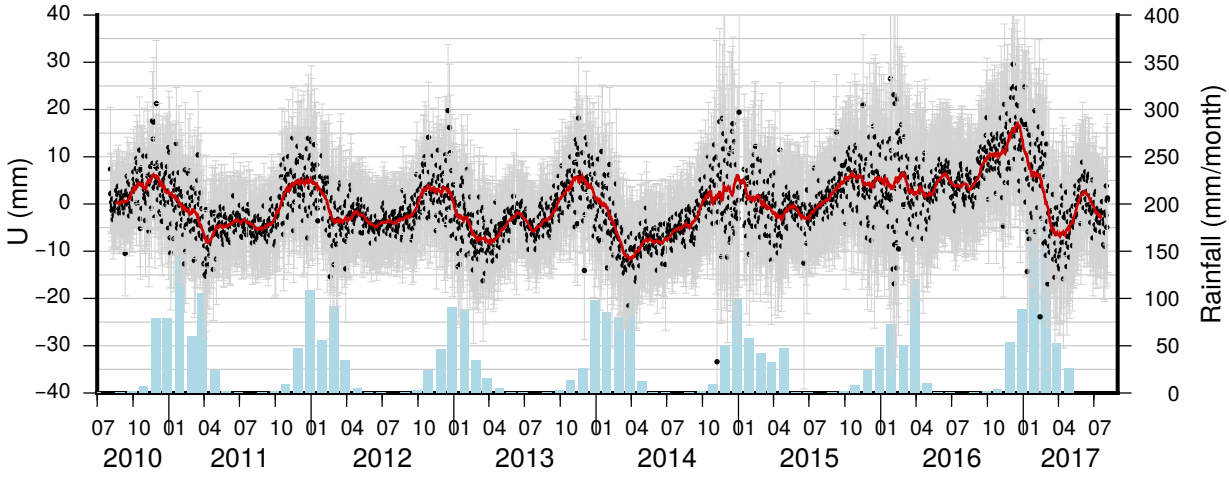

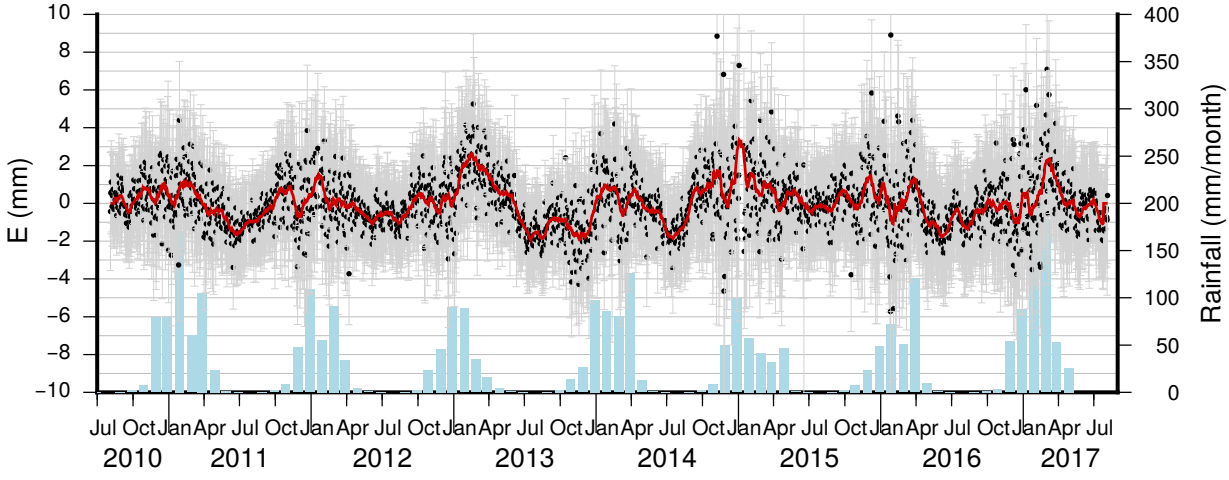

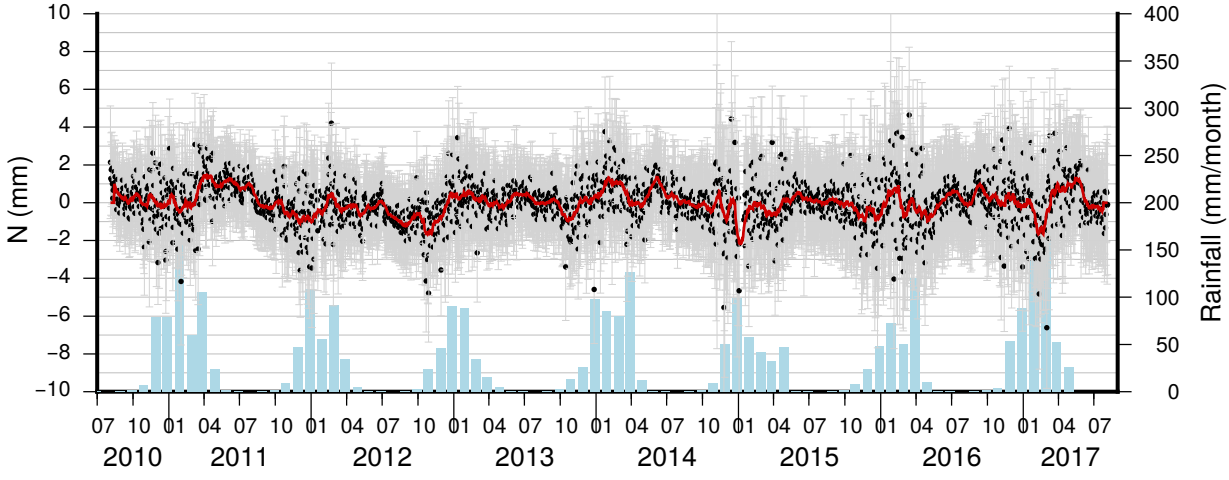

MONG

Location: Mongu, Zambia
23.1507°E, -15.2541°N, 1061.6 m

Network: UNAVCO/AfricaArray

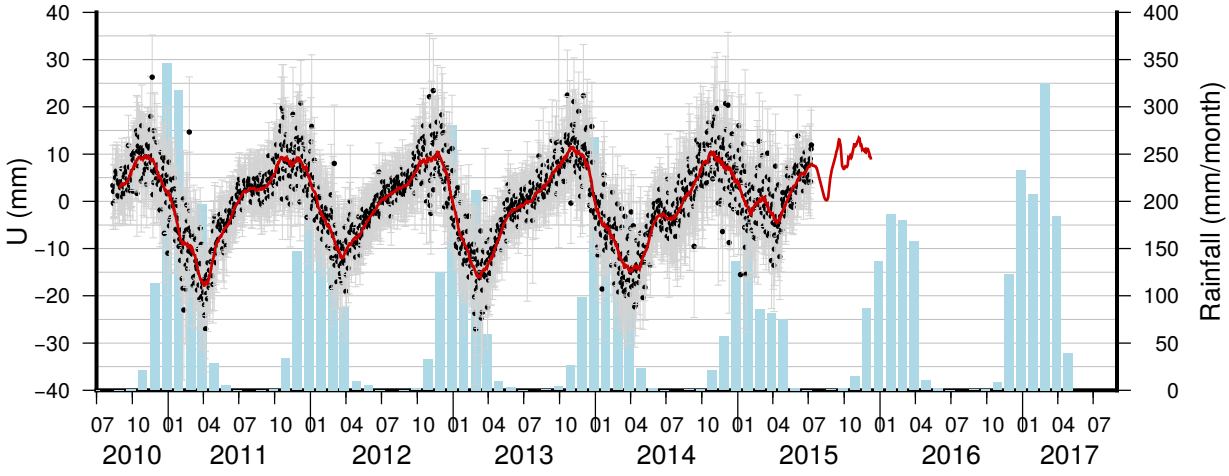

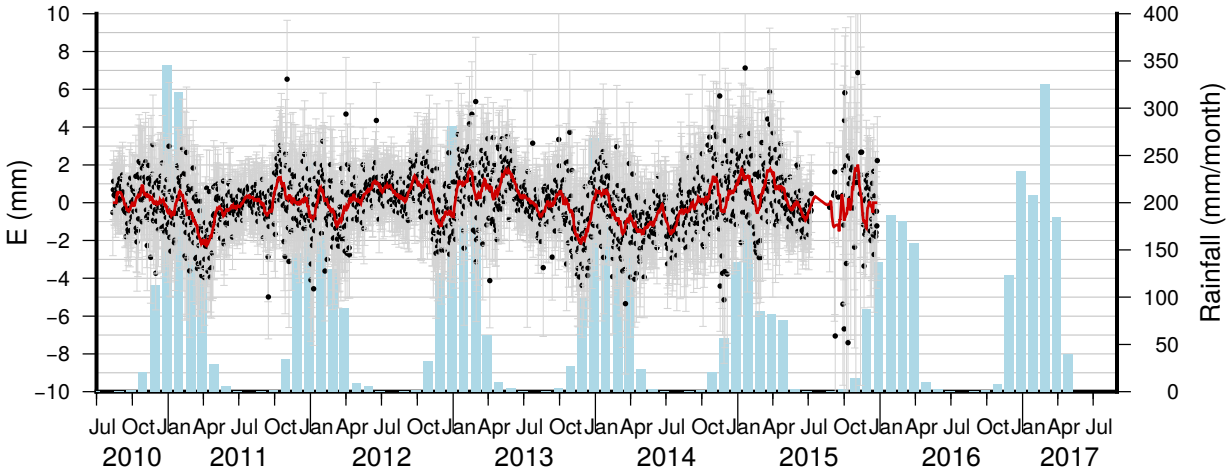

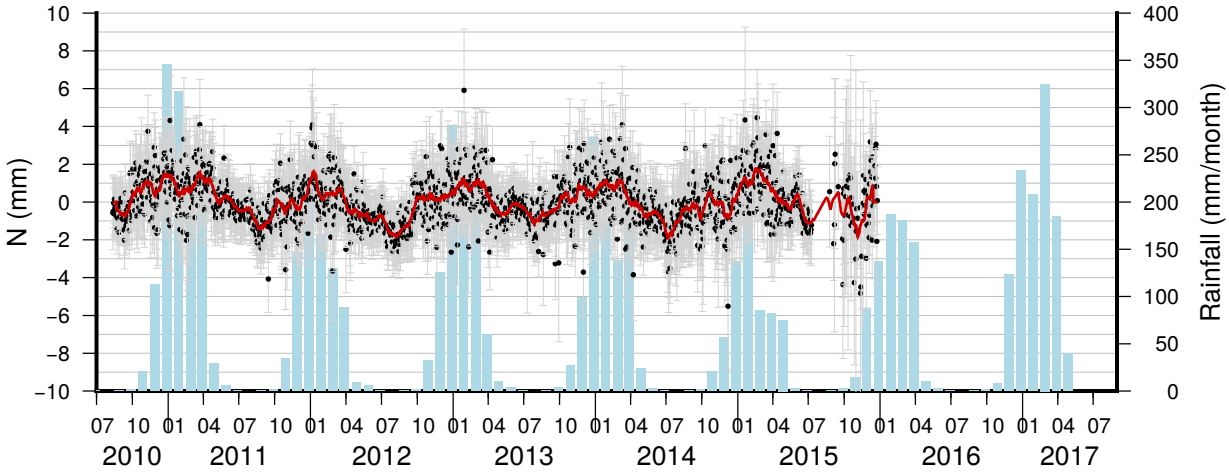

RUND

Location: Rundu, Namibia
19.7763°E, 17.9105°S, 1120.11 m

Network: UNAVCO/AfricaArray
Antenna on a building roof

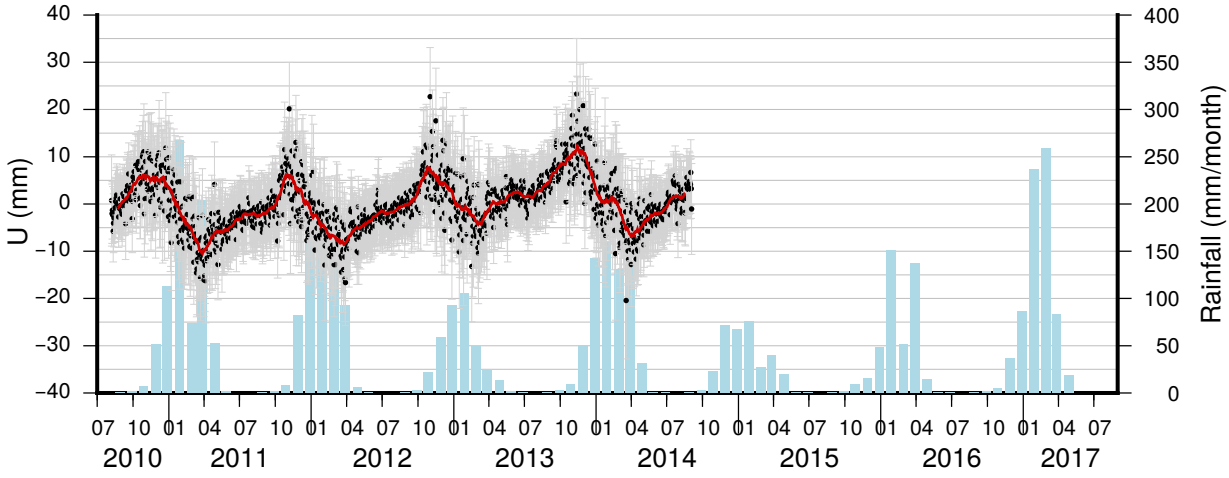

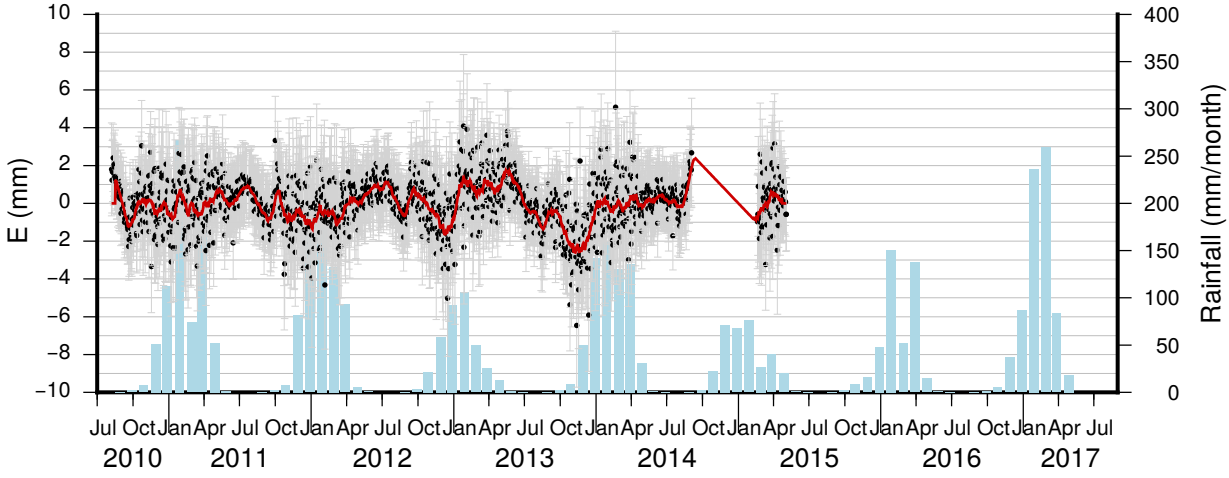

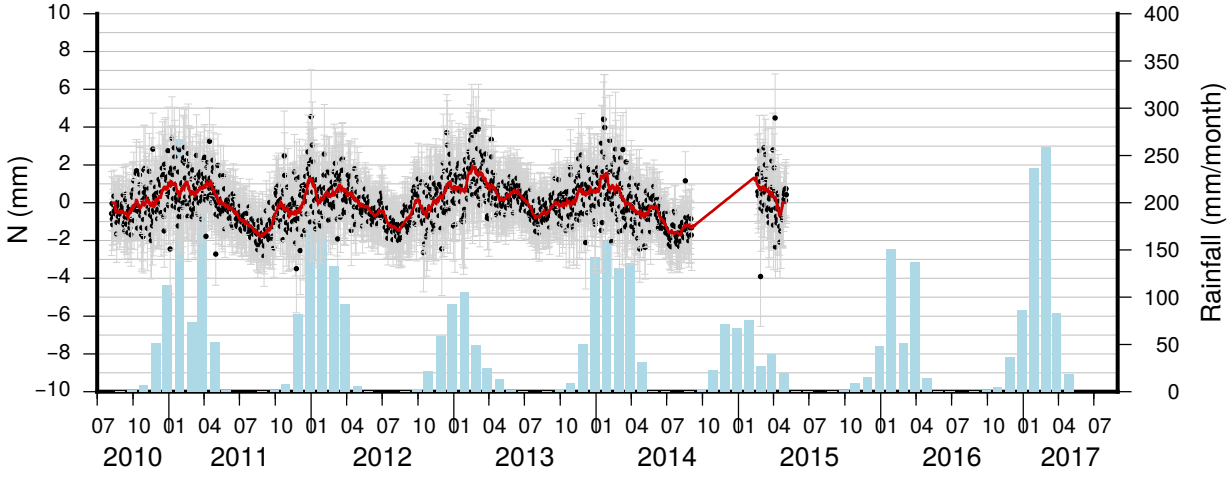

SBOK

Location: Springbok, South Africa
17.8792°E, 29.6693°S, 1043.08 m

Network: IGS
Antenna on a concrete pillar on bedrock

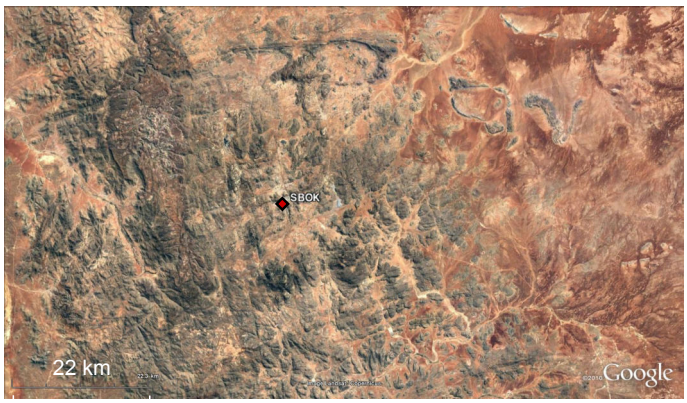

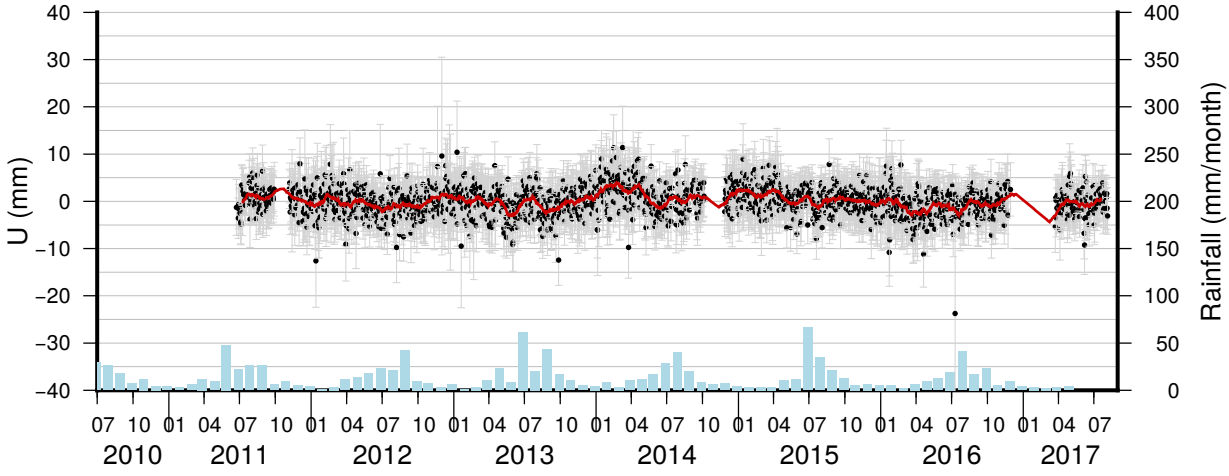

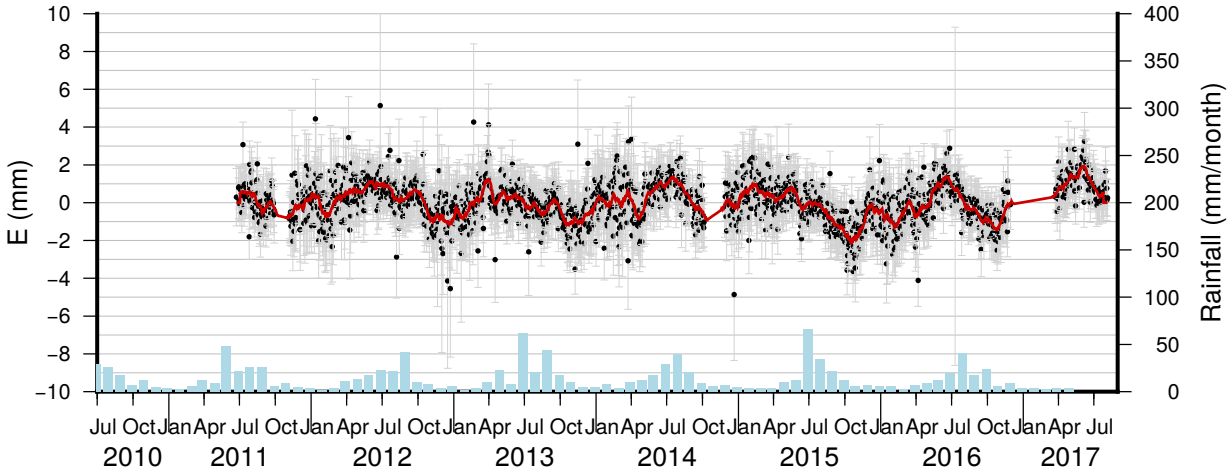

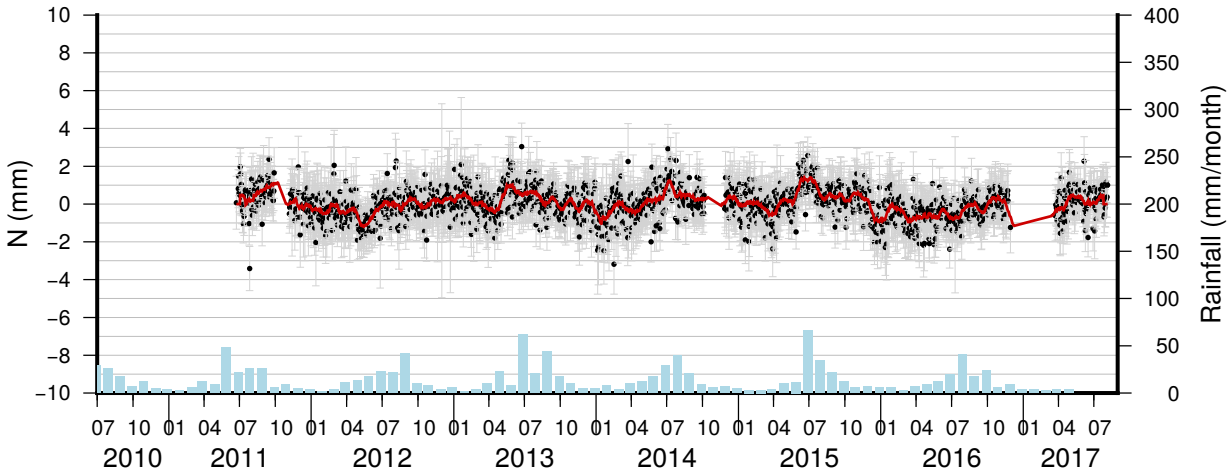

SUTH

Location: Sutherland, South Africa
20.8105°E, 32.3802°S, 1799.75 m

Twin station with SUTM

Network: IGS
Antenna on a concrete pillar on bedrock

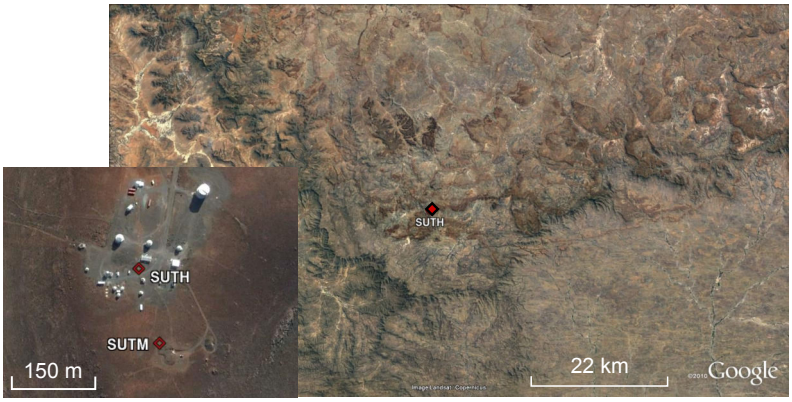

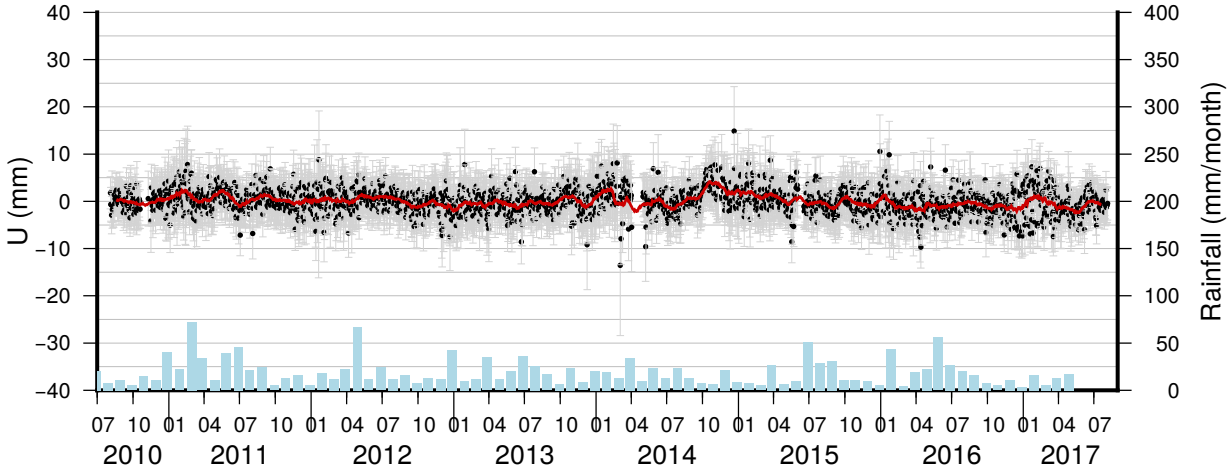

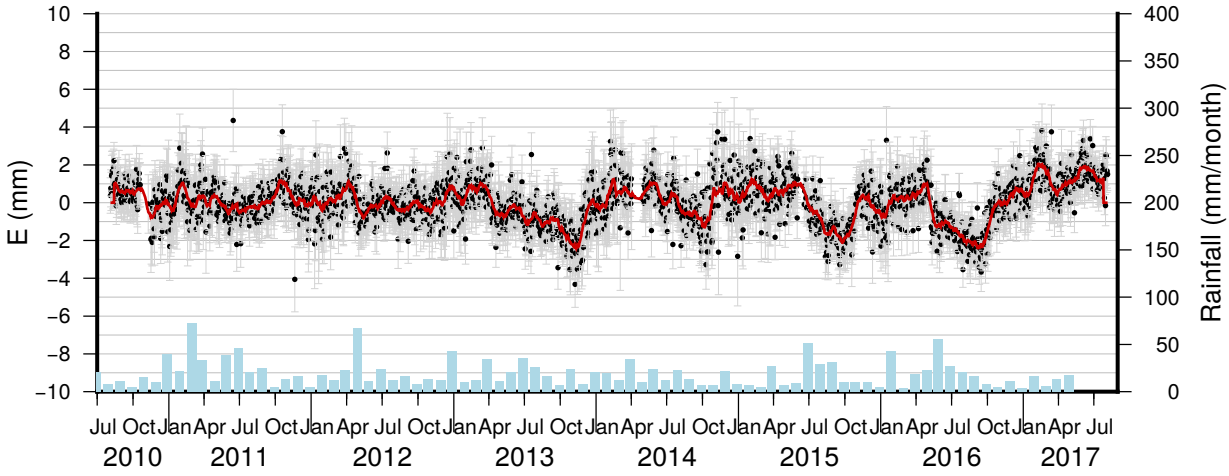

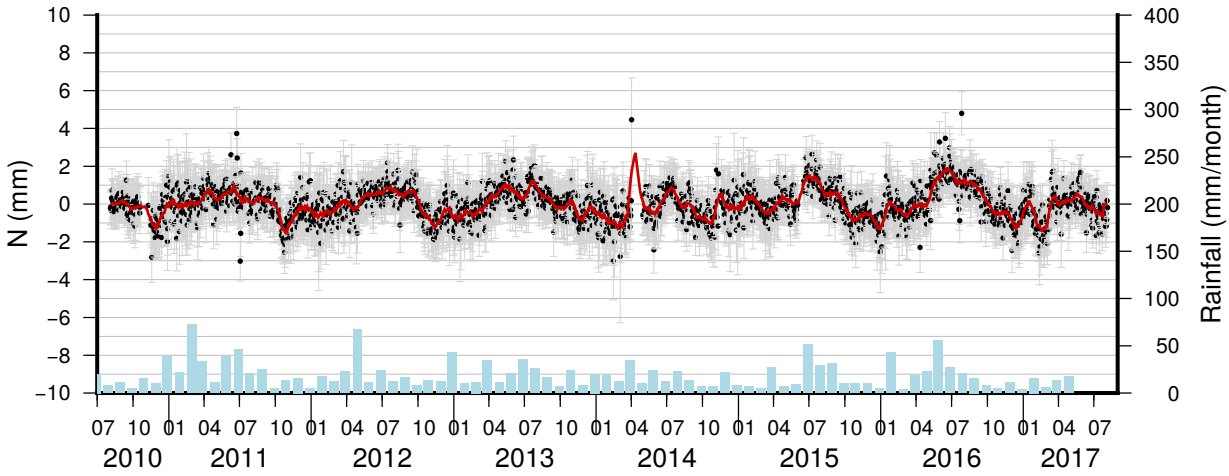

TDOU

Location: Thohoyandou, South Africa
30.384°E, 23.0799°S, 630.21 m

Network: IGS
Antenna on a concrete beacon on gravel/sand

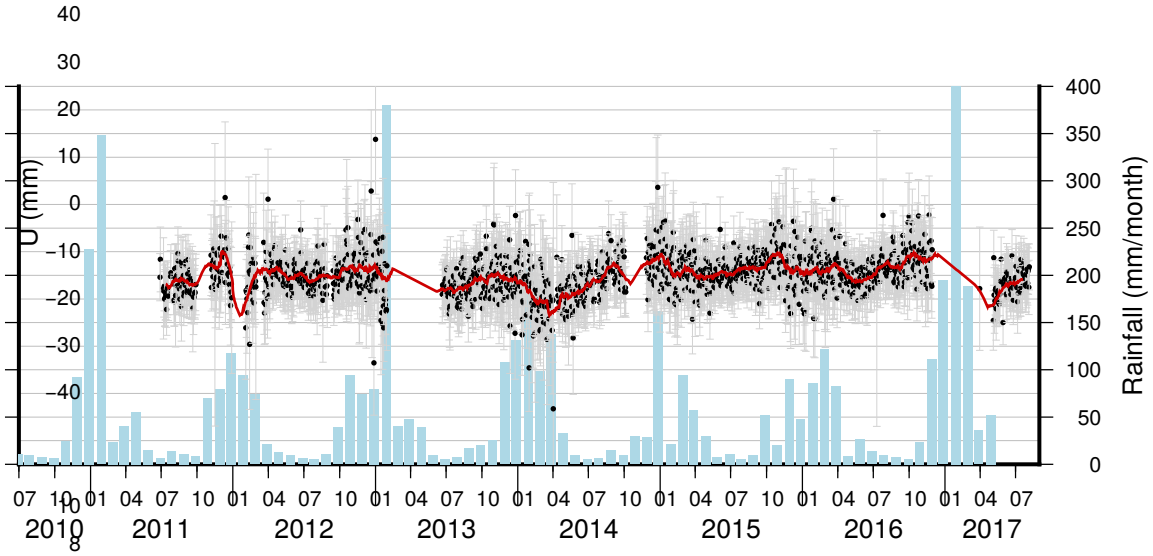

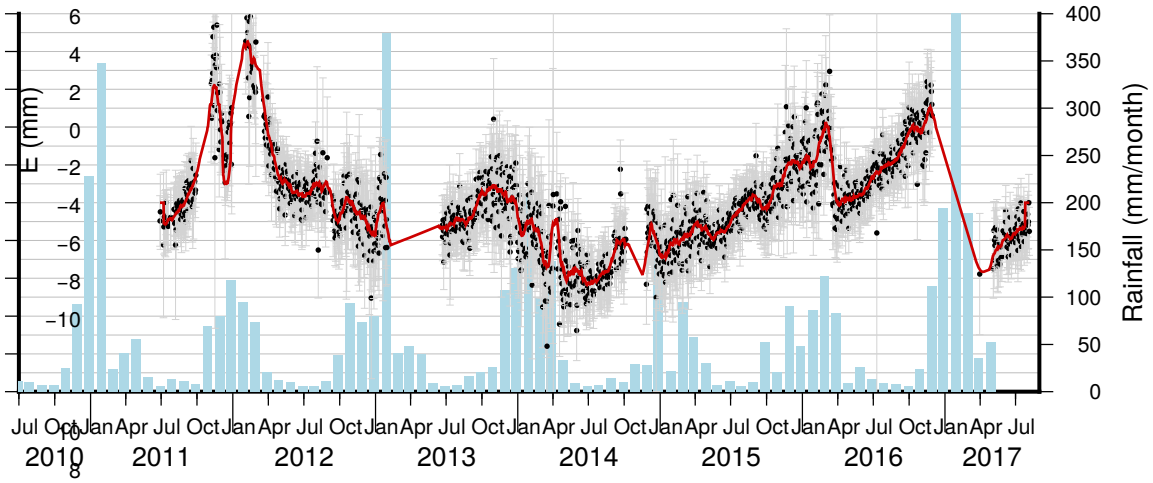

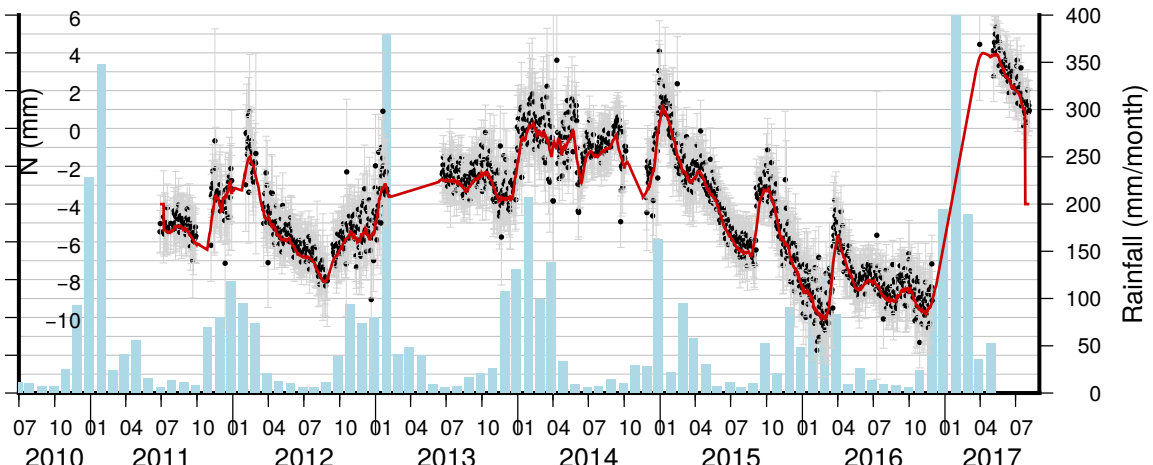

TETE

Location: Tete, Mozambique
33.5764°E, 16.1472°S, 149.23 m

Network: UNAVCO/AfricaArray
No information provided

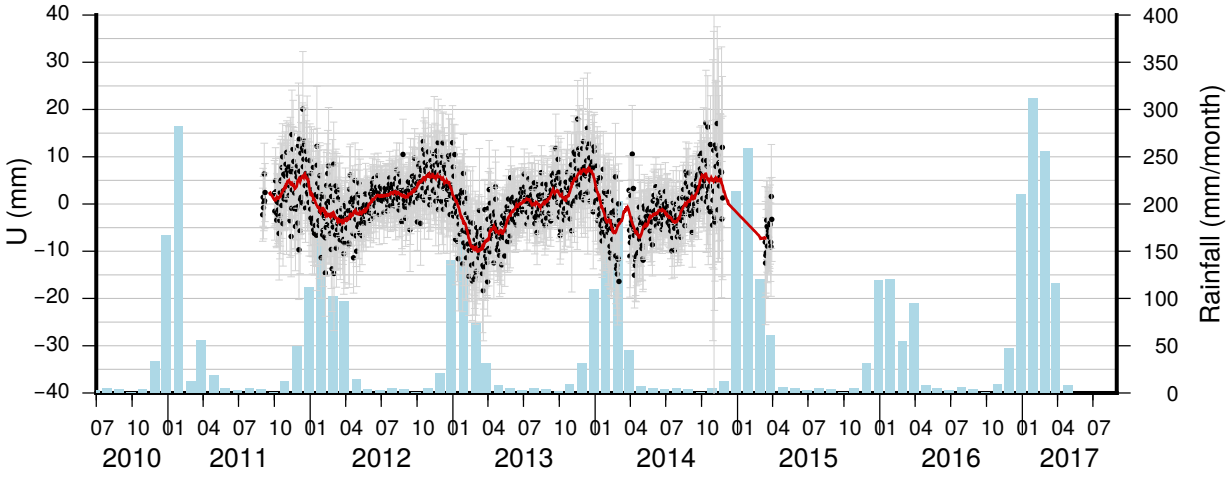

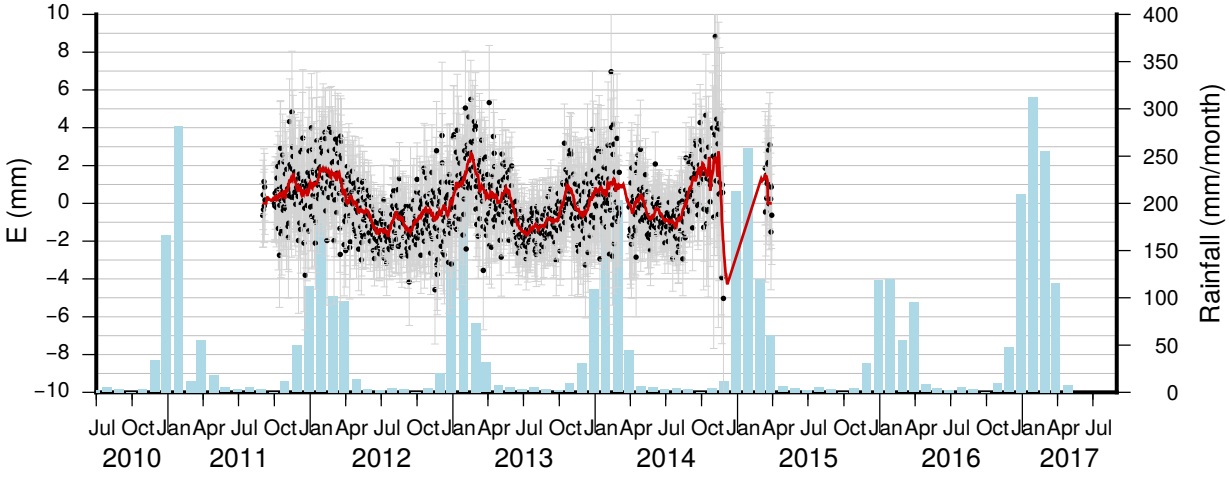

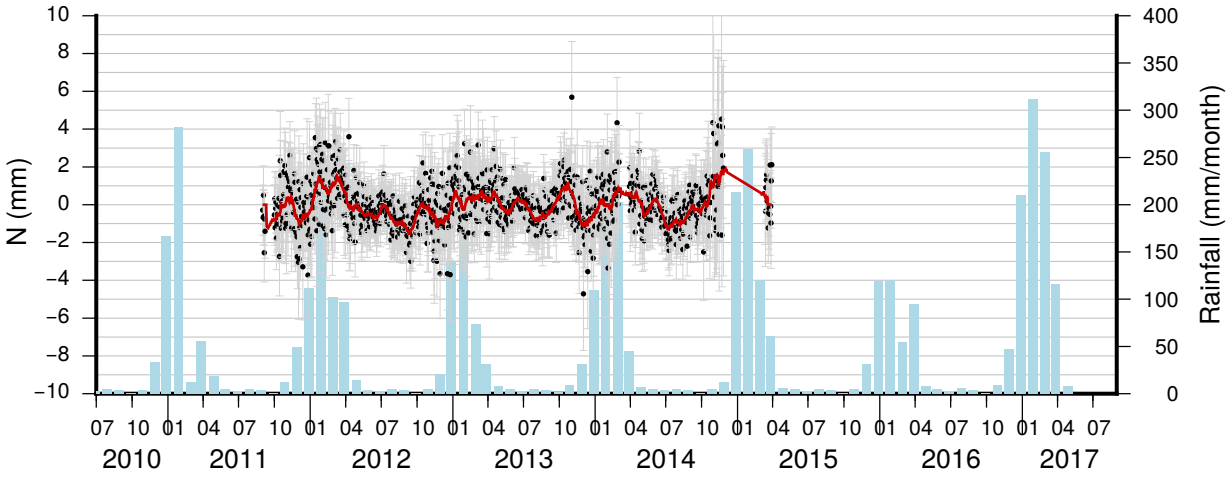

TEZI

Location: Itezhi-Tehzi, Zambia
26.0157°E, 15.7465°S, 1115.25 m

Network: UNAVCO/AfricaArray
Antenna on building roof

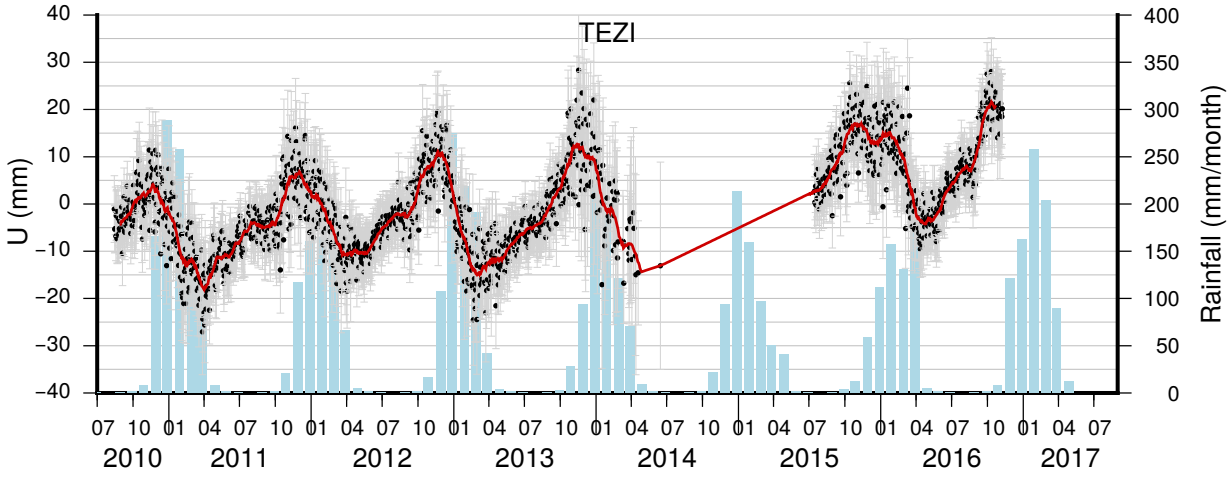

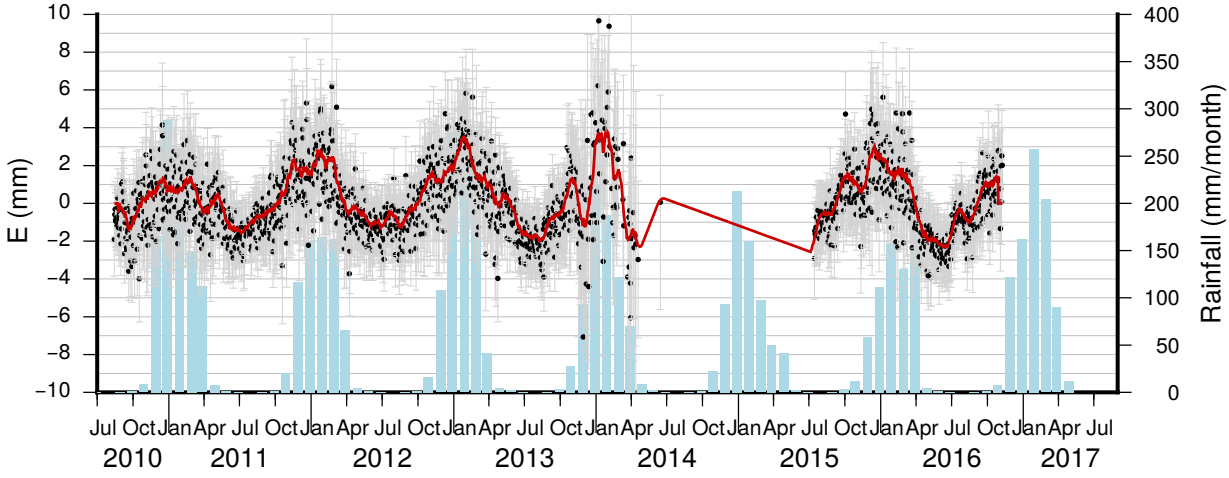

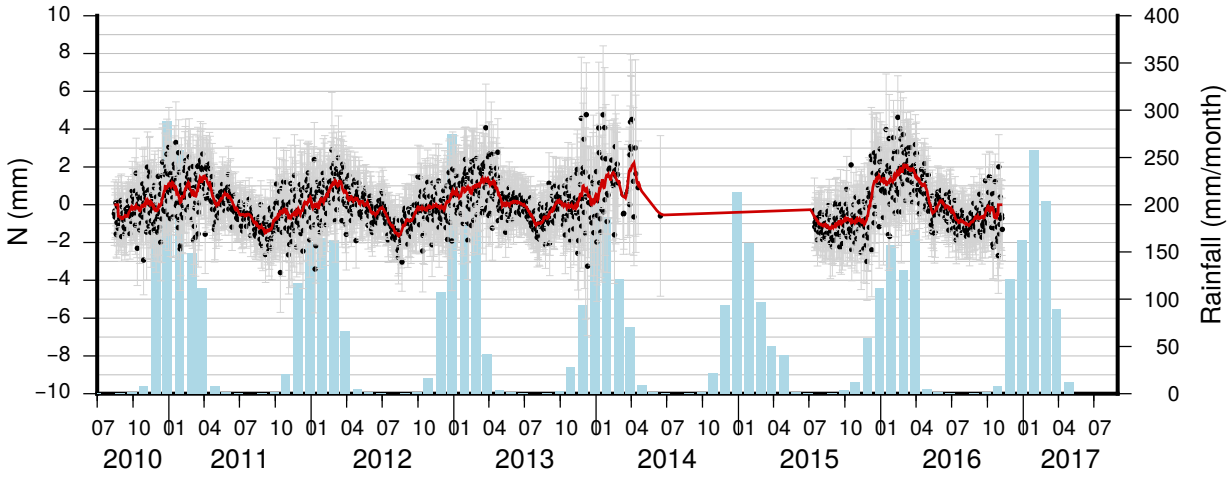

UKAM

Location: Kamina, RDC
25.0031°E, 8.7326°S, 1119.09 m

Network: UNAVCO/AfricaArray
Antenna on a shallow foundation pillar

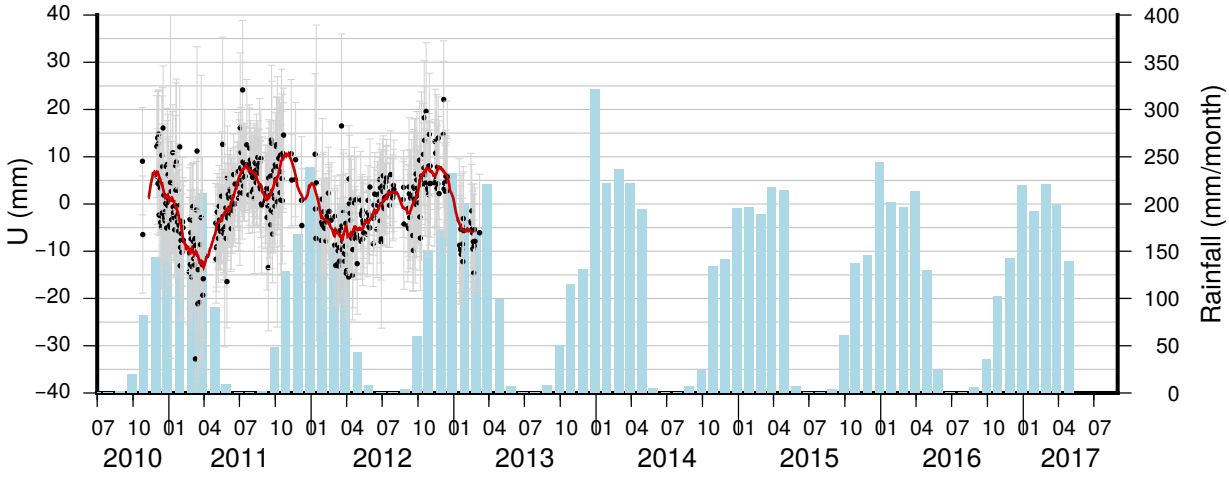

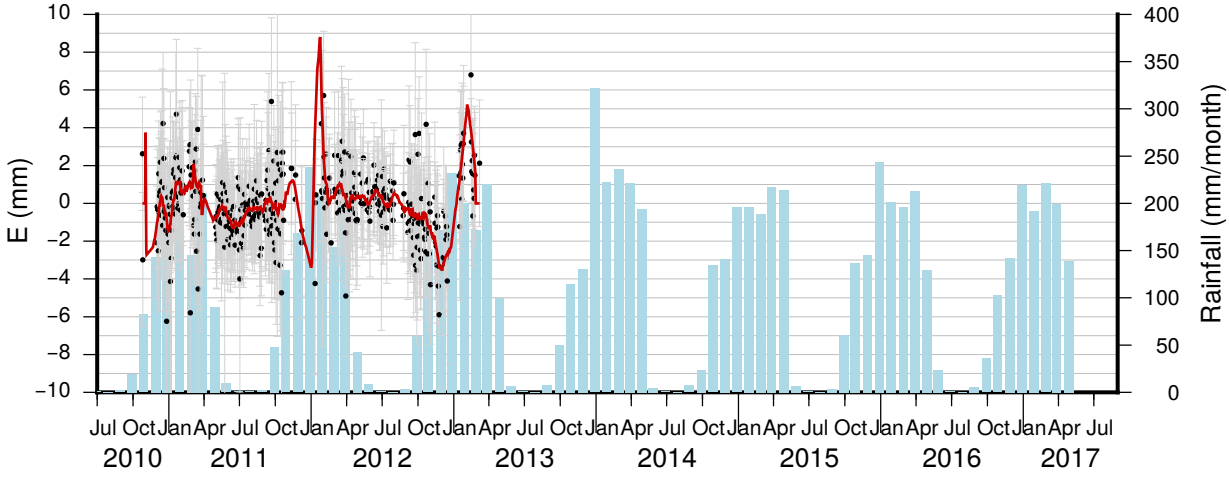

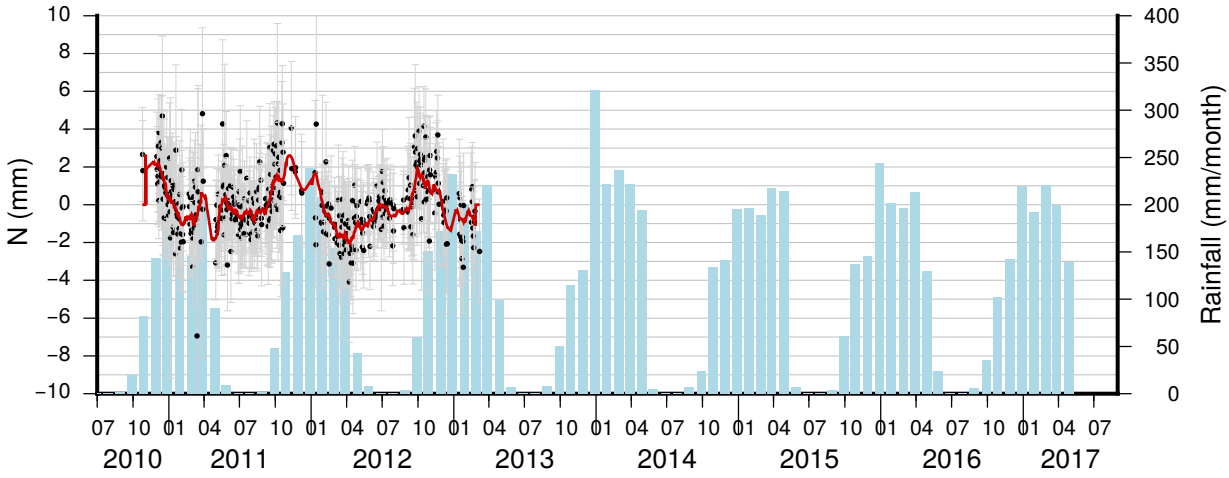

ULDI

Location: Ulundi, South Africa
31.4209°E, 28.2931°S, 607.95 m

Network: IGS
Antenna on a pipe on a parapet wall

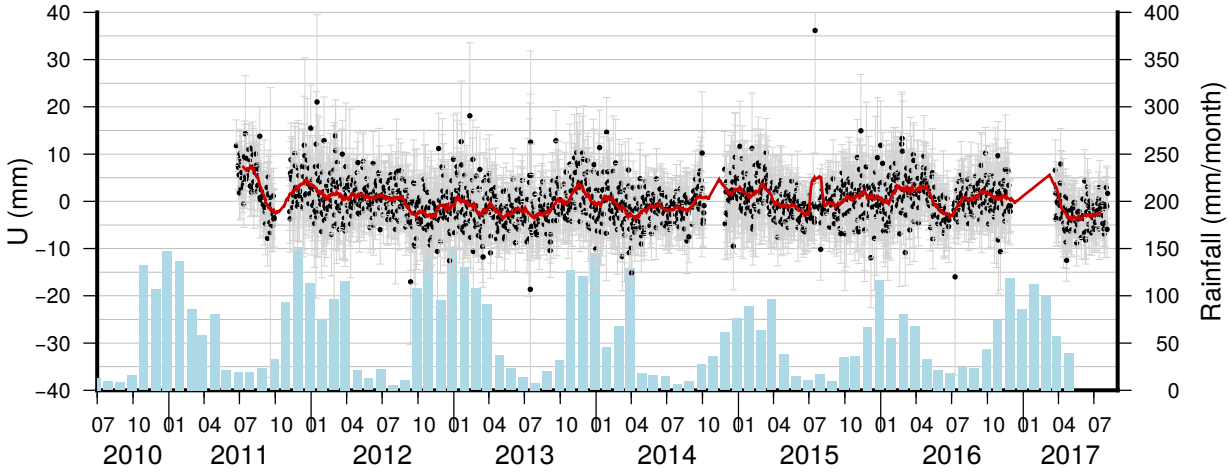

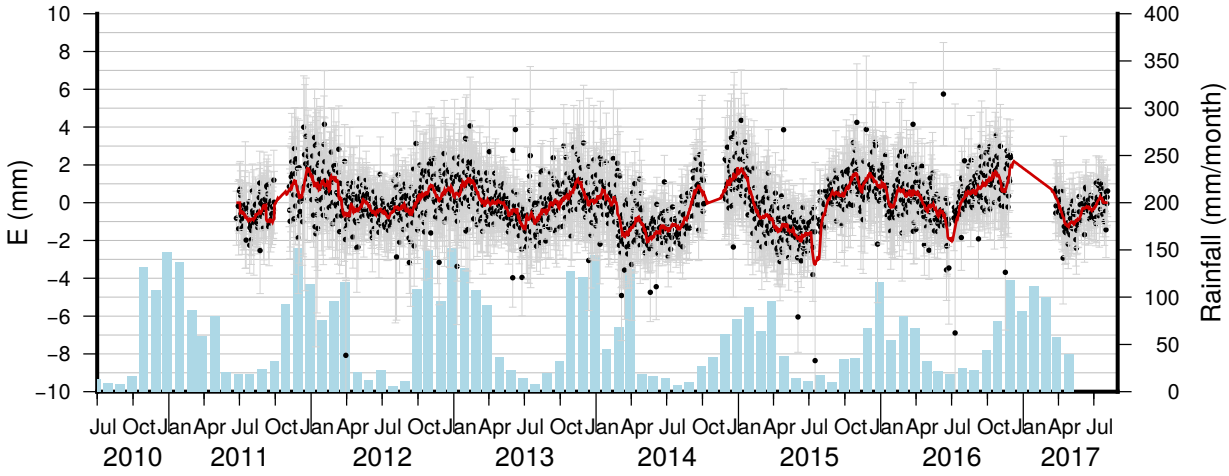

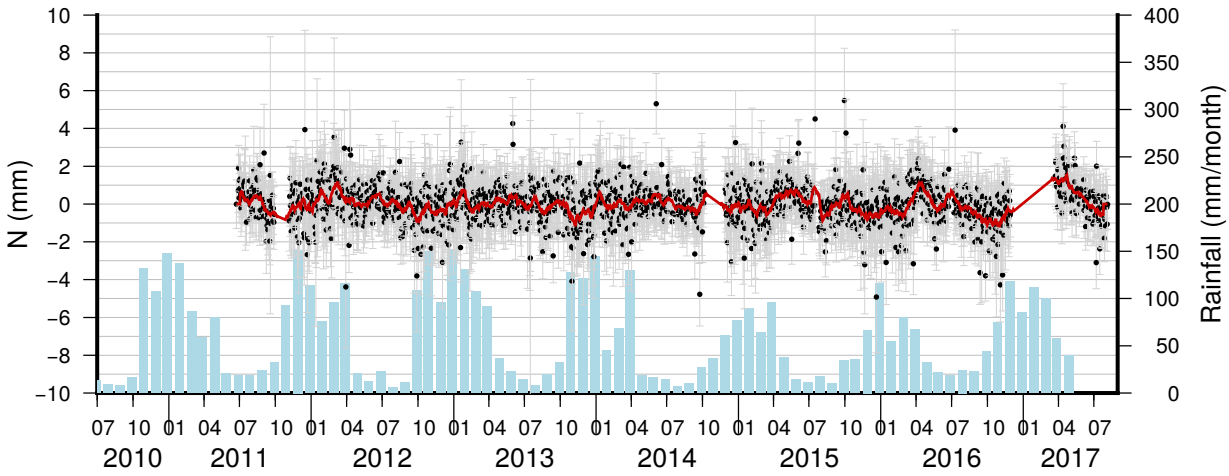

ULUB

Location: Lubumbashi, RDC
27.4849°E, 11.6306°S, 1280.21 m

Network: UNAVCO/AfricaArray
Antenna on a shallow foundation pillar

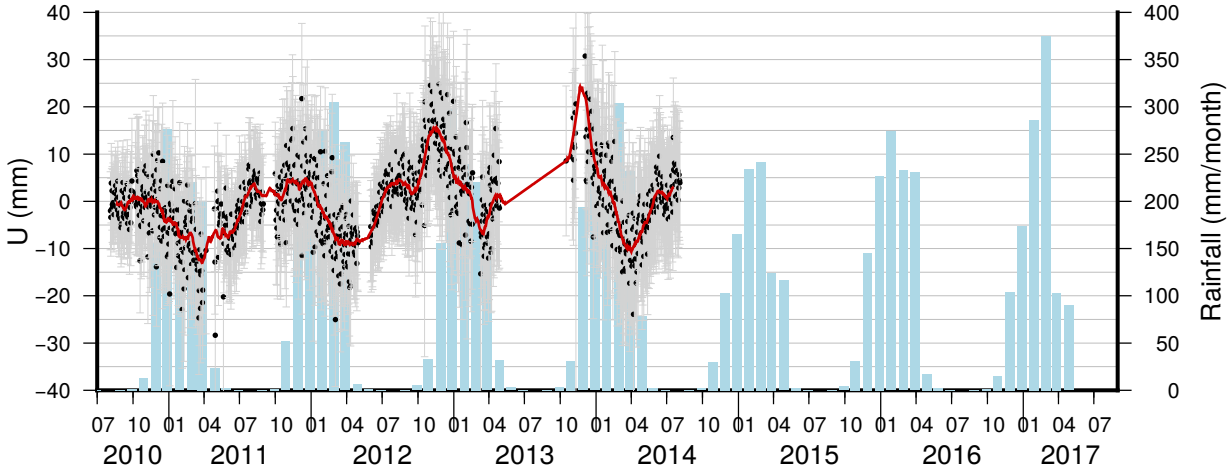

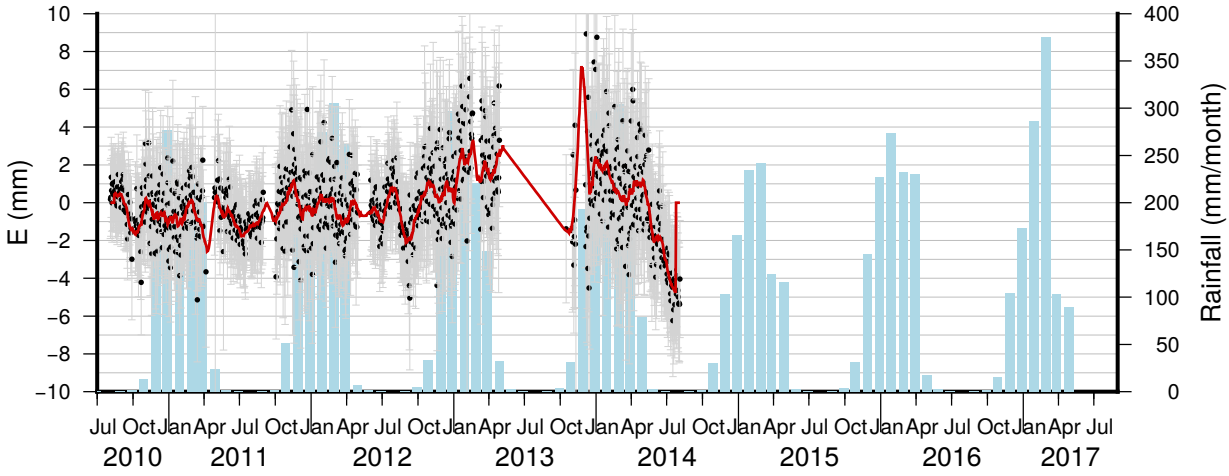

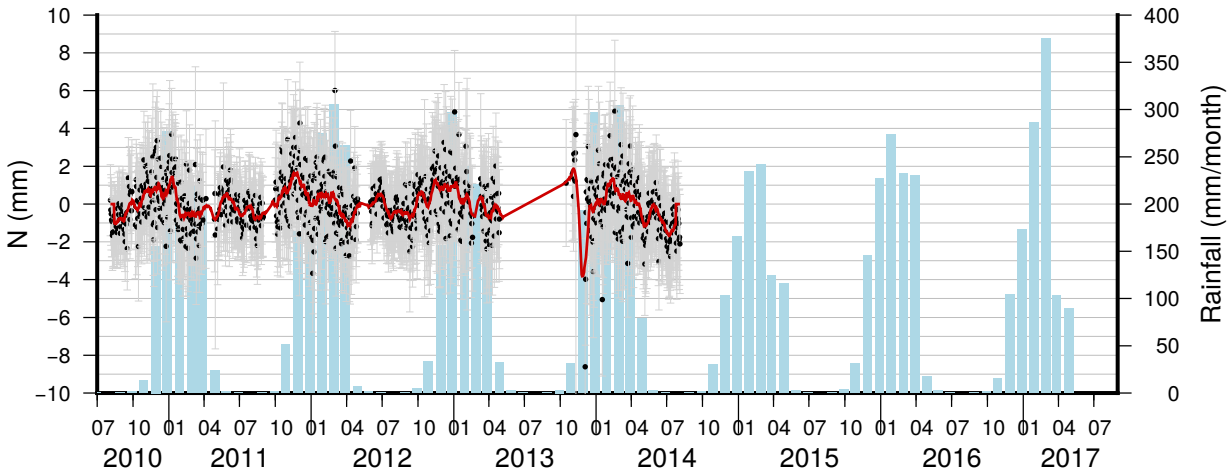

WIND

Location: Windhoek, Namibia
17.0894°E, 22.5749°S, 1734.67 m

Network: IGS
Antenna on a geodetic pillar

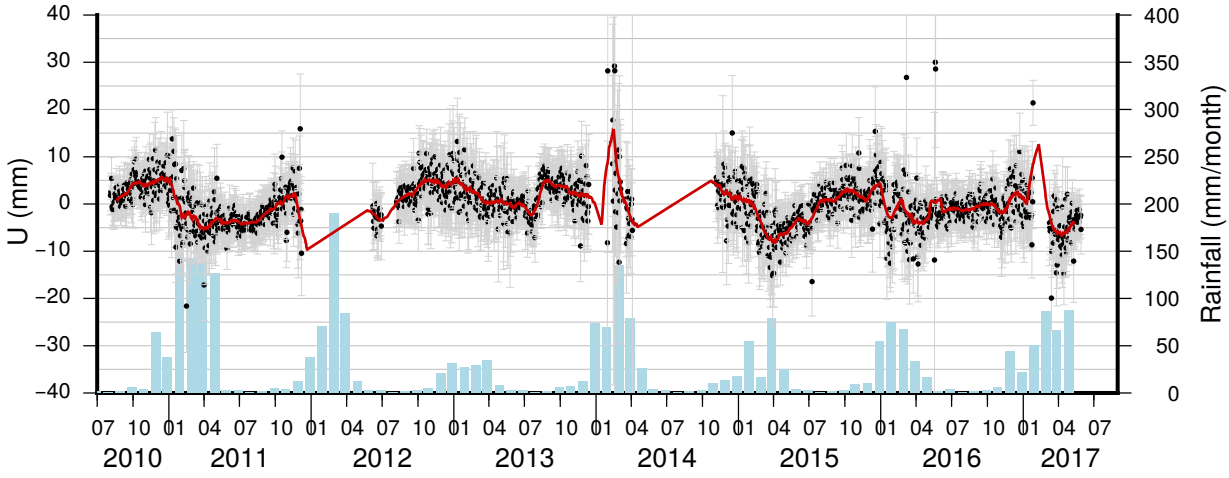

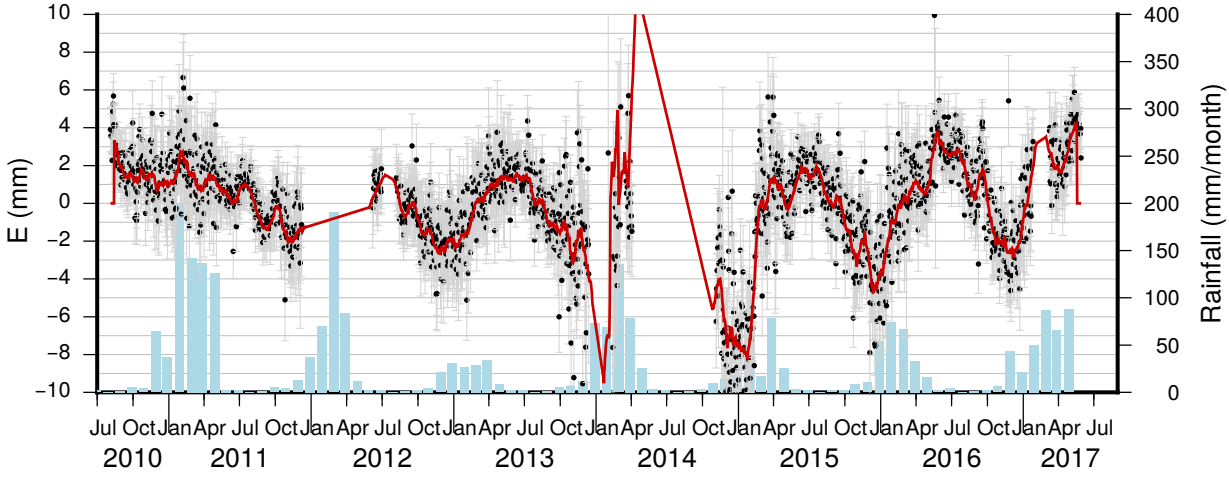

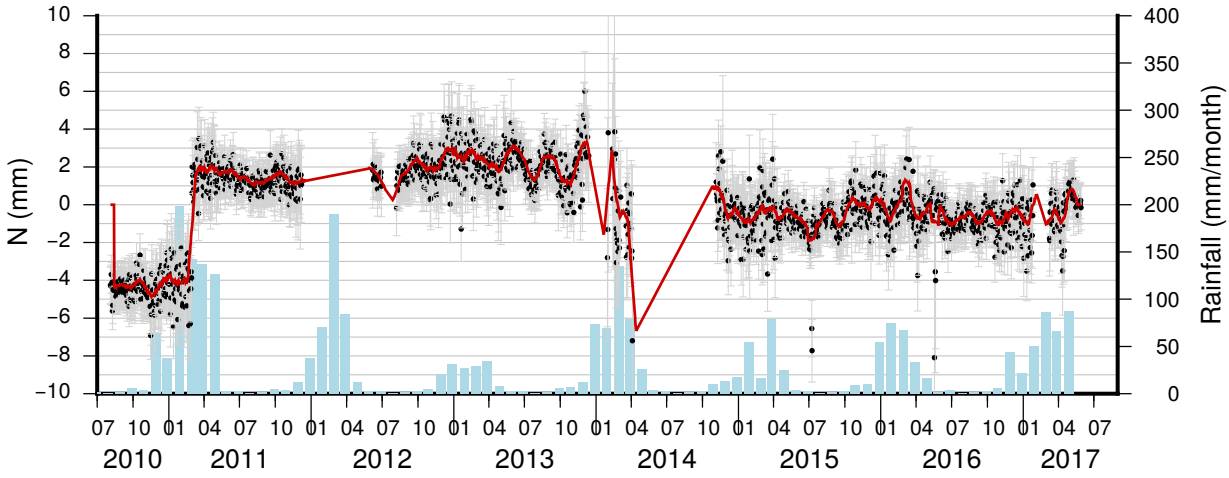

ZAMB

Location: Lusaka, Zambia
28.311°E, 15.4255°S, 1324.92 m

Network: IGS
Antenna on a roof of the premises of the Zambian Surveyor General's office

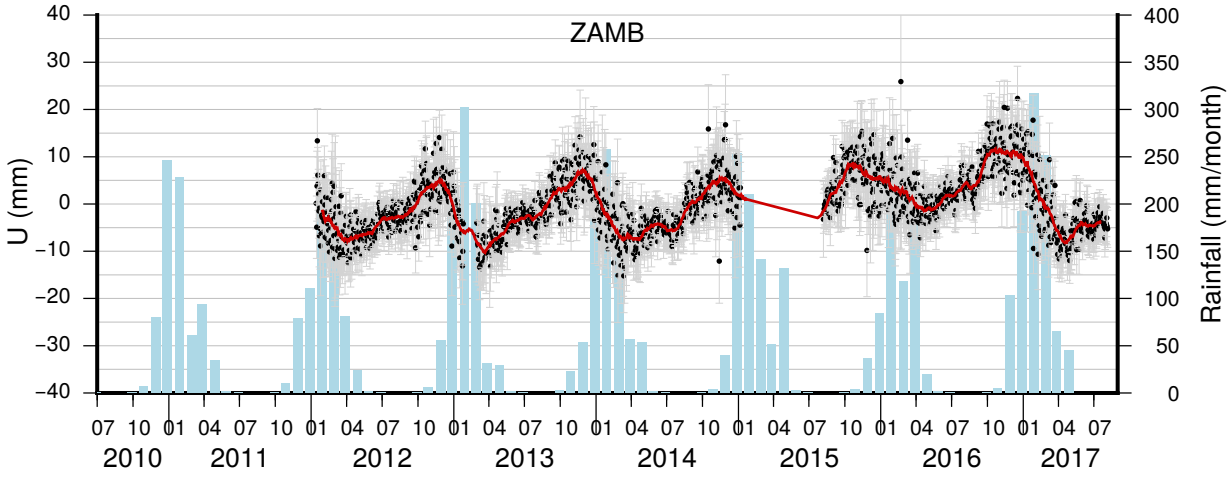

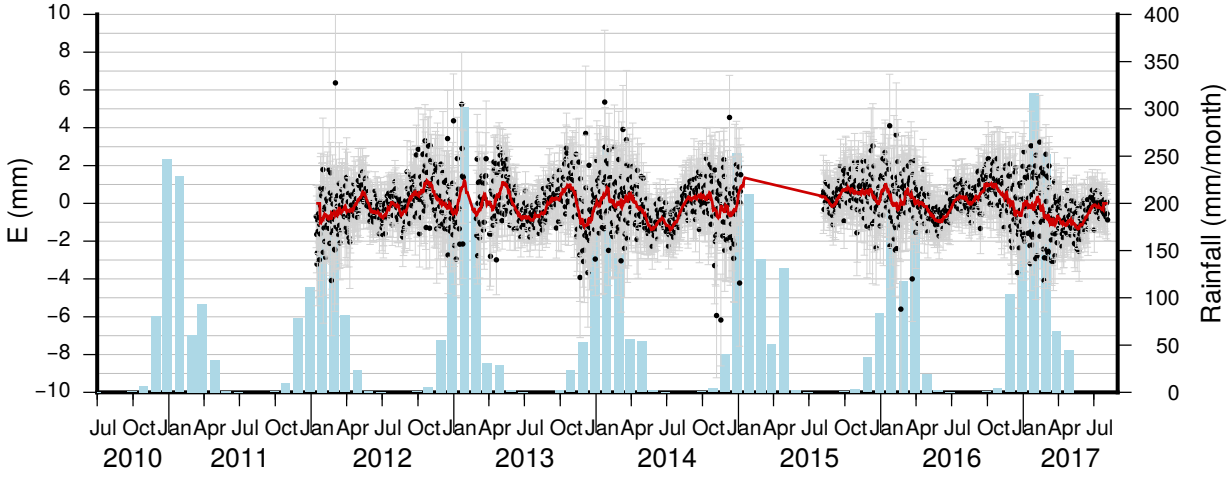

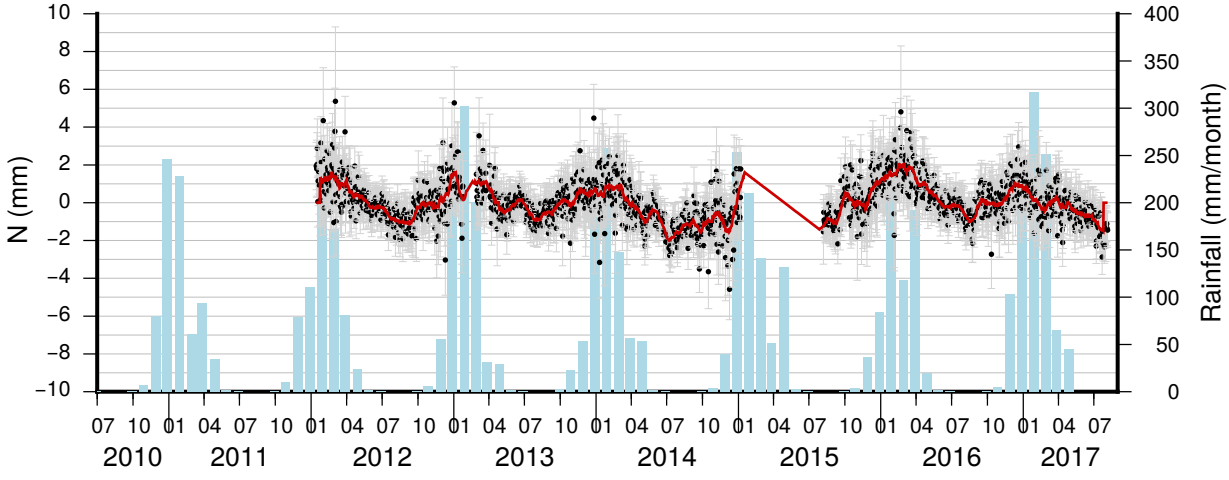

ZOMB

Location: Zomba, Malawi
35.3251°E, 15.3758°S, 972.62 m

Network: UNAVCO/AfricaArray
Antenna on a building roof

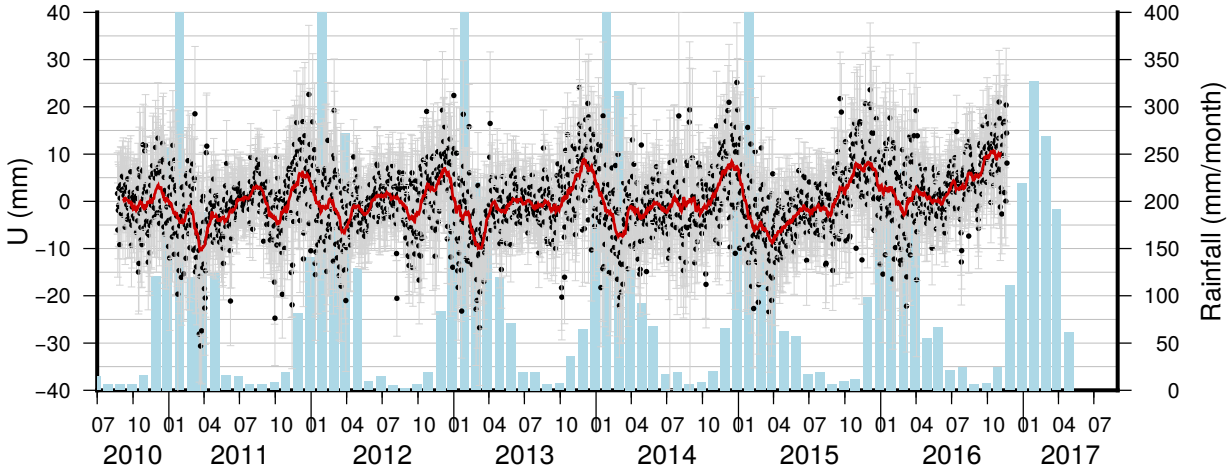

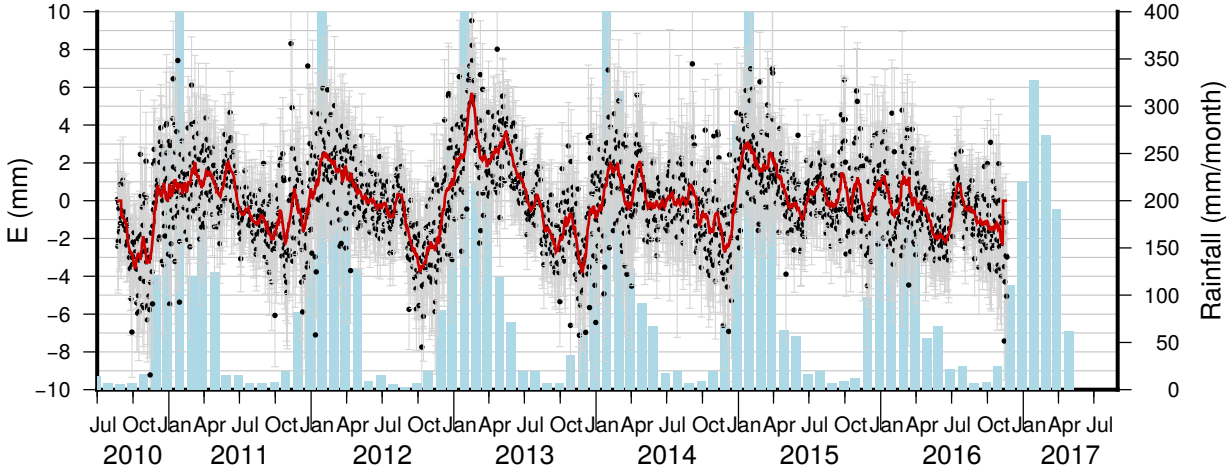

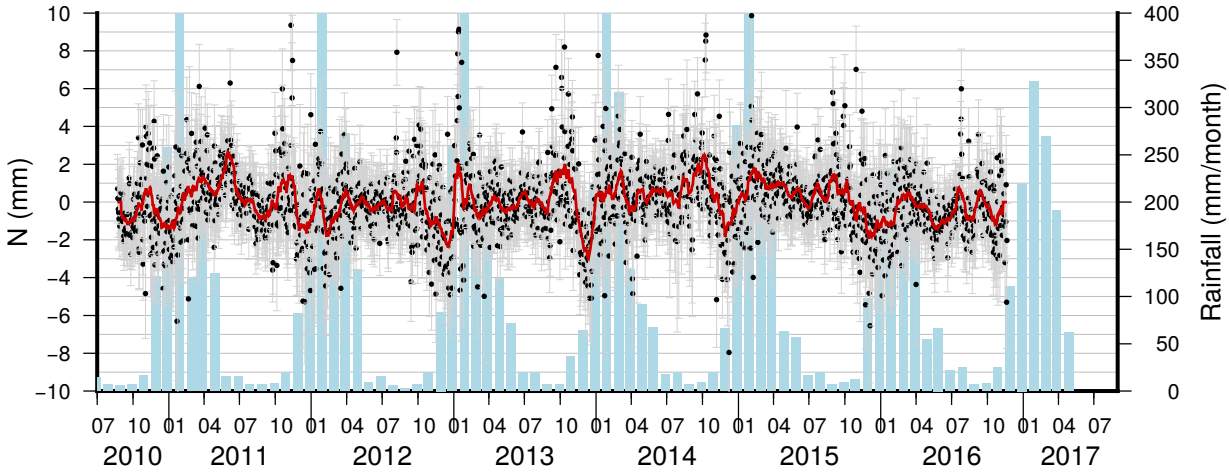

A.2 Statistics of time series of surface deformation

GPS station	CSR-60-dd4		CSR-60-gaussien		GRGS-60		GRGS-80	
	RMS	CC	RMS	CC	RMS	CC	RMS	CC
DEAR	2.229	-0.008	2.2598	-0.044	2.636	-0.377	2.750	-0.443
HNUS	2.047	0.236	2.0624	0.222	2.287	0.146	2.262	0.143
HRAO	2.211	0.665	2.1920	0.661	2.344	0.597	2.434	0.575
MAUA	3.001	0.786	3.1254	0.758	3.564	0.619	3.484	0.637
MFKG	2.322	0.449	2.6547	0.321	2.403	0.329	2.445	0.329
MONG	3.360	0.939	3.7262	0.925	3.290	0.916	3.283	0.916
RUND	2.105	0.902	2.2553	0.885	2.948	0.779	2.951	0.779
SBOK	1.711	0.161	1.7467	0.162	2.006	-0.024	2.024	-0.027
SUTH	1.736	0.042	1.8443	0.122	1.809	0.084	1.870	0.068
SUTM	1.677	0.274	1.7671	0.321	2.035	0.102	2.050	0.124
TDOU	2.680	0.531	2.7616	0.485	3.108	0.307	3.138	0.286
TETE	2.142	0.848	2.2971	0.839	2.845	0.753	2.842	0.758
TEZI	5.314	0.750	5.5716	0.720	6.523	0.647	6.571	0.641
UKAM	3.326	0.846	3.6483	0.804	3.634	0.773	3.637	0.773
ULUB	5.081	0.759	5.0546	0.747	5.433	0.679	5.437	0.676
ULDI	5.797	0.215	5.2548	0.272	5.785	0.113	5.795	0.107
WIND	3.114	0.508	3.2795	0.448	3.402	0.421	3.340	0.440
ZAMB	2.952	0.871	3.1892	0.832	3.724	0.709	3.727	0.709
ZOMB	2.780	0.775	2.8432	0.738	3.720	0.663	3.304	0.690
Okavango	2.733	0.844	2.6903	0.821	3.256	0.699	3.218	0.708
Zambezi	2.758	0.697	2.9379	0.676	3.350	0.614	3.288	0.619
Congo	4.204	0.803	4.3514	0.776	4.533	0.726	4.537	0.725
Total	2.926	0.555	3.0281	0.538	3.342	0.433	3.334	0.430

TABLE A.1 – Root mean square (RMS) and Correlation Coefficient (CC) between the GPS signal and the deformation modelled from GRACE data products, and averages for the different basins. Low CC are generally associated to a lack of seasonal loading in the area (see figure 3.5 and Appendix A.1)